ISSN 1007-9327 (print)
ISSN 2219-2840 (online)

World Journal of *Gastroenterology*

World J Gastroenterol 2020 March 7; 26(9): 883-994

Published by Baishideng Publishing Group Inc

World Journal of Gastroenterology

Contents

Weekly Volume 26 Number 9 March 7, 2020

REVIEW

ORIGINAL ARTICLE

Basic Study

Case Control Study

Retrospective Study

CASE REPORT

LETTER TO THE EDITOR

Contents

World Journal of Gastroenterology

Volume 26 Number 9 March 7, 2020

ABOUT COVER

Associate Editor of *World Journal of Gastroenterology*, Seung Up Kim, MD, PhD, Associate Professor, Department of Internal Medicine, Yonsei University College of Medicine, Severance Hospital, Seoul 03722, South Korea

AIMS AND SCOPE

The primary aim of *World Journal of Gastroenterology* (*WJG*, *World J Gastroenterol*) is to provide scholars and readers from various fields of gastroenterology and hepatology with a platform to publish high-quality basic and clinical research articles and communicate their research findings online.

WJG mainly publishes articles reporting research results and findings obtained in the field of gastroenterology and hepatology and covering a wide range of topics including gastroenterology, hepatology, gastrointestinal endoscopy, gastrointestinal surgery, gastrointestinal oncology, and pediatric gastroenterology.

INDEXING/ABSTRACTING

The *WJG* is now indexed in Current Contents®/Clinical Medicine, Science Citation Index Expanded (also known as SciSearch®), Journal Citation Reports®, Index Medicus, MEDLINE, PubMed, PubMed Central, and Scopus. The 2019 edition of Journal Citation Report® cites the 2018 impact factor for *WJG* as 3.411 (5-year impact factor: 3.579), ranking *WJG* as 35th among 84 journals in gastroenterology and hepatology (quartile in category Q2). CiteScore (2018): 3.43.

RESPONSIBLE EDITORS FOR THIS ISSUE

Responsible Electronic Editor: *Yu-Jie Ma*

Proofing Production Department Director: *Xiang Li*

NAME OF JOURNAL
World Journal of Gastroenterology

ISSN
ISSN 1007-9327 (print) ISSN 2219-2840 (online)

LAUNCH DATE
October 1, 1995

FREQUENCY
Weekly

EDITORS-IN-CHIEF
Subrata Ghosh, Andrzej S Tarnawski

EDITORIAL BOARD MEMBERS
http://www.wjgnet.com/1007-9327/editorialboard.htm

EDITORIAL OFFICE
Ze-Mao Gong, Director

PUBLICATION DATE
March 7, 2020

INSTRUCTIONS TO AUTHORS
https://www.wjgnet.com/bpg/gerinfo/204

GUIDELINES FOR ETHICS DOCUMENTS
https://www.wjgnet.com/bpg/GerInfo/287

GUIDELINES FOR NON-NATIVE SPEAKERS OF ENGLISH
https://www.wjgnet.com/bpg/gerinfo/240

PUBLICATION MISCONDUCT
https://www.wjgnet.com/bpg/gerinfo/208

ARTICLE PROCESSING CHARGE
https://www.wjgnet.com/bpg/gerinfo/242

STEPS FOR SUBMITTING MANUSCRIPTS
https://www.wjgnet.com/bpg/GerInfo/239

ONLINE SUBMISSION
https://www.f6publishing.com

World Journal of Gastroenterology

Submit a Manuscript: https://www.f6publishing.com

World J Gastroenterol 2020 March 7; 26(9): 883-903

DOI: 10.3748/wjg.v26.i9.883

ISSN 1007-9327 (print) ISSN 2219-2840 (online)

REVIEW

Role of alcohol in pathogenesis of hepatitis B virus infection

Murali Ganesan, Allison Eikenberry, Larisa Y Poluektova, Kusum K Kharbanda, Natalia A Osna

ORCID number: Murali Ganesan (0000-0002-2981-568X); Allison Eikenberry (0000-0001-6469-7036); Larisa Y Poluektova (0000-0001-7339-8732); Kusum K Kharbanda (0000-0001-7759-8889); Natalia A Osna (0000-0001-7498-0556).

Author contributions: All authors contributed to this review with conception and design, literature review, drafting and critical revision, editing, and approval of the final version.

Supported by National Institutes of Health, No. NIAAA-K01AA026864.

Conflict-of-interest statement: No potential conflicts of interest.

Manuscript source: Invited Manuscript

Received: December 5, 2019
Peer-review started: December 5, 2019
First decision: December 30, 2019
Revised: February 9, 2020
Accepted: February 15, 2020

Murali Ganesan, Allison Eikenberry, Kusum K Kharbanda, Natalia A Osna, Research Service, Veterans Affairs Nebraska-Western Iowa Health Care System, Omaha, NE 68105, United States

Murali Ganesan, Allison Eikenberry, Kusum K Kharbanda, Natalia A Osna, Department of Internal Medicine, Division of Gastroenterology and Hepatology, University of Nebraska Medical Center, Omaha, NE 68105, United States

Larisa Y Poluektova, Department of Pharmacology and Experimental Neuroscience, University of Nebraska Medical Center, Omaha, NE 68198, United States

Corresponding author: Murali Ganesan, PhD, Assistant Professor, Department of Internal Medicine, Division of Gastroenterology and Hepatology, University of Nebraska Medical Center, Omaha, NE 68198, United States. murali.ganesan@unmc.edu

Abstract

Hepatitis B virus (HBV) and alcohol abuse often contribute to the development of end-stage liver disease. Alcohol abuse not only causes rapid progression of liver disease in HBV infected patients but also allows HBV to persist chronically. Importantly, the mechanism by which alcohol promotes the progression of HBV-associated liver disease are not completely understood. Potential mechanisms include a suppressed immune response, oxidative stress, endoplasmic reticulum and Golgi apparatus stresses, and increased HBV replication. Certainly, more research is necessary to gain a better understanding of these mechanisms such that treatment(s) to prevent rapid liver disease progression in alcohol-abusing HBV patients could be developed. In this review, we discuss the aforementioned factors for the higher risk of liver diseases in alcohol-induced HBV pathogenies and suggest the areas for future studies in this field.

Key words: Hepatitis B virus; Alcohol; Immunity; Oxidative stress; Liver disease

Core tip: In this review, we discussed the literature and some of our recent findings on the combined effects of alcohol and hepatitis B virus (HBV)-infection in the progression of liver diseases, such as steatosis, fibrosis, cirrhosis and hepatocellular carcinoma. Worldwide, 1.5 billion people had chronic liver disease in 2017, most commonly resulting from HBV (29%) and alcoholic liver disease (2%). Clinical evidence supports the synergistic effect of alcohol and HBV- infection on progression of end-stage liver diseases. The possible mechanisms for the chronic liver diseases induced by the combination of alcohol and HBV-infection are increased HBV replication, oxidative stress, cell organelles stress [such as endoplasmic reticulum and Golgi stress] and

Article in press: February 15, 2020
Published online: March 7, 2020

P-Reviewer: Guo YM, Kollmann D, Yuan Y, Zheng H
S-Editor: Tang JZ
L-Editor: A
E-Editor: Ma YJ

importantly, weakened immune responses. Better understanding of these mechanisms will improve the treatment options for the HBV-alcoholic patients.

Citation: Ganesan M, Eikenberry A, Poluektova LY, Kharbanda KK, Osna NA. Role of alcohol in pathogenesis of hepatitis B virus infection. *World J Gastroenterol* 2020; 26(9): 883-903
URL: https://www.wjgnet.com/1007-9327/full/v26/i9/883.htm
DOI: https://dx.doi.org/10.3748/wjg.v26.i9.883

INTRODUCTION

Hepatitis B virus (HBV) infection is an important public health problem. Two billion population worldwide infected with HBV, including 257 million chronic carriers[1]. The current number of chronic HBV infection cases in United States is 2.2 million[2]. However, many people living with HBV are unaware that they are infected. Usually, patients with acute hepatitis B clear HBV from their blood and liver within 6 mo. However, certain factors, such as alcohol abuse, make HBV to chronically persist which put patients at a higher risk for developing fibrosis, cirrhosis, and hepatocellular carcinoma (HCC)[3-5]. The combination of HBV infection and alcohol abuse enhances liver injury progression[6,7], especially to HCC, which is 5th most common cancer type and 2nd leading cause of cancer death in world[5,8]. The mechanisms underlying these detrimental effects of alcohol in HBV-infected patients are not fully understood and are less clear than with chronic hepatitis C virus (HCV) infection. Current treatment for chronic HBV patients is limited to antiviral medications, interferon (IFN) injections, and liver transplants. These treatments do not fully cure the HBV infection but prevent its spread to uninfected people and decrease the chance of developing end-stage liver disease. However, these medications are often largely ineffective when chronic HBV infected patients have alcohol use disorders (AUD). Elucidation of the mechanisms behind the exacerbation of HBV pathogenesis by alcohol is crucial for the development of new drugs and treatment options in alcohol-abusing HBV patients. This article reviews the current literature concerning alcohol-mediated HBV persistence by exploring ethanol-induced immune system impairment, HBV replication, oxidative stress, endoplasmic reticulum (ER) stress, Golgi apparatus fragmentation, and a higher risk of the end-stage liver diseases. It also indicates the gaps in our knowledge base for future studies in this field.

INCIDENCE OF HBV INFECTION

The epidemiology of HBV infection is geographically diverse, with population prevalence, age, acquisition mode and chance of progression to chronic state being mutually interdependent[9]. In United States, about 22100 acute hepatitis B cases were reported in 2017. The prevalence of chronic HBV infection is categorized into low, intermediate and high prevalence areas based on the percent of HBV infection's incidence: Less than 2% is observed in low-prevalence areas (United States, Canada, and Western Europe), 2% to 7% is in intermediate-prevalence areas (Mediterranean countries, Japan, Central Asia, Middle East, and parts of South America) and more than 8% is in high-prevalence areas (Western Africa and South Sudan)[9].

DEVELOPMENT OF END STAGE LIVER DISEASES IN CHRONIC HBV INFECTION

The progression to chronic hepatitis B infection enhances the risk for development end- stage liver diseases leading to increased mortality[4,5]. The hepatic steatosis induced by HBV infection is mainly caused by HBx protein by increasing the mitochondrial reactive oxygen species (ROS) levels, oxidative stress and through the interaction with liver-enriched transcription factors, hepatocyte nuclear factor 3-β, CCAAT/enhancer-binding protein α, peroxisome proliferator-activated receptor α axis, and fatty acid–binding protein 1[10,11]. Interaction between viral proteins in the

liver and immune system induces hepatocyte damage, followed by tissue repair[12]. This repair process causes deposition of extracellular matrix leading to progressive liver fibrosis. HBV X protein may also have fibrogenic and oncogenic effects on liver[13]. Progression to advanced fibrosis can be either rapid or slow, or sporadic based on disease stages and levels of liver inflammation and injury[14]. A recent study reported that elevated α-fetoprotein levels and hepatitis B e antigen (HbeAg)-negative hepatitis are risk factors for liver fibrosis. In addition, these authors found that interleukin (IL)-1β elevation is important for the progression of liver fibrosis during chronic HBV infection[15]. The mean age of cirrhosis onset in chronic HBV infection acquired during childhood is about 40 years, and the complications become clinically evident 3 years to 5 years later[3,16]. Cirrhosis development is 3-fold more frequent in chronic HBV patients with high viral load than in those with low viral load[17-19]. HBeAg-positivity and elevated HBV DNA levels were reported as risk factors for the onset of liver cirrhosis in patients with chronic hepatitis B[20]. Liver cirrhosis is a pre-malignant condition that increase incidence of genetic aberrations and cellular transformations. The chronic hepatic inflammation as well as increased hepatocyte turnover found in cirrhosis lead to genetic mutations. Uncontrolled proliferation and the high rate of genetic mutations promote progression to liver cancer[21]. HBV infection is one of the major risk factors for the development of HCC. Below, we will overview the role of alcohol in progression of HBV-infection to end-stage liver disease.

ROLE OF ETHANOL METABOLISM ON VIRAL HEPATITIS

Alcohol abuse is another major health problem prevalent throughout the world. AUD is characterized by compulsive alcohol intake and a pessimistic mood when not using alcohol. The National Survey on Drug Use and Health found that 15.1 million adults and 623000 adolescents (age 12-17) had AUD. Only 6.7% of these adults and 5.2% of these adolescents received treatment. Furthermore, alcohol abuse poses an extraordinary economic burden. Excessive alcohol use cost the United States $249 billion per year[22], and alcoholic liver disease (ALD) is an escalating global problem accounting for more than 3 million deaths annually[23].

Chronic alcohol intake alters the architecture and compromises the functional capacity of the liver. Alcohol metabolism is catalyzed by alcohol dehydrogenase and cytochrome P450 2E1 (CYP2E1) to acetaldehyde and this major metabolite is the culprit for the majority of the toxic effects associated with alcohol use[24,25]. Acetaldehyde is both highly toxic and carcinogenic[26]. CYP2E1 is involved in the induction of ROS, which interact with fat molecules thereby causing lipid peroxidation[27]. In addition, both acetaldehyde and CYP2E1 induce oxidative stress[28]. Overall, the effect of alcohol metabolism on protein function, DNA, changes to the immune system and oxidative stress affect both hepatocytes and other liver cells. They take place under both acute and chronic exposure to alcohol and induce significant functional impairments resulting in cell death, tumorigenesis, altered cell to cell communication, and become more prone to viral infections[29,30].

Ethanol metabolism is often associated with viral hepatitis, because liver is a primary site for both hepatotropic viruses (HCV and HBV) replication and ethanol metabolism. ALD accompanied with the hepatitis virus accelerates the disease course[31]. Synergic hepatotoxic effect caused by alcohol and HCV infection increased the risk of advanced liver disease, rapid progression of fibrosis, and higher prevalence of HCC[32,33]. It has been reported that combination of HCV infection and daily alcohol intake (> 80 g) increased the risk of HCC development > 100-fold[34]. The incidence of HBV is higher among alcoholics than among the general population[35,36]. Studies has been conducted on the combined effect of alcohol and viral hepatitis in the progression of liver diseases, but the role of alcohol metabolism as risk factors in pathogenesis of HBV infection has not been studied yet[30].

CLINICAL EVIDENCE OF HBV INFECTION ASSOCIATED LIVER DISEASES IN ALCOHOLICS

Alcohol abuse pattern has wide geographical distribution depending on alcohol drinking habits in various parts of the world. As reported, about 50% of HBV carriers drink alcohol and more than 10% are heavy drinkers in Korean population[37]. A study from Taiwan reported that alcohol drinking is linked to a lower prevalence of hepatitis B surface antigen (HbsAg) alone but to higher prevalence of HBeAg among HbsAg-positive drinkers compared with nondrinkers[38]. Recently, Iida-Ueno *et al*[27]

extensively reviewed the role of alcohol in the exacerbation of HBV infection and progression to end-stage liver diseases. Marcellin *et al*[39] found a strong association between alcohol consumption and mortality in HBV patients. Two prospective community-based cohort studies from Taiwan and Korea reported that alcohol consumption had an increased risk of HCC in HBsAg-positive men when compared HBsAg-positive patients with HbsAg negative patients without alcohol consumption, but relative risk was not significant[40,41]. It has been shown that chronic HBV infection potentiated by co-factors, such as alcohol consumption, may act in synergy with the virus in determining an early onset and a more rapid progression of HCC[42,43]. Furthermore, the risk of HCC development is 6-fold higher in alcohol abusers[44]. In addition, according to Loomba *et al*[45] both obesity and alcohol have synergistic effects in increasing the incidence of HCC in HBsAg–positive men. It has been reported in cohort of Italian cirrhotic patients that the combined effect of alcohol and HBV was high risk factor for HCC (18-fold increase) than the HBV alone[34,46]. In addition, people who use alcohol for at least 15 years had enhanced the risk of liver cancer in chronic HbsAg carriers for 3-4 times[46].

Alcohol also increases the risk of fibrosis in patients with coexisting HBV[47], as well as enhances liver necroinflammatory changes in HBsAg positive patients[48]. There is an increased alteration of liver tests in HBsAg alcohol abusers[49]. In addition, self-resolved HBV infection (defined as HBsAg-negative and HBcAb-positive) can be qualified as a risk factor for developing HCC in patients with alcoholic cirrhosis[50]. Interestingly, a recent study on liver disease progression in subjects with simultaneous presence of HBV/HCV dual infection and history of alcohol abuse suggests that females are at a higher risk of liver cirrhosis than males[51]. Future studies should focus on the unresolved issues, such as the influence of alcohol in inactive HBsAg carriers, immune tolerant or long-term virally suppressed patients for the risk of liver disease progression[34]. Importantly the mechanisms of synergistic effects between alcohol and HBV infection, which increases the risk of end-stage liver diseases should be the subject of extensive research[52].

HBV REPLICATION CYCLE AND ALCOHOL

Under normal circumstances, HBV behaves as a stealth virus, escaping the immune response[53,54]. HBV is an enveloped DNA virus containing a partially double-stranded relaxed circular DNA genome tropic to hepatocytes[55]. The HBV replication cycle requires binding and entry of the virus *via* its receptors, cytosolic transport and uncoating of the nucleocapsid, formation of covalently closed circular DNA in the nucleus, the transcription and translation of virus-specific genes, assembly of capsids and initiation of reverse transcription, followed by budding and secretion of virions and sub-viral particles as shown in Figure 1.

HBV replication cycle is a classical process, which is regulated by both host and viral factors[55-57]. Double-stranded DNA genome encodes only 7 viral proteins including DNA polymerase, capsid protein (Core), HBeAg, X protein, and three envelope proteins: LHBs (L), MHBs (M) and SHBs (S)[57,58]. A hallmark of all Hepadnaviridae is the secretion of surface proteins as sub-viral particles (for HBV, HBsAg particles) in spherical or filamentous form and HBsAg do not contain viral DNA and are non-infectious[59].

Alcoholic patients often have higher levels of HBV markers. Under experimental conditions, Larkin *et al*[35] found that ethanol-fed mice had up to 7-fold higher levels of HBsAg and HBV DNA compared to control diet- fed mice. HBV RNA levels were increased in alcohol-fed mice, also showing higher expression of core, surface, and X antigens in the liver. This is consistent with the higher HBV marker levels present among alcoholics and supports the idea that alcohol abuse increases HBV replication. The ability of HBV to evade and/or suppress the immune system also supports this idea, especially when the immune system is impaired by excessive alcohol consumption. Recently, based on *in vitro* studies, we reported that ethanol metabolism increased the HBV RNA, covalently closed circular DNA, and HBsAg in HBV transfected cells[60]. This report is in agreement with a previous study which demonstrated that ethanol significantly increased HBV replication in mice[61]. The mechanism behind the ethanol- induced HBV replication may be related to increased CYP2E1 activity and subsequent oxidative stress induction. As shown by Min *et al*[62] ethanol-induced overexpression of CYP2E1 significantly increased the expression of HNF-4a, a major transcription factor for the HBV core promoter, thereby increasing the HBV replication in ethanol exposed HepAD38 cells. The same authors reported that alcohol per se stimulates the HBV genome transcription by increasing the liver-specific transcription factors/nuclear receptors in an oxidative stress-independent

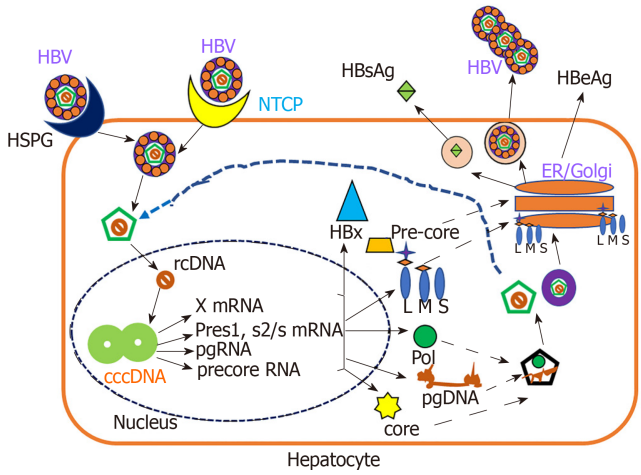

Figure 1 Schematic presentation of hepatitis B virus replication cycle. Hepatitis B virus (HBV) enters hepatocytes *via* hepatocyte-expressing receptors for viral entry, either sodium taurocholate co-transporting polypeptide or heparan sulfate proteoglycan. The next stage is uncoating of the nucleocapsid, which takes place in cytosol and then formation of covalently closed circular DNA occurs in nucleus. Next, the transcription and translation of HBV specific genes take place and finally, the HBV virions are released to circulation. X protein, and three envelope proteins: LHBs (L), MHBs (M) and SHBs (S). HBV: Hepatitis B virus; NTCP: sodium taurocholate co-transporting polypeptide; cccDNA: Covalently closed circular DNA; HSPG: Heparan sulfate proteoglycan; rcDNA: Relaxed circular DNA; ER: Endoplasmic reticulum; Pol: DNA polymerase; Core: Capsid protein; HBeAg: Hepatitis B e antigen.

mechanism. In addition, there are other factors, PPARa, FXRa, and PGC involved in regulation of HBV RNA transcription[63,64]. They also bind to HBV core promoter, thereby increasing the transcription of HBV pgRNA[65-67]. The above-mentioned mechanisms are attributed to ethanol-induced activation of HBV transcription[62]. Recently, Lin *et al*[68] showed that alcoholic HBV patients have higher hepatitis B viral load. In addition, acetaldehyde affects the lipid composition of cellular membranes in lipid rafts, thereby influencing HBV infectivity[30,69]. Thus, the increased HBV replication plays a role in establishment of chronic hepatitis and/or liver end-stage disease in alcohol abusing HBV patients.

HBV PATHOGENESIS/IMMUNOPATHOGENESIS AND ALCOHOL

The natural history of HBV has been subdivided into two types of infection. In adults, 90%-95% of HBV infections is acute where immune-competent people clear the viral infection effectively[70,71]. Acute infection is characterized by inflammation and necrosis of hepatocytes and has low mortality rate (0.5%-1%)[71]. The persistence of HBsAg in blood for longer than 6 months after the initial infection is a sign of chronic hepatitis B[70]. This infection is mainly asymptomatic without any intense liver damage, but in some cases, it leads to chronic hepatitis, followed by fibrosis, cirrhosis development, and HCC. Majority of infected children aged 1-5 years, are not able to clear HBV and represent the source of chronic patients[71,72], whereas 5%–10% of HBV-infected adults are prone to develop chronic HBV infection with the mortality rate of 15%-25% from cirrhosis and HCC[71,73].

Based on the virus-host interactions, the natural course of chronic HBV infection is sub-divided into 4 stages[3,74]: (1) Immune-tolerant phase is characterized by HBeAg positivity, and high levels of serum HBV DNA due to active HBV replication[75,76]. Mostly, children and young adults who are HBsAg positive for 10-30 years from the initial infection are in this phase[71]; (2) Immune clearance phase accompanied by elevated serum ALT levels and decreased HBV DNA load; and (3) Immune-control phase is characterized by low-replication, patients lose HBeAg with seroconversion to anti-HBeAg, accompanied by liver disease remission; this is typical for the inactive carrier state. However, about 20%–30% of these patients may have a viral relapse followed by reactivation phase during follow-up period[75,76].

There are very limited reports available to support the role of alcohol in HBV pathogenesis in relation to HBV markers. For example, it has been reported that alcohol abused cirrhotic patients with higher levels of serum HBV DNA are more

prone to liver cancer than those with low serum HBV DNA. An increasing HBV DNA levels precipitate the progression of liver cirrhosis to HCC[77]. In another study, the synergism between HBsAg positivity and drinking were reported, suggesting a stronger influence of viral infections and alcohol drinking on the risk of liver cancer[78]. In contrast, as reported by an older study, increased alcohol consumption is related to higher prevalence of HBeAg seroconversion to anti-HBe, increased prevalence of ALD and lower prevalence of chronic hepatitis[79]. Furthermore, some early studies demonstrated more frequent presence of anti-HBs and anti-HBc antibodies in blood of alcoholics than in the non-alcoholics[80-82]. In addition, it has been shown that alcohol consumption increased liver necro-inflammatory changes in HBsAg positive patients[48] and elevated liver tests[49].

ROLE OF ALCOHOL IN HBV INNATE IMMUNITY

Host cells activate innate immune response when they contact pathogen to prevent the spread of infection and to stimulate efficient adaptive immune response[71,83]. Pattern-recognition receptors, through identifying the specific pathogen determinants activate innate immunity to protect against pathogens. Viral sensing, induction of type I IFNs and production of different cytokines are performed *via* toll-like receptors (TLRs), RNA helicases, RIG-I-like receptors, NOD-like receptors, melanoma differentiation-associated protein 5 and protein kinase R. Namely, TLR5, and TLR9 are receptors for viral DNA, TLR7 and TLR8 for single-stranded RNA, while TLR3 can bind double-stranded RNA[71,83-89].

Production of IFN type 1 -α/β and activation of natural killers (NK) cells are induced at the initial phase of viral infections. Infected plasmacytoid dendritic cells (pDC) are the main producers of IFN-α/β, while NK and natural killer T (NKT) cells produce IFN-γ. In addition to IFN-α/β, other cytokines, like IL-12 and IL-18, control viral replication[54,90-93].

HBV is relatively inefficient at inducing the anti-viral cytokines, including IFN-α/β. This appears to be due to limited sensing of HBV stealth virus combined with active suppression of innate immunity[94,95]. IFN-α/β induced interferon inducible genes (ISGs) are responsible for antiviral effects that minimize pathogenetic processes by limiting the viral production and spread[96,97]. Studies conducted on acutely infected chimpanzees as well as in humans showed decreased production of type-1 interferons and ISGs[94,97-100]. Interestingly, McClary *et al*[101] using transgenic mouse model or hepatoma cell lines have shown that HBV replicates in IFN-γ knockouts and IFN-α/β receptor knockouts mice at levels higher than those observed in wild type mice, implying that baseline levels of these cytokines control HBV replication in the absence of inflammation. In support to the above study, Lucifora *et al*[102] demonstrated that HBV elicits a strong and specific innate antiviral response (production of IFN-β and activation of ISGs) that results in a non-cytopathic clearance of HBV DNA in HepaRG cells. In contrast, in a chimeric mouse model, HBV inhibited the nuclear translocation of STAT1 in response to IFNα, thereby preventing ISG transcription in human hepatocytes[103]. The effect of ethanol on IFN-α/β innate responses and ISGs activation in HBV infection pathogenesis has not been investigated, but there are several studies which suggests that alcohol impairs IFN-α/β innate responses and anti-viral gene expressions in HCV pathogenesis[24,104-106]. Future studies should focus on understanding the effect of alcohol metabolism on IFN-α/β innate responses and ISGs activation during HBV infection pathogenesis as well as examine whether IFN-α/β therapy could be a useful strategy for HBV alcoholics.

HBV infection may elicit differential cytokine responses among various liver cell types different from hepatocytes, depending on the stage or route of infection. Guidotti *et al*[107] elegantly demonstrated that HBV can be controlled by immune cells in a non-cytolytic manner through the release of cytokines and other immune mediators. Both *in vitro* and *in vivo* studies showed that TNF-α, IL-12, and IL-18 are involved in controlling HBV replication in addition to IFN-γ and IFN-α/β induction[108-110]. Several cytokines control HBV transcription through liver-enriched transcription factors[111]. It has been demonstrated that IL-4, IL-6, IL-1β, and transforming growth factor-β (TGF-β) were effective in diminishing HBV replication markers[112-116] *via* regulating HBV transcriptional activity. However, while all these cytokines are protective during acute HBV infection, their persistence in chronic infection may cause liver inflammation.

While the effect of alcohol in modulating these cytokines in HBV infection has not been investigated, but it has been well documented that pro-inflammatory cytokines levels were increased and anti-inflammatory cytokines were decreased in ALD patients[117,118]. Taken together, it is reasonable to expect that alcohol could affect the

anti-viral activity of these cytokines during acute infection and potentiate persistent liver inflammation in chronic HBV infection, thereby promoting progressive end-stage liver diseases. The excessive or persistent presence of immune mediators in tissues have been recognized to play important roles in the pathogenesis of human diseases[117,118]. It is very important to conduct future studies to understand and fill the gaps in our understanding of the role of alcohol in both acute and chronic HBV infection induced cytokine responses.

Being important innate immunity component, NK cells control viruses *via* direct or indirect cytolytic effects, namely, through the release of cytokines, IFN-γ, TNF-α, TGF-β and IL-10[83,119]. In this regard, NK cell can directly lyse infected hepatocytes through granzyme/perforin or death receptor pathways causing the death of infected hepatocytes[119,120]. Non-cytolytic mechanisms of HBV clearance through cytokines like IFN-γ[121] also control virus in the infected liver without affecting cell integrity[119].

The antiviral capacity of NK cells in HBV-infection has been extensively reviewed by two different groups[119,120]. In this regard, NK cells efficiently inhibited HBV replication in a transgenic mice mouse model of HBV infection[122] and contributed to HBV clearance using acute HBV mouse model[123]. In chimpanzees, NK cells participated early in non-cytolytic clearance of HBV-infected hepatocytes accompanied by increase in intrahepatic content of IFN-gamma and TNF-α[107]. However, subsequent experiments revealed a critical role for T cells rather than NK cells in HBV control in this model[124]. In the pre-clinical ramp-up phase of acute hepatitis B patients, it was observed an increase in the number of circulating NK cells[125,126], while activation and effector function was suppressed; this led to viral load increase[98]. There was inversive correlation between low NK cell activation and induction of the immunosuppressive cytokine IL-10, raising the possibility that HBV can actively evade immune responses[98].

NK cells display varying changes in proportion, phenotype and/or function in different studies of chronic HBV infection. The defects in NK cells are reflected in many aspects: In chronic HBV patients: (1) The proportions of hepatic and peripheral NK cells are reduced with or without changes in their subsets[127-129]; (2) There are changes in expression of activating or inhibitory receptors on NK cells[130,131]; (3) There is an increase of some molecules with negative effects, such as T cell immunoglobulin and mucin domain containing molecule-3[132]; (4) The cytolytic activity is maintained or even enhanced, which correlates with the severity of liver injury[128,129,131]; and (5) There is defect in the production of cytokines, like IFN-γ and TNF-α, making them inefficient in promotion of direct non-cytolytic antiviral roles as well as in T-cell responses[128,130-132].

Activated NK cells play a role in early HBV-infected hepatocyte clearance. However, with the progression of chronic infection, both NK and T cells can be suppressed by tolerogenic effects of hepatic ligands and cytokines which limit their antiviral efficacy[119,133]. Further studies are needed for better understanding of the factors triggering and mediating the opposing roles of NK cells in chronic HBV infection which could allow these cells to be successfully exploited as therapeutic targets[119]. Importantly, the role of alcohol on NK cell responsiveness in the HBV-infected liver has not been addressed. As reported, NK cells are impaired by alcohol[134], which ultimately affects antiviral activity of NK cells during acute HBV infection. Another possible mechanism is the alcohol-induced impairment of IFN-γ signaling which would decrease the protective ISGs gene expression. We recently reported that ethanol metabolite, acetaldehyde impaired IFN-γ signaling *via* the JAK-STAT1 pathway in HBV transfected cells[60]. Future studies in this topical area will improve our understanding of NK cell immunity in HBV-infected alcoholic patients.

Dendritic cells (DCs), (both conventional/myeloid DCs, mDCs and plasmacytoid DCs, pDCs) effectively connect the adaptive and innate immune responses[135]. Subpopulations of DCs can be distinguished from other immune cells by specific surface markers[136,137]. pDCs play a crucial role against viral infection by producing vast amounts of type I interferon due to up-regulated TLR7 and TLR9 expression[138-140]. It has also been reported that pDCs increase the co-stimulatory and major histocompatibility complex (MHC) molecules expression on target cells enabling them to present antigen to T cells[141].

Cui *et al*[142] elucidated three main ways of recognition of HBV antigens by DCs. First is that HBV DNA can be recognized by DCs through TLR9, second DCs internalize HBV DNA and third, HBsAg can be internalized by DCs through the mannose receptor. DCs phagocytize HBV, process viral antigens to antigenic peptides and present them to CD4+ and CD8+ T cells[143]. DCs activate antibody-dependent cytotoxicity cells and NK cells, which stimulate these cells to secrete immunosuppressive cytokines, IL-10 and TGF-β, assisting in the induction of regulatory T cells (Tregs) with the participation of mDC to destroy HBV-infected hepatocytes[144]. To date, there have been no studies which investigated the effect of

alcohol on DCs function in pathogenesis of HBV infection. There are several reports support that alcohol consumption decrease the DCs functional ability which leads to impaired adaptive immunity and gives more chances to detrimental events upon pathogens exposure[145-148]. It is possible that ethanol-induced dysfunction of DCs leads to reduction in their HBV antigen presentation property, thereby causing prolonged persistence of virus and progression to end-stage liver disease.

EFFECT OF ALCOHOL ON ADAPTIVE IMMUNITY IN HBV INFECTION

The adaptive immune response is responsible for viral clearance and disease pathogenesis during HBV infection[54,149]. Cell-to-cell interactions may play either protective or pathogenic roles, and are important for anti-viral adaptive immune response in HBV infection[150]. These immune cells are: (1) CD4+ T cells, the helper T cells, robust producers of cytokines required for the efficient development of effector cytotoxic CD8+ T cells and B cell antibody production; (2) CD8+ T cells directly recognizing virus-infected cells and responsible for HBV-infected hepatocytes clearance *via* cytolytic and non-cytolytic mechanisms[151,152]; and (3) B cells neutralizing free viral particles by antibodies to prevent (re) infection[153,154] and affect participation of helper T cell in HBV antigen presentation[150]. The development of antiviral immune response is typical for acute HBV infection, while chronic HBV patients do not generate efficient antiviral response[149].

ROLE OF ALCOHOL ON B CELL RESPONSES IN HBV INFECTION

Minimal information is available regarding the specificity of B cell responses to HBV, although different antibodies are routinely used to distinguish between clinical phases of infection[155]. Recently, two different groups, extensively reviewed the role of B cell responses in acute and chronic HBV infection[155,156]. It has been reported that in chronic HBV patients, B cells are capable of producing polyclonal antibodies, which targeted a range of HBV antigens, including HBcAg, HbeAg, and the large, medium and small forms of HBsAg[157]. Antibodies against HBV surface antigen and HBV core antigen are produced in acute HBV infection with different kinetics. Anti-HBs is considered as a marker of disease resolution whereas anti-HBc is marker of active or past infection[158]. Some studies showed that anti-HBc response has also been associated with acute liver damage[159,160]. Antibodies targeting HBsAg and HBeAg (anti-HBs and anti-HBe) appear later in acute infection and are associated with favorable outcomes of infection[161]. The well-identified antiviral effector function of B cells is related to their differentiation into plasma cells, which produce neutralizing antibodies, preventing entry of the virus into target cells either through steric obstruction or through direct binding to the receptor-binding site on virions[162,163]. During HBV infection, only antibodies directed against the envelope protein (anti-HBs) have neutralizing activity, underscored by their ability to recognize and bind to key viral epitopes required for infectivity[164,165]. The function of B cells is not only in production of neutralizing antibodies, but they also act as potent antigen presenting cells (APCs), specifically for helper T cells[166]. During the flares of chronic hepatitis B, there is an enrichment of IL-10 producing B cells which modulate inflammatory events as well as HBV-specific T cell responses[167]. Again, there is a huge gap on the role of alcohol in terms of the regulation of B cells function and its input in HBV pathogenesis. It has been previously reported that alcohol decreased the B cell numbers and especially lowered the circulating B cell levels[168-170]. Alcohol-induced loss of peripheral B cells primarily affects certain subpopulations of cells, which develop into long-lived memory B cells critical in protection from the infection with same pathogen[171]. It is possible that alcohol may weaken the B cell immune responses by decreasing the level of B cells leading to reduction in antibodies against HBV antigens, thereby causing chronic HBV. Geissler *et al*[172] demonstrated that in female mice fed ethanol diet and immunized by DNA-based construct containing the pre-S2/S gene, the levels of anti-HBs were marginally reduced compared with those in control mice.

ROLE OF ALCOHOL ON CYTOTOXIC T-LYMPOCYTE RESPONSES IN HBV INFECTION

Regarding acute HBV-infection, there is less information available on B-cell response but HBV-specific CD4+ and CD8+ mediated responses become normally measurable during the period of exponential rise in HBV replication[125,126]. Capsid protein epitopes were specifically recognized by CD4+ T helper cells, whereas CD8+ T cells naturally recognize epitopes positioned within diverse HBV proteins. HBV-specific T cells are Th1 focused and vigorous in self-limiting acute infection compared to chronic infection[97,173-175]. CD4+ T cell response to HBV is vigorous, and multi-specific in patients with acute hepatitis who ultimately clear the virus, but it is comparatively weak in persistently infected patients with chronic hepatitis[176]. Many studies provided evidence for a strong relationship and association between CD4+ T cell response, acute hepatitis, and viral clearance[177-179]. As also reported, there is no effect on viral clearance and liver disease when CD4+ T cells are depleted at the peak of HBV infection in chimpanzees[124], suggesting that CD4+ T cells do not directly participate in viral clearance and tissue damage. It is possible that CD4+ T cells indirectly control HBV infection by facilitating the induction and maintenance of the virus-specific B cell and CD8+ T cell response[54].

HBV-specific CD8+ T cell response acts as the principal effector mechanism of viral clearance and liver inflammation[156]. HBV-specific CD8+ T cells are enriched within the infected liver, lyse HBV infected hepatocytes[124,180] and secrete cytokines (mainly IFN-γ) that trigger a process of non-cytolytic HBV clearance[121] and recruitment of inflammatory immune cells[122,181]. As mentioned earlier, like CD4+ T cells, CD8+ T cell response is detectable in acute HBV. But in chronically infected patients, the peripheral blood T cell response is weak and narrowly focused[182-184]. Maini *et al*[185] examined a relationship between the number of intrahepatic HBV specific CD8+ T cells, extent of liver disease, and levels of HBV replication in chronically infected patients, demonstrating that inhibition of virus replication could be independent of liver damage and that the functionality of HBV-specific CD8+ T cells was more important than total number of T cells to control HBV replication. Experiments in chimpanzees have shown that the viral clearance and the onset of liver disease coincide with the accumulation of virus-specific CD8+ T cells and the induction of IFN-γ, as well as ISGs in the liver[107,124].

In 2010, Chisari *et al*[54] clearly outlined the role of cytotoxic T lymphocyte (CTL) response in viral clearance by killing infected cells. Although CTL killing is an inefficient process, in order to kill the infected cells, a direct contact between CTLs and infected cells is required. Hence, it is not possible to kill all infected cells by CTLs because unlike HCV infection, HBV can infect as many as up to 10^{11} hepatocytes[107,186]. Therefore, although hepatitis in HBV infection is due to the cytopathic activity of the CTLs, viral clearance may require more efficient CTL functions than just killing. There are few studies which investigated the pathogenetic and non-cytopathic antiviral functions of the CTL response in HBV transgenic mice that develop an acute necroinflammatory liver disease after adoptive transfer of HBsAg specific CTL clones[121,180,181]. They found that CTLs rapidly enter the liver and recognize viral antigen which triggers two events: (1) Apoptosis of the hepatocytes that are physically engaged with CTLs; and (2) Secretion of IFN-γ which non-cytopathically inhibits HBV gene expression and replication in the rest of the hepatocytes[121,187]. It has also been reported that the cytopathic and antiviral functions of CTLs are completely independent from each other[121]. All these results suggest that CD8+-dependent cytopathic and non-cytopathic clearance of HBV are effective in the limitation of HBV viral infection[100,107,121,124]. Studies conducted in both animals and humans clearly showed that alcohol reduces the number of T- cells, changes the ratio of T- cell types, decrease the T- cells activation and function and finally, promote the T- cell apoptosis[171]. Geissler *et al*[172] showed in a transgenic mouse model that ethanol-induced effects on CTL activity against the middle envelope protein (MHBs) as well as on T-cell proliferation and cytokine release may partially contribute to a higher incidence of persistent HBV infection in alcoholics. Again, there are no studies directly investigating the role of alcohol in the context of CTL responses in HBV infection. It is very important to study the association between alcohol and HBV adaptive immune response for understanding of the exact mechanisms of alcohol-induced impairment of various arms of the adaptive immunity. The clarity in this matter will be useful for the development of treatment strategy for the end stage liver diseases in alcoholic HBV patients.

ROLE OF ALCOHOL IN HBV MHC CLASS I AND II ANTIGEN PRESENTATION

MHC class I antigen presentation pathway plays important role in the detection of virally infected cells by CTLs. MHC class I molecules are expressed on the cell surface of all nucleated cells and present peptide fragments derived from intracellular proteins[188]. As mentioned above, in HBV infection, CTLs expressing specific T- cell receptors are responsible for elimination of HBV-presenting hepatocytes. When the display of viral peptide/MHC class I complex on HBV-infected hepatocytes is altered, it may reduce CTL activation and thereby, suppress HBV-infected hepatocyte clearance[60]. Hence, the presentation of HBV-viral peptide-MHC class I complex on hepatocytes surface is necessary for the effective elimination of HBV infected cells. Sastry *et al*[189] and Khakpoor *et al*[190] reported that the recognition of different HBV viral peptides-MHC class I complex (HBV epitopes) are important for efficient immune therapeutic control of chronic HBV infection and that determination of these epitopes will be useful in delivering antiviral drugs or cytokines directly to virus-infected cells. As we mentioned earlier, MHC class I pathway is usually fueled by endogenous antigens whereas main source of Ag entering the MHC class II pathway is exogenous protein, which is endocytosed/phagocytosed by professional APCs[191]. CD4+ T cell activation is triggered when the specific antigenic peptide is presented on MHC class II molecules. Exogenous antigens may also enter MHC class I pathway, which is called cross-presentation by DCs and macrophages. Furthermore, antigens expressed in the context of HBsAg virus-like particles can access MHC class I and class II pathways of primary DCs to elicit adaptive immune responses. In addition, Murata *et al*[192] reported that intrahepatic cross-presentation by DCs in the liver augments HBV-specific CD8+ T cell expansion, while concomitant or subsequent hepatocellular presentation of endogenously synthesized antigen is essential for expansion and cytolytic differentiation of HBV-specific CD8+ T cells induced by DC activation. There are two old studies which reported that strong MHC class II-restricted CD4+ T cell response to HBV core is associated with viral clearance in acute HBV infection[177,193]. There are limited number of studies investigating the role of alcohol on MHC class I and II presentation in HBV- infected cells. Pasala *et al*[171] reported that immune response to the HBV vaccination yielded a smaller immune response in patients who abuse alcohol compared with healthy patients. We have recently reported that in hepatocytes, the combination of HBV and ethanol metabolites impairs proteasome function as well as IFN-γ-signaling through the Jak-STAT1 pathway and suppresses HBV peptide cleavage by immunoproteasome. It also disactivates protein loading complex components, TAP and tapasin, which are required for HBV peptide-MHC class I trafficking to the membrane, finally, affecting the expression of HBV core peptide 18-27- MHC class I complex on cell surface[60]. All these events may prevent CTLs activation to limit their ability to identify/clear HBV-infected hepatocytes resulting in liver inflammation and its progression to fibrosis and HCC. Importantly, future studies should be focused on the effects of ethanol on MHC-class II presentation, which is mainly catalyzed by effector cells, such as APCs. Overall, the combination of a weakened innate and adaptive immune response due to ethanol consumption could decrease the ability to clear HBV from the body, allowing the virus to persist chronically, followed by development of end - liver diseases, such as cirrhosis and HCC.

ALCOHOL INDUCED IMPAIRMENT OF GUT-MICROBIOME AND HBV PATHOGENESIS

The unique intestinal blood supply containing microbe-derived products and metabolites affect the composition of hepatic immune cells, immune microenvironment and the regulation of antiviral immune responses. The immune response in the liver is closely controlled by the intestinal commensal microbiota signals. The host's ability to clear HBV is correlated with the establishment of commensal microbiota. Wu *et al*[194] using HBV- transfected mice, demonstrated the critical role of CD4+ T cells in HBV clearance mediated by commensal microbiota. Both human and animal studies have shown that the intestinal barrier of the gastrointestinal tract has exceptionally high permeability as a result of alcohol abuse. The tight junctions between epithelial cells in the gastrointestinal tract are also disturbed as a result of alcohol abuse, allowing bacterial substances to leak into the bloodstream[195-197]. It is possible that alcohol influenced bacterial composition due to depletion of beneficial commensal bacteria and high pathogenic bacteria colonization[198]. All these changes could contribute to impairment in the HBV

clearance dependent on the establishment of commensal microbiota.

ROLE OF ETHANOL AND HBV- INDUCED OXIDATIVE STRESS IN LIVER INJURY

As mentioned earlier, ethanol metabolism in the liver can lead to an increase in the production of ROS, mainly hydrogen peroxide and superoxide anion[27]. Moderate drinking (< 50 g/d) has been shown to increase the probabilities of developing oxidative stress three-fold, while heavy drinking (> 50 g/d) has been shown to increase these odds by 13 to 24 times[199]. Few studies have investigated the role of alcohol-induced oxidative stress in HBV infection pathogenesis and associated liver injury. In addition, oxidative stress may play a key role in the progression of liver disease where alcohol consumption is associated with chronic hepatitis B[27]. Ha *et al*[200] reported that even moderate ethanol consumption promotes oxidative stress and liver injury in HBx transgenic mice, implying that compromised antioxidant defense increases alcohol-associated liver injury. In addition, Min *et al*[62] found that CYP2E1-induced oxidative stress potentiates the ethanol-related transactivation of HBV. Recently, we reported the ethanol metabolite, acetaldehyde induces lipid peroxidation, and adduction of proteins with 4-hydroxynonenal and malonaldehydes (oxidative stress markers) suppress the proteasome activity, necessary for generation of antigenic peptides for MHC class I -restricted antigen presentation. This results in decreased presentation of HBV peptide-MHC class I complex for the recognition by CTLs and limits elimination of infected cells[60] leading to persistence of HBV and subsequent end-stage liver diseases.

However, it is very difficult to dissect the role of alcohol- induced oxidative stress in HBV infection and associated liver injury since HBV has also been shown to cause oxidative stress[201-203]. In a study on 158 HBV patients and 42 healthy individuals, total oxidative stress levels were significantly higher for the patients infected with chronic HBV compared to the other groups[204]. Findings from a recent study consist of 296 chronic HBV patients suggesting that oxidative stress might be a useful indicator of the progression of HBV-induced liver disease in patients[202]. HBV has also been shown to induce oxidative stress in transgenic mice and human primary hepatocytes[205,206]. Also, HBx protein-induced ROS plays an important role in autophagosome formation and the ensuing viral replication[207]. In addition, the development of HCC in HBx transgenic mice is preceded by oxidative stress[208]. Overall, both alcohol and HBV proteins induced ROS activated pathways (such as the mitogen-activated protein kinase pathway) that aid in the formation of chronic liver disease[200]. Since, alcohol and HBV act as an individual factor in causing oxidative stress, there are no studies which investigated the combined effect alcohol- and HBV-induced oxidative stress in the pathogenesis of liver injury. Hence, it is very important to conduct more studies to find out the synergistic effect of alcohol- and HBV-induced oxidative stress in the progression of end stage liver disease.

ETHANOL AND HBV INDEPENDENTLY INDUCE ER STRESS

When the protein load exceeds the protein-folding capacity of the ER, the unfolded protein response (UPR) is induced as an attempt to decrease the load. A strong, prolonged UPR leads to ER stress. Both ethanol and HBV have been shown to induce the UPR and ER stress[209-212].

It is known that ALD leads to an impaired ability of the liver to secrete serum proteins, such as serum albumin and clotting factor proteins. There is evidence to support that this impairment is caused by a malfunctioning ER, which makes sense because the ER is involved in folding and modification of proteins that will eventually be secreted. Howarth *et al*[213] reported that the exposure to ethanol metabolites caused ER fragmentation and increased expression of UPR genes in hepatocytes. The same group found that ethanol exposure caused ER morphological abnormalities, defects in hepatocyte secretion, and a strong UPR in zebrafish[213]. Several investigators reported that acetaldehyde and its adducts cause ER stress[214-218].

HBV infection has also been shown to cause ER stress. Li *et al*[219], found that the UPR was induced in HBV-infected hepatocytes. However, only specific branches of the UPR were induced, while the branch leading to apoptosis was not affected. This allowed UPR and ER stress to persist while preventing apoptosis[219]. Kim *et al*[220] reported that chronic HBV infection results in chronic ER stress. This chronic ER stress plays a major role in the pathogenesis of liver diseases, including viral hepatitis and liver cancer.

Since both HBV and ethanol abuse cause ER stress, these stress responses may be additive or even synergistic. It has been reported that ER stress is synergistically induced by alcohol in the presence of environmental factors, drugs, or viral infection[221]. The possible mechanism behind the alcohol- induced ER stress in HBV infection may be due to the alcohol-triggered viral replication (as we mentioned in the earlier section) by increasing HBV DNA, HbsAg, and HBx protein. These viral components have been involved in the UPR activation and ER stress, playing a role in HBV pathogenesis[212,220,222,223]. It has been reported that alcohol and anti-HIV drugs induced the ER stress and liver injury[224]. Importantly, for the effective elimination of HBV- infected cells by CTLs, the proteasome generated antigenic peptides should be loaded into MHC class I molecules and form peptide loading complex in the ER for the HBV peptide-MHC class I complex presentation on hepatocytes surface. We have recently reported that acetaldehyde suppressed the presentation of HBV peptide-MHC class I in HBV transfected cell, in part, due to the acetaldehyde-induced ER stress which leads to the impaired trafficking of this peptide complex in ER to Golgi then to the cell surface[60].

ETHANOL INDUCES GOLGI FRAGMENTATION

A stressed ER often corresponds with a stressed Golgi apparatus since proteins from the ER are trafficked to the Golgi before they are secreted from the cell. There is no well-characterized system of Golgi stress markers as exists for the UPR proteins in ER, so the best way to determine the presence of Golgi stress is to view Golgi fragmentation morphologically. Siddhanta *et al*[225] demonstrated that ethanol exposure leads to Golgi fragmentation and fragmented Golgi cannot function properly. A malfunctioning of Golgi along with a malfunctioning ER impairs the ability of hepatocytes to secrete serum and membrane proteins[225]. Recently Petrosyan *et al*[226-228] revealed that abnormalities in the Golgi apparatus function is crucial for the development of alcoholic liver injury. They reported that ethanol-induced Golgi fragmentation and disorganization of Golgi matrix proteins is one of the main contributors of Golgi scattering. They also found that alcohol-induced Golgi fragmentation alters the Golgi-to-plasma membrane trafficking. Interestingly, it has been reported that under viral infection, Golgi is partially fragmented[229] and that HCV also caused Golgi fragmentation[230]. There are no studies conducted on the role of alcohol and HBV-induced Golgi fragmentation in HBV infection pathogenesis and subsequent progression of liver injury.

CONCLUSION

The combination of HBV infection and alcohol abuse can provide detrimental consequences. To gain better understanding of the mechanisms behind this dangerous combination could save millions of lives. Many possible mechanisms explain the synergistic progression of end-stage liver disease and the development of chronic hepatitis B infection in alcohol-abused patients (Figure 2). These factors include alcohol-induced increase in HBV replication, oxidative stress and suppressed immune response, which finally leads to fibrosis and HCC development. Other potential contributors to this rapid disease progression are ER and Golgi stress, which are induced by each alcohol and HBV, but effects are synergized by the combination of both insults. While many potential mechanisms for the synergistic effects of HBV and alcohol abuse exist, most of them have not been explicitly studied and characterized. More research is required to understand the complex interactions between alcohol consumption and HBV infection. Once elucidated, these mechanisms could aid in the development of new treatments to prevent the progression of end-stage liver disease in alcohol abusing HBV patients.

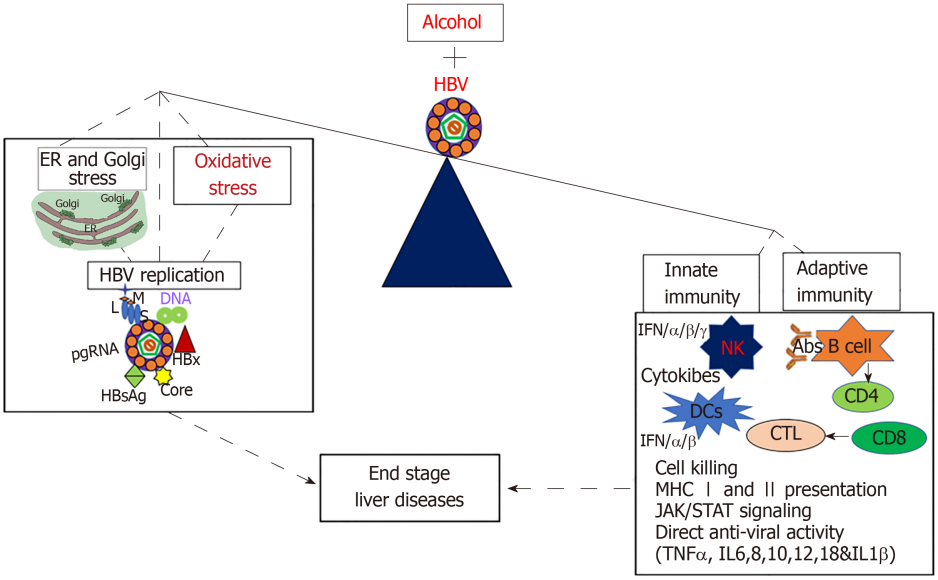

Figure 2 Mechanisms of alcohol and hepatitis B virus-infection induced liver injury. Alcohol and hepatitis B virus together increase hepatitis B virus replication, oxidative stress, and cell organelle stress (endoplasmic reticulum and Golgi stress) which ultimately suppresses both adaptive and innate immune response, thereby leading to end- stage liver diseases. HBV: Hepatitis B virus; ER: Endoplasmic reticulum; IFN: Interferon; IL: Interleukin; MHC: Major histocompatibility complex; NK: Natural killers.

REFERENCES

1 **Westin J**, Aleman S, Castedal M, Duberg AS, Eilard A, Fischler B, Kampmann C, Lindahl K, Lindh M, Norkrans G, Stenmark S, Weiland O, Wejstål R. Management of hepatitis B virus infection, updated Swedish guidelines. *Infect Dis (Lond)* 2020; **52**: 1-22 [PMID: 31613181 DOI: 10.1080/23744235.2019.1675903]

2 **Kowdley KV**, Wang CC, Welch S, Roberts H, Brosgart CL. Prevalence of chronic hepatitis B among foreign-born persons living in the United States by country of origin. *Hepatology* 2012; **56**: 422-433 [PMID: 22105832 DOI: 10.1002/hep.24804]

3 **Terrault NA**, Bzowej NH, Chang KM, Hwang JP, Jonas MM, Murad MH; American Association for the Study of Liver Diseases. AASLD guidelines for treatment of chronic hepatitis B. *Hepatology* 2016; **63**: 261-283 [PMID: 26566064 DOI: 10.1002/hep.28156]

4 **Suliman I**, Abdelgelil N, Kassamali F, Hassanein TI. The Effects of Hepatic Steatosis on the Natural History of HBV Infection. *Clin Liver Dis* 2019; **23**: 433-450 [PMID: 31266618 DOI: 10.1016/j.cld.2019.05.001]

5 **Li TY**, Yang Y, Zhou G, Tu ZK. Immune suppression in chronic hepatitis B infection associated liver disease: A review. *World J Gastroenterol* 2019; **25**: 3527-3537 [PMID: 31367154 DOI: 10.3748/wjg.v25.i27.3527]

6 **El-Serag HB**. Hepatocellular carcinoma. *N Engl J Med* 2011; **365**: 1118-1127 [PMID: 21992124 DOI: 10.1056/NEJMra1001683]

7 **Sayiner M**, Golabi P, Younossi ZM. Disease Burden of Hepatocellular Carcinoma: A Global Perspective. *Dig Dis Sci* 2019; **64**: 910-917 [PMID: 30835028 DOI: 10.1007/s10620-019-05537-2]

8 **El-Serag HB**, Rudolph KL. Hepatocellular carcinoma: epidemiology and molecular carcinogenesis. *Gastroenterology* 2007; **132**: 2557-2576 [PMID: 17570226 DOI: 10.1053/j.gastro.2007.04.061]

9 **MacLachlan JH**, Cowie BC. Hepatitis B virus epidemiology. *Cold Spring Harb Perspect Med* 2015; **5**: a021410 [PMID: 25934461 DOI: 10.1101/cshperspect.a021410]

10 **Kim KH**, Shin HJ, Kim K, Choi HM, Rhee SH, Moon HB, Kim HH, Yang US, Yu DY, Cheong J. Hepatitis B virus X protein induces hepatic steatosis via transcriptional activation of SREBP1 and PPARgamma. *Gastroenterology* 2007; **132**: 1955-1967 [PMID: 17484888 DOI: 10.1053/j.gastro.2007.03.039]

11 **Wu YL**, Peng XE, Zhu YB, Yan XL, Chen WN, Lin X. Hepatitis B Virus X Protein Induces Hepatic Steatosis by Enhancing the Expression of Liver Fatty Acid Binding Protein. *J Virol* 2016; **90**: 1729-1740 [PMID: 26637457 DOI: 10.1128/JVI.02604-15]

12 **McMahon BJ**. The natural history of chronic hepatitis B virus infection. *Hepatology* 2009; **49**: S45-S55 [PMID: 19399792 DOI: 10.1002/hep.22898]

13 **Guo GH**, Tan DM, Zhu PA, Liu F. Hepatitis B virus X protein promotes proliferation and upregulates TGF-beta1 and CTGF in human hepatic stellate cell line, LX-2. *Hepatobiliary Pancreat Dis Int* 2009; **8**: 59-64 [PMID: 19208517]

14 **Parikh P**, Ryan JD, Tsochatzis EA. Fibrosis assessment in patients with chronic hepatitis B virus (HBV) infection. *Ann Transl Med* 2017; **5**: 40 [PMID: 28251119 DOI: 10.21037/atm.2017.01.28]

15 **Wu JF**, Song SH, Lee CS, Chen HL, Ni YH, Hsu HY, Wu TC, Chang MH. Clinical Predictors of Liver Fibrosis in Patients With Chronic Hepatitis B Virus Infection From Children to Adults. *J Infect Dis* 2018; **217**: 1408-1416 [PMID: 29390144 DOI: 10.1093/infdis/jiy048]

16 **Guan R**, Lui HF. Treatment of hepatitis B in decompensated liver cirrhosis. *Int J Hepatol* 2011; **2011**: 918017 [PMID: 21994876 DOI: 10.4061/2011/918017]

17 **Liaw YF**, Tai DI, Chu CM, Chen TJ. The development of cirrhosis in patients with chronic type B

hepatitis: a prospective study. *Hepatology* 1988; **8**: 493-496 [PMID: 3371868 DOI: 10.1002/hep.1840080310]
18 **Sumi H**, Yokosuka O, Seki N, Arai M, Imazeki F, Kurihara T, Kanda T, Fukai K, Kato M, Saisho H. Influence of hepatitis B virus genotypes on the progression of chronic type B liver disease. *Hepatology* 2003; **37**: 19-26 [PMID: 12500184 DOI: 10.1053/jhep.2003.50036]
19 **Kanda T**, Goto T, Hirotsu Y, Moriyama M, Omata M. Molecular Mechanisms Driving Progression of Liver Cirrhosis towards Hepatocellular Carcinoma in Chronic Hepatitis B and C Infections: A Review. *Int J Mol Sci* 2019; **20** [PMID: 30889843 DOI: 10.3390/ijms20061358]
20 **Höner Zu Siederdissen C**, Cornberg M. Management of HBV and HBV/HDV-Associated Liver Cirrhosis. *Visc Med* 2016; **32**: 86-94 [PMID: 27413725 DOI: 10.1159/000445518]
21 **Riccardo Nevola LR**, Giordano M, Marrone A, Adinolfi LE. Mechanisms and clinical behavior of hepatocellular carcinoma in HBV and HCV infection and alcoholic and non-alcoholic fatty liver disease. *Hepatoma Research* 2018; **4**: 55 [DOI: 10.20517/2394-5079.2018.38]
22 **Sacks JJ**, Gonzales KR, Bouchery EE, Tomedi LE, Brewer RD. 2010 National and State Costs of Excessive Alcohol Consumption. *Am J Prev Med* 2015; **49**: e73-e79 [PMID: 26477807 DOI: 10.1016/j.amepre.2015.05.031]
23 **Riva A**, Chokshi S. Immune checkpoint receptors: homeostatic regulators of immunity. *Hepatol Int* 2018; **12**: 223-236 [PMID: 29740793 DOI: 10.1007/s12072-018-9867-9]
24 **Ganesan M**, Zhang J, Bronich T, Poluektova LI, Donohue TM, Tuma DJ, Kharbanda KK, Osna NA. Acetaldehyde accelerates HCV-induced impairment of innate immunity by suppressing methylation reactions in liver cells. *Am J Physiol Gastrointest Liver Physiol* 2015; **309**: G566-G577 [PMID: 26251470 DOI: 10.1152/ajpgi.00183.2015]
25 **Peana AT**, Sánchez-Catalán MJ, Hipólito L, Rosas M, Porru S, Bennardini F, Romualdi P, Caputi FF, Candeletti S, Polache A, Granero L, Acquas E. Mystic Acetaldehyde: The Never-Ending Story on Alcoholism. *Front Behav Neurosci* 2017; **11**: 81 [PMID: 28553209 DOI: 10.3389/fnbeh.2017.00081]
26 **Testino G**, Leone S, Borro P. Alcohol and hepatocellular carcinoma: a review and a point of view. *World J Gastroenterol* 2014; **20**: 15943-15954 [PMID: 25473148 DOI: 10.3748/wjg.v20.i43.15943]
27 **Iida-Ueno A**, Enomoto M, Tamori A, Kawada N. Hepatitis B virus infection and alcohol consumption. *World J Gastroenterol* 2017; **23**: 2651-2659 [PMID: 28487602 DOI: 10.3748/wjg.v23.i15.2651]
28 **Ramadori P**, Cubero FJ, Liedtke C, Trautwein C, Nevzorova YA. Alcohol and Hepatocellular Carcinoma: Adding Fuel to the Flame. *Cancers (Basel)* 2017; **9** [PMID: 28946672 DOI: 10.3390/cancers9100130]
29 **Ganne-Carrié N**, Nahon P. Hepatocellular carcinoma in the setting of alcohol-related liver disease. *J Hepatol* 2019; **70**: 284-293 [PMID: 30658729 DOI: 10.1016/j.jhep.2018.10.008]
30 **Dolganiuc A**. Alcohol and Viral Hepatitis: Role of Lipid Rafts. *Alcohol Res* 2015; **37**: 299-309 [PMID: 26695752]
31 **Yuan JM**, Govindarajan S, Arakawa K, Yu MC. Synergism of alcohol, diabetes, and viral hepatitis on the risk of hepatocellular carcinoma in blacks and whites in the U.S. *Cancer* 2004; **101**: 1009-1017 [PMID: 15329910 DOI: 10.1002/cncr.20427]
32 **Novo-Veleiro I**, Alvela-Suárez L, Chamorro AJ, González-Sarmiento R, Laso FJ, Marcos M. Alcoholic liver disease and hepatitis C virus infection. *World J Gastroenterol* 2016; **22**: 1411-1420 [PMID: 26819510 DOI: 10.3748/wjg.v22.i4.1411]
33 **Shoreibah M**, Anand BS, Singal AK. Alcoholic hepatitis and concomitant hepatitis C virus infection. *World J Gastroenterol* 2014; **20**: 11929-11934 [PMID: 25232227 DOI: 10.3748/wjg.v20.i34.11929]
34 **Serfaty L**. Clinical Implications of Concomitant Alcohol Use, Obesity, and Viral Hepatitis. *Gastroenterology* 2016; **150**: 1718-1722 [PMID: 26873400 DOI: 10.1053/j.gastro.2016.02.001]
35 **Larkin J**, Clayton MM, Liu J, Feitelson MA. Chronic ethanol consumption stimulates hepatitis B virus gene expression and replication in transgenic mice. *Hepatology* 2001; **34**: 792-797 [PMID: 11584377 DOI: 10.1053/jhep.2001.27565]
36 **Wilkening S**, Bader A. Influence of culture time on the expression of drug-metabolizing enzymes in primary human hepatocytes and hepatoma cell line HepG2. *J Biochem Mol Toxicol* 2003; **17**: 207-213 [PMID: 12898644 DOI: 10.1002/jbt.10085]
37 **Park B**, Jung KW, Oh CM, Choi KS, Suh M, Jun JK. Factors associated with alcohol consumption in hepatitis B carriers: a nationwide study in the Republic of Korea. *PLoS One* 2014; **9**: e110144 [PMID: 25387237 DOI: 10.1371/journal.pone.0110144]
38 **Yang HI**, Lu SN, Liaw YF, You SL, Sun CA, Wang LY, Hsiao CK, Chen PJ, Chen DS, Chen CJ; Taiwan Community-Based Cancer Screening Project Group. Hepatitis B e antigen and the risk of hepatocellular carcinoma. *N Engl J Med* 2002; **347**: 168-174 [PMID: 12124405 DOI: 10.1056/NEJMoa013215]
39 **Marcellin P**, Pequignot F, Delarocque-Astagneau E, Zarski JP, Ganne N, Hillon P, Antona D, Bovet M, Mechain M, Asselah T, Desenclos JC, Jougla E. Mortality related to chronic hepatitis B and chronic hepatitis C in France: evidence for the role of HIV coinfection and alcohol consumption. *J Hepatol* 2008; **48**: 200-207 [PMID: 18086507 DOI: 10.1016/j.jhep.2007.09.010]
40 **Jee SH**, Ohrr H, Sull JW, Samet JM. Cigarette smoking, alcohol drinking, hepatitis B, and risk for hepatocellular carcinoma in Korea. *J Natl Cancer Inst* 2004; **96**: 1851-1856 [PMID: 15601641 DOI: 10.1093/jnci/djh334]
41 **Wang LY**, You SL, Lu SN, Ho HC, Wu MH, Sun CA, Yang HI, Chien-Jen C. Risk of hepatocellular carcinoma and habits of alcohol drinking, betel quid chewing and cigarette smoking: a cohort of 2416 HBsAg-seropositive and 9421 HBsAg-seronegative male residents in Taiwan. *Cancer Causes Control* 2003; **14**: 241-250 [PMID: 12814203 DOI: 10.1023/a:1023636619477]
42 **El-Serag HB**, Tran T, Everhart JE. Diabetes increases the risk of chronic liver disease and hepatocellular carcinoma. *Gastroenterology* 2004; **126**: 460-468 [PMID: 14762783 DOI: 10.1053/j.gastro.2003.10.065]
43 **Yu MC**, Yuan JM, Lu SC. Alcohol, cofactors and the genetics of hepatocellular carcinoma. *J Gastroenterol Hepatol* 2008; **23** Suppl 1: S92-S97 [PMID: 18336674 DOI: 10.1111/j.1440-1746.2007.05293.x]
44 **Marrero JA**, Fontana RJ, Fu S, Conjeevaram HS, Su GL, Lok AS. Alcohol, tobacco and obesity are synergistic risk factors for hepatocellular carcinoma. *J Hepatol* 2005; **42**: 218-224 [PMID: 15664247 DOI: 10.1016/j.jhep.2004.10.005]
45 **Loomba R**, Yang HI, Su J, Brenner D, Iloeje U, Chen CJ. Obesity and alcohol synergize to increase the risk of incident hepatocellular carcinoma in men. *Clin Gastroenterol Hepatol* 2010; **8**: 891-898 [PMID: 20621202 DOI: 10.1016/j.cgh.2010.06.027]
46 **Corrao G**, Zambon A, Torchio P, Aricò S, La Vecchia C, di Orio F. Attributable risk for symptomatic liver cirrhosis in Italy. Collaborative Groups for the Study of Liver Diseases in Italy. *J Hepatol* 1998; **28**:

608-614 [PMID: 9566829 DOI: 10.1016/s0168-8278(98)80284-5]
47 **Stroffolini T**, Cotticelli G, Medda E, Niosi M, Del Vecchio-Blanco C, Addolorato G, Petrelli E, Salerno MT, Picardi A, Bernardi M, Almasio P, Bellentani S, Surace LA, Loguercio C. Interaction of alcohol intake and cofactors on the risk of cirrhosis. *Liver Int* 2010; **30**: 867-870 [PMID: 20492499 DOI: 10.1111/j.1478-3231.2010.02261.x]
48 **Murata T**, Takanari H, Watanabe S, Tanaka T, Suzuki S. Enhancement of chronic viral hepatitic changes by alcohol intake in patients with persistent HBs-antigenemia. *Am J Clin Pathol* 1990; **94**: 270-273 [PMID: 2396602 DOI: 10.1093/ajcp/94.3.270]
49 **Nomura H**, Kashiwagi S, Hayashi J, Kajiyama W, Ikematsu H, Noguchi A, Tani S, Goto M. An epidemiologic study of effects of alcohol in the liver in hepatitis B surface antigen carriers. *Am J Epidemiol* 1988; **128**: 277-284 [PMID: 3394696 DOI: 10.1093/oxfordjournals.aje.a114968]
50 **Uetake S**, Yamauchi M, Itoh S, Kawashima O, Takeda K, Ohata M. Analysis of risk factors for hepatocellular carcinoma in patients with HBs antigen- and anti-HCV antibody-negative alcoholic cirrhosis: clinical significance of prior hepatitis B virus infection. *Alcohol Clin Exp Res* 2003; **27**: 47S-51S [PMID: 12960507 DOI: 10.1097/01.ALC.0000079449.47468.B0]
51 **Stroffolini T**, Sagnelli E, Andriulli A, Colloredo G, Furlan C, Gaeta GB, Morisco F, Pirisi M, Rosina F, Sagnelli C, Smedile A, Almasio PL; EPACRON study group. Sex difference in the interaction of alcohol intake, hepatitis B virus, and hepatitis C virus on the risk of cirrhosis. *PLoS One* 2017; **12**: e0185710 [PMID: 29140988 DOI: 10.1371/journal.pone.0185710]
52 **Matsushita H**, Takaki A. Alcohol and hepatocellular carcinoma. *BMJ Open Gastroenterol* 2019; **6**: e000260 [PMID: 31139422 DOI: 10.1136/bmjgast-2018-000260]
53 **Ait-Goughoulte M**, Lucifora J, Zoulim F, Durantel D. Innate antiviral immune responses to hepatitis B virus. *Viruses* 2010; **2**: 1394-1410 [PMID: 21994686 DOI: 10.3390/v2071394]
54 **Chisari FV**, Isogawa M, Wieland SF. Pathogenesis of hepatitis B virus infection. *Pathol Biol (Paris)* 2010; **58**: 258-266 [PMID: 20116937 DOI: 10.1016/j.patbio.2009.11.001]
55 **Jieliang Chen M**, Kuancheng Liu, Wen Zhang, Yaming Li, Xiaohui Zhou, Lu Bai, Zhenghong Yuan. New insights into hepatitis B virus biology and implications for novel antiviral strategies. *Natl Sci Rev* 2015; **2**: 296–313 [DOI: 10.1093/nsr/nwv044]
56 **Thomas E**, Liang TJ. Experimental models of hepatitis B and C - new insights and progress. *Nat Rev Gastroenterol Hepatol* 2016; **13**: 362-374 [PMID: 27075261 DOI: 10.1038/nrgastro.2016.37]
57 **Mitra B**, Thapa RJ, Guo H, Block TM. Host functions used by hepatitis B virus to complete its life cycle: Implications for developing host-targeting agents to treat chronic hepatitis B. *Antiviral Res* 2018; **158**: 185-198 [PMID: 30145242 DOI: 10.1016/j.antiviral.2018.08.014]
58 **Montalbano R**, Honrath B, Wissniowski TT, Elxnat M, Roth S, Ocker M, Quint K, Churin Y, Roederfeld M, Schroeder D, Glebe D, Roeb E, Di Fazio P. Exogenous hepatitis B virus envelope proteins induce endoplasmic reticulum stress: involvement of cannabinoid axis in liver cancer cells. *Oncotarget* 2016; **7**: 20312-20323 [PMID: 26967385 DOI: 10.18632/oncotarget.7950]
59 **Glebe D**, König A. Molecular virology of hepatitis B virus and targets for antiviral intervention. *Intervirology* 2014; **57**: 134-140 [PMID: 25034480 DOI: 10.1159/000360946]
60 **Ganesan M**, Krutik VM, Makarov E, Mathews S, Kharbanda KK, Poluektova LY, Casey CA, Osna NA. Acetaldehyde suppresses the display of HBV-MHC class I complexes on HBV-expressing hepatocytes. *Am J Physiol Gastrointest Liver Physiol* 2019; **317**: G127-G140 [PMID: 31141391 DOI: 10.1152/ajpgi.00064.2019]
61 **Li ZM**, Kong CY, Zhang SL, Han B, Zhang ZY, Wang LS. Alcohol and HBV synergistically promote hepatic steatosis. *Ann Hepatol* 2019; **18**: 913-917 [PMID: 31147179 DOI: 10.1016/j.aohep.2019.04.013]
62 **Min BY**, Kim NY, Jang ES, Shin CM, Lee SH, Park YS, Hwang JH, Jeong SH, Kim N, Lee DH, Kim JW. Ethanol potentiates hepatitis B virus replication through oxidative stress-dependent and -independent transcriptional activation. *Biochem Biophys Res Commun* 2013; **431**: 92-97 [PMID: 23274499 DOI: 10.1016/j.bbrc.2012.12.081]
63 **Bar-Yishay I**, Shaul Y, Shlomai A. Hepatocyte metabolic signalling pathways and regulation of hepatitis B virus expression. *Liver Int* 2011; **31**: 282-290 [PMID: 21281428 DOI: 10.1111/j.1478-3231.2010.02423.x]
64 **Quasdorff M**, Protzer U. Control of hepatitis B virus at the level of transcription. *J Viral Hepat* 2010; **17**: 527-536 [PMID: 20546497 DOI: 10.1111/j.1365-2893.2010.01315.x]
65 **Ramière C**, Scholtès C, Diaz O, Icard V, Perrin-Cocon L, Trabaud MA, Lotteau V, André P. Transactivation of the hepatitis B virus core promoter by the nuclear receptor FXRalpha. *J Virol* 2008; **82**: 10832-10840 [PMID: 18768987 DOI: 10.1128/JVI.00883-08]
66 **Shlomai A**, Paran N, Shaul Y. PGC-1alpha controls hepatitis B virus through nutritional signals. *Proc Natl Acad Sci USA* 2006; **103**: 16003-16008 [PMID: 17043229 DOI: 10.1073/pnas.0607837103]
67 **Yu X**, Mertz JE. Differential regulation of the pre-C and pregenomic promoters of human hepatitis B virus by members of the nuclear receptor superfamily. *J Virol* 1997; **71**: 9366-9374 [PMID: 9371596 DOI: 10.1128/JVI.71.12.9366-9374.1997]
68 **Lin CW**, Hsu CC, Perng DS, Yeh MM, Yang SS. The Histological Assessment of Hepatitis B Viral Activity in Patients with Heavy Alcohol Consumption. *J Liver* 2016; **5**: 204 [DOI: 10.4172/2167-0889.1000204]
69 **Dolganiuc A**, Bakis G, Kodys K, Mandrekar P, Szabo G. Acute ethanol treatment modulates Toll-like receptor-4 association with lipid rafts. *Alcohol Clin Exp Res* 2006; **30**: 76-85 [PMID: 16433734 DOI: 10.1111/j.1530-0277.2006.00003.x]
70 **Lamontagne RJ**, Bagga S, Bouchard MJ. Hepatitis B virus molecular biology and pathogenesis. *Hepatoma Res* 2016; **2**: 163-186 [PMID: 28042609 DOI: 10.20517/2394-5079.2016.05]
71 **Peeridogaheh H**, Meshkat Z, Habibzadeh S, Arzanlou M, Shahi JM, Rostami S, Gerayli S, Teimourpour R. Current concepts on immunopathogenesis of hepatitis B virus infection. *Virus Res* 2018; **245**: 29-43 [PMID: 29273341 DOI: 10.1016/j.virusres.2017.12.007]
72 **Tseng TC**, Huang LR. Immunopathogenesis of Hepatitis B Virus. *J Infect Dis* 2017; **216**: S765-S770 [PMID: 29156047 DOI: 10.1093/infdis/jix356]
73 **Yim HJ**, Lok AS. Natural history of chronic hepatitis B virus infection: what we knew in 1981 and what we know in 2005. *Hepatology* 2006; **43**: S173-S181 [PMID: 16447285 DOI: 10.1002/hep.20956]
74 **Tu T**, Budzinska MA, Shackel NA, Urban S. HBV DNA Integration: Molecular Mechanisms and Clinical Implications. *Viruses* 2017; **9** [PMID: 28394272 DOI: 10.3390/v9040075]
75 **Liaw YF**, Chu CM. Hepatitis B virus infection. *Lancet* 2009; **373**: 582-592 [PMID: 19217993 DOI: 10.1016/S0140-6736(09)60207-5]

76 **Tseng TC**, Kao JH. Clinical utility of quantitative HBsAg in natural history and nucleos(t)ide analogue treatment of chronic hepatitis B: new trick of old dog. *J Gastroenterol* 2013; **48**: 13-21 [PMID: 23090000 DOI: 10.1007/s00535-012-0668-y]

77 **Lin CW**, Lin CC, Mo LR, Chang CY, Perng DS, Hsu CC, Lo GH, Chen YS, Yen YC, Hu JT, Yu ML, Lee PH, Lin JT, Yang SS. Heavy alcohol consumption increases the incidence of hepatocellular carcinoma in hepatitis B virus-related cirrhosis. *J Hepatol* 2013; **58**: 730-735 [PMID: 23220252 DOI: 10.1016/j.jhep.2012.11.045]

78 **Donato F**, Tagger A, Chiesa R, Ribero ML, Tomasoni V, Fasola M, Gelatti U, Portera G, Boffetta P, Nardi G. Hepatitis B and C virus infection, alcohol drinking, and hepatocellular carcinoma: a case-control study in Italy. Brescia HCC Study. *Hepatology* 1997; **26**: 579-584 [PMID: 9303486 DOI: 10.1002/hep.510260308]

79 **Itoh S**, Shimoji K. Effects of alcohol on the liver in HBsAg carriers. *Am J Gastroenterol* 1986; **81**: 779-782 [PMID: 3752040]

80 **Bassendine MF**, Della Seta L, Salmeron J, Thomas HC, Sherlock S. Incidence of hepatitis B virus infection in alcoholic liver disease, HBsAg negative chronic active liver disease and primary liver cell cancer in Britain. *Liver* 1983; **3**: 65-70 [PMID: 6877051 DOI: 10.1111/j.1600-0676.1983.tb00852.x]

81 **Fong TL**, Govindarajan S, Valinluck B, Redeker AG. Status of hepatitis B virus DNA in alcoholic liver disease: a study of a large urban population in the United States. *Hepatology* 1988; **8**: 1602-1604 [PMID: 3192173 DOI: 10.1002/hep.1840080621]

82 **Yokosuka O**, Omata M, Imazeki F, Ito Y, Okuda K. Hepatitis B virus RNA transcripts and DNA in chronic liver disease. *N Engl J Med* 1986; **315**: 1187-1192 [PMID: 3762642 DOI: 10.1056/NEJM198611063151903]

83 **Busca A**, Kumar A. Innate immune responses in hepatitis B virus (HBV) infection. *Virol J* 2014; **11**: 22 [PMID: 24507433 DOI: 10.1186/1743-422X-11-22]

84 **Kawai T**, Akira S. Antiviral signaling through pattern recognition receptors. *J Biochem* 2007; **141**: 137-145 [PMID: 17190786 DOI: 10.1093/jb/mvm032]

85 **Sato S**, Li K, Kameyama T, Hayashi T, Ishida Y, Murakami S, Watanabe T, Iijima S, Sakurai Y, Watashi K, Tsutsumi S, Sato Y, Akita H, Wakita T, Rice CM, Harashima H, Kohara M, Tanaka Y, Takaoka A. The RNA sensor RIG-I dually functions as an innate sensor and direct antiviral factor for hepatitis B virus. *Immunity* 2015; **42**: 123-132 [PMID: 25557055 DOI: 10.1016/j.immuni.2014.12.016]

86 **Thompson AJ**, Locarnini SA. Toll-like receptors, RIG-I-like RNA helicases and the antiviral innate immune response. *Immunol Cell Biol* 2007; **85**: 435-445 [PMID: 17667934 DOI: 10.1038/sj.icb.7100100]

87 **Loo YM**, Fornek J, Crochet N, Bajwa G, Perwitasari O, Martinez-Sobrido L, Akira S, Gill MA, García-Sastre A, Katze MG, Gale M. Distinct RIG-I and MDA5 signaling by RNA viruses in innate immunity. *J Virol* 2008; **82**: 335-345 [PMID: 17942531 DOI: 10.1128/JVI.01080-07]

88 **Wu J**, Lu M, Meng Z, Trippler M, Broering R, Szczeponek A, Krux F, Dittmer U, Roggendorf M, Gerken G, Schlaak JF. Toll-like receptor-mediated control of HBV replication by nonparenchymal liver cells in mice. *Hepatology* 2007; **46**: 1769-1778 [PMID: 17929296 DOI: 10.1002/hep.21897]

89 **Wu J**, Meng Z, Jiang M, Pei R, Trippler M, Broering R, Bucchi A, Sowa JP, Dittmer U, Yang D, Roggendorf M, Gerken G, Lu M, Schlaak JF. Hepatitis B virus suppresses toll-like receptor-mediated innate immune responses in murine parenchymal and nonparenchymal liver cells. *Hepatology* 2009; **49**: 1132-1140 [PMID: 19140219 DOI: 10.1002/hep.22751]

90 **Belloni L**, Allweiss L, Guerrieri F, Pediconi N, Volz T, Pollicino T, Petersen J, Raimondo G, Dandri M, Levrero M. IFN-α inhibits HBV transcription and replication in cell culture and in humanized mice by targeting the epigenetic regulation of the nuclear cccDNA minichromosome. *J Clin Invest* 2012; **122**: 529-537 [PMID: 22251702 DOI: 10.1172/JCI58847]

91 **Katze MG**, He Y, Gale M. Viruses and interferon: a fight for supremacy. *Nat Rev Immunol* 2002; **2**: 675-687 [PMID: 12209136 DOI: 10.1038/nri888]

92 **Pham AM**, Santa Maria FG, Lahiri T, Friedman E, Marié IJ, Levy DE. PKR Transduces MDA5-Dependent Signals for Type I IFN Induction. *PLoS Pathog* 2016; **12**: e1005489 [PMID: 26939124 DOI: 10.1371/journal.ppat.1005489]

93 **Zheng M**, Sun R, Wei H, Tian Z. NK Cells Help Induce Anti-Hepatitis B Virus CD8+ T Cell Immunity in Mice. *J Immunol* 2016; **196**: 4122-4131 [PMID: 27183639 DOI: 10.4049/jimmunol.1500846]

94 **Maini MK**, Gehring AJ. The role of innate immunity in the immunopathology and treatment of HBV infection. *J Hepatol* 2016; **64**: S60-S70 [PMID: 27084038 DOI: 10.1016/j.jhep.2016.01.028]

95 **Bertoletti A**, Ferrari C. Innate and adaptive immune responses in chronic hepatitis B virus infections: towards restoration of immune control of viral infection. *Gut* 2012; **61**: 1754-1764 [PMID: 22157327 DOI: 10.1136/gutjnl-2011-301073]

96 **Samuel CE**. Antiviral actions of interferon. Interferon-regulated cellular proteins and their surprisingly selective antiviral activities. *Virology* 1991; **183**: 1-11 [PMID: 1711253 DOI: 10.1016/0042-6822(91)90112-o]

97 **Wieland SF**, Chisari FV. Stealth and cunning: hepatitis B and hepatitis C viruses. *J Virol* 2005; **79**: 9369-9380 [PMID: 16014900 DOI: 10.1128/JVI.79.15.9369-9380.2005]

98 **Dunn C**, Peppa D, Khanna P, Nebbia G, Jones M, Brendish N, Lascar RM, Brown D, Gilson RJ, Tedder RJ, Dusheiko GM, Jacobs M, Klenerman P, Maini MK. Temporal analysis of early immune responses in patients with acute hepatitis B virus infection. *Gastroenterology* 2009; **137**: 1289-1300 [PMID: 19591831 DOI: 10.1053/j.gastro.2009.06.054]

99 **Stacey AR**, Norris PJ, Qin L, Haygreen EA, Taylor E, Heitman J, Lebedeva M, DeCamp A, Li D, Grove D, Self SG, Borrow P. Induction of a striking systemic cytokine cascade prior to peak viremia in acute human immunodeficiency virus type 1 infection, in contrast to more modest and delayed responses in acute hepatitis B and C virus infections. *J Virol* 2009; **83**: 3719-3733 [PMID: 19176632 DOI: 10.1128/JVI.01844-08]

100 **Wieland S**, Thimme R, Purcell RH, Chisari FV. Genomic analysis of the host response to hepatitis B virus infection. *Proc Natl Acad Sci USA* 2004; **101**: 6669-6674 [PMID: 15100412 DOI: 10.1073/pnas.0401771101]

101 **McClary H**, Koch R, Chisari FV, Guidotti LG. Relative sensitivity of hepatitis B virus and other hepatotropic viruses to the antiviral effects of cytokines. *J Virol* 2000; **74**: 2255-2264 [PMID: 10666256 DOI: 10.1128/jvi.74.5.2255-2264.2000]

102 **Lucifora J**, Durantel D, Testoni B, Hantz O, Levrero M, Zoulim F. Control of hepatitis B virus replication by innate response of HepaRG cells. *Hepatology* 2010; **51**: 63-72 [PMID: 19877170 DOI: 10.1002/hep.23230]

103 **Lütgehetmann M**, Bornscheuer T, Volz T, Allweiss L, Bockmann JH, Pollok JM, Lohse AW, Petersen J, Dandri M. Hepatitis B virus limits response of human hepatocytes to interferon-α in chimeric mice. *Gastroenterology* 2011; **140**: 2074-2083, 2083.e1-2083.e2 [PMID: 21376046 DOI: 10.1053/j.gastro.2011.02.057]

104 **McCartney EM**, Semendric L, Helbig KJ, Hinze S, Jones B, Weinman SA, Beard MR. Alcohol metabolism increases the replication of hepatitis C virus and attenuates the antiviral action of interferon. *J Infect Dis* 2008; **198**: 1766-1775 [PMID: 18956976 DOI: 10.1086/593216]

105 **Plumlee CR**, Lazaro CA, Fausto N, Polyak SJ. Effect of ethanol on innate antiviral pathways and HCV replication in human liver cells. *Virol J* 2005; **2**: 89 [PMID: 16324217 DOI: 10.1186/1743-422X-2-89]

106 **Ganesan M**, Poluektova LY, Tuma DJ, Kharbanda KK, Osna NA. Acetaldehyde Disrupts Interferon Alpha Signaling in Hepatitis C Virus-Infected Liver Cells by Up-Regulating USP18. *Alcohol Clin Exp Res* 2016; **40**: 2329-2338 [PMID: 27716962 DOI: 10.1111/acer.13226]

107 **Guidotti LG**, Rochford R, Chung J, Shapiro M, Purcell R, Chisari FV. Viral clearance without destruction of infected cells during acute HBV infection. *Science* 1999; **284**: 825-829 [PMID: 10221919 DOI: 10.1126/science.284.5415.825]

108 **Xia Y**, Stadler D, Lucifora J, Reisinger F, Webb D, Hösel M, Michler T, Wisskirchen K, Cheng X, Zhang K, Chou WM, Wettengel JM, Malo A, Bohne F, Hoffmann D, Eyer F, Thimme R, Falk CS, Thasler WE, Heikenwalder M, Protzer U. Interferon-γ and Tumor Necrosis Factor-α Produced by T Cells Reduce the HBV Persistence Form, cccDNA, Without Cytolysis. *Gastroenterology* 2016; **150**: 194-205 [PMID: 26416327 DOI: 10.1053/j.gastro.2015.09.026]

109 **Cavanaugh VJ**, Guidotti LG, Chisari FV. Interleukin-12 inhibits hepatitis B virus replication in transgenic mice. *J Virol* 1997; **71**: 3236-3243 [PMID: 9060687 DOI: 10.1128/JVI.71.4.3236-3243.1997]

110 **Kimura K**, Kakimi K, Wieland S, Guidotti LG, Chisari FV. Interleukin-18 inhibits hepatitis B virus replication in the livers of transgenic mice. *J Virol* 2002; **76**: 10702-10707 [PMID: 12368312 DOI: 10.1128/jvi.76.21.10702-10707.2002]

111 **Xia Y**, Protzer U. Control of Hepatitis B Virus by Cytokines. *Viruses* 2017; **9** [PMID: 28117695 DOI: 10.3390/v9010018]

112 **Bouezzedine F**, Fardel O, Gripon P. Interleukin 6 inhibits HBV entry through NTCP down regulation. *Virology* 2015; **481**: 34-42 [PMID: 25765005 DOI: 10.1016/j.virol.2015.02.026]

113 **Hong MH**, Chou YC, Wu YC, Tsai KN, Hu CP, Jeng KS, Chen ML, Chang C. Transforming growth factor-β1 suppresses hepatitis B virus replication by the reduction of hepatocyte nuclear factor-4α expression. *PLoS One* 2012; **7**: e30360 [PMID: 22276183 DOI: 10.1371/journal.pone.0030360]

114 **Hösel M**, Quasdorff M, Wiegmann K, Webb D, Zedler U, Broxtermann M, Tedjokusumo R, Esser K, Arzberger S, Kirschning CJ, Langenkamp A, Falk C, Büning H, Rose-John S, Protzer U. Not interferon, but interleukin-6 controls early gene expression in hepatitis B virus infection. *Hepatology* 2009; **50**: 1773-1782 [PMID: 19937696 DOI: 10.1002/hep.23226]

115 **Isorce N**, Testoni B, Locatelli M, Fresquet J, Rivoire M, Luangsay S, Zoulim F, Durantel D. Antiviral activity of various interferons and pro-inflammatory cytokines in non-transformed cultured hepatocytes infected with hepatitis B virus. *Antiviral Res* 2016; **130**: 36-45 [PMID: 26971407 DOI: 10.1016/j.antiviral.2016.03.008]

116 **Lin SJ**, Shu PY, Chang C, Ng AK, Hu CP. IL-4 suppresses the expression and the replication of hepatitis B virus in the hepatocellular carcinoma cell line Hep3B. *J Immunol* 2003; **171**: 4708-4716 [PMID: 14568946 DOI: 10.4049/jimmunol.171.9.4708]

117 **McClain CJ**, Barve S, Deaciuc I, Kugelmas M, Hill D. Cytokines in alcoholic liver disease. *Semin Liver Dis* 1999; **19**: 205-219 [PMID: 10422201 DOI: 10.1055/s-2007-1007110]

118 **Wang HJ**, Gao B, Zakhari S, Nagy LE. Inflammation in alcoholic liver disease. *Annu Rev Nutr* 2012; **32**: 343-368 [PMID: 22524187 DOI: 10.1146/annurev-nutr-072610-145138]

119 **Maini MK**, Peppa D. NK cells: a double-edged sword in chronic hepatitis B virus infection. *Front Immunol* 2013; **4**: 57 [PMID: 23459859 DOI: 10.3389/fimmu.2013.00057]

120 **Wu SF**, Wang WJ, Gao YQ. Natural killer cells in hepatitis B virus infection. *Braz J Infect Dis* 2015; **19**: 417-425 [PMID: 26119852 DOI: 10.1016/j.bjid.2015.05.006]

121 **Guidotti LG**, Ishikawa T, Hobbs MV, Matzke B, Schreiber R, Chisari FV. Intracellular inactivation of the hepatitis B virus by cytotoxic T lymphocytes. *Immunity* 1996; **4**: 25-36 [PMID: 8574849 DOI: 10.1016/s1074-7613(00)80295-2]

122 **Kakimi K**, Guidotti LG, Koezuka Y, Chisari FV. Natural killer T cell activation inhibits hepatitis B virus replication in vivo. *J Exp Med* 2000; **192**: 921-930 [PMID: 11015434 DOI: 10.1084/jem.192.7.921]

123 **Yang PL**, Althage A, Chung J, Chisari FV. Hydrodynamic injection of viral DNA: a mouse model of acute hepatitis B virus infection. *Proc Natl Acad Sci USA* 2002; **99**: 13825-13830 [PMID: 12374864 DOI: 10.1073/pnas.202398599]

124 **Thimme R**, Wieland S, Steiger C, Ghrayeb J, Reimann KA, Purcell RH, Chisari FV. CD8(+) T cells mediate viral clearance and disease pathogenesis during acute hepatitis B virus infection. *J Virol* 2003; **77**: 68-76 [PMID: 12477811 DOI: 10.1128/jvi.77.1.68-76.2003]

125 **Fisicaro P**, Valdatta C, Boni C, Massari M, Mori C, Zerbini A, Orlandini A, Sacchelli L, Missale G, Ferrari C. Early kinetics of innate and adaptive immune responses during hepatitis B virus infection. *Gut* 2009; **58**: 974-982 [PMID: 19201769 DOI: 10.1136/gut.2008.163600]

126 **Webster GJ**, Reignat S, Maini MK, Whalley SA, Ogg GS, King A, Brown D, Amlot PL, Williams R, Vergani D, Dusheiko GM, Bertoletti A. Incubation phase of acute hepatitis B in man: dynamic of cellular immune mechanisms. *Hepatology* 2000; **32**: 1117-1124 [PMID: 11050064 DOI: 10.1053/jhep.2000.19324]

127 **Li Y**, Wang JJ, Gao S, Liu Q, Bai J, Zhao XQ, Hao YH, Ding HH, Zhu F, Yang DL, Zhao XP. Decreased peripheral natural killer cells activity in the immune activated stage of chronic hepatitis B. *PLoS One* 2014; **9**: e86927 [PMID: 24520324 DOI: 10.1371/journal.pone.0086927]

128 **Tjwa ET**, van Oord GW, Hegmans JP, Janssen HL, Woltman AM. Viral load reduction improves activation and function of natural killer cells in patients with chronic hepatitis B. *J Hepatol* 2011; **54**: 209-218 [PMID: 21095036 DOI: 10.1016/j.jhep.2010.07.009]

129 **Zhang Z**, Zhang S, Zou Z, Shi J, Zhao J, Fan R, Qin E, Li B, Li Z, Xu X, Fu J, Zhang J, Gao B, Tian Z, Wang FS. Hypercytolytic activity of hepatic natural killer cells correlates with liver injury in chronic hepatitis B patients. *Hepatology* 2011; **53**: 73-85 [PMID: 21254163 DOI: 10.1002/hep.23977]

130 **Li F**, Wei H, Wei H, Gao Y, Xu L, Yin W, Sun R, Tian Z. Blocking the natural killer cell inhibitory receptor NKG2A increases activity of human natural killer cells and clears hepatitis B virus infection in mice. *Gastroenterology* 2013; **144**: 392-401 [PMID: 23103614 DOI: 10.1053/j.gastro.2012.10.039]

131 **Oliviero B**, Varchetta S, Paudice E, Michelone G, Zaramella M, Mavilio D, De Filippi F, Bruno S, Mondelli MU. Natural killer cell functional dichotomy in chronic hepatitis B and chronic hepatitis C virus infections. *Gastroenterology* 2009; **137**: 1151-1160, 1160.e1-1160.e7 [PMID: 19470388 DOI: 10.1053/j.gastro.2009.05.047]

132 **Ju Y**, Hou N, Meng J, Wang X, Zhang X, Zhao D, Liu Y, Zhu F, Zhang L, Sun W, Liang X, Gao L, Ma C. T cell immunoglobulin- and mucin-domain-containing molecule-3 (Tim-3) mediates natural killer cell suppression in chronic hepatitis B. *J Hepatol* 2010; **52**: 322-329 [PMID: 20133006 DOI: 10.1016/j.jhep.2009.12.005]

133 **Peppa D**, Micco L, Javaid A, Kennedy PT, Schurich A, Dunn C, Pallant C, Ellis G, Khanna P, Dusheiko G, Gilson RJ, Maini MK. Blockade of immunosuppressive cytokines restores NK cell antiviral function in chronic hepatitis B virus infection. *PLoS Pathog* 2010; **6**: e1001227 [PMID: 21187913 DOI: 10.1371/journal.ppat.1001227]

134 **Zhang P**, Bagby GJ, Happel KI, Raasch CE, Nelson S. Alcohol abuse, immunosuppression, and pulmonary infection. *Curr Drug Abuse Rev* 2008; **1**: 56-67 [PMID: 19630706 DOI: 10.2174/1874473710801010056]

135 **Sun HH**, Zhou DF, Zhou JY. The role of DCs in the immunopathogenesis of chronic HBV infection and the methods of inducing DCs maturation. *J Med Virol* 2016; **88**: 13-20 [PMID: 26104380 DOI: 10.1002/jmv.24306]

136 **Cohn L**, Delamarre L. Dendritic cell-targeted vaccines. *Front Immunol* 2014; **5**: 255 [PMID: 24910635 DOI: 10.3389/fimmu.2014.00255]

137 **Schlitzer A**, McGovern N, Teo P, Zelante T, Atarashi K, Low D, Ho AW, See P, Shin A, Wasan PS, Hoeffel G, Malleret B, Heiseke A, Chew S, Jardine L, Purvis HA, Hilkens CM, Tam J, Poidinger M, Stanley ER, Krug AB, Renia L, Sivasankar B, Ng LG, Collin M, Ricciardi-Castagnoli P, Honda K, Haniffa M, Ginhoux F. IRF4 transcription factor-dependent CD11b+ dendritic cells in human and mouse control mucosal IL-17 cytokine responses. *Immunity* 2013; **38**: 970-983 [PMID: 23706669 DOI: 10.1016/j.immuni.2013.04.011]

138 **Kadowaki N**. The divergence and interplay between pDC and mDC in humans. *Front Biosci (Landmark Ed)* 2009; **14**: 808-817 [PMID: 19273101 DOI: 10.2741/3279]

139 **Reizis B**, Bunin A, Ghosh HS, Lewis KL, Sisirak V. Plasmacytoid dendritic cells: recent progress and open questions. *Annu Rev Immunol* 2011; **29**: 163-183 [PMID: 21219184 DOI: 10.1146/annurev-immunol-031210-101345]

140 **Tibúrcio R**, Nunes S, Nunes I, Rosa Ampuero M, Silva IB, Lima R, Machado Tavares N, Brodskyn C. Molecular Aspects of Dendritic Cell Activation in Leishmaniasis: An Immunobiological View. *Front Immunol* 2019; **10**: 227 [PMID: 30873156 DOI: 10.3389/fimmu.2019.00227]

141 **Merad M**, Sathe P, Helft J, Miller J, Mortha A. The dendritic cell lineage: ontogeny and function of dendritic cells and their subsets in the steady state and the inflamed setting. *Annu Rev Immunol* 2013; **31**: 563-604 [PMID: 23516985 DOI: 10.1146/annurev-immunol-020711-074950]

142 **Cui GY**, Diao HY. Recognition of HBV antigens and HBV DNA by dendritic cells. *Hepatobiliary Pancreat Dis Int* 2010; **9**: 584-592 [PMID: 21134826]

143 **Ma YJ**, He M, Han JA, Yang L, Ji XY. A clinical study of HBsAg-activated dendritic cells and cytokine-induced killer cells during the treatment for chronic hepatitis B. *Scand J Immunol* 2013; **78**: 387-393 [PMID: 23841728 DOI: 10.1111/sji.12097]

144 **Zhang Z**, Zhang JY, Wang LF, Wang FS. Immunopathogenesis and prognostic immune markers of chronic hepatitis B virus infection. *J Gastroenterol Hepatol* 2012; **27**: 223-230 [PMID: 22004062 DOI: 10.1111/j.1440-1746.2011.06940.x]

145 **Heinz R**, Waltenbaugh C. Ethanol consumption modifies dendritic cell antigen presentation in mice. *Alcohol Clin Exp Res* 2007; **31**: 1759-1771 [PMID: 17850646 DOI: 10.1111/j.1530-0277.2007.00479.x]

146 **Lau AH**, Abe M, Thomson AW. Ethanol affects the generation, cosignaling molecule expression, and function of plasmacytoid and myeloid dendritic cell subsets in vitro and in vivo. *J Leukoc Biol* 2006; **79**: 941-953 [PMID: 16478920 DOI: 10.1189/jlb.0905517]

147 **Feng D**, Eken A, Ortiz V, Wands JR. Chronic alcohol-induced liver disease inhibits dendritic cell function. *Liver Int* 2011; **31**: 950-963 [PMID: 21733084 DOI: 10.1111/j.1478-3231.2011.02514.x]

148 **Thompson MG**, Navarro F, Chitsike L, Ramirez L, Kovacs EJ, Watkins SK. Alcohol exposure differentially effects anti-tumor immunity in females by altering dendritic cell function. *Alcohol* 2016; **57**: 1-8 [PMID: 27916138 DOI: 10.1016/j.alcohol.2016.10.007]

149 **Tan A**, Koh S, Bertoletti A. Immune Response in Hepatitis B Virus Infection. *Cold Spring Harb Perspect Med* 2015; **5**: a021428 [PMID: 26134480 DOI: 10.1101/cshperspect.a021428]

150 **Bertoletti A**, Tan AT, Gehring AJ. HBV-Specific Adaptive Immunity. *Viruses* 2009; **1**: 91-103 [PMID: 21994540 DOI: 10.3390/v1020091]

151 **Chisari FV**. Cytotoxic T cells and viral hepatitis. *J Clin Invest* 1997; **99**: 1472-1477 [PMID: 9119989 DOI: 10.1172/JCI119308]

152 **Guidotti LG**, Chisari FV. To kill or to cure: options in host defense against viral infection. *Curr Opin Immunol* 1996; **8**: 478-483 [PMID: 8794011 DOI: 10.1016/s0952-7915(96)80034-3]

153 **Alberti A**, Diana S, Sculard GH, Eddleston AL, Williams R. Detection of a new antibody system reacting with Dane particles in hepatitis B virus infection. *Br Med J* 1978; **2**: 1056-1058 [PMID: 81702 DOI: 10.1136/bmj.2.6144.1056]

154 **Grady GF**, Lee VA, Prince AM, Gitnick GL, Fawaz KA, Vyas GN, Levitt MD, Senior JR, Galambos JT, Bynum TE, Singleton JW, Clowdus BF, Akdamar K, Aach RD, Winkelman EI, Schiff GM, Hersh T. Hepatitis B immune globulin for accidental exposures among medical personnel: final report of a multicenter controlled trial. *J Infect Dis* 1978; **138**: 625-638 [PMID: 361899 DOI: 10.1093/infdis/138.5.625]

155 **Maini MK**, Burton AR. Restoring, releasing or replacing adaptive immunity in chronic hepatitis B. *Nat Rev Gastroenterol Hepatol* 2019; **16**: 662-675 [PMID: 31548710 DOI: 10.1038/s41575-019-0196-9]

156 **Bertoletti A**, Ferrari C. Adaptive immunity in HBV infection. *J Hepatol* 2016; **64**: S71-S83 [PMID: 27084039 DOI: 10.1016/j.jhep.2016.01.026]

157 **Gerlich WH**. Medical virology of hepatitis B: how it began and where we are now. *Virol J* 2013; **10**: 239 [PMID: 23870415 DOI: 10.1186/1743-422X-10-239]

158 **Hoofnagle JH**, Gerety RJ, Barker LF. Antibody to hepatitis-B-virus core in man. *Lancet* 1973; **2**: 869-873 [PMID: 4126916 DOI: 10.1016/s0140-6736(73)92004-7]

159 **Chen Z**, Diaz G, Pollicino T, Zhao H, Engle RE, Schuck P, Shen CH, Zamboni F, Long Z, Kabat J, De Battista D, Bock KW, Moore IN, Wollenberg K, Soto C, Govindarajan S, Kwong PD, Kleiner DE, Purcell

RH, Farci P. Role of humoral immunity against hepatitis B virus core antigen in the pathogenesis of acute liver failure. *Proc Natl Acad Sci USA* 2018; **115**: E11369-E11378 [PMID: 30420516 DOI: 10.1073/pnas.1809028115]

160 **Farci P**, Diaz G, Chen Z, Govindarajan S, Tice A, Agulto L, Pittaluga S, Boon D, Yu C, Engle RE, Haas M, Simon R, Purcell RH, Zamboni F. B cell gene signature with massive intrahepatic production of antibodies to hepatitis B core antigen in hepatitis B virus-associated acute liver failure. *Proc Natl Acad Sci USA* 2010; **107**: 8766-8771 [PMID: 20421498 DOI: 10.1073/pnas.1003854107]

161 **Yuen MF**, Chen DS, Dusheiko GM, Janssen HLA, Lau DTY, Locarnini SA, Peters MG, Lai CL. Hepatitis B virus infection. *Nat Rev Dis Primers* 2018; **4**: 18035 [PMID: 29877316 DOI: 10.1038/nrdp.2018.35]

162 **Corti D**, Lanzavecchia A. Broadly neutralizing antiviral antibodies. *Annu Rev Immunol* 2013; **31**: 705-742 [PMID: 23330954 DOI: 10.1146/annurev-immunol-032712-095916]

163 **Hangartner L**, Zinkernagel RM, Hengartner H. Antiviral antibody responses: the two extremes of a wide spectrum. *Nat Rev Immunol* 2006; **6**: 231-243 [PMID: 16498452 DOI: 10.1038/nri1783]

164 **Cerino A**, Bremer CM, Glebe D, Mondelli MU. A Human Monoclonal Antibody against Hepatitis B Surface Antigen with Potent Neutralizing Activity. *PLoS One* 2015; **10**: e0125704 [PMID: 25923526 DOI: 10.1371/journal.pone.0125704]

165 **Glebe D**, Aliakbari M, Krass P, Knoop EV, Valerius KP, Gerlich WH. Pre-s1 antigen-dependent infection of Tupaia hepatocyte cultures with human hepatitis B virus. *J Virol* 2003; **77**: 9511-9521 [PMID: 12915565 DOI: 10.1128/jvi.77.17.9511-9521.2003]

166 **Milich DR**, McLachlan A, Thornton GB, Hughes JL. Antibody production to the nucleocapsid and envelope of the hepatitis B virus primed by a single synthetic T cell site. *Nature* 1987; **329**: 547-549 [PMID: 2443856 DOI: 10.1038/329547a0]

167 **Das A**, Ellis G, Pallant C, Lopes AR, Khanna P, Peppa D, Chen A, Blair P, Dusheiko G, Gill U, Kennedy PT, Brunetto M, Lampertico P, Mauri C, Maini MK. IL-10-producing regulatory B cells in the pathogenesis of chronic hepatitis B virus infection. *J Immunol* 2012; **189**: 3925-3935 [PMID: 22972930 DOI: 10.4049/jimmunol.1103139]

168 **Cook RT**, Waldschmidt TJ, Cook BL, Labrecque DR, McLatchie K. Loss of the CD5+ and CD45RAhi B cell subsets in alcoholics. *Clin Exp Immunol* 1996; **103**: 304-310 [PMID: 8565316 DOI: 10.1046/j.1365-2249.1996.d01-621.x]

169 **Zhang H**, Meadows GG. Chronic alcohol consumption in mice increases the proportion of peripheral memory T cells by homeostatic proliferation. *J Leukoc Biol* 2005; **78**: 1070-1080 [PMID: 16260584 DOI: 10.1189/jlb.0605317]

170 **Matos LC**, Batista P, Monteiro N, Ribeiro J, Cipriano MA, Henriques P, Girão F, Carvalho A. Lymphocyte subsets in alcoholic liver disease. *World J Hepatol* 2013; **5**: 46-55 [PMID: 23646229 DOI: 10.4254/wjh.v5.i2.46]

171 **Pasala S**, Barr T, Messaoudi I. Impact of Alcohol Abuse on the Adaptive Immune System. *Alcohol Res* 2015; **37**: 185-197 [PMID: 26695744]

172 **Geissler M**, Gesien A, Wands JR. Chronic ethanol effects on cellular immune responses to hepatitis B virus envelope protein: an immunologic mechanism for induction of persistent viral infection in alcoholics. *Hepatology* 1997; **26**: 764-770 [PMID: 9303510 DOI: 10.1002/hep.510260332]

173 **Bertoletti A**, Ferrari C. Innate and adaptive immune responses in chronic hepatitis B virus infections: towards restoration of immune control of viral infection. *Postgrad Med J* 2013; **89**: 294-304 [PMID: 23596257 DOI: 10.1136/postgradmedj-2011-301073rep]

174 **Bertoletti A**, Maini MK, Ferrari C. The host-pathogen interaction during HBV infection: immunological controversies. *Antivir Ther* 2010; **15** Suppl 3: 15-24 [PMID: 21041900 DOI: 10.3851/IMP1620]

175 **Rehermann B**, Nascimbeni M. Immunology of hepatitis B virus and hepatitis C virus infection. *Nat Rev Immunol* 2005; **5**: 215-229 [PMID: 15738952 DOI: 10.1038/nri1573]

176 **Moss B**, Smith GL, Gerin JL, Purcell RH. Live recombinant vaccinia virus protects chimpanzees against hepatitis B. *Nature* 1984; **311**: 67-69 [PMID: 6472464 DOI: 10.1038/311067a0]

177 **Ferrari C**, Penna A, Bertoletti A, Valli A, Antoni AD, Giuberti T, Cavalli A, Petit MA, Fiaccadori F. Cellular immune response to hepatitis B virus-encoded antigens in acute and chronic hepatitis B virus infection. *J Immunol* 1990; **145**: 3442-3449 [PMID: 2230128]

178 **Jung MC**, Spengler U, Schraut W, Hoffmann R, Zachoval R, Eisenburg J, Eichenlaub D, Riethmüller G, Paumgartner G, Ziegler-Heitbrock HW. Hepatitis B virus antigen-specific T-cell activation in patients with acute and chronic hepatitis B. *J Hepatol* 1991; **13**: 310-317 [PMID: 1808224 DOI: 10.1016/0168-8278(91)90074-l]

179 **Tsui LV**, Guidotti LG, Ishikawa T, Chisari FV. Posttranscriptional clearance of hepatitis B virus RNA by cytotoxic T lymphocyte-activated hepatocytes. *Proc Natl Acad Sci USA* 1995; **92**: 12398-12402 [PMID: 8618909 DOI: 10.1073/pnas.92.26.12398]

180 **Moriyama T**, Guilhot S, Klopchin K, Moss B, Pinkert CA, Palmiter RD, Brinster RL, Kanagawa O, Chisari FV. Immunobiology and pathogenesis of hepatocellular injury in hepatitis B virus transgenic mice. *Science* 1990; **248**: 361-364 [PMID: 1691527 DOI: 10.1126/science.1691527]

181 **Ando K**, Moriyama T, Guidotti LG, Wirth S, Schreiber RD, Schlicht HJ, Huang SN, Chisari FV. Mechanisms of class I restricted immunopathology. A transgenic mouse model of fulminant hepatitis. *J Exp Med* 1993; **178**: 1541-1554 [PMID: 8228807 DOI: 10.1084/jem.178.5.1541]

182 **Bertoletti A**, Ferrari C, Fiaccadori F, Penna A, Margolskee R, Schlicht HJ, Fowler P, Guilhot S, Chisari FV. HLA class I-restricted human cytotoxic T cells recognize endogenously synthesized hepatitis B virus nucleocapsid antigen. *Proc Natl Acad Sci USA* 1991; **88**: 10445-10449 [PMID: 1660137 DOI: 10.1073/pnas.88.23.10445]

183 **Penna A**, Chisari FV, Bertoletti A, Missale G, Fowler P, Giuberti T, Fiaccadori F, Ferrari C. Cytotoxic T lymphocytes recognize an HLA-A2-restricted epitope within the hepatitis B virus nucleocapsid antigen. *J Exp Med* 1991; **174**: 1565-1570 [PMID: 1720813 DOI: 10.1084/jem.174.6.1565]

184 **Rehermann B**, Fowler P, Sidney J, Person J, Redeker A, Brown M, Moss B, Sette A, Chisari FV. The cytotoxic T lymphocyte response to multiple hepatitis B virus polymerase epitopes during and after acute viral hepatitis. *J Exp Med* 1995; **181**: 1047-1058 [PMID: 7532675 DOI: 10.1084/jem.181.3.1047]

185 **Maini MK**, Boni C, Lee CK, Larrubia JR, Reignat S, Ogg GS, King AS, Herberg J, Gilson R, Alisa A, Williams R, Vergani D, Naoumov NV, Ferrari C, Bertoletti A. The role of virus-specific CD8(+) cells in liver damage and viral control during persistent hepatitis B virus infection. *J Exp Med* 2000; **191**: 1269-1280 [PMID: 10770795 DOI: 10.1084/jem.191.8.1269]

186 **Asabe S**, Wieland SF, Chattopadhyay PK, Roederer M, Engle RE, Purcell RH, Chisari FV. The size of the viral inoculum contributes to the outcome of hepatitis B virus infection. *J Virol* 2009; **83**: 9652-9662

[PMID: 19625407 DOI: 10.1128/JVI.00867-09]
187 **Guidotti LG**, Ando K, Hobbs MV, Ishikawa T, Runkel L, Schreiber RD, Chisari FV. Cytotoxic T lymphocytes inhibit hepatitis B virus gene expression by a noncytolytic mechanism in transgenic mice. *Proc Natl Acad Sci USA* 1994; **91**: 3764-3768 [PMID: 8170985 DOI: 10.1073/pnas.91.9.3764]
188 **Hewitt EW**. The MHC class I antigen presentation pathway: strategies for viral immune evasion. *Immunology* 2003; **110**: 163-169 [PMID: 14511229 DOI: 10.1046/j.1365-2567.2003.01738.x]
189 **Sastry KS**, Too CT, Kaur K, Gehring AJ, Low L, Javiad A, Pollicino T, Li L, Kennedy PT, Lopatin U, Macary PA, Bertoletti A. Targeting hepatitis B virus-infected cells with a T-cell receptor-like antibody. *J Virol* 2011; 1935-1942 [PMID: 21159876 DOI: 10.1128/JVI.01990-10]
190 **Khakpoor A**, Ni Y, Chen A, Ho ZZ, Oei V, Yang N, Giri R, Chow JX, Tan AT, Kennedy PT, Maini M, Urban S, Bertoletti A. Spatiotemporal Differences in Presentation of CD8 T Cell Epitopes during Hepatitis B Virus Infection. *J Virol* 2019; 93(4) [PMID: 30518652 DOI: 10.1128/JVI.01457-18]
191 **Storni T**, Bachmann MF. Loading of MHC class I and II presentation pathways by exogenous antigens: a quantitative in vivo comparison. *J Immunol* 2004; **172**: 6129-6135 [PMID: 15128799 DOI: 10.4049/jimmunol.172.10.6129]
192 **Murata Y**, Kawashima K, Sheikh K, Tanaka Y, Isogawa M. Intrahepatic Cross-Presentation and Hepatocellular Antigen Presentation Play Distinct Roles in the Induction of Hepatitis B Virus-Specific $CD8^+$ T Cell Responses. *J Virol* 2018; **92** [PMID: 30089700 DOI: 10.1128/JVI.00920-18]
193 **Jung MC**, Diepolder HM, Spengler U, Wierenga EA, Zachoval R, Hoffmann RM, Eichenlaub D, Frösner G, Will H, Pape GR. Activation of a heterogeneous hepatitis B (HB) core and e antigen-specific CD4+ T-cell population during seroconversion to anti-HBe and anti-HBs in hepatitis B virus infection. *J Virol* 1995; **69**: 3358-3368 [PMID: 7538172 DOI: 10.1128/JVI.69.6.3358-3368.1995]
194 **Wu T**, Li F, Chen Y, Wei H, Tian Z, Sun C, Sun R. $CD4^+$ T Cells Play a Critical Role in Microbiota-Maintained Anti-HBV Immunity in a Mouse Model. *Front Immunol* 2019; **10**: 927 [PMID: 31114580 DOI: 10.3389/fimmu.2019.00927]
195 **Bishehsari F**, Magno E, Swanson G, Desai V, Voigt RM, Forsyth CB, Keshavarzian A. Alcohol and Gut-Derived Inflammation. *Alcohol Res* 2017; **38**: 163-171 [PMID: 28988571]
196 **Lowe PP**, Gyongyosi B, Satishchandran A, Iracheta-Vellve A, Cho Y, Ambade A, Szabo G. Reduced gut microbiome protects from alcohol-induced neuroinflammation and alters intestinal and brain inflammasome expression. *J Neuroinflammation* 2018; **15**: 298 [PMID: 30368255 DOI: 10.1186/s12974-018-1328-9]
197 **Meroni M**, Longo M, Dongiovanni P. Alcohol or Gut Microbiota: Who Is the Guilty? *Int J Mol Sci* 2019; **20** [PMID: 31540133 DOI: 10.3390/ijms20184568]
198 **Fan X**, Peters BA, Jacobs EJ, Gapstur SM, Purdue MP, Freedman ND, Alekseyenko AV, Wu J, Yang L, Pei Z, Hayes RB, Ahn J. Drinking alcohol is associated with variation in the human oral microbiome in a large study of American adults. *Microbiome* 2018; **6**: 59 [PMID: 29685174 DOI: 10.1186/s40168-018-0448-x]
199 **Safdar K**, Schiff ER. Alcohol and hepatitis C. *Semin Liver Dis* 2004; **24**: 305-315 [PMID: 15349807 DOI: 10.1055/s-2004-832942]
200 **Ha HL**, Shin HJ, Feitelson MA, Yu DY. Oxidative stress and antioxidants in hepatic pathogenesis. *World J Gastroenterol* 2010; **16**: 6035-6043 [PMID: 21182217 DOI: 10.3748/wjg.v16.i48.6035]
201 **Liu Y**, Xu L, Lu B, Zhao M, Li L, Sun W, Qiu Z, Zhang B. LncRNA H19/microRNA-675/PPARα axis regulates liver cell injury and energy metabolism remodelling induced by hepatitis B X protein via Akt/mTOR signalling. *Mol Immunol* 2019; **116**: 18-28 [PMID: 31574452 DOI: 10.1016/j.molimm.2019.09.006]
202 **Xianyu J**, Feng J, Yang Y, Tang J, Xie G, Fan L. Correlation of oxidative stress in patients with HBV-induced liver disease with HBV genotypes and drug resistance mutations. *Clin Biochem* 2018; **55**: 21-27 [PMID: 29596793 DOI: 10.1016/j.clinbiochem.2018.03.014]
203 **Yang J**, Xiong Y, Zhou L, Huang Y, Chen W, Wang B. Soluble E-cadherin is associated with oxidative stress in patients with chronic HBV infection. *J Med Virol* 2020; **92**: 34-44 [PMID: 31429942 DOI: 10.1002/jmv.25571]
204 **Duygu F**, Karsen H, Aksoy N, Taskin A. Relationship of oxidative stress in hepatitis B infection activity with HBV DNA and fibrosis. *Ann Lab Med* 2012; **32**: 113-118 [PMID: 22389877 DOI: 10.3343/alm.2012.32.2.113]
205 **Hsieh YH**, Su IJ, Wang HC, Chang WW, Lei HY, Lai MD, Chang WT, Huang W. Pre-S mutant surface antigens in chronic hepatitis B virus infection induce oxidative stress and DNA damage. *Carcinogenesis* 2004; **25**: 2023-2032 [PMID: 15180947 DOI: 10.1093/carcin/bgh207]
206 **Severi T**, Ying C, Vermeesch JR, Cassiman D, Cnops L, Verslype C, Fevery J, Arckens L, Neyts J, van Pelt JF. Hepatitis B virus replication causes oxidative stress in HepAD38 liver cells. *Mol Cell Biochem* 2006; **290**: 79-85 [PMID: 16960659 DOI: 10.1007/s11010-006-9167-x]
207 **Zhong L**, Shu W, Dai W, Gao B, Xiong S. Reactive Oxygen Species-Mediated c-Jun NH_2-Terminal Kinase Activation Contributes to Hepatitis B Virus X Protein-Induced Autophagy via Regulation of the Beclin-1/Bcl-2 Interaction. *J Virol* 2017; **91** [PMID: 28515304 DOI: 10.1128/JVI.00001-17]
208 **Ha HL**, Yu DY. HBx-induced reactive oxygen species activates hepatocellular carcinogenesis via dysregulation of PTEN/Akt pathway. *World J Gastroenterol* 2010; **16**: 4932-4937 [PMID: 20954279 DOI: 10.3748/wjg.v16.i39.4932]
209 **Choi YM**, Lee SY, Kim BJ. Naturally Occurring Hepatitis B Virus Mutations Leading to Endoplasmic Reticulum Stress and Their Contribution to the Progression of Hepatocellular Carcinoma. *Int J Mol Sci* 2019; **20** [PMID: 30704071 DOI: 10.3390/ijms20030597]
210 **George AK**, Behera J, Kelly KE, Mondal NK, Richardson KP, Tyagi N. Exercise Mitigates Alcohol Induced Endoplasmic Reticulum Stress Mediated Cognitive Impairment through ATF6-Herp Signaling. *Sci Rep* 2018; **8**: 5158 [PMID: 29581524 DOI: 10.1038/s41598-018-23568-z]
211 **Ji C**. New Insights into the Pathogenesis of Alcohol-Induced ER Stress and Liver Diseases. *Int J Hepatol* 2014; **2014**: 513787 [PMID: 24868470 DOI: 10.1155/2014/513787]
212 **Li Y**, Xia Y, Cheng X, Kleiner DE, Hewitt SM, Sproch J, Li T, Zhuang H, Liang TJ. Hepatitis B Surface Antigen Activates Unfolded Protein Response in Forming Ground Glass Hepatocytes of Chronic Hepatitis B. *Viruses* 2019; **11** [PMID: 31027244 DOI: 10.3390/v11040386]
213 **Howarth DL**, Vacaru AM, Tsedensodnom O, Mormone E, Nieto N, Costantini LM, Snapp EL, Sadler KC. Alcohol disrupts endoplasmic reticulum function and protein secretion in hepatocytes. *Alcohol Clin Exp Res* 2012; **36**: 14-23 [PMID: 21790674 DOI: 10.1111/j.1530-0277.2011.01602.x]
214 **Li SY**, Gilbert SA, Li Q, Ren J. Aldehyde dehydrogenase-2 (ALDH2) ameliorates chronic alcohol

ingestion-induced myocardial insulin resistance and endoplasmic reticulum stress. *J Mol Cell Cardiol* 2009; **47**: 247-255 [PMID: 19344727 DOI: 10.1016/j.yjmcc.2009.03.017]
215 **Li SY**, Ren J. Cardiac overexpression of alcohol dehydrogenase exacerbates chronic ethanol ingestion-induced myocardial dysfunction and hypertrophy: role of insulin signaling and ER stress. *J Mol Cell Cardiol* 2008; **44**: 992-1001 [PMID: 18377926 DOI: 10.1016/j.yjmcc.2008.02.276]
216 **Mills KR**, Ward K, Martin F, Peters TJ. Peripheral neuropathy and myopathy in chronic alcoholism. *Alcohol Alcohol* 1986; **21**: 357-362 [PMID: 3028439]
217 **Nishitani Y**, Matsumoto H. Ethanol rapidly causes activation of JNK associated with ER stress under inhibition of ADH. *FEBS Lett* 2006; **580**: 9-14 [PMID: 16343492 DOI: 10.1016/j.febslet.2005.11.030]
218 **Sun YH**, Li YQ, Feng SL, Li BX, Pan ZW, Xu CQ, Li TT, Yang BF. Calcium-sensing receptor activation contributed to apoptosis stimulates TRPC6 channel in rat neonatal ventricular myocytes. *Biochem Biophys Res Commun* 2010; **394**: 955-961 [PMID: 20307499 DOI: 10.1016/j.bbrc.2010.03.096]
219 **Li J**, He J, Fu Y, Hu X, Sun LQ, Huang Y, Fan X. Hepatitis B virus X protein inhibits apoptosis by modulating endoplasmic reticulum stress response. *Oncotarget* 2017; **8**: 96027-96034 [PMID: 29221184 DOI: 10.18632/oncotarget.21630]
220 **Kim SY**, Kyaw YY, Cheong J. Functional interaction of endoplasmic reticulum stress and hepatitis B virus in the pathogenesis of liver diseases. *World J Gastroenterol* 2017; **23**: 7657-7665 [PMID: 29209107 DOI: 10.3748/wjg.v23.i43.7657]
221 **Ji C**. Mechanisms of alcohol-induced endoplasmic reticulum stress and organ injuries. *Biochem Res Int* 2012; **2012**: 216450 [PMID: 22110961 DOI: 10.1155/2012/216450]
222 **Li B**, Gao B, Ye L, Han X, Wang W, Kong L, Fang X, Zeng Y, Zheng H, Li S, Wu Z, Ye L. Hepatitis B virus X protein (HBx) activates ATF6 and IRE1-XBP1 pathways of unfolded protein response. *Virus Res* 2007; **124**: 44-49 [PMID: 17092596 DOI: 10.1016/j.virusres.2006.09.011]
223 **Li X**, Pan E, Zhu J, Xu L, Chen X, Li J, Liang L, Hu Y, Xia J, Chen J, Chen W, Hu J, Wang K, Tang N, Huang A. Cisplatin Enhances Hepatitis B Virus Replication and PGC-1α Expression through Endoplasmic Reticulum Stress. *Sci Rep* 2018; **8**: 3496 [PMID: 29472690 DOI: 10.1038/s41598-018-21847-3]
224 **Han H**, He Y, Hu J, Lau R, Lee H, Ji C. Disrupted ER-to-Golgi Trafficking Underlies Anti-HIV Drugs and Alcohol-Induced Cellular Stress and Hepatic Injury. *Hepatol Commun* 2017; **1**: 122-139 [PMID: 28626835 DOI: 10.1002/hep4.1030]
225 **Siddhanta A**, Radulescu A, Stankewich MC, Morrow JS, Shields D. Fragmentation of the Golgi apparatus. A role for beta III spectrin and synthesis of phosphatidylinositol 4,5-bisphosphate. *J Biol Chem* 2003; **278**: 1957-1965 [PMID: 12411436 DOI: 10.1074/jbc.M209137200]
226 **Casey CA**, Thomes P, Manca S, Petrosyan A. Giantin Is Required for Post-Alcohol Recovery of Golgi in Liver Cells. *Biomolecules* 2018; **8** [PMID: 30453527 DOI: 10.3390/biom8040150]
227 **Petrosyan A**, Casey CA, Cheng PW. The role of Rab6a and phosphorylation of non-muscle myosin IIA tailpiece in alcohol-induced Golgi disorganization. *Sci Rep* 2016; **6**: 31962 [PMID: 27535804 DOI: 10.1038/srep31962]
228 **Petrosyan A**, Cheng PW, Clemens DL, Casey CA. Downregulation of the small GTPase SAR1A: a key event underlying alcohol-induced Golgi fragmentation in hepatocytes. *Sci Rep* 2015; **5**: 17127 [PMID: 26607390 DOI: 10.1038/srep17127]
229 **Avitabile E**, Di Gaeta S, Torrisi MR, Ward PL, Roizman B, Campadelli-Fiume G. Redistribution of microtubules and Golgi apparatus in herpes simplex virus-infected cells and their role in viral exocytosis. *J Virol* 1995; **69**: 7472-7482 [PMID: 7494253 DOI: 10.1128/JVI.69.12.7472-7482.1995]
230 **Hansen MD**, Johnsen IB, Stiberg KA, Sherstova T, Wakita T, Richard GM, Kandasamy RK, Meurs EF, Anthonsen MW. Hepatitis C virus triggers Golgi fragmentation and autophagy through the immunity-related GTPase M. *Proc Natl Acad Sci USA* 2017; **114**: E3462-E3471 [PMID: 28389568 DOI: 10.1073/pnas.1616683114]

World Journal of Gastroenterology

Submit a Manuscript: https://www.f6publishing.com

World J Gastroenterol 2020 March 7; 26(9): 904-917

DOI: 10.3748/wjg.v26.i9.904

ISSN 1007-9327 (print) ISSN 2219-2840 (online)

ORIGINAL ARTICLE

Basic Study

Magnetic resonance imaging biomarkers for pulsed focused ultrasound treatment of pancreatic ductal adenocarcinoma

Ezekiel Maloney, Yak-Nam Wang, Ravneet Vohra, Helena Son, Stella Whang, Tatiana Khokhlova, Joshua Park, Kayla Gravelle, Stephanie Totten, Joo Ha Hwang, Donghoon Lee

ORCID number: Ezekiel Maloney (0000-0002-7614-4399); Yak-Nam Wang (0000-0003-0396-6057); Ravneet Vohra (0000-0001-6258-2710); Helena Son (0000-0003-1776-531X); Stella Whang (0000-0001-5893-6029); Tatiana Khokhlova (0000-0002-1711-0404); Joshua Park (0000-0002-6434-879X); Kayla Gravelle (0000-0002-9724-3134); Stephanie Totten (0000-0002-8848-4745); Joo Ha Hwang (0000-0002-7534-230X); Donghoon Lee (0000-0001-5220-3991).

Author contributions: Maloney E, Wang YN, Vorha R, Son H, Whang S, Khokhlova T, Park J, Gravelle K, and Lee D performed the majority of experiments; Maloney E, Wang YN, Vorha R, and Park J performed the majority of data analysis; Maloney E, Wang YN, and Lee D performed the majority of data interpretation; S Totten assisted Wang YN, S Whang, H Son and K Gravelle in treatment and care of the involved animals, as well as tissue processing/testing; Lee D and Hwang JH designed and coordinated the research; Maloney E wrote the initial draft of the manuscript; Maloney E and Wang YN created the figures; all authors contributed to manuscript content over multiple subsequent rounds of internal editing and revision prior to submission; all authors agreed upon the final content of the manuscript.

Supported by National Institutes of Health, National Cancer Institute, No. R01 CA188654 and No. R01

Ezekiel Maloney, Ravneet Vohra, Joshua Park, Donghoon Lee, Department of Radiology, University of Washington, Seattle, WA 98195, United States

Yak-Nam Wang, Applied Physics Laboratory, University of Washington, Seattle, WA 98195, United States

Helena Son, Stella Whang, Tatiana Khokhlova, Kayla Gravelle, Stephanie Totten, Division of Gastroenterology, University of Washington, Seattle 98195, WA, United States

Joo Ha Hwang, Division of Gastroenterology & Hepatology, Stanford University School of Medicine, Redwood City, CA 94063, United States

Corresponding author: Donghoon Lee, PhD, Research Professor, Department of Radiology, University of Washington, SLU C256, 850 Republican Street, Seattle, WA 98109, United States. dhoonlee@uw.edu

Abstract

BACKGROUND

The robust fibroinflammatory stroma characteristic of pancreatic ductal adenocarcinoma (PDA) impedes effective drug delivery. Pulsed focused ultrasound (pFUS) can disrupt this stroma and has improved survival in an early clinical trial. Non-invasive methods to characterize pFUS treatment effects are desirable for advancement of this promising treatment modality in larger clinical trials.

AIM

To identify promising, non-invasive pre-clinical imaging methods to characterize acute pFUS treatment effects for *in vivo* models of PDA.

METHODS

We utilized quantitative magnetic resonance imaging methods at 14 tesla in three mouse models of PDA (subcutaneous, orthotopic and transgenic - *KrasLSL-G12D/+*, *Trp53LSL-R172H/+*, *Cre* or "KPC") to assess immediate tumor response to pFUS treatment (VIFU 2000 Alpinion Medical Systems; 475 W peak electric power, 1 ms pulse duration, 1 Hz, duty cycle 0.1%) *vs* sham therapy, and correlated our results with histochemical data. These pFUS treatment parameters were previously shown to enhance tumor permeability to chemotherapeutics. T1 and T2 relaxation maps, high (126, 180, 234, 340, 549) *vs* low (7, 47, 81) *b*-value apparent diffusion coefficient (ADC) maps, magnetization transfer ratio (MTR)

CA154451.

Institutional animal care and use committee statement: All animal experiments were conducted in accordance with policies of the NIH Guide for the Care and Use of Laboratory Animals and the Institutional Animal Care and Use Committee (IACUC) of the University of Washington. Specific protocols used in this study were approved by the University of Washington IACUC (approved protocols are: "4210-01: MR Methods for Small Animal Imaging" and "4242-05: Enhanced chemotherapeutic drug delivery by High Intensity Focused Ultrasound").

Conflict-of-interest statement: All other authors have nothing to disclose.

ARRIVE guidelines statement: The authors have read the ARRIVE guidelines, and the manuscript was prepared and revised according to the ARRIVE guidelines.

Manuscript source: Unsolicited manuscript

Received: November 17, 2019
Peer-review started: November 17, 2019
First decision: December 23, 2019
Revised: January 12, 2020
Accepted: February 15, 2020
Article in press: February 15, 2020
Published online: March 7, 2020

P-Reviewer: Huang LY, Mastoraki A
S-Editor: Ma YJ
L-Editor: A
E-Editor: Ma YJ

maps, and chemical exchange saturation transfer (CEST) maps for the amide proton spectrum (3.5 parts per million or "ppm") and the glycosaminoglycan spectrum (0.5-1.5 ppm) were generated and analyzed pre-treatment, and immediately post-treatment, using ImageJ. Animals were sacrificed immediately following post-treatment imaging. The whole-tumor was selected as the region of interest for data analysis and subsequent statistical analysis. *T*-tests and Pearson correlation were used for statistical inference.

RESULTS
Mean high-*b* value ADC measurements increased significantly with pFUS treatment for all models. Mean glycosaminoglycan CEST and T2 measurements decreased significantly post-treatment for the KPC group. Mean MTR and amide CEST values increased significantly for the KPC group. Hyaluronic acid focal intensities in the treated regions were significantly lower following pFUS treatment for all animal models. The magnetic resonance imaging changes observed acutely following pFUS therapy likely reflect: (1) Sequelae of variable degrees of microcapillary hemorrhage (T1, MTR and amide CEST); (2) Lower PDA glycosaminoglycan content and associated water content (glycosaminoglycan CEST, T2 and hyaluronic acid focal intensity); and (3) Improved tumor diffusivity (ADC) post pFUS treatment.

CONCLUSION
T2, glycosaminoglycan CEST, and ADC maps may provide reliable quantitation of acute pFUS treatment effects for patients with PDA.

Key words: Pancreatic adenocarcinoma; Multiparametric magnetic resonance imaging; Focused ultrasound

Core tip: In a genetic model of pancreatic ductal adenocarcinoma, clinically translatable, quantitative magnetic resonance imaging methods of T2, glycosaminoglycan chemical exchange saturation transfer, and apparent diffusion coefficient mapping were effective in non-invasively characterizing the treatment effects of pulsed focused ultrasound treatment. Pulsed focused ultrasound treatment has already been shown to improve survival for patients with pancreatic ductal adenocarcinoma in an early clinical trial, and these complimentary magnetic resonance imaging methods could help to advance this promising therapy in larger clinical trials.

Citation: Maloney E, Wang YN, Vohra R, Son H, Whang S, Khokhlova T, Park J, Gravelle K, Totten S, Hwang JH, Lee D. Magnetic resonance imaging biomarkers for pulsed focused ultrasound treatment of pancreatic ductal adenocarcinoma. *World J Gastroenterol* 2020; 26(9): 904-917
URL: https://www.wjgnet.com/1007-9327/full/v26/i9/904.htm
DOI: https://dx.doi.org/10.3748/wjg.v26.i9.904

INTRODUCTION

Pancreatic cancer is the fourth leading cause of cancer-related deaths in the United States[1]. Pancreatic ductal adenocarcinomas (PDAs) have a robust fibroinflammatory stroma and a dense extracellular matrix that accumulates water molecules in a poorly mobile, gel-fluid phase[2]. In combination, these features result in a high interstitial fluid pressure (IFP; approximately 99 mmHg *vs* 10.4 in normal pancreas) that collapses tumor vasculature and impedes therapeutic drug delivery[2-4]. Glycosaminoglycans produced by PDA tumor cells are often present at exceedingly high concentrations in the tumor interstitium, and their presence correlates with high IFP. In a genetic mouse model of PDA, pulsed focused ultrasound (pFUS) therapy has disrupted the tumor stroma and improved delivery of chemotherapy to the tumor[4,5]. A recent phase 1 clinical trial of pFUS therapy in combination with chemotherapy doubled median overall survival in patients with inoperable PDA *vs* chemotherapy

alone[6]. In clinical trials and in clinical practice, both the time and invasiveness required to assess treatment efficacy are critical considerations for the majority of patients with PDA who have rapidly progressive, non-surgical disease in a highly sensitive anatomic area. Quantitative magnetic resonance imaging (MRI) assessments at 14 tesla (T) have previously been shown to correlate well with the degree of PDA fibrosis in preclinical models[7]. In this study, our objective was to identify non-invasive MRI methods that can be used to assess pFUS treatment effects for PDA, based on data derived from three murine models of PDA, including a genetic model. These methods have translational relevance to future, larger clinical trials that might help to advance pFUS therapy as a valuable supplement to traditional treatment modalities for patients with PDA.

MATERIALS AND METHODS

Animal models

All animal studies were approved by the Institutional Animal Care and Use Committee of the University of Washington. The animal protocol was designed to minimize pain or discomfort to the animals included in our study. Subcutaneous, orthotopic, and genetic murine models of PDA were employed. We used the *KrasLSL-G12D/+*, *Trp53LSL-R172H/+*, *Cre* (KPC) genetic PDA mouse model[8]. KPC animals conditionally express endogenous mutant *Kras* and point mutant *Trp53* alleles, spontaneously develop PDA, and closely mimic the pathophysiology and molecular progression of the human disease[8]. All mice were housed in an specific pathogen free, controlled environment (14 h/10 h light/dark cycle, 73.5 ± 5 °F) with ad libitum access to tap water and chow. We used previously described methods to develop orthotopic models[7,9]. Briefly, 8-10 wk old, immunocompetent mixed *129/SvJae/C57Bl/6* mice were anesthetized and, following sterile preparation, a 2 cm incision was made along the left flank to access the tail of the pancreas. One million cells derived from KPC liver metastases, suspended in 50 microliters of Matrigel (Corning Incorporated), were injected into the pancreatic tail. The incision was sutured closed and the animal was recovered. For subcutaneous models, the same cell suspension was injected at the left flank, near the hindlimb. At 12-14 wk old, all animal models underwent weekly tumor burden monitoring with direct palpation and diagnostic ultrasound (US). Animals were enrolled in the study when their primary tumor mass was ≥ 5 mm in greatest diameter. Six KPC animals, 6 orthotopic model animals, and 6 subcutaneous model animals were enrolled and underwent the MRI and pFUS treatment protocols. Between 3 and 5 additional animals for each tumor model underwent the same MRI protocol, but with sham treatment. The size of each experimental group was previously approved by the National Institutes of Health funding agency, based on result from prior similarly designed studies, to ensure reasonable ability to detect any meaningful data trends in this early phase research.

MRI protocol

Our group has previously used quantitative MRI methods at 14T magnet strength to characterize both untreated PDA tumors in subcutaneous, orthotopic, and KPC models, as well as enzymatically treated PDA tumors in KPC models[7,10]. Similar quantitative methods were employed in the current study for in-vivo assessments on a 14T Avance 600 MHz/89 mm wide-bore vertical MR spectrometer with a microimaging accessory (Bruker BioSpin corp., Bellerica, MA, United States) using a ^{1}H radiofrequency birdcage coil and coil holder with 25 mm inner diameter. Quantitative MRI parameter acquisition methods are detailed in Table 1. The water saturation shift referencing approach to chemical exchange saturation transfer (CEST) imaging has also been used by other laboratories at 3-9.4 T magnet strength for pre-clinical applications, including murine tumor model imaging, with reliable quantitative results[11-13].

As previously described, animals were anesthetized, lubricant was applied to their eyes, they were placed into a radiofrequency coil and secure custom cradle that was inserted vertically into the thermally-regulated (32 °C) magnet bore[7]. An adjustable isoflurane gas/vacuum system was used to maintain appropriate sedation throughout the experiments. The animals' respiratory rates were monitored continuously for the approximately 60 min scan time via abdominal sensor (SA Instruments Inc., Stony Brook, NY). A baseline MRI assessment was performed for each animal within 1.5 wk of enrollment and 48 h prior to pFUS or sham therapy. Immediately post-therapy, animals underwent a follow-up MRI assessment. Animals were sacrificed for histochemical analysis after being removed from the scanner at the conclusion of the follow-up MRI.

Table 1 14T magnetic resonance imaging parameter acquisition methods

Method	Sequence type	TR/TE (ms)	Comments
T1	RARE	5500, 3000, 1500, 1000, 385.8/9.66	NA = 1; FOV = 30 mm × 30 mm; rare factor = 2, matrix size = 256 × 128 (reconstructed phase encoding steps = 128; acquisition phase encoding steps = 96); yielding spatial resolution of 0.117 × 0.234 mm/pixel. Approximately 9 min acquisition time.
T2	MSME, fat suppressed	4000/twelve echoes equally spaced from 6.28 to 75.4	NA = 1; FOV = 30 mm × 30 mm; matrix size = 256 × 128 (reconstructed phase encoding steps = 128; acquisition phase encoding steps = 91); spatial resolution of 0.117 × 0.234 mm/pixel. 10 contiguous slices were acquired with respiration gating to cover the entire abdomen. Approximately 6 min acquisition time.
ADC	EPI	2500/17.7	Echo train length = 16; Pulse duration = 3.0 ms; Diffusion time = 7.46 ms; NA = 1; FOV = 30 × 30 mm^2; matrix size = 128 × 128; spatial resolution of 0.234 × 0.234 mm/pixel; 8 *b* values (7, 47, 81, 126, 180, 234, 340, 549) s/mm^2. 10 contiguous slices were acquired to cover the entire abdomen. Approximately 2 min 40 s acquisition time.
CEST	(1) RARE	(1) 2200 / 7	(1) Center frequency estimate: Continuous-wave block saturation pulse with B1 = 3 μT and duration = 1 s; 25 frequency offsets from -360 Hz to 360 Hz with an interval of 0.5 ppm (WASSR approach). FOV = 30 mm x 30 mm; Matrix size = 128 x 128; Flip angle = 180°; NA = 1. A single, 1 mm slice delineating the tumor was acquired.
	(2) RARE	(2) 5000 / 7	(2) Frequency shift saturation: 14 frequency offsets at ± 0.5, ± 1.0. ± 1.5, ± 2.0, ± 2.5, ± 3.0, ± 3.5 ppm were acquired through the same single slice using respiration gating with an off-resonance radiofrequency pulse applied for 1 s at a power of 3 μT. Matrix = 128 × 128 (reconstructed phase encoding steps = 128; acquisition phase encoding steps = 96); FOV = 30 mm × 30 mm; rare factor = 8.
	(3) RARE	(3) 5000 / 7	(3) Control image: A control image was acquired through the same slice using the same settings as #2, except with saturation offset at 300 ppm. Approximately 30 min total acquisition time.
MTR	GRE	625 / 2	Flip angle = 30°; off-resonance frequency 7000 Hz; saturation pulse block pulse shape = 50 ms width and 10 μT amplitude; FOV = 30 mm × 30 mm; matrix size = 256 × 256; spatial resolution of 0.117 x 0.117 mm/pixel. 10 contiguous images were acquired to cover the entire abdomen. Approximately 3 min acquisition time.

ADC: Apparent diffusion coefficient; CEST: Chemical exchange saturation transfer; MTR: Magnetization transfer ratio.

MRI quantitative map creation and data analysis

Raw MR images were processed for map creation using Image-J software (Rasband, W.S., ImageJ, United States National Institutes of Health, Bethesda, ML, http://imagej.nih.gov/ij, 1997-2012)[14]. T1 and T2 relaxation maps were generated from T1 and T2 weighted images. Apparent diffusion coefficient (ADC) maps were generated using a mono-exponential model: Sb/S0 = exp(-b·ADC). Sb represents the MRI signal intensity with diffusion weighting b and S0 represents the non-diffusion-weighted signal intensity. A bi-exponential model was also used to estimate intra voxel incoherent motion (IVIM) related parameters of perfusion fraction (or pseudo-diffusion) and diffusion[15]. The 3 lowest b values (7, 47, and 81 s/mm^2) were used to calculate perfusion / pseudo-diffusion component, and the remaining higher 5 *b* values (126, 180, 234, 340, 549 s/mm^2) were used to calculate the tissue diffusivity parameter. Magnetization transfer ratio (MTR) maps were generated using: (SI0–SIs)/SI0, where SI0 represents the tissue signal intensity prior to application of the saturation pulse, and SIs represents the tissue signal intensity during the saturation pulse application. CEST maps were generated for the amide proton using: [Ssat (-3.5 ppm) - Ssat (3.5 ppm)]/S0, where S0 and Ssat are the water signal intensities measured prior to the saturation pulse, and during the water saturation pulse, respectively. For the glycosaminoglycan spectrum (gagCEST), maps were generated using a similar calculation for the 0.5, 1.0 and 1.5 ppm frequency shifts. Summative saturation sampled at these shifts has previously been validated in human cartilage for quantification of glycosaminoglycans[16], and is representative of the spectral signal observed in prior 7T MRI studies of glycosaminoglycan phantoms[17], as well as our own phantom studies at 14T[10]. Ultimately, CEST measurements were not performed in the subcutaneous mice due to the difficulty in properly performing the shimming process for these animals. A susceptibility change near the interface between a subcutaneous tumor and air often precluded adequate shimming and tumor signal suppression.

pFUS treatment protocol and cavitation quantitation

Animals were anesthetized and the abdomen was shaved, depilated, and wiped with isopropyl alcohol to decrease risk of cavitation at the skin surface. Animals were then mounted to a custom holder capable of 3 dimensional movement for positioning during treatment, and partially submerged in a 37 °C, transparent water tank, where respiratory rate could be constantly visually monitored during continuous anesthesia throughout the experiment. pFUS treatments were performed under US guidance with an Alpinion VIFU 2000 small animal system. A 1.5 MHz focused US transducer with a 64 mm aperture and 45 mm radius of curvature was mounted to the side of the water tank[18]. A miniature flat passive cavitation detector (Panametrics XMS-310; Olympus, Waltham, Mass) was positioned at the side of the transducer and aligned to detect broadband emissions from inertially collapsing bubbles in the focal area during each FUS pulse. The passive cavitation detector was 3 mm in aperture, with the frequency band of 6.3-14.2 MHz at a 6-dB level. The signals received by the passive cavitation detector were amplified by 20 dB (Panametrics PR5072; Olympus) and recorded by using a digital oscilloscope[19]. The US imaging probe employed a C4-12 phased array, with center frequency 7 MHz (Alpinion Medical Systems). The tumor was identified as a predominantly hypoechoic mass, typically in the epigastrium or along the left paracolic gutter adjacent to the spleen. Assessment was made for an appropriate acoustic treatment window that was free of intervening loops of bowel or significant vasculature. For the KPC animal cohort, whose tumors were less commonly superficial, the presence of an appropriate treatment window always determined whether the animal would receive pFUS *vs* sham treatment. For the orthotopic and subcutaneous model cohorts, receipt of sham *vs* pFUS treatment was randomized.

Exposure parameters were: Peak electric power 475 watts, pulse duration 1 ms, pulse repetition frequency 1 Hz, duty cycle 0.1%. The focal spot was raster-scanned throughout the acoustically accessible volume of the tumor with a step size of 1 mm, and 60 pulses were delivered at each focal spot. These parameters were previously shown to enhance tumor permeability to chemotherapeutics[4]. Cavitation activity was quantitated based on broadband noise emission as previously described[18]. Sham treatment animals remained submerged in the water tank under anesthesia for the same duration of time required to deliver the pFUS therapy, but did not receive the therapy. At the completion of the pFUS or sham treatment session (approximately 20 min duration), while maintaining anesthesia, animals were removed from the water tank, dried, and placed on a warming pad for transport to the adjacent MRI suite and follow-up imaging. At the end of the study, the animals were immediately euthanized according to approved procedures for the collection of biological samples.

Histology and biochemistry

Tumors were excised and embedded in an optimum cutting temperature medium. Three serial 5 micrometer sections were cut every 1 mm through the entire tumor (CM1950, Leica, Bannockburn, IL, United States). Tissue between the section steps was collected for biochemical analysis. Samples taken for biochemical analysis were evaluated for sulfated glycosaminoglycans (sGAG) and hyaluronan (HA) using commercial assays (Blyscan™ for sGAG and Purple-Jelley for HA, Biocolor Ltd., United Kingdom).

Tissue sections were stained with Hematoxylin and Eosin (H&E), Masson's trichrome for connective tissue and for HA using a HA binding protein (HABP, Millipore Sigma, Burlington, MA, United States). Sections were examined using a Nikon Eclipse 80i light microscope (Nikon, Melville, NY, United States) and whole slide images were captured for image analysis with a 10 × objective lens using the same settings for each type of stain. Fibrotic tissue, identified by blue staining in the Masson's trichrome stained sections was quantified using methods described previously. For quantification of the HABP stained sections, a random grid of circular regions of interest (ROIs) were placed on each slide. Two random numbers were generated with the first number designating the offset ROI and the second number indicating the sampling number for the ROI selection resulting in several ROIs being evaluated per section. New random numbers were generated for each section. For each ROI selected, the mean intensity was measured ImageJ (ImageJ 1.42 National Institutes of Health, Bethesda, MD, United States). Data was separated into three groups: background (no tissue), non-treated tumor tissue, and FUS treated tissue. FUS treated tissue was identified and confirmed by looking at H&E stained serial sections.

Statistical analysis

For all quantitative maps, the whole tumor that was visible on each analyzed slice was selected as the ROI, and mean quantitative values were recorded for each slice analyzed. On T1, T2, MTR, and ADC maps, this involved selection of 3 separate slices that included the tumor, and the area of the tumor that was ultimately treated for animals who underwent pFUS therapy, on both baseline and follow up MRI exams. The average of the 3 values generated from these slices was used as the single parameter value for the corresponding animal at each point in time. Since CEST maps were only generated for a single slice through the tumor, only 1 whole tumor ROI was used to estimate this parameter at each point in time for the primary analysis comparing pre and post-treatment maps. A secondary analysis of the gagCEST maps using only the follow-up MRI examination maps was performed for the KPC cohort. This secondary analysis method also closely mirrored our histochemical analysis, which was limited to the follow-up time point. In the secondary MRI analysis, an ROI was drawn to select the treated region of the tumor, and a second ROI was drawn to select an untreated region for comparison. For the histological samples, the mean intensities from the treated and untreated ROIs of each tumor were calculated for comparison.

Paired *t*-tests were performed using Microsoft Excel software (Redmond, WA, United States) to compare baseline and follow-up whole-tumor ROI quantitations and to compare treated-tumor *vs* untreated-tumor ROIs. Unpaired t-tests were performed to compare treated and sham treated mice. Statistical significance was assigned to P values less than 0.05. To compare gagCEST values obtained from CEST maps to sGAG values obtained from biochemical analysis, the correlation coefficient (r) was determined using Pearson correlation analysis using StatPlus software (AnalystSoft Inc. Walnut, CA, United States) in Microsoft Excel. Statistical review of the study was performed by a biomedical statistician employed at the University of Washington.

RESULTS

At enrollment into the study the animals had a good body condition score with an average age (± SD) and weight (± SD) of 179 ± 35 d and 26.3 ± 2.8 g respectively. Cavitation activity was achieved in all three murine PDA models and all acquired data from all animals in each group were included in the analysis, with the exception of erroneous amide CEST data from 2 pFUS treated KPC animals and all CEST data from 1 pFUS treated orthotopic animal. No adverse events, such as skin burns or unexpected morbidity/mortality, were observed. Quantitative MRI map analysis results from the pFUS treated animal cohorts are presented in Table 2. Following pFUS treatment (Figure 1), mean high-*b* value ADC values increased significantly for all animal models, and this increase was most pronounced in the KPC model (Figure 2A and B). Mean gagCEST and T2 values decreased significantly post-treatment only

for the KPC group (Figure 2C and D). Mean MTR and amide CEST values increased significantly for the KPC group. Treated areas demonstrated predominantly isointense signal on proton density weighted images, in some instances with an associated peripheral ring of hypointense signal (Figure 1C and F). Overall, there was no significant difference in mean tumor T1 relaxation time values. Parameters tested were otherwise not significantly changed post-pFUS treatment in all three murine PDA models. There were no significant differences in any parameters tested for the sham group animals. There was greater variability within these paired data groups, likely related to their smaller group size, but on review of individual parameter data obtained from each sham animal, no consistent trends were evident between the two timepoints.

There was no statistical difference in HA or sGAG concentration between KPC or orthotopic mice. HA and sGAG mean tissue concentrations were found to be lower in all of the pFUS-treated animals *vs* sham-treatment controls, but these differences were not statistically significant (Figure 3A). The evaluation of the regional concentrations of HA using HABP, showed that the treated regions had significantly lower mean HA labelling intensity in the treated regions compared to the non-treated regions for all animal models (Figure 3B and C). The HA intensities were similar for the KPC and orthotopic mice and lower for the subcutaneous mice (Figure 3B). There was no statistical difference in the mean collagen concentration in the treated region vs the non-treated regions or the sham treated mice.

There was a strong positive correlation between the HA concentrations (as determined by the biochemical assay) and the gagCEST measurements (Figure 4) for the orthotopic (correlation coefficients: 0.72 treated; 0.74 sham) and KPC mice (correlation coefficient: 0.60 treated). There were not enough values to evaluate any correlation for the sham treated KPC mice.

DISCUSSION

T1, MTR and amide CEST

Variable changes in T1 relaxation, and significantly increased MTR and amide CEST signals post-pFUS-treatment most likely represent sequelae of hyperacute hemorrhage from microcapillary vessels. T1 weighted images combined with susceptibility weighted images (SWI) are standard of care for hemorrhage detection and characterization. At the hyperacute time point, T1 weighted images of hemorrhage are typically isointense, and thus would contribute a variable amount of signal to the values generated, as we observed. Amide proton imaging has recently been shown to be even more sensitive and specific for detection and characterization of intracranial hemorrhage than SWI, including at the hyperacute timepoint[20]. Since the broad spectrum of the MTR asymmetry signal includes the region of the amide proton at 3.5 ppm, the increased values from both of these maps would not be surprising in the context of acute hemorrhage.

There are additional factors that also might contribute, in part, to these signal changes. Tumor metabolites such as glucose (3.83 ppm), taurine (3.27 ppm) and ethanolamine (3.13 ppm) are known to be upregulated in PDA, and these could potentially also contribute signal near the amide proton 3.5 ppm frequency shift[21]. However, given the short amount of time that elapsed between pFUS treatment and post-treatment MRI characterization (approximately 15 min), a significant change in the concentration of these metabolites is unlikely. MTR values have also previously been shown to have a positive correlation with the degree of fibrosis in murine PDA tumor models[7,22]. Since the pFUS protocol we employed for our treatments is known to disrupt the collagenous tumor stroma[4], as was observed on Masson's trichrome stains in our study, the signal increase observed on MTR maps post-pFUS is unlikely to be representative of this change. Rather, the signal likely derived from microcapillary hemorrhage at the amide proton portion of the MTR spectrum appears to have dominated MTR values at this time point.

gagCEST, T2 and ADC

Significant decreases in gagCEST and T2 relaxation may represent disruption of glycosaminoglycans within the tumor stroma and associated liberation of complexed water molecules from the gel-fluid phase. This, in combination with disruption of the collagenous matrix, could lead to decreased intra-tumoral IFP and increased diffusivity within the tumor microenvironment[2]. This theory is supported by our quantitative immunohistochemistry results – demonstrating a trend of lower HA and sGAG concentrations on average in pFUS-treated animals *vs* sham treated controls. Although multiple species of sulfated (*e.g.*, chondroitin sulfate) and unsulfated (*e.g.*,

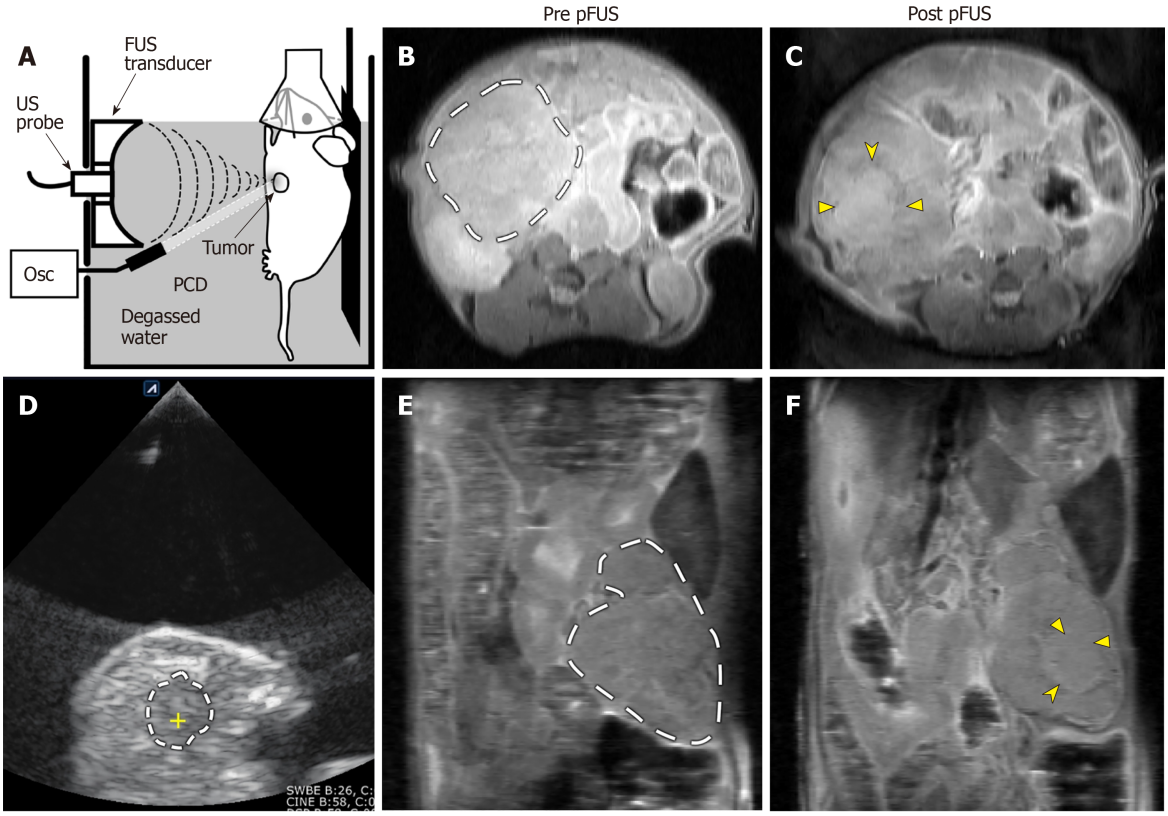

Figure 1 Representative images of pulsed focused ultrasound treatment and 14T magnetic resonance imaging assessment. (A) Sagittal plane line drawing and (D) axial plane ultrasound (US) image of a pulsed focused ultrasound (pFUS) treatment. Animals were anesthetized, placed on a mobile platform, and partially submerged in degassed water. Tumors were identified using B-mode images from a diagnostic US probe. The KPC mouse tumors generally appear as predominantly hypoechoic masses along the distribution of the pancreas (dashed line in D; the yellow cross within marks the focus of the pFUS transducer). Axial (B and C) and coronal (E and F) pre- and post-treatment proton density weighted anatomic images from a different KPC mouse. Dashed lines in B and E demarcate the pancreatic tumor mass. The treated area demonstrates predominantly isointense signal (solid arrowheads in C and F), with a peripheral ring of hypointense signal (notched arrowheads in C and F), most likely representing sequelae of hyperacute hemorrhage. pFUS: Pulsed focused ultrasound; SC: Subcutaneous; Osc: Oscilloscope; PCD: Passive cavitation detector.

HA) glycosasminoglycans are commonly overexpressed in the PDA microenvironment, the HA subtype exerts the dominant effect on IFP[2,23]. Previous phantom imaging experiments by our group, employing a range of relevant concentrations of both chondroitin sulfate and HA, have demonstrated that HA produces a significantly stronger signal on gagCEST imaging at 14T compared to CS, even at 10 fold lower concentrations (*e.g.*, an area under the MTR asymmetry curve of 7.5 for a 0.01% aqueous HA resuspension, *vs* 1.6 for a 0.1% aqueous chondroitin sulfate resuspension)[10]. In addition, we have previously shown that targeted depletion of HA via a systemic enzymatic therapy results in decreased gagCEST signal in KPC mice[10]. These findings support the theory that the signal changes observed post-pFUS treatment on the gagCEST sequence are driven by changes induced in HA concentrations.

There are other, less likely considerations that might explain, or at least contribute to the observed changes in gagCEST signal. Nuclear Overhause Effects (NOE) can spuriously contribute to CEST signal at any portion of the spectrum, and are known to be more prevalent at higher magnet strengths, however we employed high saturation power (3.0 μT) to minimize this potential confounding influence on the signal we obtained.

PDA typically demonstrates restricted diffusion (at or below an arbitrary, sometimes clinically used ADC threshold of 1×10^{-3} mm^2/s), and this is most consistently demonstrated clinically with b values between 500 and 1000[24]. The degree of restriction has been inconsistently correlated with fibrotic content, histopathologic grade, and tumor stage[24]. The degree of restriction may correlate with greater HA content in PDA tumors, given the known positive correlation between HA content and IFP in these tumors[2]. We did not detect such a correlation between whole-tumor HA content and ADC values in the animals we studied. However, there was small variability in the whole-tumor HA content of the animals included in our study, and this limited our ability to detect such a correlation. The limited variability

Table 2 Magnetic resonance imaging quantitative map results pre and post focused ultrasound treatment for three mouse models of pancreatic ductal adenocarcinoma

	Pre-pFUS	Post-pFUS	Difference	*P* value
High-b ADC (10^{-3} mm^2/s)				
KPC	1.0 ± 0.33 (n = 6)	3.32 ± 0.61 (n = 6)	2.32 ± 0.60	**0.01**
Ortho	0.72 ± 0.07 (n = 6)	1.15 ± 0.15 (n = 6)	0.43 ± 0.13	**0.02**
SC	0.97 ± 0.21 (n = 6)	1.80 ± 0.14 (n = 6)	0.83 ± 0.27	**0.03**
GagCEST (%)				
KPC[1]	25.89 ± 3.10 (n = 6)	10.61 ± 3.09 (n = 6)	-15.28 ± 2.67	**2.2×10^{-3}**
Ortho	20.83 ± 4.02 (n = 5)	20.04 ± 5.34 (n = 5)	-0.79 ± 6.41	0.91
Amide CEST (%)				
KPC	10.37 ± 2.76 (n = 4)	24.89 ± 5.17 (n = 4)	14.52 ± 2.89	**0.01**
Ortho	4.11 ± 1.25(n = 5)	4.79 ± 1.64 (n = 5)	0.68 ± 1.99	0.29
MTR (%)				
KPC	38.15 ± 4.17 (n = 6)	59.80 ± 1.46 (n = 6)	21.65 ± 2.96	**7.5×10^{-4}**
Ortho	53.92 ± 7.20 (n = 6)	60.91 ± 3.39 (n = 6)	6.99 ± 6.33	0.32
SC	58.1 ± 7.01 (n = 6)	60.50 ± 7.85 (n = 6)	2.40 ± 7.22	0.75
T2 (ms)				
KPC	39.38 ± 2.32 (n = 6)	34.41 ± 1.93 (n = 6)	-4.97 ± 1.37	**0.02**
Ortho	32.74 ± 1.12 (n = 6)	31.91 ± 0.89 (n = 6)	-0.83 ± 1.54	0.62
SC	44.52 ± 8.97 (n = 6)	32.77 ± 1.67 (n = 6)	-11.75 ± 10.08	0.30
T1 (ms)				
KPC	986.95 ± 236.99 (n = 6)	847.69 ± 255.94 (n = 6)	-139.26 ± 314.92	0.68
Ortho	453.62 ± 116.72 (n = 6)	618.10 ± 183.85 (n = 6)	164.48 ± 194.29	0.44
SC	508.82 ± 192.64 (n = 6)	1032.44 ± 293.46 (n = 6)	523.62 ± 255.40	0.10

Pre and post treatment quantitative values are presented as mean ± SE from the mean. Paired t-tests were used to generate P-values, and values < 0.05, considered significant, are in bold.

[1]Post-hoc secondary analysis, performed to compare the pre and post-treatment KPC groups with gagCEST maps, that employed within-tumor regions of interest (ROIs) rather than whole tumor ROIs, as detailed in the text, generated mean gagCEST values (%) of 25.20 ± 4.63 pre-treatment *vs* 7.71 ± 2.22 post-treatment, for a difference of -17.49 ± 3.07, $P = 6.7 \times 10^{-3}$. pFUS: Pulsed focused ultrasound treatment; ADC: Apparent diffusion coefficient; KPC: Genetic mouse model; Ortho: Orthotopic; SC: Subcutaneous; gagCEST: Glycosaminoglycan chemical exchange saturation transfer; MTR: Magnetization transfer ratio.

in whole-tumor HA content in our animal cohort is likely explained by two factors: (1) We recruited animals into the study when their tumors reached a similar size, and tumor HA content has been shown in a recent clinical series to correlate with tumor size[25]; and (2) For animals undergoing pFUS treatment, the area of treatment, as judged by changes evident on whole-tumor immunohistochemistry slides, involved less than approximately 20% of the overall tumor volume.

It is interesting that a statistically significant decrease in gagCEST and T2 values was only observed in the KPC animal cohort. The gagCEST values correlated well with the total HA concentration in the treated KPC mice and both the treated and sham treated orthotopic mice. When looking at the localized concentrations of HA in the treated tumors, there was a significant decrease in HA in the treated area compared to the surrounding non-treated area. The decrease in HA could potentially result in a decrease in IFP in these regions given the positive correlation between the two[2]. However, this would need to be confirmed experimentally.

Limitations

Limitations of this study include the fact that the whole tumor was selected as the ROI for the primary a priori MR analysis plan. In the treated animals this combined the signal coming from the treated and non-treated regions of the tumor, and decreased our sensitivity for detecting significant treatment effects on tumor signal. This approach was chosen due to the difficulty in determining the precise treatment effect margins on MRI for every tumor treated on any given sequence, which we had encountered in prior experiments with this tumor model. While the general area of treatment could in all cases be identified by correlation between US treatment images and variable changes on T1 and T2 anatomic imaging during MRI scanning, treatment signal effect margins were often ill-defined. Non-standardized, potentially error prone ROI selection in the area of treatment signal changes would have introduced

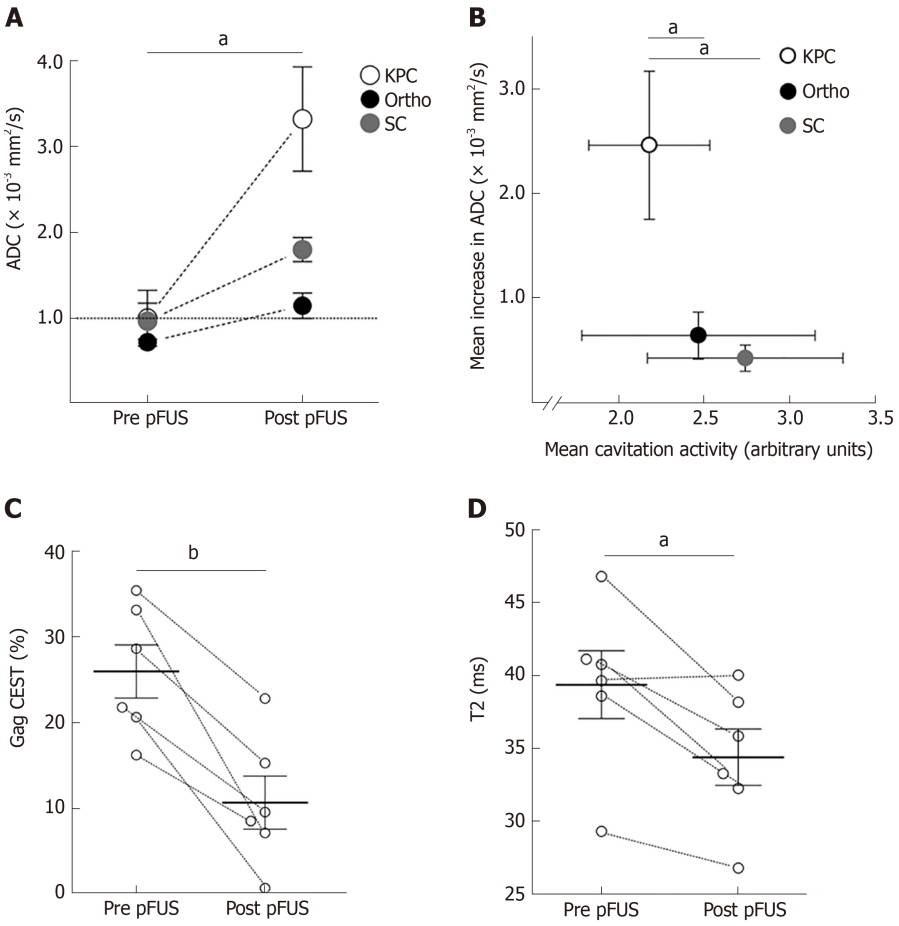

Figure 2 14T magnetic resonance imaging parameter changes due to pulsed focused ultrasound treatments. A: There was significant increase in mean apparent diffusion coefficient (ADC) quantitation for all three murine pancreatic ductal adenocarcinoma models (n = 6 in each group). The horizontal dotted line at ADC = 1 demarcates a frequently used clinical threshold for "restricted" diffusion; B: Cavitation was successfully achieved in all treated animals. On average, cavitation activity tended to be lower in the KPC animals, yet the absolute increase in ADC values for these animals was significantly higher than the other two models post-pulsed focused ultrasound (pFUS) treatment; C and D: GagCEST (C) and T2 (D) quantifications in KPC animals revealed significant decrease in mean values (solid horizontal lines) post-pFUS treatment (n = 6). There was no significant change in these parameters in the other tumor models. [a]P < 0.05; [b]P < 0.01. ADC: Apparent diffusion coefficient; pFUS: Pulsed focused ultrasound; Ortho: Orthotopic; KPC: Genetic mouse model; SC: Subcutaneous.

too great a risk of excluding meaningful data and including irrelevant data in the primary analysis for our relatively small cohort. Whole tumor ROI selection allowed for standard, reliable methodology across all tumor models. Nonetheless, we chose to perform one post-hoc secondary analysis attempting within-tumor ROI selections for the gagCEST sequence in the KPC animals. This was done to compare background tumor *vs* the treated area at a single time point immediately post treatment, to most closely mimic our histologic within-tumor gag quantitative methods. The result of this secondary analysis was consistent with the whole-tumor ROI analysis that compared data from two separate time-points (pre-treatment *vs* immediately post-treatment) – both demonstrated a significant reduction in gagCEST post pFUS treatment.

Subject motion and bowel peristalsis / motion within the abdomen are also inherent limitations of abdominal MRI examinations, and are particularly challenging in small animal models such as ours. Although we attempted to mitigate this effect by continuously monitoring subject respiratory rate throughout image acquisition and use of respiratory gating within sequence protocols, some signal degradation was still observed on longer sequence acquisitions. This was most commonly seen in the highest b value subcomponents of the ADC maps, and likely explains the observed range of ADC quantitations that at times reach supra-physiologic values. Future studies in larger animal models, or as part of human trials, might achieve larger or more significant differences in the measurements evaluated by employing protocol design to mitigate these effects. In addition, we only evaluated a single time point, immediately post-therapy, to optimize our correlation with histopathologic results. Further study of T2, gagCEST and ADC at additional post-treatment time points in

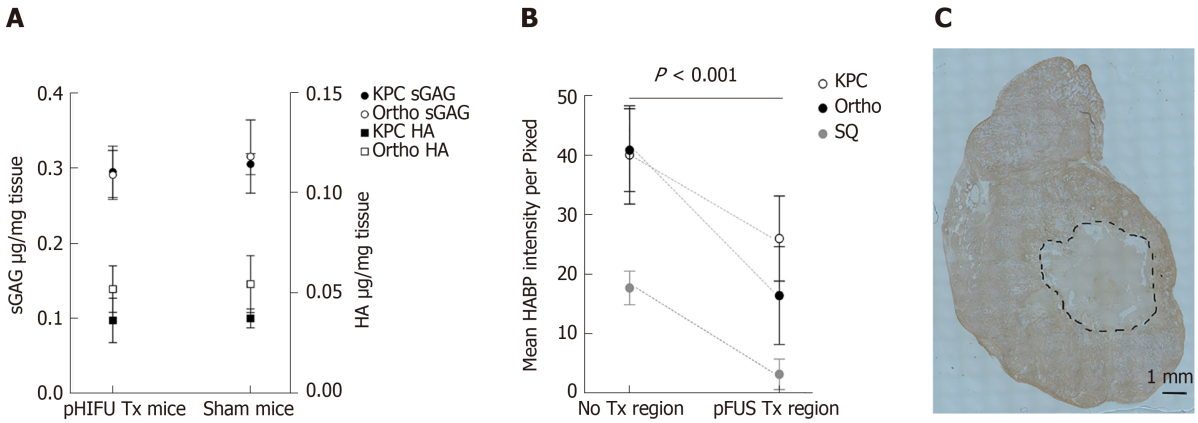

Figure 3 Histochemical and biochemical parameter changes due to pulsed focused ultrasound treatments. A: Hyaluronic acid (HA) and sulfated glycosaminoglycan concentrations in treated and sham treated KPC and orthotopic mice; B: HA intensities in treated and non-treated regions of the tumor in KPC, orthotopic, and subcutaneous models; C: Representative histological image of HA binding protein stained section for a KPC mouse. The treated region is outline by a dashed line. KPC: Genetic mouse model; Ortho: Orthotopic; HA: Hyaluronic acid.

survival studies would help to determine the optimal interval for post-treatment imaging and further elucidate the prognostic value of our results.

Conclusions

The use of a non-invasive technique such as MRI could be a useful tool for the evaluation of therapies used to treat PDA. It is likely that several different sequences would be needed to provide information on the microenvironment of the tumor. From this study, T2 relaxation, gagCEST, and ADC values have been identified to be part of the portfolio of scans which may provide reliable quantitation of pFUS treatment effects for patients with PDA.

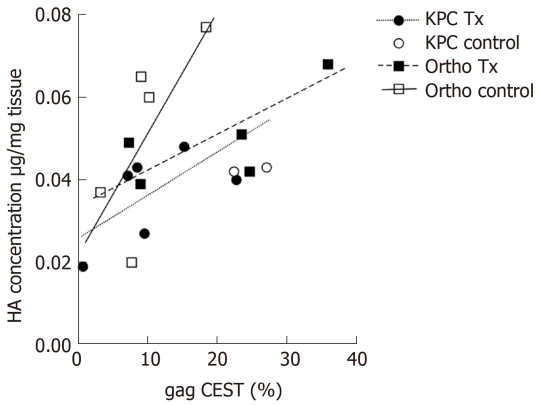

Figure 4 Total hyaluronic acid concentration compared to glycosaminoglycan chemical exchange saturation transfer for treated and sham treated (control) KPC and orthotopic mice. Regression lines for each animal model and condition demonstrate strong positive correlation between the hyaluronic acid concentrations as determined by the biochemical assay and glycosaminoglycan chemical exchange saturation transfer measurements. HA: Hyaluronic acid; CEST: Chemical exchange saturation transfer.

ARTICLE HIGHLIGHTS

Research background

The robust fibroinflammatory stroma characteristic of pancreatic ductal adenocarcinoma (PDA) impedes effective drug delivery. Pulsed focused ultrasound (pFUS) can disrupt this stroma and has improved survival in an early clinical trial. Non-invasive methods to characterize pFUS treatment effects are desirable for advancement of this promising treatment modality in larger clinical trials.

Research motivation

In this study, our objective was to identify non-invasive MRI methods that can be used to assess pFUS treatment effects for PDA, based on data derived from three murine models of PDA, including a genetic model. These methods have translational relevance to future, larger clinical trials that might help to advance pFUS therapy as a valuable supplement to traditional treatment modalities for patients with PDA.

Research objectives

Our primary objective was to identify promising, non-invasive pre-clinical imaging methods to characterize acute pFUS treatment effects for *in vivo* models of PDA. Robust pre-clinical data such as this builds critical foundation to facilitate efficient clinical trials. Knowledge of reliable methods to characterize the acute phase of treatment also helps to inform selection of methods to characterize long-term treatment follow up assessments in future studies.

Research methods

We utilized quantitative MRI methods at 14 tesla in three mouse models of PDA (subcutaneous, orthotopic and transgenic - *KrasLSL-G12D/+*, *Trp53LSL-R172H/+*, *Cre* or "KPC") to assess immediate tumor response to pFUS treatment (VIFU 2000 Alpinion Medical Systems; 475 W peak electric power, 1 millisecond pulse duration, 1 Hz, duty cycle 0.1%) *vs* sham therapy, and correlated our results with histochemical data. These pFUS treatment parameters were previously shown to enhance tumor permeability to chemotherapeutics. T1 and T2 relaxation maps, high (126, 180, 234, 340, 549) *vs* low (7, 47, 81) *b*-value apparent diffusion coefficient (ADC) maps, magnetization transfer ratio (MTR) maps, and chemical exchange saturation transfer (CEST) maps for the amide proton spectrum (3.5 parts per million or "ppm") and the glycosaminoglycan spectrum (0.5-1.5 ppm) were generated and analyzed pre-treatment, and immediately post-treatment, using ImageJ. Animals were sacrificed immediately following post-treatment imaging. The whole-tumor was selected as the region of interest for data analysis and subsequent statistical analysis. *T*-tests and Pearson correlation were used for statistical inference.

Research results

Mean high-*b* value ADC measurements increased significantly with pFUS treatment for all models. Mean glycosaminoglycan CEST and T2 measurements decreased significantly post-treatment for the KPC group. Mean MTR and amide CEST values increased significantly for the KPC group. Hyaluronic acid focal intensities in the treated regions were significantly lower following pFUS treatment for all animal models. The MRI changes observed acutely following pFUS therapy likely reflect: (1) Sequelae of variable degrees of microcapillary hemorrhage (T1, MTR and amide CEST); (2) Lower PDA glycosaminoglycan content and associated water content (glycosaminoglycan CEST, T2 and hyaluronic acid focal intensity); and (3) Improved tumor diffusivity (ADC) post pFUS treatment.

Research conclusions

T2, glycosaminoglycan CEST, and ADC maps proved to be reliable means of quantifying pFUS treatment effects in murine models of PDA, and may provide reliable, non-invasive quantitation of acute pFUS treatment effects for patients with PDA in future clinical trials.

Research perspectives

We have identified specific MRI methods as reliable non-invasive means of quantitating acute pFUS treatment effects for murine models of PDA. Future studies of long-term post-treatment disease burden may also benefit from employing the methods we describe. Clinical trials of pFUS therapy for PDA will be more easily accomplished if similar non-invasive methods of tracking immediate treatment endpoints can replace potentially morbid biopsies of this highly sensitive anatomic area. pFUS therapy may also be more efficacious for certain subpopulations of patients with PDA, and the methods we describe may help to non-invasively select enriched patient populations that will derive the greatest benefit from pFUS treatments in future studies.

ACKNOWLEDGEMENTS

We would like to thank Daniel S Hippe, biostatistician at the University of Washington, for reviewing the content of our manuscript to confirm appropriateness of biostatistical methods for study design.

REFERENCES

1 **Siegel RL**, Miller KD, Jemal A. Cancer statistics, 2019. *CA Cancer J Clin* 2019; **69**: 7-34 [PMID: 30620402 DOI: 10.3322/caac.21551]
2 **DuFort CC**, DelGiorno KE, Carlson MA, Osgood RJ, Zhao C, Huang Z, Thompson CB, Connor RJ, Thanos CD, Scott Brockenbrough J, Provenzano PP, Frost GI, Michael Shepard H, Hingorani SR. Interstitial Pressure in Pancreatic Ductal Adenocarcinoma Is Dominated by a Gel-Fluid Phase. *Biophys J* 2016; **110**: 2106-2119 [PMID: 27166818 DOI: 10.1016/j.bpj.2016.03.040]
3 **Jacobetz MA**, Chan DS, Neesse A, Bapiro TE, Cook N, Frese KK, Feig C, Nakagawa T, Caldwell ME, Zecchini HI, Lolkema MP, Jiang P, Kultti A, Thompson CB, Maneval DC, Jodrell DI, Frost GI, Shepard HM, Skepper JN, Tuveson DA. Hyaluronan impairs vascular function and drug delivery in a mouse model of pancreatic cancer. *Gut* 2013; **62**: 112-120 [PMID: 22466618 DOI: 10.1136/gutjnl-2012-302529]
4 **Li T**, Wang YN, Khokhlova TD, D'Andrea S, Starr F, Chen H, McCune JS, Risler LJ, Mashadi-Hossein A, Hingorani SR, Chang A, Hwang JH. Pulsed High-Intensity Focused Ultrasound Enhances Delivery of Doxorubicin in a Preclinical Model of Pancreatic Cancer. *Cancer Res* 2015; **75**: 3738-3746 [PMID: 26216548 DOI: 10.1158/0008-5472.CAN-15-0296]
5 **Yu MH**, Lee JY, Kim HR, Kim BR, Park EJ, Kim HS, Han JK, Choi BI. Therapeutic Effects of Microbubbles Added to Combined High-Intensity Focused Ultrasound and Chemotherapy in a Pancreatic Cancer Xenograft Model. *Korean J Radiol* 2016; **17**: 779-788 [PMID: 27587968 DOI: 10.3348/kjr.2016.17.5.779]
6 **Dimcevski G**, Kotopoulis S, Bjånes T, Hoem D, Schjøtt J, Gjertsen BT, Biermann M, Molven A, Sorbye H, McCormack E, Postema M, Gilja OH. A human clinical trial using ultrasound and microbubbles to enhance gemcitabine treatment of inoperable pancreatic cancer. *J Control Release* 2016; **243**: 172-181 [PMID: 27744037 DOI: 10.1016/j.jconrel.2016.10.007]
7 **Farr N**, Wang YN, D'Andrea S, Gravelle KM, Hwang JH, Lee D. Noninvasive characterization of pancreatic tumor mouse models using magnetic resonance imaging. *Cancer Med* 2017; **6**: 1082-1090 [PMID: 28390098 DOI: 10.1002/cam4.1062]
8 **Hingorani SR**, Wang L, Multani AS, Combs C, Deramaudt TB, Hruban RH, Rustgi AK, Chang S, Tuveson DA. Trp53R172H and KrasG12D cooperate to promote chromosomal instability and widely metastatic pancreatic ductal adenocarcinoma in mice. *Cancer Cell* 2005; **7**: 469-483 [PMID: 15894267 DOI: 10.1016/j.ccr.2005.04.023]
9 **Tseng WW**, Winer D, Kenkel JA, Choi O, Shain AH, Pollack JR, French R, Lowy AM, Engleman EG. Development of an orthotopic model of invasive pancreatic cancer in an immunocompetent murine host. *Clin Cancer Res* 2010; **16**: 3684-3695 [PMID: 20534740 DOI: 10.1158/1078-0432.CCR-09-2384]
10 **Maloney E**, DuFort CC, Provenzano PP, Farr N, Carlson MA, Vohra R, Park J, Hingorani SR, Lee D. Non-Invasive Monitoring of Stromal Biophysics with Targeted Depletion of Hyaluronan in Pancreatic Ductal Adenocarcinoma. *Cancers (Basel)* 2019; **11** [PMID: 31167451 DOI: 10.3390/cancers11060772]
11 **Desmond KL**, Moosvi F, Stanisz GJ. Mapping of amide, amine, and aliphatic peaks in the CEST spectra of murine xenografts at 7 T. *Magn Reson Med* 2014; **71**: 1841-1853 [PMID: 23801344 DOI: 10.1002/mrm.24822]
12 **Jin T**, Wang P, Zong X, Kim SG. MR imaging of the amide-proton transfer effect and the pH-insensitive nuclear overhauser effect at 9.4 T. *Magn Reson Med* 2013; **69**: 760-770 [PMID: 22577042 DOI: 10.1002/mrm.24315]
13 **Kim M**, Gillen J, Landman BA, Zhou J, van Zijl PC. Water saturation shift referencing (WASSR) for chemical exchange saturation transfer (CEST) experiments. *Magn Reson Med* 2009; **61**: 1441-1450 [PMID: 19358232 DOI: 10.1002/mrm.21873]
14 **Schneider CA**, Rasband WS, Eliceiri KW. NIH Image to ImageJ: 25 years of image analysis. *Nat Methods* 2012; **9**: 671-675 [PMID: 22930834 DOI: 10.1038/nmeth.2089]
15 **Kim S**, Decarlo L, Cho GY, Jensen JH, Sodickson DK, Moy L, Formenti S, Schneider RJ, Goldberg JD, Sigmund EE. Interstitial fluid pressure correlates with intravoxel incoherent motion imaging metrics in a mouse mammary carcinoma model. *NMR Biomed* 2012; **25**: 787-794 [PMID: 22072561 DOI: 10.1002/nbm.1793]
16 **Schmitt B**, Zbýn S, Stelzeneder D, Jellus V, Paul D, Lauer L, Bachert P, Trattnig S. Cartilage quality assessment by using glycosaminoglycan chemical exchange saturation transfer and (23)Na MR imaging at 7 T. *Radiology* 2011; **260**: 257-264 [PMID: 21460030 DOI: 10.1148/radiol.11101841]

17 **Haris M**, Singh A, Reddy S, Bagga P, Kneeland JB, Tjoumakaris FP, Hariharan H, Marincola FM, Reddy R. Characterization of viscosupplementation formulations using chemical exchange saturation transfer (ViscoCEST). *J Transl Med* 2016; **14**: 92 [PMID: 27071650 DOI: 10.1186/s12967-016-0850-8]

18 **Li T**, Chen H, Khokhlova T, Wang YN, Kreider W, He X, Hwang JH. Passive cavitation detection during pulsed HIFU exposures of ex vivo tissues and in vivo mouse pancreatic tumors. *Ultrasound Med Biol* 2014; **40**: 1523-1534 [PMID: 24613635 DOI: 10.1016/j.ultrasmedbio.2014.01.007]

19 **Chevillet JR**, Khokhlova TD, Giraldez MD, Schade GR, Starr F, Wang YN, Gallichotte EN, Wang K, Hwang JH, Tewari M. Release of Cell-free MicroRNA Tumor Biomarkers into the Blood Circulation with Pulsed Focused Ultrasound: A Noninvasive, Anatomically Localized, Molecular Liquid Biopsy. *Radiology* 2017; **283**: 158-167 [PMID: 27802108 DOI: 10.1148/radiol.2016160024]

20 **Ma X**, Bai Y, Lin Y, Hong X, Liu T, Ma L, Haacke EM, Zhou J, Wang J, Wang M. Amide proton transfer magnetic resonance imaging in detecting intracranial hemorrhage at different stages: a comparative study with susceptibility weighted imaging. *Sci Rep* 2017; **7**: 45696 [PMID: 28374764 DOI: 10.1038/srep45696]

21 **Battini S**, Faitot F, Imperiale A, Cicek AE, Heimburger C, Averous G, Bachellier P, Namer IJ. Metabolomics approaches in pancreatic adenocarcinoma: tumor metabolism profiling predicts clinical outcome of patients. *BMC Med* 2017; **15**: 56 [PMID: 28298227 DOI: 10.1186/s12916-017-0810-z]

22 **Vohra R**, Park J, Wang YN, Gravelle K, Whang S, Hwang JH, Lee D. Evaluation of pancreatic tumor development in KPC mice using multi-parametric MRI. *Cancer Imaging* 2018; **18**: 41 [PMID: 30409175 DOI: 10.1186/s40644-018-0172-6]

23 **Theocharis AD**, Tsara ME, Papageorgacopoulou N, Karavias DD, Theocharis DA. Pancreatic carcinoma is characterized by elevated content of hyaluronan and chondroitin sulfate with altered disaccharide composition. *Biochim Biophys Acta* 2000; **1502**: 201-206 [PMID: 11040445 DOI: 10.1016/s0925-4439(00)00051-x]

24 **Lee SS**, Byun JH, Park BJ, Park SH, Kim N, Park B, Kim JK, Lee MG. Quantitative analysis of diffusion-weighted magnetic resonance imaging of the pancreas: usefulness in characterizing solid pancreatic masses. *J Magn Reson Imaging* 2008; **28**: 928-936 [PMID: 18821618 DOI: 10.1002/jmri.21508]

25 **Gebauer F**, Kemper M, Sauter G, Prehm P, Schumacher U. Is hyaluronan deposition in the stroma of pancreatic ductal adenocarcinoma of prognostic significance? *PLoS One* 2017; **12**: e0178703 [PMID: 28582436 DOI: 10.1371/journal.pone.0178703]

World Journal of Gastroenterology

Submit a Manuscript: https://www.f6publishing.com

World J Gastroenterol 2020 March 7; 26(9): 918-932

DOI: 10.3748/wjg.v26.i9.918

ISSN 1007-9327 (print) ISSN 2219-2840 (online)

ORIGINAL ARTICLE

Basic Study

Kynurenine plays an immunosuppressive role in 2,4,6-trinitrobenzene sulfate-induced colitis in mice

Chieko Tashita, Masato Hoshi, Akihiro Hirata, Kentaro Nakamoto, Tatsuya Ando, Takayuki Hattori, Yasuko Yamamoto, Hiroyuki Tezuka, Hiroyuki Tomita, Akira Hara, Kuniaki Saito

ORCID number: Chieko Tashita (0000-0002-4124-3581); Masato Hoshi (0000-0001-6260-8300); Akihiro Hirata (0000-0003-2268-504X); Kentro Nakamoto (0000-0002-4379-8740); Tatsuya Ando (0000-0003-2274-5807); Takayuki Hattori (0000-0003-4445-6387); Yasuko Yamamoto (0000-0001-8825-9188); Hiroyuki Tezuka (0000-0003-4209-9486); Hiroyuki Tomita (0000-0002-3291-0274); Akira Hara (0000-0002-5554-8060); Kuniaki Saito (0000-0001-5800-9305).

Author contributions: Hoshi M, Hara A, and Saito K planned the studies; Tashita C, Hoshi M, Hirata A, Tezuka H, Hattori T, Yamamoto Y, and Tomita H performed the experiments; Tashita C and Hoshi M had responsibility for all data integrity and data analysis; Tashita C, Hoshi M, Hirata A, Tezuka H, Nakamoto K, Ando T, Hattori T, Yamamoto Y, Tomita H, Hara A, and Saito K discussed the results; Tashita C, Hoshi M, and Tezuka H wrote the manuscript; Hara A and Saito K conducted the research; Saito K had primary responsibility for the final content; all authors reviewed and approved the manuscript.

Supported by Grants-in-Aids for Young Scientists (B) from the Japan Society for the Promotion of Science, No. 17K15785; and Fujita Health University Grant (2018).

Institutional review board statement: This research was approved by the Ethics Committee

Chieko Tashita, Kentaro Nakamoto, Tatsuya Ando, Yasuko Yamamoto, Kuniaki Saito, Department of Disease Control and Prevention, Fujita Health University Graduate School of Health Sciences, Toyoake 470-1192, Japan

Masato Hoshi, Department of Biochemical and Analytical Science, Fujita Health University Graduate School of Health Sciences, Toyoake 470-1192, Japan

Akihiro Hirata, Division of Animal Experiment, Life Science Research Center, Gifu University, Gifu 501-1193, Japan

Tatsuya Ando, Hiroyuki Tezuka, Department of Cellular Function Analysis, Research Promotion and Support Headquarters, Fujita Health University Graduate School of Health Sciences, Toyoake 470-1192, Japan

Takayuki Hattori, Faculty of Medical Technology, Gifu University of Medical Science, Gifu 501-3892, Japan

Hiroyuki Tomita, Akira Hara, Department of Tumor Pathology, Gifu University Graduate School of Medicine, Gifu 501-1193, Japan

Corresponding author: Masato Hoshi, PhD, Assistant Professor, Department of Biochemical and Analytical Science, Fujita Health University Graduate School of Health Sciences, 1-98 Dengakugakubo, Kutsukake-cho, Toyoake 470-1192, Japan. mhoshi@fujita-hu.ac.jp

Abstract

BACKGROUND

Inflammatory bowel disease, such as Crohn's disease and ulcerative colitis, is characterized by chronic intestinal inflammation leading to intestinal mucosal damage. Inflammatory bowel disease causes dysregulation of mucosal T cell responses, especially the responses of $CD4^+$ T cells. Previously, we demonstrated that indoleamine-2,3-dioxygenase plays an immunosuppressive role in 2,4,6-trinitrobenzene sulfate (TNBS)-induced colitis. Although indoleamine-2,3-dioxygenase exerts immunosuppressive effects by altering the local concentration of tryptophan (Trp) and immunomodulatory Trp metabolites, the specific changes in immune regulation during colitis caused by Trp metabolites and its related enzymes remain unclear.

AIM

To investigate role of kynurenine 3-monooxygenase (KMO) in TNBS-induced colitis and involvement of Trp metabolites in maintenance of intestinal

of Fujita Health University.

Institutional animal care and use committee statement: This research was approved by Animal Experimental Ethical Inspection of Fujita Health University, NO. APU19040.

Conflict-of-interest statement: The authors declare that they have no conflict of interest.

ARRIVE guidelines statement: The authors have read the ARRIVE guidelines, and the manuscript was prepared and revised according to the ARRIVE guidelines.

Manuscript source: Unsolicited Manuscript

Received: November 5, 2019
Peer-review started: November 5, 2019
First decision: December 23, 2019
Revised: January 6, 2020
Accepted: February 21, 2020
Article in press: February 21, 2020
Published online: March 7, 2020

P-Reviewer: Yang MS, Sun XT
S-Editor: Wang YQ
L-Editor: A
E-Editor: Zhang YL

homeostasis.

METHODS
Colitis was induced in eight-week-old male KMO$^{+/+}$ or KMO$^{-/-}$ mice of C57BL/6N background using TNBS. Three days later, the colon was used for hematoxylin-eosin staining for histological grading, immunohistochemical or immunofluorescence staining for KMO, cytokines, and immune cells. Inflammatory and anti-inflammatory cytokines were measured using quantitative RT-PCR, and kynurenine (Kyn) pathway metabolites were measured by high-performance liquid chromatography. The cell proportions of colonic lamina propria and mesenteric lymph nodes were analyzed by flow cytometry.

RESULTS
KMO expression levels in the colonic mononuclear phagocytes, including dendritic cells and macrophages increased upon TNBS induction. Notably, KMO deficiency reduced TNBS-induced colitis, resulting in an increased frequency of Foxp3^{+} regulatory T cells and increased mRNA and protein levels of anti-inflammatory cytokines, including transforming growth factor-β and interleukin-10.

CONCLUSION
Absence of KMO reduced TNBS-induced colitis *via* generation of Foxp3^{+} regulatory T cells by producing Kyn. Thus, Kyn may play a therapeutic role in colon protection during colitis.

Key words: Kynurenine 3-monooxygenase; Kynurenine; Regulatory T cell; Inflammatory bowie diseases

Core tip: The role of kynurenine 3-monooxygenase (KMO) in immune regulation was examined in *KMO* gene deficient mice suffering from 2,4,6-trinitrobenzene sulfate-induced colitis. We demonstrated that the expression of transforming growth factor-β and interleukin-10 in the colon of these mice was upregulated by KMO inhibition and kynurenine administration, resulting in increased incidence of regulatory T cells in the inflammatory site, where they suppress progression to colitis. Thus, administration of kynurenine plays a critical role in host protection during 2,4,6-trinitrobenzene sulfate-induced colitis.

Citation: Tashita C, Hoshi M, Hirata A, Nakamoto K, Ando T, Hattori T, Yamamoto Y, Tezuka H, Tomita H, Hara A, Saito K. Kynurenine plays an immunosuppressive role in 2,4,6-trinitrobenzene sulfate-induced colitis in mice. *World J Gastroenterol* 2020; 26(9): 918-932
URL: https://www.wjgnet.com/1007-9327/full/v26/i9/918.htm
DOI: https://dx.doi.org/10.3748/wjg.v26.i9.918

INTRODUCTION

Inflammatory bowel disease (IBD), such as Crohn's disease and ulcerative colitis, is characterized by chronic intestinal inflammation leading to damage of the intestinal mucosa, which may persist for a long term. Consequently, therapy corresponding to stage and the lifestyle of the patient is important. Recent studies have suggested that IBD causes dysregulation of mucosal T cell responses, especially those of CD4^{+} T cells[1], leading to intestinal inflammation and barrier destruction[2,3]. Further, CD4^{+} T helper (Th) cells, including Th1 and Th2, and regulatory T (Treg) cells regulate the production of pro-inflammatory cytokines, such as tumor necrosis factor (TNF)-α and interferon (IFN)-γ and anti-inflammatory cytokines, such as transforming growth factor (TGF)-β and interleukin (IL)-10 in the intestines[4]. Thus, it is known that dysregulation of these cytokines is an important characteristic of IBD. For example, Crohn's disease and ulcerative colitis are associated with inflammatory Th1- and Th2-responses, respectively[5]. The regulatory function of Treg cells on colonic inflammation is mainly exerted by the production of anti-inflammatory cytokines,

such as IL-10 and TGF-β[6-8], leading to the suppression of inflammatory Th1- and Th2-responses[9]. Importantly, the deletion of Treg cells leads to the onset of chronic T cell-mediated intestinal inflammation and worsens acute intestinal inflammation[10], suggesting that Treg cells may be beneficial in the treatment of colonic inflammation[11]. Moreover, a recent study suggested that Th17 cells play an important role during IBD[12] by producing pro-inflammatory cytokines such as IFN-γ and IL-17. Therefore, the immune responses in the intestine are important because the balance between congenital and secondary responses, and negative regulation, and impairment of such balance by genetic or environmental factors leads to inflammatory disorders such as the IBD[5,13-15]. However, the roles of the pro-inflammatory processes and of immune regulation during colitis still remain unclear.

We recently demonstrated that the activity of indoleamine-2,3-dioxygenase (IDO), which catalyzes the rate-controlling step in the kynurenine pathway (KP), plays an immunosuppressive role during colitis[16]. IDO exerts immunosuppressive effects by reducing the local concentration of tryptophan (Trp) and increasing the production of immunomodulatory Trp metabolites that have a variety of effects on immune cells. For example, the Trp metabolites suppress proliferation and promote apoptosis of T cells[17,18], and induce the differentiation of naive T cells into Treg cells. In addition, recent studies have shown that increase in IDO concentrations in some tissues inhibits migration of effector T cells[19]. Although regulation of KP metabolism has attracted considerable attention as a novel target for the development of colitis therapeutics, the immunosuppressive effects of Trp metabolites and the KP enzymes associated with them are not fully understood.

Kynurenine-3-monooxygenase (KMO) is a key enzyme in KP, that biosynthesizes 3-hydroxykynurenine (3-HK) from kynurenine (Kyn) with the aid of nicotinamide adenine dinucleotide phosphate (NADPH)[20]. KMO is predominantly localized in the mitochondria and exhibits the highest activity in the liver, kidney, and immune cells, especially macrophages[21]. The transcriptional expression of KMO is induced by IFN-γ and is inhibited by IL-4[22]. Recently, we demonstrated that *KMO* gene deficiency in mice leads to high levels of Kyn and low levels of 3-HK in serum and various tissues[23]. Kyn is involved in arterial relaxation[24] and generation of Treg[25]. Based on these findings, we hypothesized that increased levels of Kyn, caused by regulating KMO, may contribute to the induction of intestinal T cells and other immune cells during colitis.

MATERIALS AND METHODS

Animals

Eight-week-old male mice were used for this study. *KMO* gene deficient ($KMO^{-/-}$) mice on a C 57BL/6N background were obtained from the Knockout Mouse Project (KOMP) repository. Homozygous $KMO^{-/-}$ and $KMO^{+/+}$ mice were generated by intercrossing heterozygous mice and genotyped using standard PCR-based genotyping of genomic DNA extracted from tail snippets. The following primer sequences were used for PCR genotyping: *KMO* gene sense: 5′-TTCTGACC CCATCTGTGTCTGTTCC-3′, antisense: 5′-ATCAGAGCTCCCTAAATA TGGTGGC-3′; and *KMO* gene deficiency sense: 5′-AACTTCGACCCTTTCCCAC-3′, antisense: 5′-GACCACCTCATCAGAGCAG-5′. The mice were housed in a specific pathogen-free environment in our animal facility. All experiments were performed in accordance with Guidelines for Animal Care of the Fujita Health University. Mice were acclimatized to controlled conditions (12 h/12 h light/dark cycle, 50% humidity, 23 °C ± 2 °C, *ad libitum* access to food and water) for two weeks prior to experimentation. The protocol for all animal experiments was approved by the Animal Experimentation Committee of Fujita Health University Graduate School of Medicine. Procedures involving mice and their care conformed to international guidelines, as described in Principles of Laboratory Animal Care (National Institutes of Health publication 85-23, revised 1985).

Induction of acute colitis

Eight-week-old $KMO^{-/-}$ or $KMO^{+/+}$ mice were allotted to four groups: TNBS-treated ($KMO^{-/-}$ mice; at least $n = 4$, $KMO^{+/+}$ mice; at least $n = 4$) and ethanol-treated (vehicle, TNBS solvent control) ($KMO^{-/-}$ mice; at least $n = 4$, $KMO^{+/+}$ mice; at least $n = 5$). Treatment of the mice with TNBS (obtained from Sigma-Aldrich, St. Louis, MO) and vehicle was performed as described previously[26]. Mice were placed under anesthesia, and intrarectally injected with either 100 μL TNBS (2.5% TNBS in 50% ethanol) or 50% ethanol. All surviving mice were sacrificed three days after the TNBS treatment. Any steps taken to minimize the effects of subjective bias when allocating mice to

treatment.

Sample preparation

The colon was opened longitudinally and cut in half in the direction of the long axis. One half was fixed in phosphate-buffered 10% formalin for 24 h at room temperature. The tissue sample was then processed for histological and immunohistological analyses as described later. The second half of the colon was used for quantitative real-time RT-PCR analysis, enzymatic assays, or analysis of Trp metabolites.

Histological analysis

Three micrometer-thick sections of the colon were used for hematoxylin-eosin staining for histological grading. The colon tissue was divided into three separate sections. The histological grades were determined for each section and the sum of the grades was reported as the inflammation score for each mouse. Histological grading of colitis was determined on a scale of 0 to 5 as described previously[16]. Grade 0: No obvious inflammation; Grade 1: Mild inflammatory cell infiltration, no structural changes observed; Grade 2: Moderate inflammatory cell infiltration, crypt elongation, bowel wall thickening that does not extend beyond the mucosal layer, no evidence of ulceration; Grade 3: Severe inflammation cell infiltration, thickening of bowel wall, high vascular density, crypt elongation with distortion, transmural bowel wall thickening with ulceration that extends beyond the mucosal layer; Grade 4: Complete loss of mucosal architecture (crypts) with ulceration and loss of mucosal vasculature; Grade 5: Coagulative necrosis of the mucosal layer. Illustrative images of the colon at each grade are shown in Supplementary Figure 1.

Measurement of KP metabolites

For Trp, Kyn, 3-HK, kynurenic acid (KA), anthranilic acid (AA), and 3-hydroxyanthranilic acid (3-HAA) measurement, colon tissues were homogenized. The homogenate samples were centrifuged at 7000 × g at 4 °C for 10 min. Fifty microliters of the supernatant was subjected to high-performance liquid chromatography (HPLC) analysis. Trp, Kyn, KA, and AA were isocratically eluted from a reverse phase column [TSKgel ODS-100V, 3 μm, 4.6 mm (ID) × 150 nm (L)] (Tosoh, Tokyo, Japan) using a mobile phase containing 10 mmol/L sodium acetate and 1% acetonitrile (adjusted pH to 4.5 with acetic acid) at a flow rate of 0.9 ml/min. Trp and Kyn were detected using an ultraviolet and visible spectrophotometric apparatus (SPD-20A, Shimadzu, Kyoto, Japan) (UV wavelength for Trp: 280 nm, UV wavelength for Kyn: 365 nm). AA, KA, and 3-HAA were detected by a fluorescence detector (RF-20Axs) (Shimadzu) under the following conditions: The excitation wavelength 320 nm and emission wavelength 420 nm for AA and 3-HAA, the excitation wavelength 334 nm and emission wavelength 380 nm for KA. Twenty microliters of the supernatant was injected into a 3 μm HPLC column (HR-80; 80 mm × 4.6 mm) (ESA, Chelmsford, MA), using a mobile phase consisting of 1.5% acetonitrile, 0.9% trimethylamine, 0.59% phosphoric acid, 0.27 mmol/L EDTA, and 8.9 mmol/L sodium heptane sulfonic acid, at a flow rate of 0.5 mL/min. 3-HK was detected electrochemically using an ECD 300 detector (oxidation potential: +0.05 V) (Eicom, Kyoto, Japan) as described previously[27].

Immunohistochemical analysis

Three micrometer-thick sections of the colon were used for immunohistochemical staining for KMO, CD4, and Foxp3. The primary antibodies used were rabbit anti-KMO antibody (ab83929, Abcam, Abcam Cambridge, United Kingdom), and rabbit anti-CD4 antibody (ab183685, Abcam), and rabbit anti-Foxp3 antibody (ab545011, Abcam). After deparaffinization and rehydration, sections were heated at 121 °C for 20 min in Histofine antigen retrieval solution (pH 9.0) (NICHIREI BIOSCIENCE INC., Tokyo, Japan) for CD4 or 0.1 mol/L sodium citrate buffer (pH 6.0) for KMO and Foxp3. The sections were soaked in 3% hydrogen peroxide in methanol for 30 min to eliminate endogenous peroxidase activity. After nonspecific binding was blocked with 1% BSA, the sections were incubated with primary antibodies overnight at 4 °C. Positive and negative controls (no primary antibody) were included for each antibody (Supplementary Figure 2). Secondary antibody, conjugated with a peroxidase polymer (ImmPRESS Reagent anti-rabbit IgG Vector Laboratories, Burlingame, CA) was added for 30 min at room temperature, followed by the addition of the substrate 3,3`-diaminobenzidine tetrahydrochloride (DAB; Dako, Santa Clara, CA). The sections were then counterstained with hematoxylin. For immunofluorescence analysis, the frozen colon sections were used for immunohistochemical staining for KMO, F4/80, CD19, CD11c, Foxp3, TGF-β, and IL-10. The nonspecific binding was blocked with 1% BSA in PBS or M.O.M mouse Ig blocking reagent for TGF-β staining (M.O.M kit, Vector Laboratories), and the sections were subsequently incubated with rabbit anti-KMO antibody (ab83929, Abcam) and rat monoclonal anti-F4/80 antibody (ab16911,

Abcam), rabbit anti-Foxp3 antibody (ab545011, Abcam), mouse monoclonal anti-TGF-β antibody (NBP2-45137, Novus Biological, Littleton, CO), rat monoclonal anti-IL-10 antibody (MBS246583, MyBioSource, San Diego, CA), rat monoclonal anti-CD19 antibody (14-0194-82, Thermo Fisher Scientific, Tokyo, Japan) and hamster monoclonal anti-CD11c antibody (70-0114, TONBO Biosciences, San Diego, CA) in 2% BSA in PBS overnight at 4 °C. Negative controls (without primary antibodies) were included for each antibody (Supplementary Figure 3). After the incubation with primary antibodies, the sections were rinsed with PBS, and incubated with secondary antibodies for 30 min at room temperature. The secondary antibodies used were Alexa Fluor® 488-conjugated donkey anti-rabbit IgG (H+L) antibody (NL004, R&D Systems, Minneapolis, MN), donkey anti-mouse IgG (H+L) antibody (NL009, R&D Systems) and goat anti-rat IgG (H+L) antibody (ab150157, Abcam), FITC-conjugated anti-hamster IgG (H+L) antibody (31587, Thermo Fisher Scientific) and nuclei were stained with 4′,6-diamidino-2-phenylindole (Dojindo, Tokyo, Japan). Immunostained slides were observed under fluorescence microscope BX51 equipped with a DP74 digital camera (Olympus, Tokyo, Japan).

Cell preparation and Flow cytometry

To prepare colonic lamina propria (LP) cells, the colon was opened longitudinally and cut into 2-3 fragments. The fragments were stirred to remove epithelial cells in 3 mmol/L ethylenediaminetetraacetic acid (EDTA) solution (220 r/min, 30 min, 37 °C) and then digested in 100 U/ml of type I collagenases (FUJIFILM Wako, Osaka, Japan) (220 r/min, 45 min, 37 °C). Digested fragments were passed through a 70-μm cell strainer and then applied to a discontinuous Percoll density gradient (GE Healthcare, Illinois, CHI) of 44% Percoll and 60%. Cells at the interface were collected and used as colonic LP cells. Mesenteric lymph nodes (MLN) were dissociated into single-cells and then passed through a 70-μm cell strainer and used as MLN cells. Cells were stained with fluorochrome-conjugated monoclonal antibodies against the following cell-surface makers: FITC anti-mouse CD4 (GK1.5, BioLegend, San Diego, CA), PE anti-mouse CD103 (2E7, BioLegend), APC anti-mouse CD11c (N418, BioLegend) and FITC anti-mouse CD45.2 (104, BioLegend). For intracellular Foxp3 staining, cells were fixed and permeabilized with Foxp3 Fix/Perm solution (BioLegend). Cells were then stained with biotin-conjugated anti-mouse Foxp3 antibody (FJK-16s, BioLegend) followed by streptavidin-conjugated APC (405207, BioLegend). The cells were analyzed on FACS Calibur in conjunction with FlowJo software (BD Bioscience, Tokyo, Japan).

RNA extraction and quantitative PCR

Total RNA was extracted from the colon tissue using Isogen II (NIPPON GENE, Tokyo, Japan). cDNA was synthesized using High-capacity cDNA Reverse Transcription Kits (Applied Biosystems, Foster city, CA) for RT-PCR according to the manufacturer's instructions. The following PCR primers were used: KMO, sense, 5′-GTTATTGGCGGTGGTTTGGTTG-3′, and antisense, 5′-GGGCCAAG TTAATGCTCCTTC-3′; 18S rRNA, sense 5′-GGATTGACAGATTGATAGC-3′, and antisense, 5′-TATCGGAATTAACCAGACAA-3′; IFN-γ, sense, 5′-AAGTTTGAGGTCAACAAC-3′, and anti-sense, 5′-GTGCTGGCAGAATTATTC-3′; TGF-β, sense, 5′-ACAATTCCTGGCGTTACCTTG-3′, and anti-sense, 5′-CGTGGA GTTTGTTATCTTTGCTG-3′; IL-10, sense, 5′-TGCACTACCAAAGCC ACAAG-3′, and anti-sense, 5′-TAAGAGCAGGCAGCATAGCAG-3′; and TNF-α, sense, 5′-TCATGCACCACCATCAAG-3′, and antisense, 5′-CAGAACTCAGGAATGGACAT-3′.

KMO, TGF-β, IL-10, IFN-γ, TNF-α and 18S rRNA were quantified by using SYBR Green Supermix (Bio Rad, Hercules, CA) on Step One Real Time PCR System (Applied Biosystems). The expression of each gene was normalized to the expression of 18S rRNA using the standard curve method.

Administration of Kyn

Kyn was administered as described previously[28]. Briefly, mice were intraperitoneally injected with L-Kyn (n = 5, 100 mg/kg, twice per day, Sigma-Aldrich, Tokyo, Japan), KA (n = 5), AA (n = 5), 3-HAA (n = 3), and 3-HK (n = 3, 10 mg/kg, twice per day, respectively, Sigma-Aldrich) at 12 h after TNBS injection and were humanely sacrificed on day 3.

Statistical analysis

Results are presented as the mean ± SE. For analyzing multiple groups, two-way ANOVA was used followed by Tukey multiple comparisons test, except for KMO expression, which was performed using one-way ANOVA followed by Tukey multiple comparison test, and Kyn-treated mice or vehicle mice were analyzed by Student's t-test. All comparison and observations were performed using GraphPad

Prism7 (GraphPad Software Inc., San Diego, CA). $P < 0.05$ was considered significant.

RESULTS

Absence of KMO suppresses TNBS-induced colitis in mice

We examined the effects of the $KMO^{-/-}$ genotype to investigate the role of KMO during colitis. There was no difference in length, weight, or histological appearance of the colon and body weight between untreated $KMO^{+/+}$ mice and untreated $KMO^{-/-}$ mice (data not shown). The histological grades of colonic inflammation were consistently higher in TNBS-treated than in vehicle-treated $KMO^{+/+}$ mice ($P < 0.01$), and the histological grades of colonic inflammation and the ratio of colon to body weight (Supplementary Figure 4) in TNBS-treated $KMO^{-/-}$ mice ($P < 0.05$) were significantly lower compared to those in TNBS-treated $KMO^{+/+}$ mice (Figure 1A and B). $KMO^{-/-}$ mice suffering from TNBS-induced colitis showed relatively mild inflammation and occasionally developed focal ulceration. In contrast, in $KMO^{+/+}$ mice, colitis was frequently associated with pathological changes in the colonic mucosa, including extensive ulceration, crypt loss, and coagulative necrosis (Figure 1B). We next assessed the expression of KMO in the colon by quantitative PCR and immunohistochemical staining. In $KMO^{+/+}$ mice, the number of KMO^{+} cells and KMO mRNA levels were significantly higher in TNBS-treated groups ($P < 0.05$) than in vehicle-treated groups (Figure 1C-E). Interestingly, KMO was expressed in $F4/80^{+}$ cells and $CD11c^{+}$ cells, but not in $CD19^{+}$ cells, as observed by immunofluorescence analysis (Figure 1F, Supplementary Figure 5). These observations indicate that TNBS-induced KMO^{+} mononuclear phagocytes (MPs), including possibly dendritic cells and macrophages, were involved in the pathological progression of colitis.

KMO gene deficiency markedly changes the levels of KP metabolites in the colon

Because KMO deficiency has been associated with significantly reduced inflammation, we next investigated the effects of KP metabolites in the TNBS-induced colitis model. The levels of Kyn and KA in the colonic tissues were significantly higher in TNBS-treated $KMO^{-/-}$ mice (Kyn: $P < 0.05$; KA: $P < 0.01$) than those in $KMO^{-/-}$ vehicle mice. In contrast, the levels of Kyn, AA, and KA in TNBS-treated (Kyn, KA: $P < 0.01$; AA: $P < 0.05$) and vehicle-treated $KMO^{-/-}$ mice (Kyn, KA: $P < 0.01$; AA: $P < 0.05$) were significantly higher compared to those in TNBS-treated and vehicle-treated $KMO^{+/+}$ mice (Figure 2). As expected, the levels of 3-HK and 3-HAA remained low in TNBS-treated $KMO^{-/-}$ mice. The levels of Trp were unaffected in all mice tested regardless of presence or absence of KMO (Figure 2). These results suggest that increased levels of KP metabolites, excluding 3-HK and 3-HAA, resulting from KMO deficiency might also contribute to the regulation of colonic inflammation.

Increase in Kyn levels in the colon of $KMO^{-/-}$ mice promotes $Foxp3^{+}$ Treg cell accumulation

Treg cells prevent the induction and progression of colitis[6-8]. Therefore, we quantified the proportion of $Foxp3^{+}$ Treg cells in the inflamed colon by immunohistochemical staining and flow cytometry. To this end, we evaluated the $Foxp3^{+}$ Treg cells on serial sections (Figure 3A). During colitis, the frequency of colonic Treg cells was significantly higher in $KMO^{-/-}$ mice ($P < 0.05$) than in $KMO^{+/+}$ mice (Figure 3B and C). Consistent with these results, the frequency of $CD103^{+}$ DCs in the MLN was higher in $KMO^{-/-}$ mice ($P < 0.05$) than in $KMO^{+/+}$ mice under inflammatory conditions (Figure 3D and E). These results suggest that $KMO^{-/-}$ mice showed enhanced induction or accumulation of $Foxp3^{+}$ Treg cells in the inflamed colon.

Upregulation of anti-inflammatory cytokines in the colon of $KMO^{-/-}$ mice

Anti-inflammatory cytokines, which are largely produced by Treg cells, regulate intestinal inflammation including colitis. To examine whether reduced inflammation in $KMO^{-/-}$ mice is due to enhanced production of anti-inflammatory cytokines, we first examined the levels of mRNA expression of TGF-β and IL-10 in the colonic tissues. The levels of TGF-β and IL-10 mRNA in the colon of TNBS-treated $KMO^{-/-}$ mice ($P < 0.05$) were significantly higher than those of TNBS-treated $KMO^{+/+}$ mice (Figure 4A). In contrast, the levels of inflammatory cytokines TNF-α and IFN-γ mRNA tended to reduce in the colon of TNBS-treated $KMO^{-/-}$ mice compared to the colon of TNBS-treated $KMO^{+/+}$ mice (Figure 4A). We next performed immunofluorescence staining to determine the source of TGF-β and IL-10. In the colonic lamina propria (LP) of vehicle or TNBS-treated $KMO^{+/+}$ mice, the expression of TGF-β and IL-10 was largely observed in $Foxp3^{+}$ Treg cells, but not in colonic epithelium (Figure 4B). Furthermore, the ratio of TGF-β^{+} /$Foxp3^{+}$ cells and IL-10^{+}/

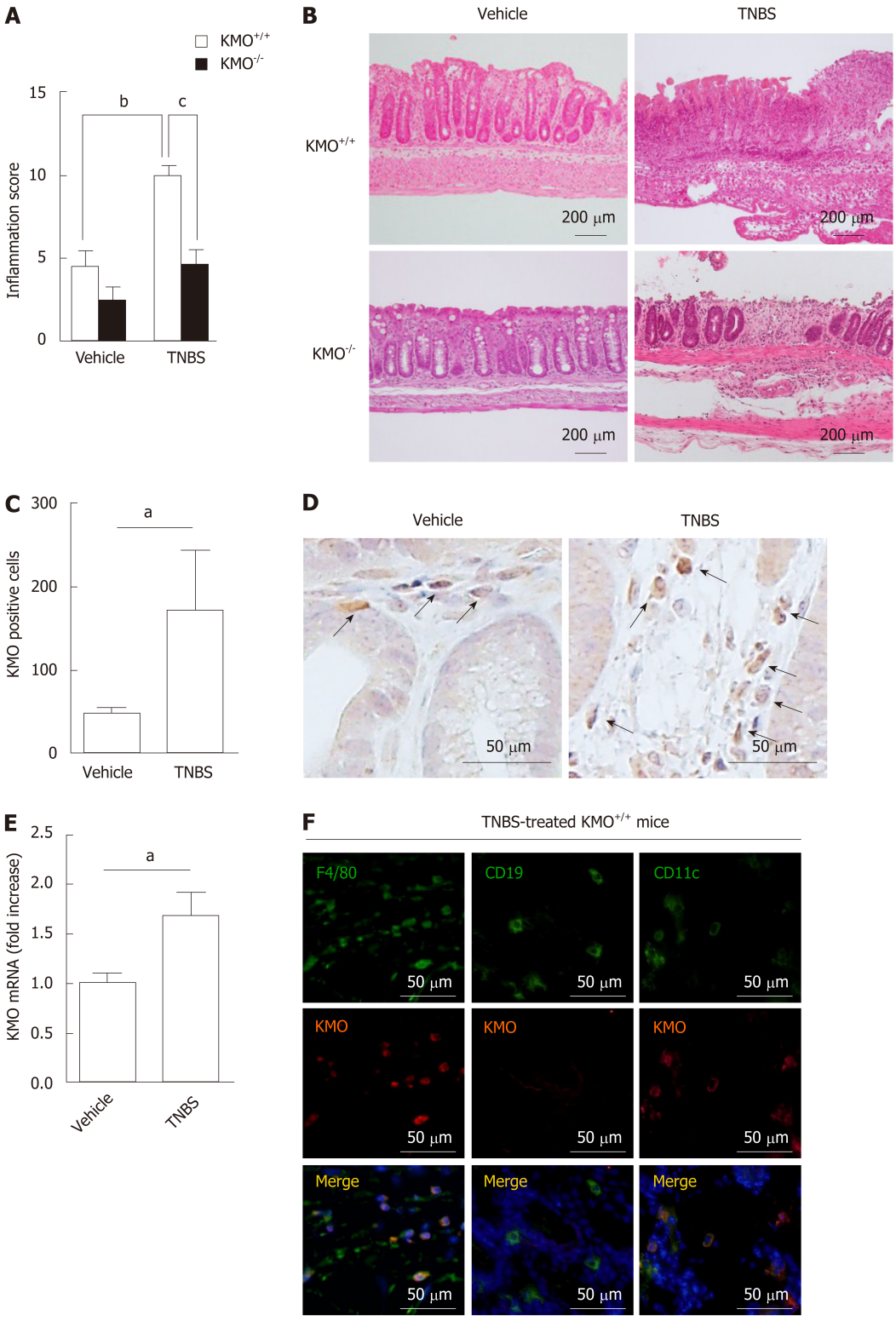

Figure 1 Increased number of F4/80⁺ KMO⁺ cells in the colon exacerbates TNBS-induced colitis. Mice were treated with either TNBS or vehicle, and colons were collected three days after treatment. A: Histological scores determined based on a histological grading as described in Materials and Methods. B: Representative images of H&E-stained colons of the said mice. C, D: The KMO⁺ cells in the colons of the said mice were counted using immunohistochemical staining for KMO. E: KMO mRNA expression in the colon was determined by quantitative PCR. F: The colons of TNBS-treated mice were stained for F4/80, CD19, CD11c, KMO, and DAPI (nuclei) using immunofluorescence staining. The negative controls for F4/80, CD19, CD11c, and KMO were not stained (Supplementary Figure 2 and 3). $^{a}P < 0.05$ *vs* Vehicle group, $^{b}P < 0.01$ *vs* Vehicle group, $^{c}P < 0.05$ *vs* TNBS-treated KMO$^{+/+}$ mice group. KMO: Kynurenine 3-monooxygenase; TNBS: Trinitrobenzene sulfonic acid.

Foxp3⁺ cells in the isolated lymphoid follicles (ILF) in the colon was significantly higher in TNBS-treated KMO$^{-/-}$ mice ($P < 0.01$) than in TNBS-treated KMO$^{+/+}$ mice (Figure 4D). However, the ratio of TGF-β⁺/Foxp3⁺ cells and IL-10⁺/ Foxp3⁺ cells in the

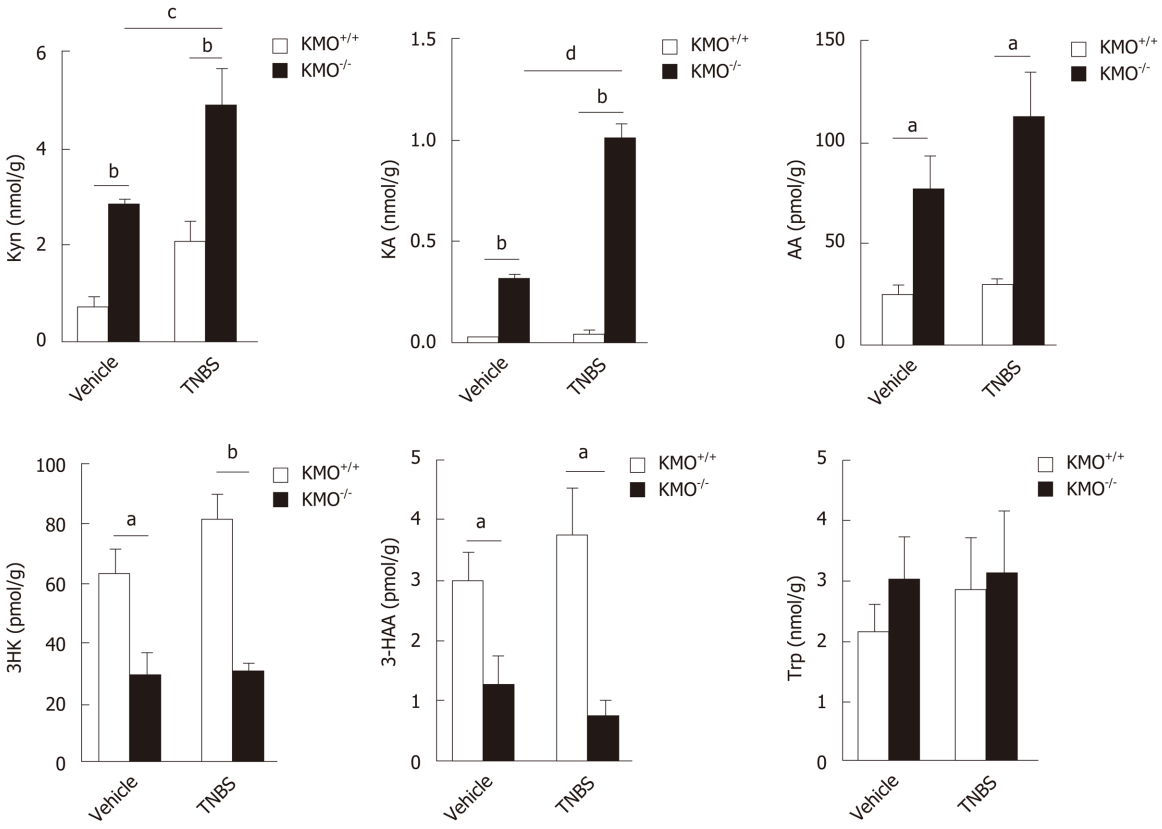

Figure 2 TNBS treatment increased the levels of colon L-Kyn in absence of KMO. KP metabolite levels in the colon of the indicated mice were measured using HPLC. The data are represented as mean ± SE from at least four independent experiments: [a]$P < 0.05$ *vs* Vehicle or TNBS-treated KMO$^{+/+}$ mice group; [b]$P < 0.01$ *vs* Vehicle or TNBS-treated KMO$^{+/+}$ mice group; [c]$P < 0.05$ *vs* KMO$^{-/-}$ Vehicle group; and [d]$P < 0.01$ *vs* Vehicle group. KMO: Kynurenine 3-monooxygenase; TNBS: Trinitrobenzene sulfonic acid.

colonic LP and mesenteric lymph nodes (MLN) was not significantly altered between these mice (data not shown). These results suggest that Foxp3$^+$ Treg cells accumulate in the colonic ILF and suppress colitis through enhanced Kyn-dependent production of TGF-β and IL-10.

Treatment with Kyn improves TNBS-induced colitis

To evaluate the effects of Trp metabolites in TNBS-induced colitis, we administrated Kyn, KA, or AA to TNBS-treated KMO$^{+/+}$ mice and 3-HK or 3HAA to KMO$^{-/-}$ mice. The histological grades of colonic inflammation and the ratio of colon to body weight in Kyn-treated mice (inflammation score: $P = 0.05$; colon/B.W.: $P < 0.05$) were reduced compared to those in KA, AA, and PBS-treated KMO$^{+/+}$ mice (Figure 5A left and Supplementary Figure 6). Moreover, these indicators for colonic inflammation in 3-HK-treated KMO$^{-/-}$ mice were increased compared to those in 3HAA- or PBS-treated mice ($P < 0.05$) (Figure 5A right). Kyn-treated KMO$^{+/+}$ mice had relatively mild inflammation and occasionally developed focal ulceration. In contrast, KA, AA, and PBS-treated KMO$^{+/+}$ mice and 3-HK-treated KMO$^{-/-}$ mice exhibited severe inflammation with pathogenic changes in the colonic mucosal architecture including extensive ulceration and coagulative necrosis (Figure 5B and Supplementary Figure 7). Furthermore, the ratio of Foxp3$^+$/CD4$^+$ cells in the colon was significantly higher in Kyn-treated mice ($P < 0.05$) than in PBS-treated mice (Figure 5C, D). We finally confirmed the mRNA expression levels of IL-10 and TGF-β in Kyn-treated mice. The levels of IL-10 mRNA in Kyn-treated mice ($P < 0.05$) were significantly upregulated compared to those in PBS-treated mice, whereas there was no significant change in the levels of TGF-β mRNA (Figure 5E). Similarly, the ratio of TGF-β$^+$/Foxp3$^+$ cells or IL-10$^+$/ Foxp3$^+$ cells in the ILF were significantly higher in Kyn-treated KMO$^{-/-}$ mice than in PBS-treated KMO$^{+/+}$ mice (data not shown). These results suggest that the administration of Kyn as well as the inhibition of KMO reverse the exacerbation of TNBS-induced colitis via the induction or accumulation of anti-inflammatory cytokine producing Foxp3$^+$ Treg cells.

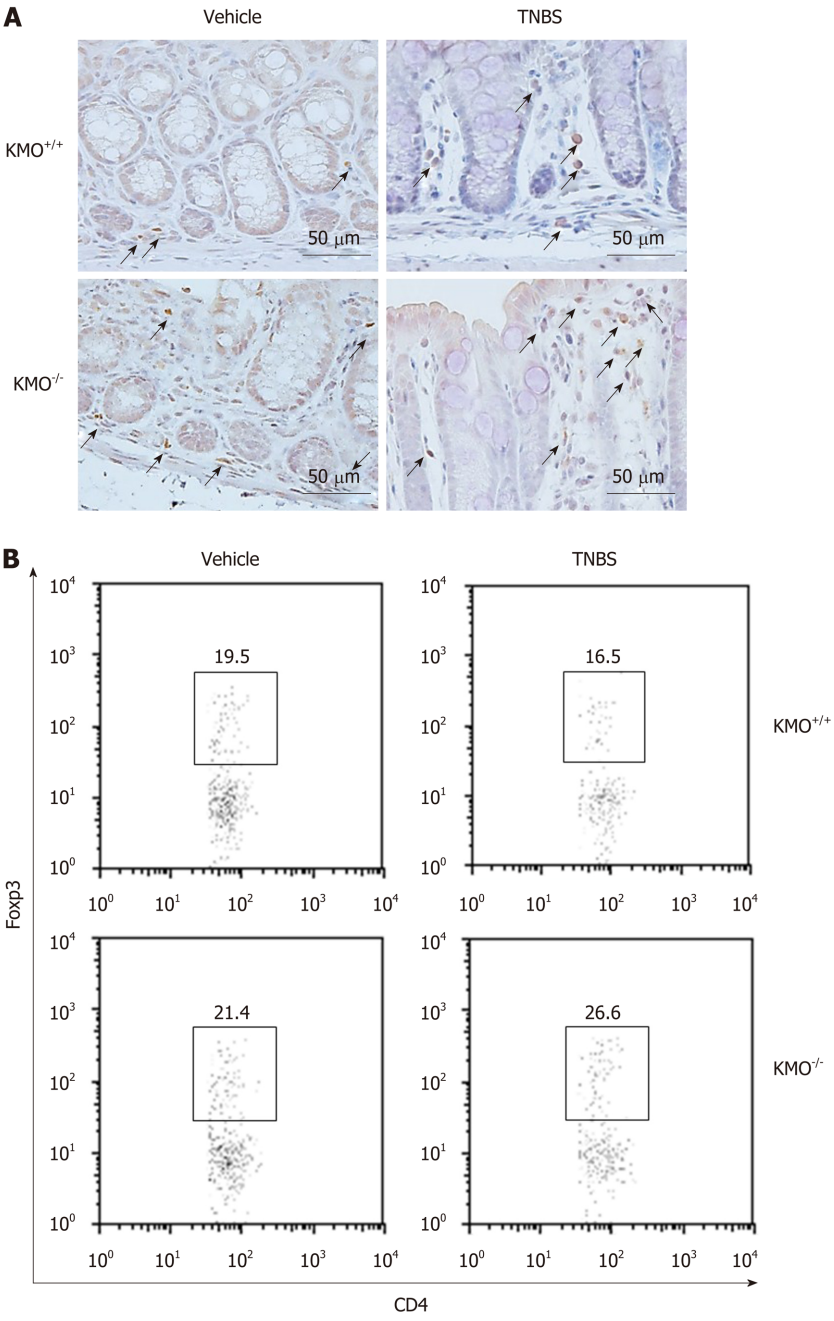
A
Vehicle
TNBS
KMO+/+
KMO-/-
50 μm
B
Vehicle
TNBS
19.5
16.5
21.4
26.6
KMO+/+
KMO-/-
Foxp3
CD4
C
% Foxp3+ cells/CD4+ cells
KMO+/+
KMO-/-
c
a
Vehicle
TNBS

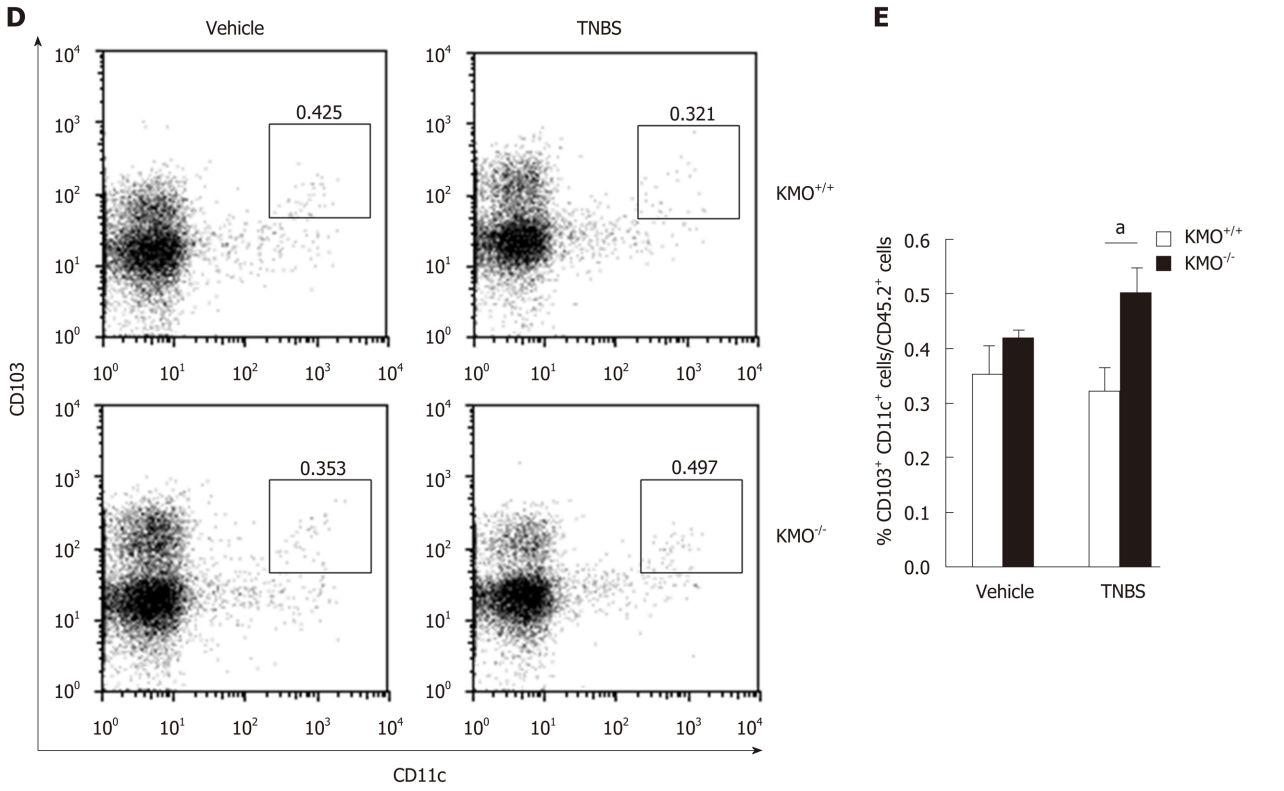

Figure 3 Regulation of KMO is involved in induction of Foxp3⁺ Treg cells. A: Serial sections of the colons of the indicated mice were stained for Foxp3 and counterstained with hematoxylin. B–E: $CD4^+Foxp3^+$ cells and $CD11c^+CD103^+$ cells were analyzed using flow cytometry on colonic LP cells and MLN cells, respectively, from indicated mice, gated on $7\text{-}AAD^-CD45.2^+$ cells. Representative flow cytometry plots and cumulative datagraphical summary are depicted. Data are representative of at least five independent experiments with similar results: $^aP < 0.05$ *vs* TNBS-treated $KMO^{+/+}$ mice group; $^cP < 0.05$ *vs* $KMO^{-/-}$ Vehicle group. KMO: Kynurenine 3-monooxygenase; TNBS: Trinitrobenzene sulfonic acid.

DISCUSSION

In this study, the role of KMO in immune regulation was examined in *KMO* gene deficient mice suffering from TNBS-induced colitis. We demonstrated that the expression of TGF-β and IL-10 in the colon of these colitic mice was upregulated by KMO inhibition and Kyn administration, resulting in increased recruitment of Treg cells into the inflammatory site, where they suppress the progression of colitis.

KMO plays a major role in physiological and pathological events involving KP[20]. KMO activity is high in MPs, especially macrophages[21] and its expression is dependent on IFN-γ signaling[22]. Our results showed that the number of KMO^+ cells, which are composed of $F4/80^+$ and $CD11c^+$ MPs, and mRNA expression level of KMO were significantly upregulated in the colon of TNBS-treated $KMO^{+/+}$ mice compared to vehicle mice. Interestingly, the absence or inhibition of KMO caused reduced inflammation and mucosal damage in the colon, suggesting that KMO^+ MPs play a pivotal role in initiating inflammation in this model. In this context, various functions of KMO in immune regulation have been reported[23-31]. For example, the absence of KMO is associated with reduction of mortality in acute viral myocarditis[23] and prevention of multiple organ failure in acute pancreatitis[29]. Therefore, KMO^+ MPs may be involved in the induction and progression of various inflammatory disorders.

Several studies have shown that the downstream metabolites of Trp possess immunomodulatory functions. Kyn, the first Trp metabolite, is known to act as an endogenous ligand for the aryl hydrocarbon receptor (AHR) that induces the generation of Treg cells through the expression of Foxp3[32,33]. Indeed, in the CpG-activated plasmacytoid dendritic cell-T cell co-culture system, the addition of 1-methyltryptophan, a representative inhibitor of IDO, significantly reduces the generation of Treg cells, whereas the addition of Kyn induces Treg generation even in the absence of endogenous IDO[25,34]. In line with these findings, the number of Treg cells in the colon is significantly increased in colitic $KMO^{-/-}$ mice, which have an elevated level of Kyn. Furthermore, the administration of Kyn to TNBS-treated $KMO^{+/+}$ mice increased the number of Treg cells in the colon and reduced the pathology of colitis. Thus, the number of Treg cells in inflamed colon may be regulated by Kyn levels in the tissue. We also found that the level of 3-HK remained

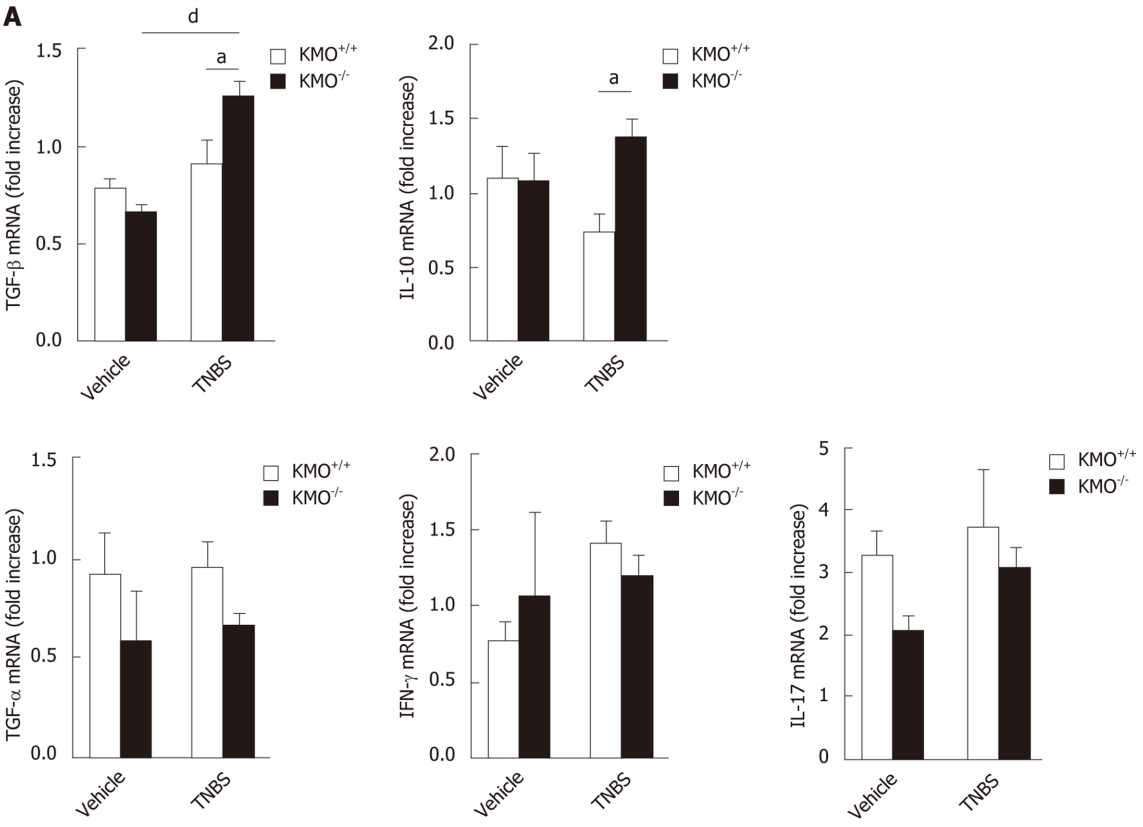
A
d
a
KMO+/+
KMO-/-
TGF-β mRNA (fold increase)
IL-10 mRNA (fold increase)
TGF-α mRNA (fold increase)
IFN-γ mRNA (fold increase)
IL-17 mRNA (fold increase)
Vehicle
TNBS

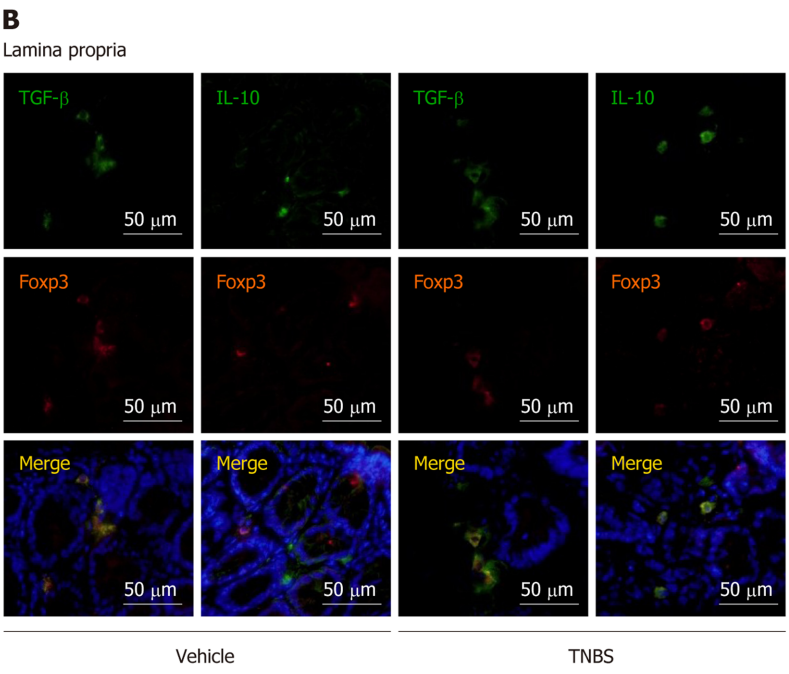
B
Lamina propria
TGF-β
IL-10
Foxp3
Merge
50 μm
Vehicle
TNBS

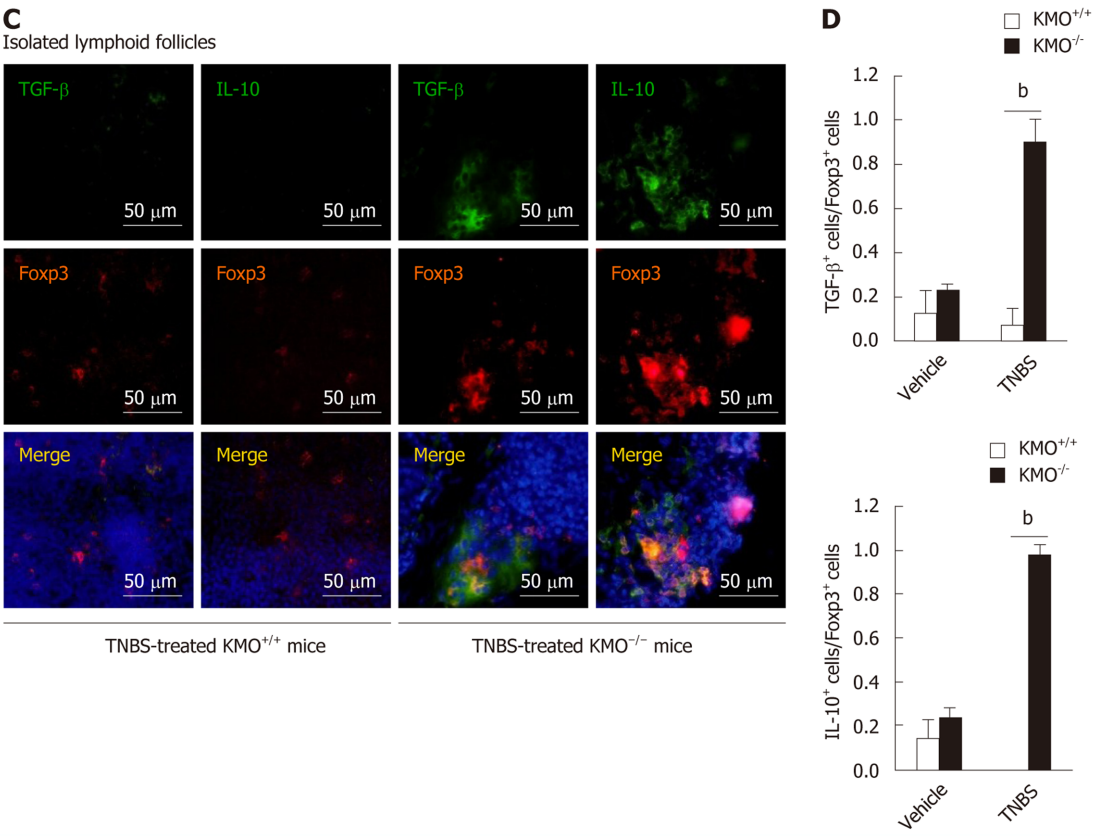

Figure 4 TNBS-treatment increased the levels of anti-inflammatory cytokines in the colon of KMO-deficient mice. A: mRNA levels of TGF-β, IL-10, TNF-α, IFN-γ, and IL-17 in the colons of indicated mice were determined by quantitative PCR. B–C: Serial sections of the colons from vehicle or TNBS-treated $KMO^{+/+}$ mice and TNBS-treated $KMO^{+/+}$ or $KMO^{-/-}$ mice were stained for TGF-β, IL-10, Foxp3, and DAPI (nuclei). D: The ratio of $TGF\text{-}\beta^+$ cells or $IL\text{-}10^+$ cells to $Foxp3^+$ Treg cells in ILF of TNBS-treated $KMO^{+/+}$ mice or TNBS-treated $KMO^{-/-}$ mice. Negative controls for of TGF-β, IL-10 and Foxp3 were not stained (Supplementary Figure 3). The data are represented as mean ± SE from at least four independent experiments: $^aP < 0.05$ *vs* TNBS-treated $KMO^{+/+}$ mice group; $^bP < 0.01$ *vs* TNBS-treated $KMO^{+/+}$ mice group; $^dP < 0.01$ *vs* $KMO^{-/-}$ Vehicle group. KMO: Kynurenine 3-monooxygenase; TNBS: Trinitrobenzene sulfonic acid; TGF-β: Transforming growth factor-β; IL-10: Interleukin-10; TNF-α: Tumor necrosis factor-α; IFN-γ: Interferon-γ; IL-17: Interleukin-17; Foxp3: Forkhead boxprotein P3.

low in colitic $KMO^{-/-}$ mice and the administration of 3-HK to $KMO^{-/-}$ mice exacerbated colitis. These results suggest that KMO^+ MPs might be a key player in the induction of colitis through their production of 3-HK.

Treg cells suppress Th1- and Th17-responses in colitis[35], and the removal of Treg cells worsens acute intestinal inflammation[10]. The suppressive effects of Treg cells on colitis are mediated by their production of IL-10 and TGF-β[36-38], suggesting that the regulation of Treg cells can aid in the treatment of IBD[39]. Indeed, in our study, TNBS-treated $KMO^{-/-}$ mice showed significantly increased frequency of IL-10- and TGF-β-producing Treg cells. However, the administration of Kyn in TNBS-treated $KMO^{+/+}$ mice significantly increased the levels of IL-10, but not those of TGF-β in the colon. In addition, although the frequency of TGF-β- or IL-10-producing $Foxp3^+$ cells was significantly higher in the ILF of TNBS-treated $KMO^{-/-}$ mice and Kyn-treated $KMO^{+/+}$ mice than in TNBS-treated $KMO^{+/+}$ mice, the frequency in the LP and MLN was unaffected, raising the question of how the Treg cells are generated in the ILF during colitis. In this regard, $CD103^+$ DCs have been shown to induce the differentiation from naive T cells into Treg cells in the MLN and possibly the ILF in a TGF-β- and retinoic acid-dependent manner, and the Treg cells then migrate into the LP[40,41]. We found that the frequency of $CD103^+$DCs in the MLN of colitic $KMO^{-/-}$ mice was higher than that in colitic $KMO^{+/+}$ mice. Importantly, intestinal $CD103^+$DCs that express IDO selectively induce Treg cells through their production of Kyn, thereby preventing colitis[42]. These findings suggest that the total number of Treg cells in the LP derived from the MLN and the ILF may be dependent on Kyn-producing $CD103^+$DCs. Besides MLN-generated Treg cells, thymus-generated natural Treg cells have also been shown to contribute to the suppression of chronic colitis in a T-cell transfer model[43]. During colitis, the ILF and their related lymphoid-like structures are developed by the recruitment of various immune cells[44], including possibly Treg cells. Therefore, the generation of Treg cells in the ILF may be due to their recruitment from the MLN and the thymus.

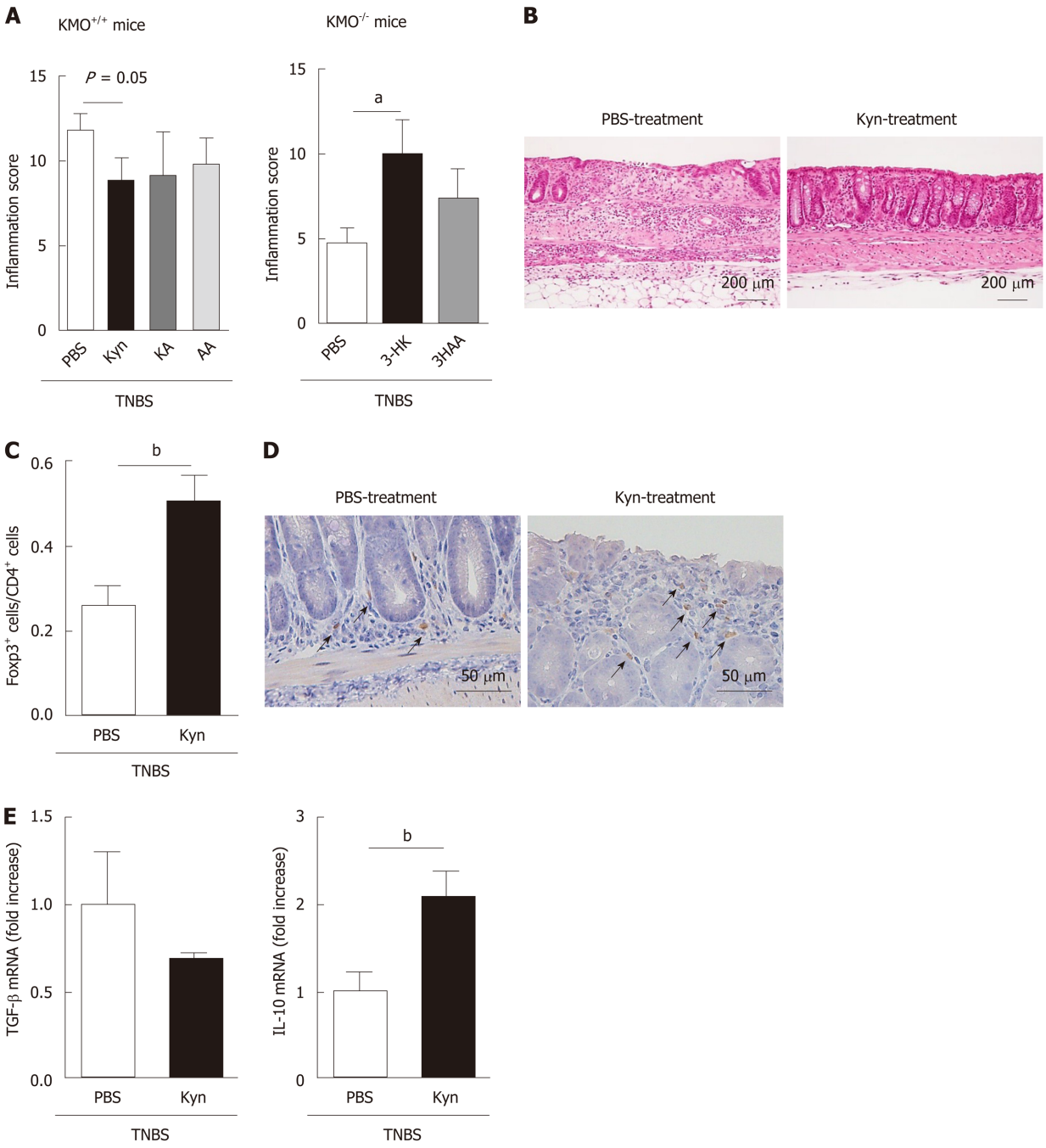

Figure 5 Administration of Kyn improved TNBS-induced colitis. KMO$^{+/+}$ and KMO$^{-/-}$ mice were treated with the indicated KP metabolites 12 h after TNBS injection, and the colons were collected on day 3. A: Histological inflammation scores for the colons of KP metabolite-treated mice or PBS-treated mice. B: Representative images of H&E-staining in the colon of indicated mice. C: The ratios of Foxp3$^+$ Treg cells to total CD4$^+$ T cells in the colons of mice. D: Serial sections of the colons of from indicated mice were stained for Foxp3 and counterstained with hematoxylin, allowing indication of Foxp3$^+$ cells. E: The mRNA expression levels of TGF-β and IL-10 were determined by quantitative PCR. The data are represented as mean ± SE from at least four independent experiments: $^aP < 0.05$ *vs* PBS-treated KMO$^{-/-}$ mice group; $^bP < 0.01$ *vs* PBS-treated KMO$^{+/+}$ mice group. KMO: Kynurenine 3-monooxygenase; TNBS: Trinitrobenzene sulfonic acid; Kyn: Kynurenine; KA: Kynurenic acid; AA: Anthranilic acid; 3-HK: 3-hydroxykynurenine; 3-HAA: 3-hydroxyanthranilic acid; TGF-β: Transforming growth factor-β; IL-10: Interleukin-10; Foxp3: Forkhead boxprotein P3.

In conclusion, we showed that the inhibition of KMO in the colon leads to increased levels of colonic Kyn, thereby suppressing colitis through Treg cell induction. Given that the administration of Kyn or inhibition of KMO are essential for Treg cell induction, our findings may contribute to the development of new therapeutic applications targeting Treg cells.

REFERENCES

1 **Strober W**, Fuss I, Mannon P. The fundamental basis of inflammatory bowel disease. *J Clin Invest* 2007; **117**: 514-521 [PMID: 17332878 DOI: 10.1172/jci30587]
2 **Xavier RJ**, Podolsky DK. Unravelling the pathogenesis of inflammatory bowel disease. *Nature* 2007; **448**: 427-434 [PMID: 17653185 DOI: 10.1038/nature06005]
3 **Antignano F**, Burrows K, Hughes MR, Han JM, Kron KJ, Penrod NM, Oudhoff MJ, Wang SK, Min PH, Gold MJ, Chenery AL, Braam MJ, Fung TC, Rossi FM, McNagny KM, Arrowsmith CH, Lupien M, Levings MK, Zaph C. Methyltransferase G9A regulates T cell differentiation during murine intestinal inflammation. *J Clin Invest* 2014; **124**: 1945-1955 [PMID: 24667637 DOI: 10.1172/JCI69592]
4 **Maynard CL**, Weaver CT. Intestinal effector T cells in health and disease. *Immunity* 2009; **31**: 389-400 [PMID: 19766082 DOI: 10.1016/j.immuni.2009.08.012]
5 **Bouma G**, Strober W. The immunological and genetic basis of inflammatory bowel disease. *Nat Rev Immunol* 2003; **3**: 521-533 [PMID: 12876555 DOI: 10.1038/nri1132]
6 **Nakamura K**, Kitani A, Fuss I, Pedersen A, Harada N, Nawata H, Strober W. TGF-beta 1 plays an important role in the mechanism of CD4+CD25+ regulatory T cell activity in both humans and mice. *J Immunol* 2004; **172**: 834-842 [PMID: 14707053 DOI: 10.4049/jimmunol.172.2.834]
7 **Asseman C**, Mauze S, Leach MW, Coffman RL, Powrie F. An essential role for interleukin 10 in the function of regulatory T cells that inhibit intestinal inflammation. *J Exp Med* 1999; **190**: 995-1004 [PMID: 10510089 DOI: 10.1084/jem.190.7.995]
8 **Read S**, Malmström V, Powrie F. Cytotoxic T lymphocyte-associated antigen 4 plays an essential role in the function of CD25(+)CD4(+) regulatory cells that control intestinal inflammation. *J Exp Med* 2000; **192**: 295-302 [PMID: 10899916 DOI: 10.1084/jem.192.2.295]
9 **Xu D**, Liu H, Komai-Koma M, Campbell C, McSharry C, Alexander J, Liew FY. CD4+CD25+ regulatory T cells suppress differentiation and functions of Th1 and Th2 cells, Leishmania major infection, and colitis in mice. *J Immunol* 2003; **170**: 394-399 [PMID: 12496424 DOI: 10.4049/jimmunol.170.1.394]
10 **Boehm F**, Martin M, Kesselring R, Schiechl G, Geissler EK, Schlitt HJ, Fichtner-Feigl S. Deletion of Foxp3+ regulatory T cells in genetically targeted mice supports development of intestinal inflammation. *BMC Gastroenterol* 2012; **12**: 97 [PMID: 22849659 DOI: 10.1186/1471-230x-12-97]
11 **Mottet C**, Uhlig HH, Powrie F. Cutting edge: cure of colitis by CD4+CD25+ regulatory T cells. *J Immunol* 2003; **170**: 3939-3943 [PMID: 12682220 DOI: 10.4049/jimmunol.170.8.3939]
12 **Fouser LA**, Wright JF, Dunussi-Joannopoulos K, Collins M. Th17 cytokines and their emerging roles in inflammation and autoimmunity. *Immunol Rev* 2008; **226**: 87-102 [PMID: 19161418 DOI: 10.1111/j.1600-065X.2008.00712.x]
13 **Izcue A**, Powrie F. Special regulatory T-cell review: Regulatory T cells and the intestinal tract--patrolling the frontier. *Immunology* 2008; **123**: 6-10 [PMID: 18154611 DOI: 10.1111/j.1365-2567.2007.02778.x]
14 **Izcue A**, Coombes JL, Powrie F. Regulatory lymphocytes and intestinal inflammation. *Annu Rev Immunol* 2009; **27**: 313-338 [PMID: 19302043 DOI: 10.1146/annurev.immunol.021908.132657]
15 **Izcue A**, Coombes JL, Powrie F. Regulatory T cells suppress systemic and mucosal immune activation to control intestinal inflammation. *Immunol Rev* 2006; **212**: 256-271 [PMID: 16903919 DOI: 10.1111/j.0105-2896.2006.00423.x]
16 **Takamatsu M**, Hirata A, Ohtaki H, Hoshi M, Hatano Y, Tomita H, Kuno T, Saito K, Hara A. IDO1 plays an immunosuppressive role in 2,4,6-trinitrobenzene sulfate-induced colitis in mice. *J Immunol* 2013; **191**: 3057-3064 [PMID: 23956437 DOI: 10.4049/jimmunol.1203306]
17 **Munn DH**, Shafizadeh E, Attwood JT, Bondarev I, Pashine A, Mellor AL. Inhibition of T cell proliferation by macrophage tryptophan catabolism. *J Exp Med* 1999; **189**: 1363-1372 [PMID: 10224276 DOI: 10.1084/jem.189.9.1363]
18 **Fallarino F**, Grohmann U, Vacca C, Orabona C, Spreca A, Fioretti MC, Puccetti P. T cell apoptosis by kynurenines. *Adv Exp Med Biol* 2003; **527**: 183-190 [PMID: 15206731 DOI: 10.1007/978-1-4615-0135-0_21]
19 **Von Bubnoff D**, Scheler M, Wilms H, Fimmers R, Bieber T. Identification of IDO-positive and IDO-negative human dendritic cells after activation by various proinflammatory stimuli. *J Immunol* 2011; **186**: 6701-6709 [PMID: 21543643 DOI: 10.4049/jimmunol.1003151]
20 **Kolodziej LR**, Paleolog EM, Williams RO. Kynurenine metabolism in health and disease. *Amino Acids* 2011; **41**: 1173-1183 [PMID: 20972599 DOI: 10.1007/s00726-010-0787-9]
21 **DE CASTRO FT**, BROWN RR, PRICE JM. The intermediary metabolism of tryptophan by cat and rat tissue preparations. *J Biol Chem* 1957; **228**: 777-784 [PMID: 13475359]
22 **Mándi Y**, Vécsei L. The kynurenine system and immunoregulation. *J Neural Transm (Vienna)* 2012; **119**: 197-209 [PMID: 21744051 DOI: 10.1007/s00702-011-0681-y]
23 **Kubo H**, Hoshi M, Mouri A, Tashita C, Yamamoto Y, Nabeshima T, Saito K. Absence of kynurenine 3-monooxygenase reduces mortality of acute viral myocarditis in mice. *Immunol Lett* 2017; **181**: 94-100 [PMID: 27889626 DOI: 10.1016/j.imlet.2016.11.012]
24 **Wang Y**, Liu H, McKenzie G, Witting PK, Stasch JP, Hahn M, Changsirivathanathamrong D, Wu BJ, Ball HJ, Thomas SR, Kapoor V, Celermajer DS, Mellor AL, Keaney JF, Hunt NH, Stocker R. Kynurenine is an endothelium-derived relaxing factor produced during inflammation. *Nat Med* 2010; **16**: 279-285 [PMID: 20190767 DOI: 10.1038/nm.2092]
25 **Chen W**, Liang X, Peterson AJ, Munn DH, Blazar BR. The indoleamine 2,3-dioxygenase pathway is essential for human plasmacytoid dendritic cell-induced adaptive T regulatory cell generation. *J Immunol* 2008; **181**: 5396-5404 [PMID: 18832696 DOI: 10.4049/jimmunol.181.8.5396]
26 **Wirtz S**, Neufert C, Weigmann B, Neurath MF. Chemically induced mouse models of intestinal inflammation. *Nat Protoc* 2007; **2**: 541-546 [PMID: 17406617 DOI: 10.1038/nprot.2007.41]
27 **Saito K**, Quearry BJ, Saito M, Nowak TS, Markey SP, Heyes MP. Kynurenine 3-hydroxylase in brain: species activity differences and effect of gerbil cerebral ischemia. *Arch Biochem Biophys* 1993; **307**: 104-109 [PMID: 8239646 DOI: 10.1006/abbi.1993.1567]
28 **Hoshi M**, Matsumoto K, Ito H, Ohtaki H, Arioka Y, Osawa Y, Yamamoto Y, Matsunami H, Hara A, Seishima M, Saito K. L-tryptophan-kynurenine pathway metabolites regulate type I IFNs of acute viral myocarditis in mice. *J Immunol* 2012; **188**: 3980-3987 [PMID: 22422885 DOI: 10.4049/jimmunol.1100997]
29 **Mole DJ**, Webster SP, Uings I, Zheng X, Binnie M, Wilson K, Hutchinson JP, Mirguet O, Walker A, Beaufils B, Ancellin N, Trottet L, Bénéton V, Mowat CG, Wilkinson M, Rowland P, Haslam C, McBride A, Homer NZ, Baily JE, Sharp MG, Garden OJ, Hughes J, Howie SE, Holmes DS, Liddle J, Iredale JP.

Kynurenine-3-monooxygenase inhibition prevents multiple organ failure in rodent models of acute pancreatitis. *Nat Med* 2016; **22**: 202-209 [PMID: 26752518 DOI: 10.1038/nm.4020]
30 **Cozzi A**, Carpenedo R, Moroni F. Kynurenine hydroxylase inhibitors reduce ischemic brain damage: studies with (m-nitrobenzoyl)-alanine (mNBA) and 3,4-dimethoxy-[-N-4-(nitrophenyl)thiazol-2yl]-benzenesulfonamide (Ro 61-8048) in models of focal or global brain ischemia. *J Cereb Blood Flow Metab* 1999; **19**: 771-777 [PMID: 10413032 DOI: 10.1097/00004647-199907000-00007]
31 **Stephens GL**, Wang Q, Swerdlow B, Bhat G, Kolbeck R, Fung M. Kynurenine 3-monooxygenase mediates inhibition of Th17 differentiation via catabolism of endogenous aryl hydrocarbon receptor ligands. *Eur J Immunol* 2013; **43**: 1727-1734 [PMID: 23568529 DOI: 10.1002/eji.201242779]
32 **Mezrich JD**, Fechner JH, Zhang X, Johnson BP, Burlingham WJ, Bradfield CA. An interaction between kynurenine and the aryl hydrocarbon receptor can generate regulatory T cells. *J Immunol* 2010; **185**: 3190-3198 [PMID: 20720200 DOI: 10.4049/jimmunol.0903670]
33 **Quintana FJ**, Basso AS, Iglesias AH, Korn T, Farez MF, Bettelli E, Caccamo M, Oukka M, Weiner HL. Control of T(reg) and T(H)17 cell differentiation by the aryl hydrocarbon receptor. *Nature* 2008; **453**: 65-71 [PMID: 18362915 DOI: 10.1038/nature06880]
34 **Fallarino F**, Grohmann U, You S, McGrath BC, Cavener DR, Vacca C, Orabona C, Bianchi R, Belladonna ML, Volpi C, Santamaria P, Fioretti MC, Puccetti P. The combined effects of tryptophan starvation and tryptophan catabolites down-regulate T cell receptor zeta-chain and induce a regulatory phenotype in naive T cells. *J Immunol* 2006; **176**: 6752-6761 [PMID: 16709834 DOI: 10.4049/jimmunol.176.11.6752]
35 **Powrie F**, Leach MW, Mauze S, Menon S, Caddle LB, Coffman RL. Inhibition of Th1 responses prevents inflammatory bowel disease in scid mice reconstituted with CD45RBhi CD4+ T cells. *Immunity* 1994; **1**: 553-562 [PMID: 7600284 DOI: 10.1016/1074-7613(94)90045-0]
36 **Sakaguchi S**. Regulatory T cells: key controllers of immunologic self-tolerance. *Cell* 2000; **101**: 455-458 [PMID: 10850488 DOI: 10.1016/s0092-8674(00)80856-9]
37 **Boden EK**, Snapper SB. Regulatory T cells in inflammatory bowel disease. *Curr Opin Gastroenterol* 2008; **24**: 733-741 [PMID: 19125486 DOI: 10.1097/mog.0b013e328311f26e]
38 **Barnes MJ**, Powrie F. Regulatory T cells reinforce intestinal homeostasis. *Immunity* 2009; **31**: 401-411 [PMID: 19766083 DOI: 10.1016/j.immuni.2009.08.011]
39 **Sumida Y**, Nakamura K, Kanayama K, Akiho H, Teshima T, Takayanagi R. Preparation of functionally preserved CD4+ CD25high regulatory T cells from leukapheresis products from ulcerative colitis patients, applicable to regulatory T-cell transfer therapy. *Cytotherapy* 2008; **10**: 698-710 [PMID: 18985477 DOI: 10.1080/14653240802345812]
40 **Annacker O**, Coombes JL, Malmstrom V, Uhlig HH, Bourne T, Johansson-Lindbom B, Agace WW, Parker CM, Powrie F. Essential role for CD103 in the T cell-mediated regulation of experimental colitis. *J Exp Med* 2005; **202**: 1051-1061 [PMID: 16216886 DOI: 10.1084/jem.20040662]
41 **Coombes JL**, Siddiqui KR, Arancibia-Cárcamo CV, Hall J, Sun CM, Belkaid Y, Powrie F. A functionally specialized population of mucosal CD103+ DCs induces Foxp3+ regulatory T cells via a TGF-beta and retinoic acid-dependent mechanism. *J Exp Med* 2007; **204**: 1757-1764 [PMID: 17620361 DOI: 10.1084/jem.20070590]
42 **Nguyen NT**, Hanieh H, Nakahama T, Kishimoto T. The roles of aryl hydrocarbon receptor in immune responses. *Int Immunol* 2013; **25**: 335-343 [PMID: 23580432 DOI: 10.1093/intimm/dxt011]
43 **Makita S**, Kanai T, Nemoto Y, Totsuka T, Okamoto R, Tsuchiya K, Yamamoto M, Kiyono H, Watanabe M. Intestinal lamina propria retaining CD4+CD25+ regulatory T cells is a suppressive site of intestinal inflammation. *J Immunol* 2007; **178**: 4937-4946 [PMID: 17404275 DOI: 10.4049/jimmunol.178.8.4937]
44 **McNamee EN**, Rivera-Nieves J. Ectopic Tertiary Lymphoid Tissue in Inflammatory Bowel Disease: Protective or Provocateur? *Front Immunol* 2016; **7**: 308 [PMID: 27579025 DOI: 10.3389/fimmu.2016.00308]

World Journal of Gastroenterology

Submit a Manuscript: https://www.f6publishing.com

World J Gastroenterol 2020 March 7; 26(9): 933-946

DOI: 10.3748/wjg.v26.i9.933

ISSN 1007-9327 (print) ISSN 2219-2840 (online)

ORIGINAL ARTICLE

Case Control Study

Exosomal miR-182 regulates the effect of RECK on gallbladder cancer

Hong Zheng, Jin-Jing Wang, Li-Jin Zhao, Xiao-Rong Yang, Yong-Lin Yu

ORCID number: Hong Zheng (0000-0002-0404-7792); Jin-Jing Wang (0000-0003-2576-4747); Li-Jin Zhao (0000-0001-6261-2262); Xiao-Rong Yang (0000-0002-7392-367X); Yong-Lin Yu (0000-0001-5803-1625).

Author contributions: Zheng H performed the majority of the experiments and analyzed the data; Wang JJ performed the molecular investigations; Zhao LJ designed and coordinated the research; Yang XR and Yu YL wrote the paper.

Institutional review board statement: This study was reviewed and approved by the Ethics Committee of Affiliated Hospital of Zunyi Medical University.

Informed consent statement: All patients in our study provided informed consent.

Conflict-of-interest statement: The authors declare no conflicts of interest.

Data sharing statement: No additional data are available.

STROBE statement: The authors have read the STROBE Statement-checklist of items, and the manuscript was prepared and revised according to the STROBE Statement-checklist of items.

Hong Zheng, Jin-Jing Wang, Xiao-Rong Yang, Yong-Lin Yu, Department of Pathology, Affiliated Hospital of Zunyi Medical University, Zunyi 563003, Guizhou Province, China

Li-Jin Zhao, Department of Hepatopancreatobiliary Surgery, Affiliated Hospital of Zunyi Medical University, Zunyi 563003, Guizhou Province, China

Corresponding author: Hong Zheng, MD, Chief Physician, Department of Pathology, Affiliated Hospital of Zunyi Medical University, No. 149 Dalian Road, Huichuan District, Zunyi 563003, Guizhou Province, China. zhengyao736925925@163.com

Abstract

BACKGROUND

As the most common biliary malignancy, gallbladder cancer (GC) is an elderly-biased disease. Although extensive studies have elucidated the molecular mechanism of microRNA 182 (miR-182) and reversion-inducing-cysteine-rich protein with kazal motifs (RECK) in various cancers, the specific role of exosomal miR-182 and RECK in GC remains poorly understood.

AIM

To explore the relationship between exosomal miR-182/RECK and metastasis of GC.

METHODS

Paired GC and adjacent normal tissues were collected from 78 patients. Quantitative polymerase chain reaction was employed to detect miR-182 and exosomal miR-182 expression, and Western blotting was conducted to determine RECK expression. In addition, the effects of exosomal miR-182/RECK on the biological function of human GC cells were observed. Moreover, the double luciferase reporter gene assay was applied to validate the targeting relationship between miR-182 and RECK.

RESULTS

Compared with normal gallbladder epithelial cells, miR-182 was highly expressed in GC cells, while RECK had low expression. Exosomal miR-182 could be absorbed and transferred by cells. Exosomal miR-182 inhibited RECK expression and promoted the migration and invasion of GC cells.

CONCLUSION

Exosomal miR-182 can significantly promote the migration and invasion of GC cells by inhibiting RECK; thus miR-182 can be used as a therapeutic target for GC.

Manuscript source: Unsolicited manuscript

Received: December 5, 2019
Peer-review started: December 5, 2019
First decision: December 30, 2019
Revised: January 8, 2020
Accepted: January 19, 2020
Article in press: January 19, 2020
Published online: March 7, 2020

P-Reviewer: Ho HK, Li C, Magnani M
S-Editor: Gong ZM
L-Editor: Filipodia
E-Editor: Ma YJ

Key words: Exosome; miR-182; RECK; Gallbladder cancer; Quantitative polymerase chain reaction; Therapeutic target

Core tip: Gallbladder cancer (GC) is the most common biliary malignancy that mostly affects the elderly. At present, however, the specific role of exosomal miR-182 and RECK in GC remains unknown. The results of this study indicated that exosomal miR-182 could markedly promote the migration and invasion of GC cells by inhibiting RECK. Therefore, miR-182 could serve as a therapeutic target for GC.

Citation: Zheng H, Wang JJ, Zhao LJ, Yang XR, Yu YL. Exosomal miR-182 regulates the effect of RECK on gallbladder cancer. *World J Gastroenterol* 2020; 26(9): 933-946
URL: https://www.wjgnet.com/1007-9327/full/v26/i9/933.htm
DOI: https://dx.doi.org/10.3748/wjg.v26.i9.933

INTRODUCTION

Gallbladder cancer (GC) is the most common biliary malignancy, ranking sixth among gastrointestinal cancers, with a high recurrence rate and poor prognosis[1,2]. Diabetes, gallstone size, age, sugary drinks, and genetic mutations are all risk factors affecting GC. At present, the effect of surgical treatment for GC is largely dependent on tumor metastasis[3], worsened by the fact that GC cells are highly invasive[1]. So gene target therapy has gradually become a research hotspot in GC. Many studies[4,5] have suggested that regulation of target gene expression by microRNA (miRNA) has potential therapeutic prospects.

MiR-182, a miRNA approximately 110 base pairs in length, is located on chromosome 7. It is well established that the abnormal expression of miR-182 is associated with cancer progression. For example, Kulkarni *et al*[6] found that miR-182 inhibited mitosis of renal cancer cells by downregulating metastasis associated lung adenocarcinoma transcript 1 expression. According to Livingstone *et al*[7], the serum expression of miR-182 in liver cancer model rats was significantly increased when aflatoxin was applied to construct liver cancer model rats, and the authors believed that the high expression of serum miR-182 was closely related to liver cancer. In addition, Perilli *et al*[8] found that the high expression of miR-182 in colorectal cancer cells could increase the activity of G0/G1 phase cells and downregulate the apoptosis pathway. MiR-182 can inhibit the Notch pathway through the NF-kB-miR-182-HES1 axis, ultimately promoting malignant invasion of medullary thyroid cancer cells[9]. While in GC, miR-182 promotes tumor metastasis by downregulating cell adhesion molecule 1 expression[10].

Reversion-inducing-cysteine-rich protein with kazal motifs (RECK) protein was expressed in 26 tissues including gallbladder, endometrium, and lung. As an important regulator of extracellular matrix remodeling, it can negatively regulate matrix metalloproteinase 9 (MMP9) and MMP2 to inhibit malignant behaviors such as migration and invasion of cancer cells[11-13]. Apart from that, RECK can promote apoptosis by altering p53, p53, B-cell lymphoma 2 (Bcl-2), Bcl-2-associated X protein (Bax), and other p53 pathway proteins[14]. Moreover, the influence of RECK on tumor progression was regulated by miRNA. For example, Chen *et al*[15] found that miR-15b promoted the proliferation and invasion of prostate cancer cells by targeting inhibition of RECK. Besides, Wang *et al*[16] demonstrated that RECK was negatively regulated by miR-21, which could upregulate the invasion and migration of colon cancer cells. In colorectal cancer, it has been reported that the effects of miR-92a[17], miR-96[18] and miR-375[19] on the biological function of cancer cells are all related to the regulation of RECK expression.

Although the molecular mechanism of miR-182 and RECK has been clarified in a variety of cancers, the co-role of exosomal miR-182 combined with RECK in GC remains unclear. Therefore here, by regulating their expression in GC, we explored the role of exosomal miR-182 and RECK in GC.

MATERIALS AND METHODS

Sample collection

Paired cancer tissues and adjacent normal tissues were obtained from 78 diagnosed GC patients, including 36 males and 42 females. Inclusion criteria were patients diagnosed with GC. In contrast, the exclusion criteria were as follows: Patients with psychiatric disorders, previous treatment history of surgery, chemotherapy, radiotherapy or antibiotic, combined with other tumors or those who did not cooperate with the treatment. The collected tissues were sectioned and stored in at -80 °C for testing. Venous blood samples from GC patients and healthy subjects were collected on an empty stomach and stored in Eppendorf tube without anticoagulant. Then it was centrifuged at room temperature for 15 min at 3×10^3 rpm to obtain the supernatant, which was then placed in a RNase-free Eppendorf tube for a 5-min centrifugation at a rotational speed of 1.2×10^4 rpm. After centrifugation, the supernatant was collected and stored at -80 °C until subsequent measurement. All participants were fully informed of the study, and the Medical Ethics Committee of the Affiliated Hospital of Zunyi Medical University approved the study.

Cell culture and transfection

GC cell lines (GBC-SD, EHGB1, NOZ) and human gallbladder epithelial cells (HGBEC) were purchased from the cell bank of American Type Culture Collection (Gaithersburg, MD, United States), and the cells were cultured in an animal cell incubator at 37 °C and 5% CO_2. The medium used for the GC cell lines was 1640 medium (HyClone Laboratories, South Logan, UT, United States) supplemented with 10% fetal bovine serum (FBS; Gibco Laboratories, Gaithersburg, MD, United States) and 1% penicillin/streptomycin (100X; Beijing Solarbio Science & Technology Co. Ltd., Beijing, China), while that used for the HGBEC cell line was Dulbecco's Modified Eagle Medium (DMEM) (Hyclone) supplemented with 10% FBS (Gibco Company) and 1% penicillin/streptomycin (100X; Solarbio). Follow-up experiments were carried out until the cells reached 80%-90% confluency.

The culture medium was renewed with FBS-free medium 1 d before transfection, and cells were seeded into 6-well plates at 1×10^5/well. MiR-182 mimics, RECK small interfering RNA (siRNA), and negative control (NC) si vectors were purchased from Sangon Biotech (Shanghai) Co., Ltd. (Shanghai, China) Then the Lipofectamine 2000 Transfection Kit (Invitrogen, Carlsbad, CA, United States) was employed to transfect the abovementioned vectors into the cell lines according to the manufacturer's instructions. The culture medium was renewed at 37 °C and 5% CO_2 8 h after transfection.

Separation and screening of exosomes

Cell (NOZ cell) suspension was prepared by enzymatic hydrolysis before centrifuging at 1×10^5 *g* for 8 h. Then the cells were cultured in RPMI 1640 medium containing 10% FBS at 37 °C and 5% CO_2. When the cells were cultured to 80%-90% confluency, the supernatant of the medium was collected, the exosomes were extracted, and the latter was centrifuged at 1×10^5 *g* for 1.5 h to collect the lower exosome sediments. Next, phosphate-buffered saline (PBS) was added to the exosome precipitate for repeated pipetting. Finally, the expression of cluster of differentiation 63 (CD63) and CD81 was detected by Western blot analysis.

Quantitative PCR

The total RNA from the tissue samples or cells was extracted by Trizol, while that of the exosomes was detected using the Total Exosome RNA & Protein Isolation Kit (No. 4475545; Invitrogen). Then the concentration and purity of total RNA at 260-280 nm was detected by an ultraviolet spectrophotometer, and RNA with OD260/OD280 > 1.8 was selected for follow-up quantitative PCR (qPCR) detection. The FastKing One-Step Reverse Transcription-Fluorescence Quantification Kit [Catalog No. FP314; Tiangen Biotech (Beijing) Co. Ltd., Beijing, China) and ABI PRISM 7000 (Applied Biosystems, Foster City, CA, United States] were applied for qPCR quantification. MiR-182 primer was designed and synthesized by Sangon Biotech (Shanghai) Co., Ltd. The reaction system was performed in strict accordance with the kit instructions (50 μL): Upstream primer: 1.25 μL, downstream primer: 1.25 μL, probe: 1.0 μL, RNA template: 10 pg/μg, 50 × ROX Reference Dye ROX: 5 μL, and RNase-FreeddH_2 was added to reach an overall reaction volume of 50 μL. Reaction process: reverse transcription at 50 °C for 30 min, cycled once; pre-denaturation at 95 °C for 3 min, cycled once; denaturation at 95 °C for 15 s, and annealing at 60 °C for 30 s, cycled 40 times. The results were analyzed by the ABI PRISM 7000 instrument with U6 and GAPDH as the internal reference genes; the primer sequences are shown in Table 1.

Table 1 Primer sequences

	Upstream primer (5'→3')	Downstream primer (5'→3')
miR-182	TGCGGTTTGGCAATGGTAGAAC	CCAGTGCAGGGTCCGAGGT
RECK	TCTGCAGGGGAAGTTGGTTG	CAGTTACAGGGCAGACCTGT
U6	CTCGCTTCGGCAGCACA	AACGCTTCACGAATTTGCGT
GAPDH	AGAAGGCTGGGGCTCATTTG	AGGGGCCATCCACAGTCTTC

miR-182: MicroRNA 182; RECK: Reversion-inducing-cysteine-rich protein with kazal motifs.

Western blot

An volume of 1 mL cell protein extract (cell lysate: protease inhibitor: phosphatase inhibitor = 98:1:1, v/v/v) was added to the cells. Then the solution was pipetted several times and centrifuged at 1.2 × 10^4 r/min for 15 min to collect the supernatant. The proteins were resolved by sodium dodecyl sulfate polyacrylamide gel electrophoresis before transfer to the nitrocellulose membrane, followed by blocking at room temperature for 1 h in 5% skim milk/PBS solution. Next, the membrane was incubated overnight at 4 °C with primary antibodies against RECK, caspase-3, caspase-9, E-cadherin, Bax, Bcl-2, N-cadherin, β-catenin and β-actin (all from Shanghai Abcam Co., Shanghai, China). Then the nitrocellulose membrane was washed three times with PBS, followed by a 1 h incubation at room temperature with goat anti-rabbit secondary antibody (horseradish peroxidase cross-linked; Shanghai Abcam Co.). Finally, the NC membrane was rinsed with PBS and proteins were visualized by enhanced chemiluminescence. With β-actin as the internal reference protein, the relative expression level of the protein to be measured was equal to the gray value of the band to be measured/the gray value of the β-actin band.

Transwell chamber detection for cell migration and invasion

The adherent cells were digested with trypsin and the supernatant was obtained by 1103 x *g* centrifugation for 1 min, and then added to the cell medium to re-suspend the cells. Then the cells were seeded in the upper migration chamber (containing 200 μL 10% FBS + 1% DMEM) at 2 × 10^4 cells/well, and the DMEM containing 10% FBS (total volume of 500 μL) was added to the lower chamber. After 24 h of cell culture, the upper chamber fluid was removed and the parenchyma cells were wiped off. Then the Transwell cells were fixed in 4% methanol for 20 min, and the Transwell chamber was washed with PBS after crystal violet staining for 15 min. Photographs of cell migration were taken under a 200-fold microscope, and three fields of view were randomly selected to calculate the number of cells, with the average value as the number of permeabilized cells. The experiment was repeated three times. The invasion experiment shared the same steps with those of migration experiment, except that the former was treated with 8% matrix glue and the number of cells per well was increased to 5 × 10^4.

MTT assay for cell viability

The transfected cells were hydrolyzed with trypsin and centrifuged to remove the enzyme solution, followed by the addition of fresh medium and pipetting to prepare the cell suspension. Then four 96-well plates were inoculated with cells of 5 × 10^3/100 μL per well, with 3 wells per set. One plate was taken out every 24 h, and 5 mg/mL MTT solution was added at 10 μL/well for additional culture for 1 h. Then the culture medium was removed and the OD value at 570 nm was measured by a microplate reader. The experiment was repeated three times to plot the cell viability-time curve.

Flow cytometry

The adherent cells were digested and prepared as a cell suspension. The CountessTM automatic counter (Invitrogen) was applied to dilute the cells to 1 × 10^6. Then cells were fixed in a 70% ethanol ice-cold solution at 4 °C for 30 min. Thereafter, the ethanol solution was removed, and the cells were incubated in Annexin V-FITC/7-AAD solution. Finally, apoptosis was analyzed using the FACScan flow cytometer (Becton Dickinson, Franklin Lakes, NJ, United States).

Double luciferase verification of targeting relationship between miR-182 and RECK

The pmirGLO-HMGB1-wt and pmirGLO-HMGB1-mut vectors were constructed and co-transfected into EH-GB1 and GBS-SD cells with miR-182 mimics and NC mimics, respectively. After 48 h of transfection, the luciferase activity was detected by double luciferase reporter gene assay (Promega, Madison, WI, United States) in strict

accordance with the instructions.

Statistical analysis

Statistical analysis of the collected data of indicators mentioned above was performed using SPSS20.0 (Asia Analytics Formerly SPSS, China) and GraphPad Prism 6.0. Each experiment was repeated three times. The data are represented by the mean ± standard deviation, and the count data are expressed as n. Intergroup comparison was conducted by an independent samples *t*-test, multi-group comparison was analyzed by one-way analysis of variance, and post-hoc pairwise comparison was performed by an least significant difference test. Pearson's analysis was applied to the correlation between miR-182 and RECK. The relationship between miR-182 and clinical features was determined by the two-sample Student's *t*-test. All data were double-tailed. With 95% as its confidence interval, a statistically significant difference was assumed at $P < 0.05$.

RESULTS

There is high expression of miR-182 and low expression of RECK in GC

Exosomes were extracted and Western blot analysis was used to detect exosome protein markers CD63 and CD81 (Figure 1). The results showed that CD63 and CD81 were highly expressed in exosomes compared with cell samples, indicating that the sample was indeed exosomes.

This study included 78 cases of paired GC and adjacent normal tissues. qPCR was employed to quantify the expression levels of miR-182 and exosomal miR-182 in tissues and cells, and the expression of RECK protein in tissues and cells was determined by Western blot analysis(Figure 2). The expression of miR-182 was markedly increased in cancer tissues (Figure 2A), whereas that of RECK was notably decreased in cancer tissues compared with normal adjacent tissues (Figure 2D). Compared with normal human blood samples, serum miR-182 level was significantly elevated in patients with GC (Figure 2B). However, compared with HGBEC, miR-182 expression was markedly increased (Figure 2C), whereas RECK was significantly decreased in GC cells (Figure 2E). The abovementioned results indicated that miR-182 was highly expressed in GC, whereas there was low expression of RECK. It is worth mentioning that the expression levels of miR-182 and RECK were the highest and lowest, respectively in NOZ cell lines.

miR-182 is associated with GC metastasis

Here, we compared the expression of miR-182 and exosomal miR-182 in different tumor-node-metastasis (TNM) phases and analyzed the correlation between miR-182 and clinical features (Figure 3, Table 2). As shown in Figure 3, miR-182 and exosomal miR-182 were highly expressed in the N1/N2/N3 and M1 phases. Table 2 illustrates that miR-182 was associated with the N and M phases and RECK expression.

Exosomal miR-182 can promote cell proliferation, migration and invasion, and inhibit apoptosis and RECK expression

As mentioned earlier, miR-182 and RECK presented the highest and lowest expression, respectively in NOZ cell lines; thus exosomal miR-182 in NOZ cells was extracted and co-cultured with EH-GB1 and GBS-SD cells to observe the effect of miR-182 on cell biological function. Cell viability was detected by MTT, cell invasion and migration were measured by the Transwell assay, protein expression was detected by Western blotting, and apoptosis was determined by flow cytometry. Compared with the NC group, the cell viability (Figure 4A and B), cell invasion (Figure 4C), and migration (Figure 4D) of the exosomal miR-182 group were enhanced, whereas apoptosis (Figure 4E, Supplementary Figure 1A and C) was attenuated. In addition, compared with the NC group, the expression levels of RECK, caspase-3, caspase-9, E-cadherin, and Bax were downregulated in the exosomal miR-182 group, whereas the expression levels of Bcl-2, N-cadherin and β-catenin were upregulated (Figure 4E). These results revealed that exosomal miR-182 promoted cell proliferation, migration and invasion, and inhibited apoptosis and RECK expression.

RECK inhibits cell proliferation, migration and invasion, and promotes apoptosis

The expression of RECK was regulated by exosomal miR-182. In order to understand whether the change of RECK expression was related to the occurrence of GC, we inhibited RECK and observed its effect on the biological function of GC cells (Figure 5). Compared with the NC group, the RECK siRNA group had increased cell viability (Figure 5A and B), enhanced cell invasion (Figure 5C) and migration (Figure 5D), and

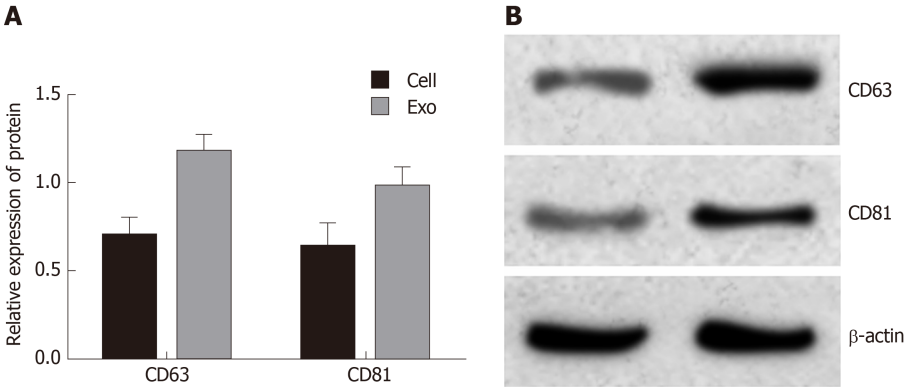

Figure 1 Western blot analysis of cluster of differentiation 63 and cluster of differentiation 81 exosomes. A: Expression levels of cluster of differentiation (CD) 63 and CD81; B: Western blot bands. Exosomes were isolated from cells; the isolation process is described in "Separation and screening of exosomes."

decreased apoptosis (Supplementary Figure 1B and D). In addition, the expression levels of caspase-3, caspase-9, E-cadherin, and Bax in the RECK siRNA group were downregulated, while the expression levels of Bcl-2, N-cadherin, and β-catenin were upregulated in contrast with the NC group. These results indicated that RECK promoted apoptosis and inhibited cell proliferation, migration, and invasion.

MiR-182 targets inhibition of RECK expression

The TargetScan database predicted that miR-182 had binding sites on RECK mRNA (Figure 6A). The double luciferase reporter gene assay confirmed that miR-182 had a targeting relationship with RECK mRNA (Figure 6B and C). In addition, a negative correlation between miR-182 and RECK protein was validated by Pearson's analysis. The above results indicated that miR-182 could target to inhibit RECK.

Rescue experiment

Exosomal miR-182 and exosomal miR-182+RECK overexpression vectors were added to GC cells to perform the MTT assay, Western blot analysis, and Transwell assay. The results showed that compared with the exosomal miR-182 group, the cell viability, migration, and invasion of the exosomal miR-182+RECK group decreased, and apoptosis increased. Meanwhile, the exosomal miR-182+RECK group showed upregulated caspase-3, caspase-9, E-cadherin and Bax and downregulated Bcl-2, N-cadherin, and β-catenin expression (Figure 7). The above results suggested that RECK overexpression could counteract the enhancement of cell proliferation, invasion, and migration caused by exosomal miR-182.

DISCUSSION

As essential carriers for cell-cell information communication, exosomes are extracellular vesicles with a diameter of 40-150 nm in nature, which contain a variety of proteins, DNA, and RNA. CD63, CD81, and CD9 on the surface of vesicles are vesicles markers[20]. Exosomes can stimulate extracellular matrix remodeling or information transmission when they are released out of the cell, which is of great significance for human health and disease[21]. Due to the presence of exosomes, miRNAs can be actively secreted outside the cell without degradation of RNA enzymes, and play a role by being absorbed by other cells through endocytosis[22].

In this study, miR-182 and exosomal miR-182 were found to be highly expressed in GC, and had the highest expression levels in NOZ cells. Therefore, exosomal miR-182 was isolated from NOZ cells and co-cultured with EH-GB1 and GBS-SD cells. The results showed that exosomal miR-182 could promote the proliferation, migration, and invasion of EH-GB1 and GBC-SD cells and inhibit cell apoptosis. Meanwhile, the expression of RECK, caspase-9, caspase-9, E-cadherin, and Bax was found to be downregulated, whereas the expression of Bcl-2, N-cadherin and β-catenin was upregulated. In the study of Qiu *et al*[10], miR-182 could act as a carcinogen to promote the metastasis of GC. The results of this study further supplemented the possibility that miR-182 could regulate other cell biological functions through exosomes.

In addition, we found that RECK was downregulated when exosomal miR-182 was co-cultured with cancer cells. TargetScan further predicted that there were binding sites between miR-182 and RECK mRNA, and the negative correlation between the

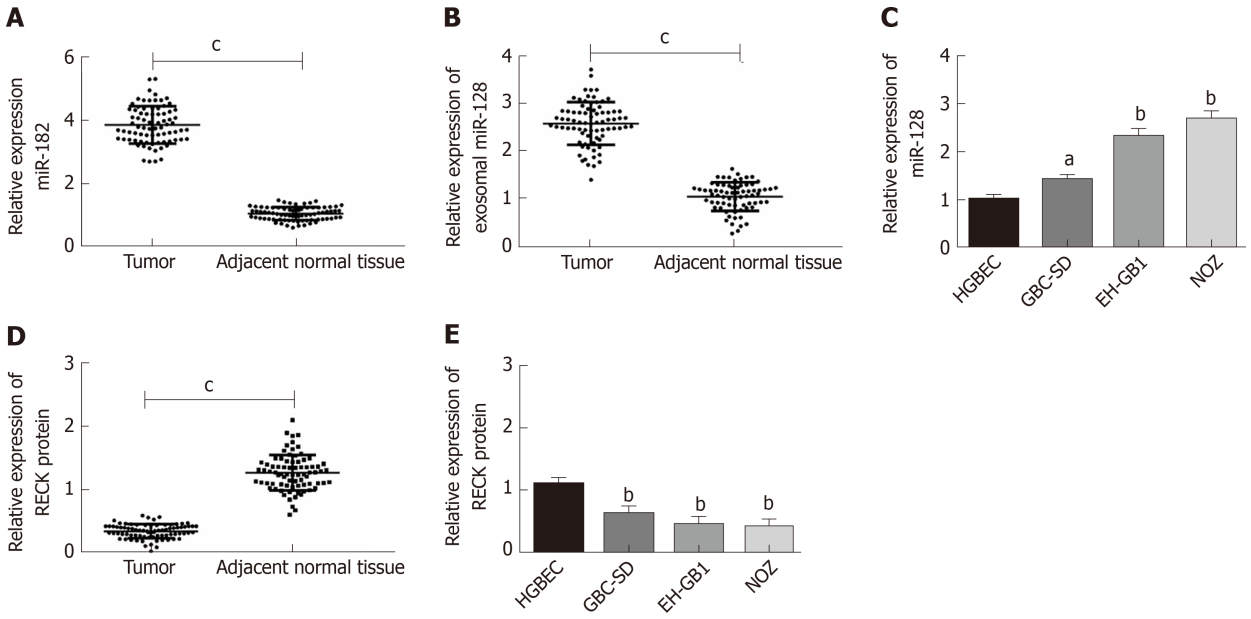

Figure 2 MicroRNA 182 was highly expressed, whereas there was low expression of reversion-inducing-cysteine-rich protein with kazal motifs in gallbladder cancer. A: MicroRNA 182 (miR-182) was highly expressed in gallbladder cancer (GC) tissues; B: Exosomal miR-182 was highly expressed in patients with GC; C: MiR-182 was highly expressed in GC cells; D: Reversion-inducing-cysteine-rich protein with kazal motifs (RECK) protein was highly expressed in GC tissues; E: RECK protein was highly expressed in GC cells. $^{a}P < 0.05$, $^{b}P < 0.01$ *vs* HGBEC. $^{c}P < 0.001$.

two. Therefore, we speculated that the effect of miR-182 on cell biological function might be achieved by regulating RECK expression. In this study, the effect of RECK on GC cells was observed by interfering with RECK expression in cancer cells by siRNA, and the targeting relationship between miR-182 and RECK was validated by the double luciferase reporter gene assay. The results demonstrated that the absence of RECK promoted cell proliferation, migration and invasion and inhibited cell apoptosis; meanwhile downregulating the levels of caspase-3, caspase-9, E-cadherin, Bax, and Bcl-2, while upregulating N-cadherin and β-catenin. In addition, it was found that luciferase activity of cells was the lowest when 182 mimics were co-transfected with pmirGLO-RECK-wt. RECK is a protein related to cell migration and invasion. By binding to RECK mRNA, exosomal miR-182 inhibited the expression of RECK at the transcriptional level, resulting in increased expression of N-cadherin, β-catenin, MMP9 and MMP2 in cells, and enhanced cell migration and invasion. Although studies[23-25] have reported that miR-182/RECK affects the development of breast, bladder and prostate cancer, the role exosomal miR-182/RECK plays in GC has not been studied. Here, we proved that, by inhibiting RECK, exosomal miR-182 could downregulate the expression levels of caspase-9, caspase-9, E-cadherin, and Bax, and upregulate Bcl-2, N-cadherin and β-catenin, ultimately promoting the proliferation, migration, and invasion of GC cells.

The present study demonstrated that by regulating RECK, exosomal miR-182 could promote cell proliferation, migration and invasion and inhibit apoptosis, ultimately leading to tumor formation or metastasis, which aggravated the deterioration of GC. Although the relationship between miR-182/RECK and tumor metastasis was preliminarily studied, there is still room for improvement. For example, the signaling pathways implicated in miR-182/RECK should be explored in future experimental design to supplement the oncogenic network of exosomal miR-182. In addition, the clinical value of exosomal miR-182 in GC remains to be discussed.

To summarize, this study investigated the effect of miR-182/RECK axis on the biological function of GC cells by studying the expression mechanism of exosomal miR-182 and RECK in GC. MiR-182 is highly expressed in GC cells, thereby acting on other cells through endocytosis to inhibit intracellular RECK expression, and ultimately promoting cell proliferation, migration, and invasion. In addition, exosomal miR-182 is positively correlated with tumor metastasis of GC. Therefore, miR-182/RECK axis has potential application value in targeted therapy of GC.

Table 2 Correlation between miR-182 and clinical features

Categories	*n*	miR-182		χ^2	*P* value
		Low expression	High expression		
Gender				0.125	0.819
Male	36	17	25		
Female	42	16	20		
Age in yr				0.273	0.646
≤ 60	45	19	26		
> 60	33	12	21		
Smoking history				0.075	0.823
Yes	41	22	19		
No	37	21	16		
Drinking history				0.396	0.645
Yes	46	22	24		
No	32	15	17		
N staging				5.128	0.035
N_0	25	12	13		
$N_1/N_2/N_3$	53	12	41		
M staging				5.349	0.027
M_0	22	10	12		
M_1	56	11	45		
RECK expression					
Low	31	15	16	5.246	0.028
High	47	11	36		

M: Metastasis; N: Node; RECK: Reversion-inducing-cysteine-rich protein with kazal motifs.

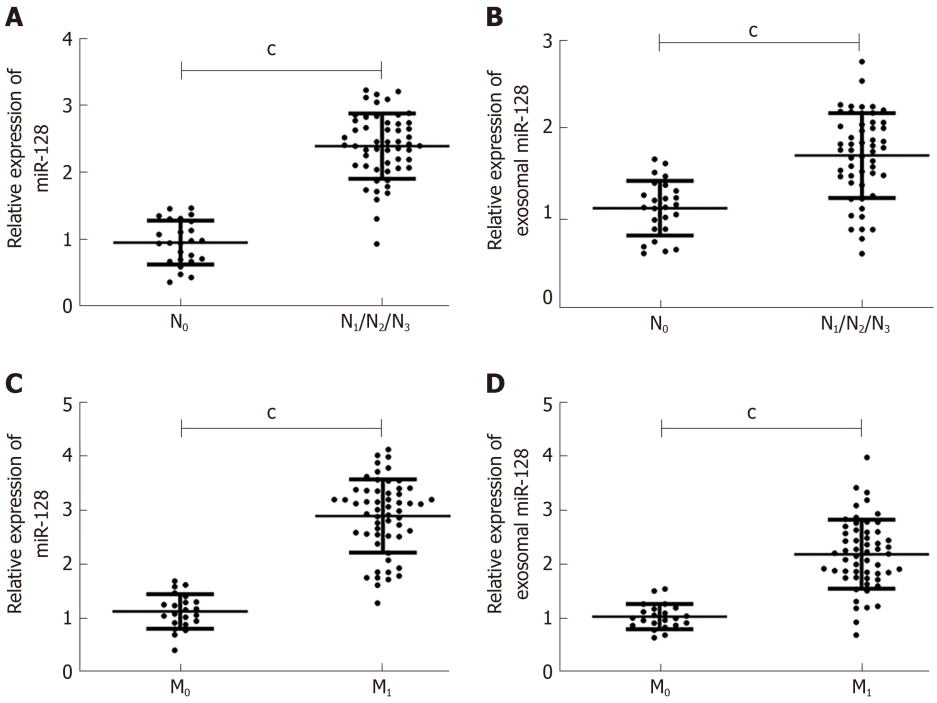

Figure 3 Relationship between microRNA 182 and tumor-node-metastasis staging. A: MicroRNA 192 (miR-182) was highly expressed in the N1/N2/N3 phase; B: Exosomal miR-182 was highly expressed in the N1/N2/N3 phase; C: MiR-182 was highly expressed in the M1 phase; D: Exosomal miR-182 was highly expressed in the M1 phase. $^cP < 0.001$.

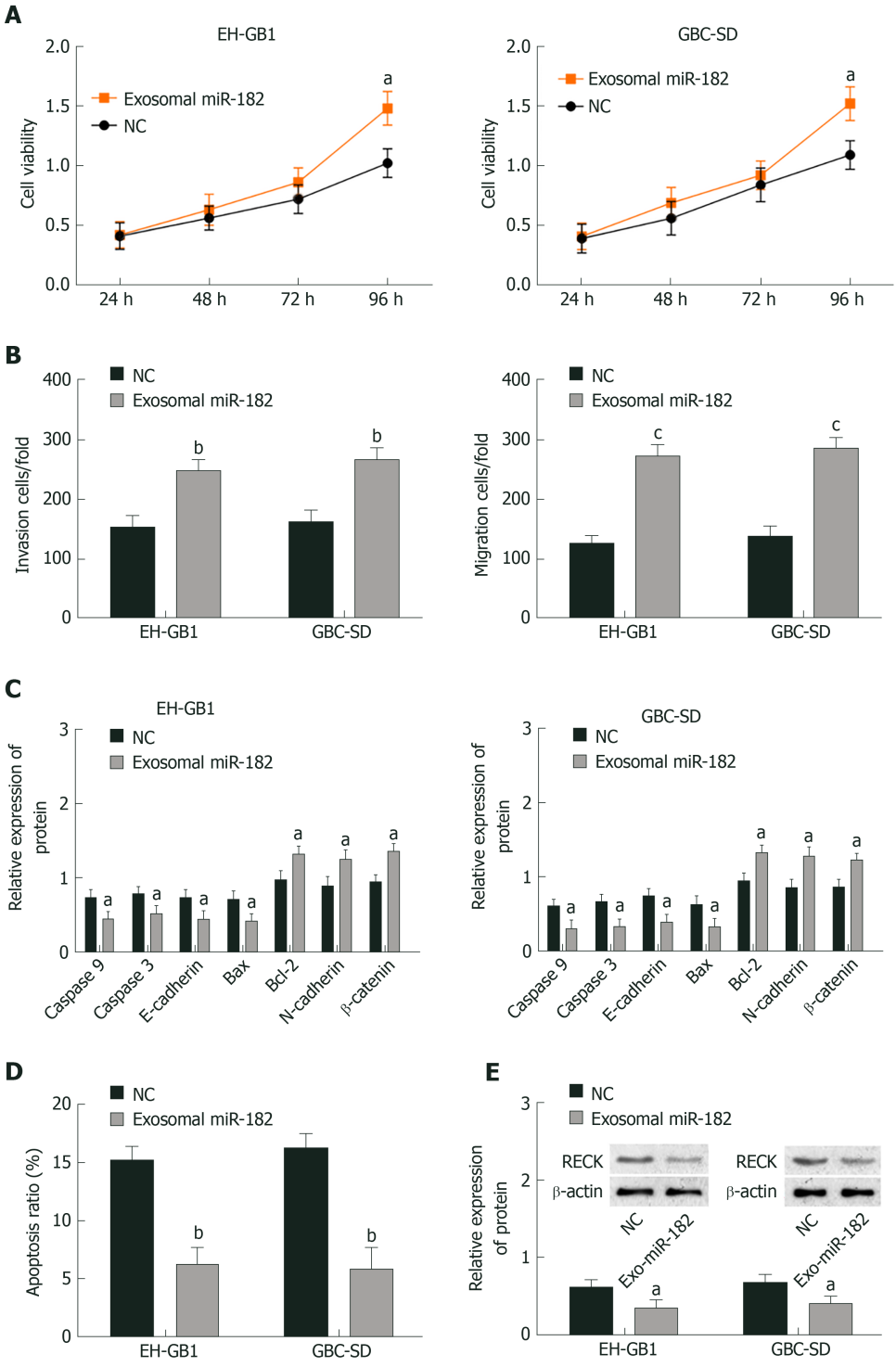

Figure 4 Exosomal microRNA 182 can promote cell proliferation, migration and invasion, and inhibit apoptosis and expression of reversion-inducing-cysteine-rich protein with kazal motifs. A: Exosomal microRNA 182 (miR-182) enhanced the viability of gallbladder cancer (GC) cells; B: Exosomal miR-182 promoted cell invasion and migration; C: Effects of exosomal miR-182 on caspase 3, caspase 9, E-cadherin, B-cell lymphoma 2 (Bcl-2), Bcl-2-associated X protein, N-cadherin, and β-catenin in GC cells; D: Exosomal miR-182 inhibited apoptosis; E: Exosomal miR-182 inhibited reversion-inducing-cysteine-rich protein with kazal motifs expression. $^{a}P < 0.05$, $^{b}P < 0.01$, and $^{c}P < 0.001$ *vs* the negative control (NC) group.

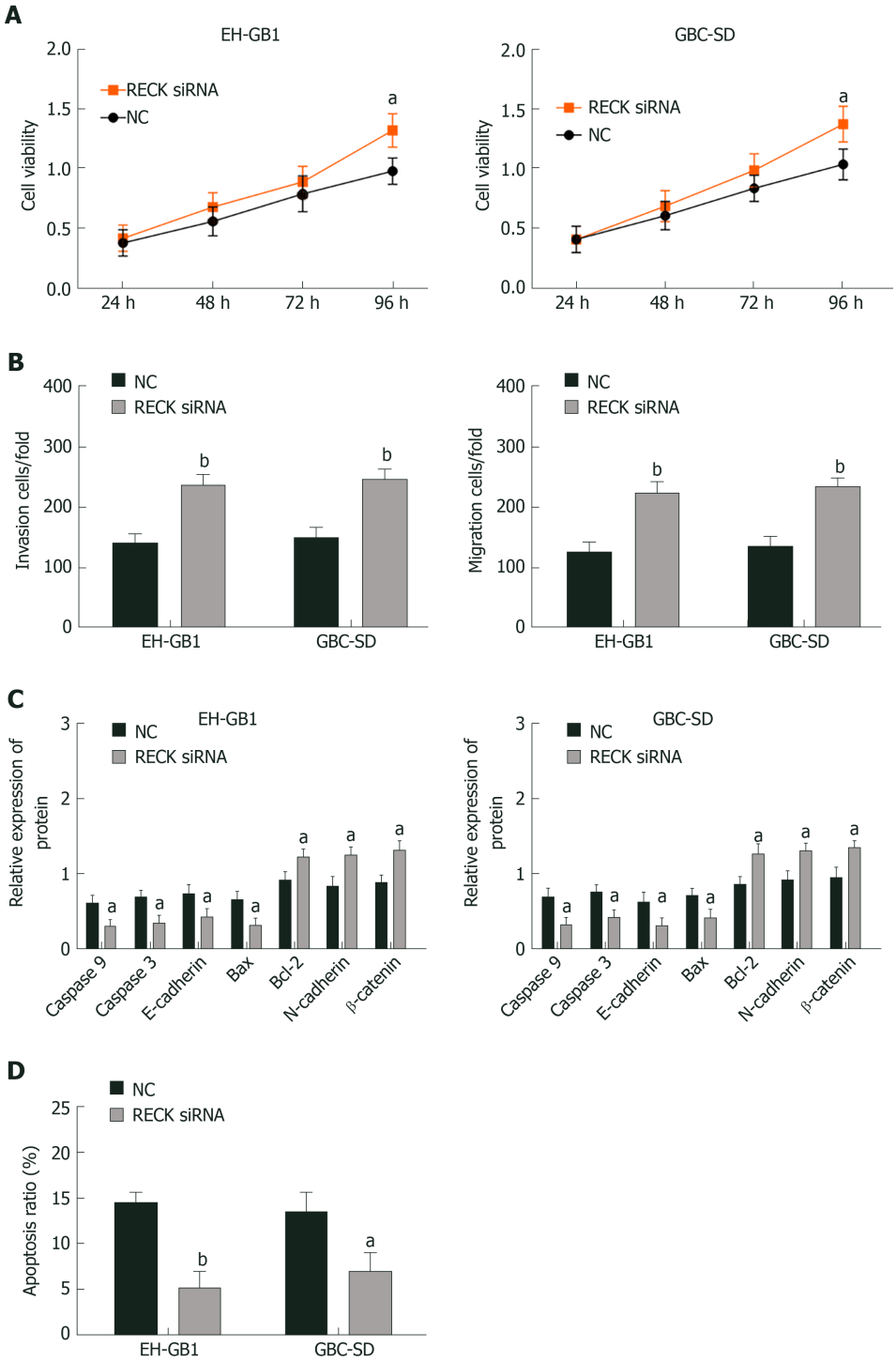

Figure 5 Reversion-inducing-cysteine-rich protein with kazal motifs inhibited cell proliferation, migration and invasion, and promoted apoptosis. A: Reversion-inducing-cysteine-rich protein with kazal motifs (RECK) inhibited viability of gallbladder cancer (GC) cells; B: RECK inhibited cell invasion and migration; C: Effects of exosomal microRNA 182 on caspase 3, caspase 9, E-cadherin, B-cell lymphoma 2 (Bcl-2), Bcl-2-associated X protein N-cadherin, and β-catenin in GC cells; D: RECK promoted apoptosis; $^{a}P < 0.05$, and $^{b}P < 0.01$ *vs* the negative control (NC) group.

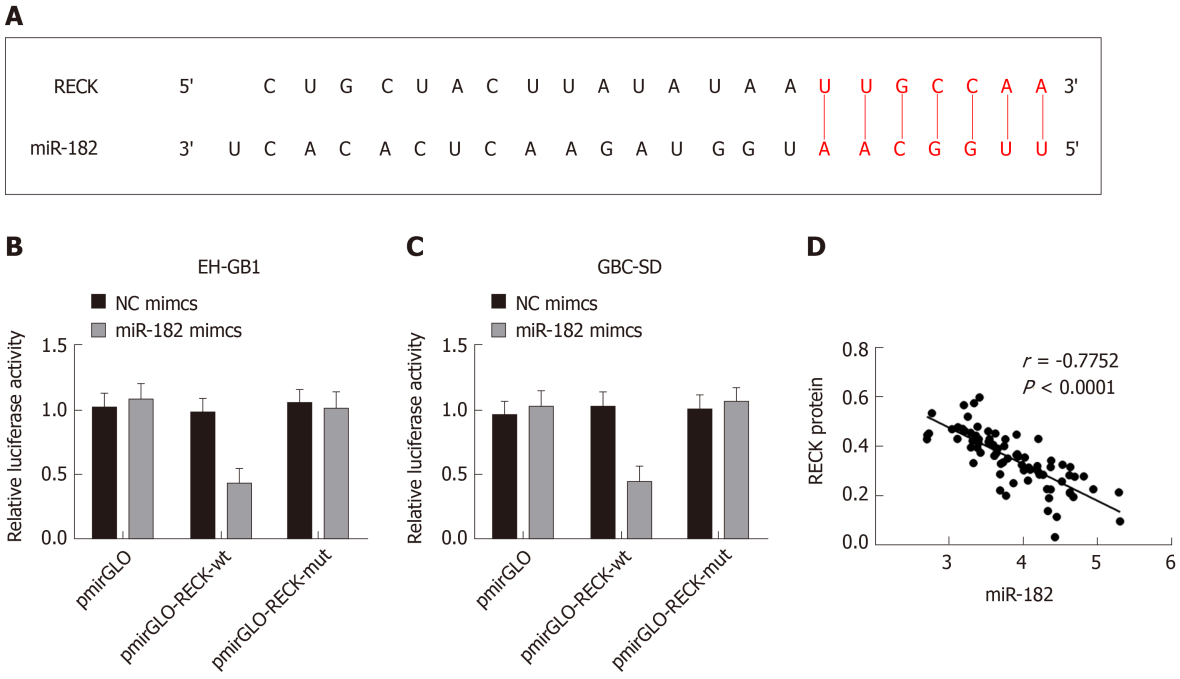

Figure 6 MiR-182 targeted inhibition of reversion-inducing-cysteine-rich protein with kazal motifs expression. A: MicroRNA 182 (miR-182) had binding sites with reversion-inducing-cysteine-rich protein with kazal motifs (RECK) mRNA; B and C: Double luciferase reporter gene assay verified the targeting relationship between miR-182 and RECK; D: MiR-182 was negatively correlated with RECK protein. NC: Negative control.

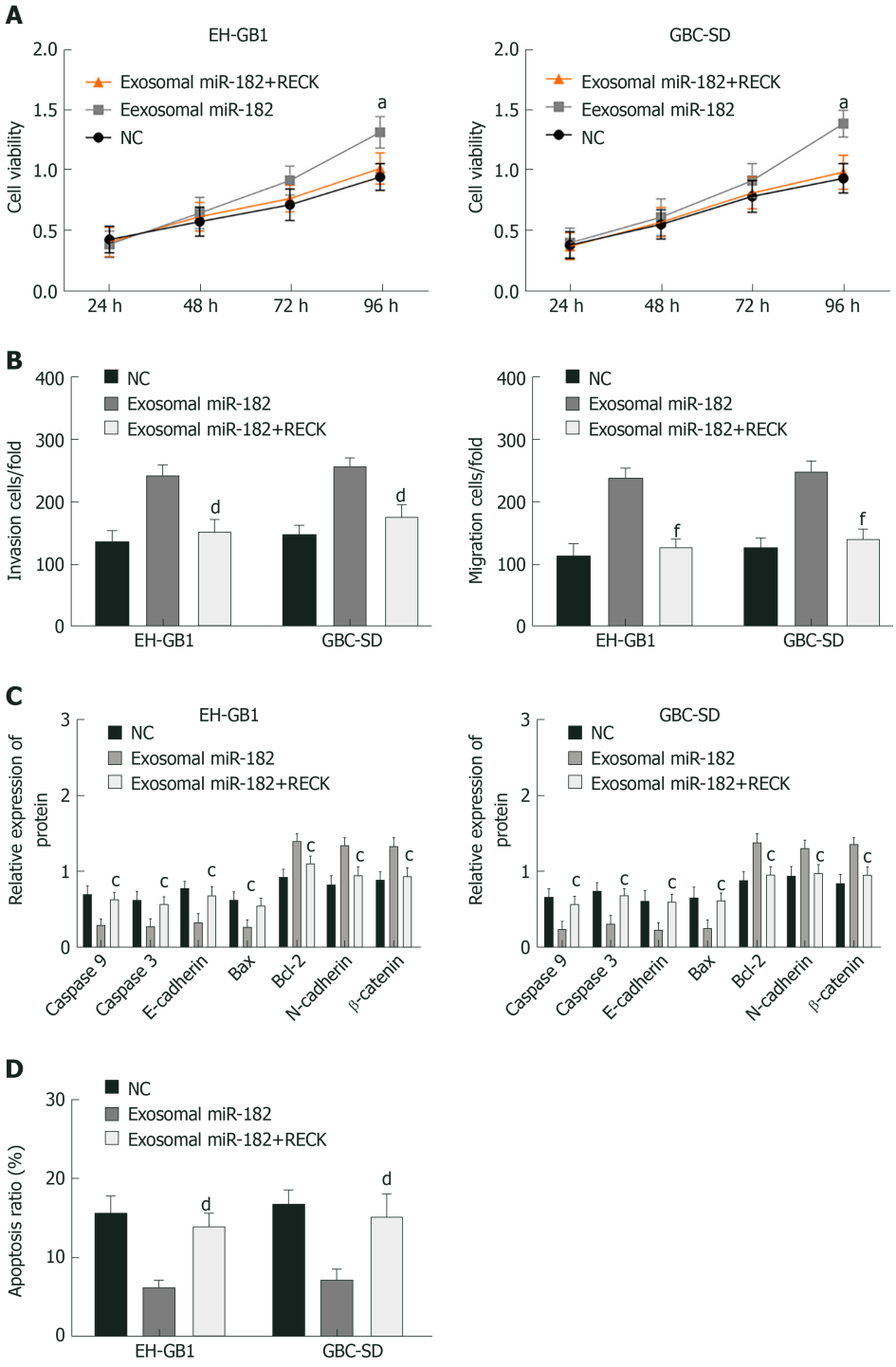

Figure 7 Rescue experiment. A: Viability comparison of gallbladder cancer cells in each group; B: Comparison of cell invasion in each group; C: Comparison of EH-GB1 cell-related proteins in each group; D: Comparison of apoptosis in each group. $^{a}P < 0.05$ *vs* the negative control (NC) group. $^{c}P < 0.05$, $^{d}P < 0.01$, and $^{f}P < 0.001$ *vs* exosomal microRNA 182 group.

ARTICLE HIGHLIGHTS

Research background

As the most common biliary malignancy, GC is an elderly-biased disease. Although extensive studies have elucidated the molecular mechanism of miR-182 and RECK in various cancers, the specific roles of exosomal miR-182 and RECK in GC remain poorly understood.

Research motivation

The expression of miR-182 and exosomal miR-182 was increased in gallbladder cancer, while RECK decreased. Targetscan7.2 predicted RECK could bind with miR-182 *via* 3'UTR. RECK was negatively correlated with miR-182.

Research objectives
This study was set out to explore the relationship between exosomal miR-182/RECK and metastasis of GC.

Research methods
Paired GC and adjacent normal tissues were collected from 78 patients. qPCR was employed to detect miR-182 and exosomal miR-182 expression, and Western blot was adopted to determine RECK expression. In addition, the effect of exosomal miR-182/RECK on the biological function of human GC cells were observed. Moreover, double luciferase reporter gene assay was applied to validate the targeting relationship between miR-182 and RECK.

Research results
Compared with normal gallbladder epithelial cells, miR-182 was highly expressed in GC cells, while RECK was lowly expressed. Exosomal miR-182 could be absorbed and transferred by cells. Exosomal miR-182 inhibited RECK expression and promoted migration and invasion of GC cells.

Research conclusions
Exosomal miR-182 can significantly promote the migration and invasion of GC cells by inhibiting RECK, and thus miR-182 can be used as a therapeutic target for GC.

Research perspectives
The signaling pathways implicated in miR-182/RECK should be explored in future experimental design to supplement the oncogenic network of exosomal miR-182. The clinical value of exosomal miR-182 in GC remains to be discussed.

REFERENCES

1 **Schmidt MA**, Marcano-Bonilla L, Roberts LR. Gallbladder cancer: epidemiology and genetic risk associations. *Chin Clin Oncol* 2019; **8**: 31 [PMID: 31484487 DOI: 10.21037/cco.2019.08.13]
2 **Hundal R**, Shaffer EA. Gallbladder cancer: epidemiology and outcome. *Clin Epidemiol* 2014; **6**: 99-109 [PMID: 24634588 DOI: 10.2147/CLEP.S37357]
3 **de Savornin Lohman EAJ**, de Bitter TJJ, van Laarhoven CJHM, Hermans JJ, de Haas RJ, de Reuver PR. The diagnostic accuracy of CT and MRI for the detection of lymph node metastases in gallbladder cancer: A systematic review and meta-analysis. *Eur J Radiol* 2019; **110**: 156-162 [PMID: 30599854 DOI: 10.1016/j.ejrad.2018.11.034]
4 **Niu J**, Li Z, Li F. Overexpressed microRNA-136 works as a cancer suppressor in gallbladder cancer through suppression of JNK signaling pathway via inhibition of MAP2K4. *Am J Physiol Gastrointest Liver Physiol* 2019; **317**: G670-G681 [PMID: 31369289 DOI: 10.1152/ajpgi.00055.2019]
5 **Jin YP**, Hu YP, Wu XS, Wu YS, Ye YY, Li HF, Liu YC, Jiang L, Liu FT, Zhang YJ, Hao YJ, Liu XY, Liu YB. miR-143-3p targeting of ITGA6 suppresses tumour growth and angiogenesis by downregulating PLGF expression via the PI3K/AKT pathway in gallbladder carcinoma. *Cell Death Dis* 2018; **9**: 182 [PMID: 29416013 DOI: 10.1038/s41419-017-0258-2]
6 **Kulkarni P**, Dasgupta P, Bhat NS, Shahryari V, Shiina M, Hashimoto Y, Majid S, Deng G, Saini S, Tabatabai ZL, Yamamura S, Tanaka Y, Dahiya R. Elevated miR-182-5p Associates with Renal Cancer Cell Mitotic Arrest through Diminished *MALAT-1* Expression. *Mol Cancer Res* 2018; **16**: 1750-1760 [PMID: 30037856 DOI: 10.1158/1541-7786.MCR-17-0762]
7 **Livingstone MC**, Johnson NM, Roebuck BD, Kensler TW, Groopman JD. Serum miR-182 is a predictive biomarker for dichotomization of risk of hepatocellular carcinoma in rats. *Mol Carcinog* 2019; **58**: 2017-2025 [PMID: 31373075 DOI: 10.1002/mc.23093]
8 **Perilli L**, Tessarollo S, Albertoni L, Curtarello M, Pastò A, Brunetti E, Fassan M, Rugge M, Indraccolo S, Amadori A, Bortoluzzi S, Zanovello P. Silencing of miR-182 is associated with modulation of tumorigenesis through apoptosis induction in an experimental model of colorectal cancer. *BMC Cancer* 2019; **19**: 821 [PMID: 31429725 DOI: 10.1186/s12885-019-5982-9]
9 **Spitschak A**, Meier C, Kowtharapu B, Engelmann D, Pützer BM. MiR-182 promotes cancer invasion by linking RET oncogene activated NF-κB to loss of the HES1/Notch1 regulatory circuit. *Mol Cancer* 2017; **16**: 24 [PMID: 28122586 DOI: 10.1186/s12943-016-0563-x]
10 **Qiu Y**, Luo X, Kan T, Zhang Y, Yu W, Wei Y, Shen N, Yi B, Jiang X. TGF-β upregulates miR-182 expression to promote gallbladder cancer metastasis by targeting CADM1. *Mol Biosyst* 2014; **10**: 679-685 [PMID: 24445397 DOI: 10.1039/c3mb70479c]
11 **Liu LT**, Chang HC, Chiang LC, Hung WC. Histone deacetylase inhibitor up-regulates RECK to inhibit MMP-2 activation and cancer cell invasion. *Cancer Res* 2003; **63**: 3069-3072 [PMID: 12810630]
12 **Noda M**, Oh J, Takahashi R, Kondo S, Kitayama H, Takahashi C. RECK: a novel suppressor of malignancy linking oncogenic signaling to extracellular matrix remodeling. *Cancer Metastasis Rev* 2003; **22**: 167-175 [PMID: 12784995 DOI: 10.1023/a:1023043315031]
13 **Takahashi C**, Sheng Z, Horan TP, Kitayama H, Maki M, Hitomi K, Kitaura Y, Takai S, Sasahara RM, Horimoto A, Ikawa Y, Ratzkin BJ, Arakawa T, Noda M. Regulation of matrix metalloproteinase-9 and inhibition of tumor invasion by the membrane-anchored glycoprotein RECK. *Proc Natl Acad Sci USA* 1998; **95**: 13221-13226 [PMID: 9789069 DOI: 10.1073/pnas.95.22.13221]
14 **Liu Y**, Li L, Liu Y, Geng P, Li G, Yang Y, Song H. RECK inhibits cervical cancer cell migration and invasion by promoting p53 signaling pathway. *J Cell Biochem* 2018; **119**: 3058-3066 [PMID: 29064588 DOI: 10.1002/jcb.26441]
15 **Chen R**, Sheng L, Zhang HJ, Ji M, Qian WQ. miR-15b-5p facilitates the tumorigenicity by targeting RECK and predicts tumour recurrence in prostate cancer. *J Cell Mol Med* 2018; **22**: 1855-1863 [PMID: 29363862 DOI: 10.1111/jcmm.13469]
16 **Wang J**, Lin Y, Jiang T, Gao C, Wang D, Wang X, Wei Y, Liu T, Zhu L, Wang P, Qi F. Up-regulation of TIMP-3 and RECK decrease the invasion and metastasis ability of colon cancer. *Arab J Gastroenterol*

2019; **20**: 127-134 [PMID: 31558368 DOI: 10.1016/j.ajg.2019.07.003]
17 **Qin J**, Luo M. MicroRNA-221 promotes colorectal cancer cell invasion and metastasis by targeting RECK. *FEBS Lett* 2014; **588**: 99-104 [PMID: 24269686 DOI: 10.1016/j.febslet.2013.11.014]
18 **Iseki Y**, Shibutani M, Maeda K, Nagahara H, Fukuoka T, Matsutani S, Hirakawa K, Ohira M. MicroRNA-96 Promotes Tumor Invasion in Colorectal Cancer *via* RECK. *Anticancer Res* 2018; **38**: 2031-2035 [PMID: 29599320 DOI: 10.21873/anticanres.12442]
19 **Wei LJ**, Bai DM, Wang ZY, Liu BC. MicroRNA-375 accelerates the invasion and migration of colorectal cancer through targeting RECK. *Eur Rev Med Pharmacol Sci* 2019; **23**: 4738-4745 [PMID: 31210300 DOI: 10.26355/eurrev_201906_18055]
20 **McAndrews KM**, Kalluri R. Mechanisms associated with biogenesis of exosomes in cancer. *Mol Cancer* 2019; **18**: 52 [PMID: 30925917 DOI: 10.1186/s12943-019-0963-9]
21 **Pegtel DM**, Gould SJ. Exosomes. *Annu Rev Biochem* 2019; **88**: 487-514 [PMID: 31220978 DOI: 10.1146/annurev-biochem-013118-111902]
22 **Pegtel DM**, Cosmopoulos K, Thorley-Lawson DA, van Eijndhoven MA, Hopmans ES, Lindenberg JL, de Gruijl TD, Würdinger T, Middeldorp JM. Functional delivery of viral miRNAs via exosomes. *Proc Natl Acad Sci USA* 2010; **107**: 6328-6333 [PMID: 20304794 DOI: 10.1073/pnas.0914843107]
23 **Chiang CH**, Hou MF, Hung WC. Up-regulation of miR-182 by β-catenin in breast cancer increases tumorigenicity and invasiveness by targeting the matrix metalloproteinase inhibitor RECK. *Biochim Biophys Acta* 2013; **1830**: 3067-3076 [PMID: 23333633 DOI: 10.1016/j.bbagen.2013.01.009]
24 **Hirata H**, Ueno K, Shahryari V, Tanaka Y, Tabatabai ZL, Hinoda Y, Dahiya R. Oncogenic miRNA-182-5p targets Smad4 and RECK in human bladder cancer. *PLoS One* 2012; **7**: e51056 [PMID: 23226455 DOI: 10.1371/journal.pone.0051056]
25 **Hirata H**, Ueno K, Shahryari V, Deng G, Tanaka Y, Tabatabai ZL, Hinoda Y, Dahiya R. MicroRNA-182-5p promotes cell invasion and proliferation by down regulating FOXF2, RECK and MTSS1 genes in human prostate cancer. *PLoS One* 2013; **8**: e55502 [PMID: 23383207 DOI: 10.1371/journal.pone.0055502]

World Journal of Gastroenterology

Submit a Manuscript: https://www.f6publishing.com

World J Gastroenterol 2020 March 7; 26(9): 947-959

DOI: 10.3748/wjg.v26.i9.947

ISSN 1007-9327 (print) ISSN 2219-2840 (online)

ORIGINAL ARTICLE

Retrospective Study

Clinical utility of treatment method conversion during single-session endoscopic ultrasound-guided biliary drainage

Kosuke Minaga, Mamoru Takenaka, Kentaro Yamao, Ken Kamata, Shunsuke Omoto, Atsushi Nakai, Tomohiro Yamazaki, Ayana Okamoto, Rei Ishikawa, Tomoe Yoshikawa, Yasutaka Chiba, Tomohiro Watanabe, Masatoshi Kudo

ORCID number: Kosuke Minaga (0000-0001-5407-7925); Mamoru Takenaka (0000-0001-7308-4311); Kentaro Yamao (0000-0003-2497-7740); Ken Kamata (0000-0003-1568-0769); Shunsuke Omoto (0000-0001-7291-3608); Atsushi Nakai (0000-0002-0569-3948); Tomohiro Yamazaki (0000-0001-8378-1268); Ayana Okamoto (0000-0002-8173-2910); Rei Ishikawa (0000-0001-8719-2866); Tomoe Yoshikawa (0000-0001-5275-2667); Yasutaka Chiba (0000-0002-7261-2351); Tomohiro Watanabe (0000-0001-7781-6305); Masatoshi Kudo (0000-0002-4102-3474).

Author contributions: All authors helped to perform the research; Minaga K, Takenaka M and Kudo M drafting conception and design; Minaga K manuscript writing; Takenaka M, Yamao K, Kamata K, Minaga K and Omoto S performing endoscopic interventions; Nakai A, Yamazaki T, Okamoto A, Ishikawa R and Yoshikawa T analysis and interpretation of data; Chiba T performing statistical analyses; Watanabe T critical manuscript revision.

Institutional review board statement: Ethical permission for this study was granted by the review board of Kindai University Faculty of Medicine (approval number: 28-173).

Informed consent statement: Patients were not required to give

Kosuke Minaga, Mamoru Takenaka, Kentaro Yamao, Ken Kamata, Shunsuke Omoto, Atsushi Nakai, Tomohiro Yamazaki, Ayana Okamoto, Rei Ishikawa, Tomoe Yoshikawa, Tomohiro Watanabe, Masatoshi Kudo, Department of Gastroenterology and Hepatology, Kindai University Faculty of Medicine, Osaka-Sayama 589-8511, Japan

Yasutaka Chiba, Clinical Research Center, Kindai University Hospital, Osaka-Sayama 589-8511, Japan

Corresponding author: Kosuke Minaga, MD, PhD, Department of Gastroenterology and Hepatology, Kindai University Faculty of Medicine, 377-2 Ohno-Higashi, Osaka-Sayama 589-8511, Japan. kousukeminaga@med.kindai.ac.jp

Abstract

BACKGROUND

Although several techniques for endoscopic ultrasound-guided biliary drainage (EUS-BD) are available at present, an optimal treatment algorithm of EUS-BD has not yet been established.

AIM

To evaluate the clinical utility of treatment method conversion during single endoscopic sessions for difficult cases in initially planned EUS-BD.

METHODS

This was a single-center retrospective analysis using a prospectively accumulated database. Patients with biliary obstruction undergoing EUS-BD between May 2008 and April 2016 were included. The primary outcome was to evaluate the improvement in EUS-BD success rates by converting the treatment methods during a single endoscopic session. Secondary outcomes were clarification of the factors leading to the conversion from the initial EUS-BD and the assessment of efficacy and safety of the conversion as judged by technical success, clinical success, and adverse events (AEs).

RESULTS

A total of 208 patients underwent EUS-BD during the study period. For 18.8% (39/208) of the patients, the treatment methods were converted to another EUS-BD technique from the initial plan. Biliary obstruction was caused by pancreatobiliary malignancies, other malignant lesions, biliary stones, and other benign lesions in 22, 11, 4, and 2 patients, respectively. The reasons for the

Conflict-of-interest statement: All authors declare no conflicts of interest related to this article. We disclose that this work was presented in part at Digestive Disease Week (DDW 2017), May 6-9, 2017, Chicago, United States (Gastrointestinal Endoscopy 2017; 85: 5 Supplement, AB493).

Data sharing statement: No additional data are available.

Manuscript source: Invited manuscript

Received: December 6, 2019
Peer-review started: December 6, 2019
First decision: January 12, 2020
Revised: February 13, 2020
Accepted: February 21, 2020
Article in press: February 21, 2020
Published online: March 7, 2020

P-Reviewer: Sun SY, Armellini E
S-Editor: Wang J
L-Editor: A
E-Editor: Liu MY

difficulty with the initial EUS-BD were classified into the following 3 procedures: Target puncture (n = 13), guidewire manipulation (n = 18), and puncture tract dilation (n = 8). Technical success was achieved in 97.4% (38/39) of the cases and clinical success was achieved in 89.5% of patients (34/38). AEs occurred in 10.3% of patients, including bile leakage (n = 2), bleeding (n = 1), and cholecystitis (n = 1). The puncture target and drainage technique were altered in subsequent EUS-BD procedures in 25 and 14 patients, respectively. The final technical success rate with 95%CI for all 208 cases was 97.1% (95%CI: 93.8%-98.9%), while that of the initially planned EUS-BD was 78.8% (95%CI: 72.6%-84.2%).

CONCLUSION
Among multi-step procedures in EUS-BD, guidewire manipulation appeared to be the most technically challenging. When initially planned EUS-BD is technically difficult, treatment method conversion in a single endoscopic session may result in successful EUS-BD without leading to severe AEs.

Key words: Endoscopic ultrasound; Endoscopic ultrasound-guided biliary drainage; Interventional endoscopic ultrasound; Biliary drainage; Biliary obstruction

Core tip: Treatment methods were converted from an initially planned endoscopic ultrasound-guided biliary drainage (EUS-BD) technique in a single endoscopic session in cases with difficulties. In 18.8% cases, treatment methods were converted to another EUS-BD technique. The technical and clinical success rates were 97.4% and 89.5%, respectively. Mild adverse events occurred in 10.5%. Final technical success rate of all 208 cases was 97.1%-much higher than that of the initially planned EUS-BD. When the initially planned EUS-BD was technically difficult, treatment method conversion during the single endoscopic session was likely to contribute to improvements in the technical success of EUS-BD, without leading to serious AEs.

Citation: Minaga K, Takenaka M, Yamao K, Kamata K, Omoto S, Nakai A, Yamazaki T, Okamoto A, Ishikawa R, Yoshikawa T, Chiba Y, Watanabe T, Kudo M. Clinical utility of treatment method conversion during single-session endoscopic ultrasound-guided biliary drainage. *World J Gastroenterol* 2020; 26(9): 947-959
URL: https://www.wjgnet.com/1007-9327/full/v26/i9/947.htm
DOI: https://dx.doi.org/10.3748/wjg.v26.i9.947

INTRODUCTION

Transpapillary biliary drainage under endoscopic retrograde cholangiopancreatography (ERCP) is a standard treatment for biliary obstruction. However, endoscopists encounter technical difficulties with biliary drainage under ERCP guidance in approximately 5%-10% of cases[1-3]. Even though percutaneous transhepatic biliary drainage (PTBD) has been established as an alternative for therapeutic relief of biliary obstruction in such situations, its morbidity and mortality rates have been reported to be high[4-6]. For overcoming the problems associated with PTBD, a novel alternative endoscopic procedure termed endoscopic ultrasound-guided biliary drainage (EUS-BD) was developed in 2001 for patients with unsuccessful conventional ERCP[7]. Over the past two decades, EUS-BD has attracted significant attention and the number of patients who have received this procedure after unsuccessful ERCP has been increasing.

At present, several EUS-BD techniques, including various approach routes and drainage methods, have been developed[8-11]. Regarding the approach routes, two major routes are used: The transgastric intrahepatic approach and the transduodenal extrahepatic approach. Biliary drainage can usually be achieved by one of three drainage methods: Transmural stenting, antegrade stenting, and the rendezvous technique (EUS-RV)[8-11]. Endoscopists select one or two safe techniques with a high probability of success among the many EUS-BD techniques. Although patient anatomy, underlying disease, location of the biliary stricture, and the diameter of the intrahepatic bile duct are regarded as important factors for the selection of the

approach routes and drainage methods[9,12], the optimal treatment strategy for EUS-BD has not yet been established. EUS-BD comprises multiple steps, including target puncture, guidewire manipulation, puncture tract dilation, and stent placement. Among these steps, technical difficulties can arise in each approach route and drainage method. However, the technically critical steps have not yet been clarified. Furthermore, no consensus has been reached regarding troubleshooting when the initial EUS-BD technique appears to be challenging. Thus, both the technical issues and treatment algorithms have been poorly defined in EUS-BD, despite overall technical success rates having been reported to be 90%-96%[13-17]. At our institution, we have attempted to change the puncture target or drainage method in a single endoscopic session upon encountering difficulty with accomplishing the initial plan. In this study, we have analyzed the outcomes of conversion during EUS-BD and identified technically difficult steps in each EUS-BD technique. We provide data regarding the utility and safety of treatment method conversion from the initially planned EUS-BD during a single endoscopic session.

MATERIALS AND METHODS

Patients

Patients who underwent EUS-BD between May 2008 and April 2016 were identified from the prospectively accumulated database of the Kindai University Hospital (Osaka-Sayama, Japan). Among these, cases with conversion of treatment methods from the initial EUS-BD plan in the same endoscopic session were extracted by reviewing electronic medical records and endoscopic reports. The protocol employed to perform this study was approved by the Institutional Review Board of Kindai University Faculty of Medicine (approval number: 28-173). The following data were retrieved from the patients' medical records: Patient characteristics (age, sex, performance status, underlying disease, blood tests), reasons for EUS-BD, reasons for changing the treatment methods, and details of the endoscopic procedures, including technical and clinical success, procedure times, and adverse events (AEs). Patients with attempted EUS-BD were defined as those who received bile duct punctures under EUS at least once. Patients who discontinued the study after observation with EUS were excluded from this study. Patients enrolled in other clinical trials were also excluded. All patients provided written informed consent before undergoing the endoscopic procedures.

Endoscopic procedures of EUS-BD

All EUS-BD procedures were performed by endoscopists trained and experienced in both ERCP and EUS procedures. Patients were placed in the prone position with moderate sedation using intravenous propofol. A linear-array echoendoscope (GF-UCT240 or 260; Olympus Medical Systems, Tokyo, Japan) was used to achieve initial biliary access from the gastrointestinal lumen. As described above, the drainage methods for EUS-BD are divided into the following: Transmural stenting, antegrade stenting, and EUS-RV. Among those three, EUS-BD with transmural stenting can be performed via two main access routes: EUS-guided choledochoduodenostomy (EUS-CDS) and EUS-guided hepaticogastrostomy (EUS-HGS). In EUS-CDS, a dilated extrahepatic bile duct was visualized from the duodenal bulb and punctured using a 19-gauge aspiration needle. After cholangiography, a 0.025-inch guidewire (VisiGlide2; Olympus Medical Systems, Revowave; Piolax, Yokohama, Japan) was placed and advanced into the biliary tree, and then a tapered catheter was inserted (StarTip V; Olympus Medical Systems, ERCP-Catheter Filiform; MTW Endoskopie, Düsseldorf, Germany). The puncture tract was dilated using a bougie dilator (Soehendra Biliary Dilation Catheter; Cook Endoscopy, Winston Salem, NC, United States) or a 4-mm balloon dilator (Hurricane RX; Boston Scientific Corporation, Natick, MA, United States) over the guidewire. Finally, a covered metal stent (8 mm in diameter, 6 or 8 cm in length) or a double-pigtail plastic stent (7 Fr in diameter, > 6 cm in length) was deployed between the extrahepatic bile duct and the duodenal bulb. In EUS-HGS, the dilated left intrahepatic bile duct was punctured from the stomach using a 19-gauge needle. After inserting the guidewire into the biliary tree and dilating the puncture site in the same manner as in EUS-CDS, a covered metal stent (8 mm in diameter, 10 or 12 mm in length) or a double-pigtail plastic stent (7 Fr in diameter, > 10 cm in length) was deployed between the left intrahepatic bile duct and the stomach.

In antegrade stenting, as with EUS-HGS, the left intrahepatic bile duct was punctured from the gastrointestinal lumen. A 0.025-inch guidewire was inserted deep into the biliary tree and was manipulated into the gastrointestinal lumen across the

papilla or anastomosis site. To prevent bile leakage, dilation of the puncture site was minimized with the ERCP catheter alone, given the puncture tract was temporarily created and unsealed after stent placement. An uncovered metal stent with a thin delivery system (8 or 10 mm in diameter, 6 or 8 cm in length) or a 7-Fr straight plastic stent was deployed to cover the biliary stricture.

In EUS-RV, initial biliary access was achieved from the stomach or duodenum under EUS guidance, then a 0.025-inch guidewire (Revowave, Piolax) was inserted into the biliary tree. The guidewire was manually advanced across the ampulla and was coiled within the duodenum. Then, the needle and the echoendoscope were withdrawn, leaving the guidewire in place. Alongside the guidewire, a duodenoscope (TJF-260V, Olympus Medical Systems) was inserted and the biliary cannulation was performed with an ERCP catheter under the guidance of the EUS-placed guidewire. After access to the bile duct was achieved, transpapillary biliary stenting was performed under conventional ERCP guidance. In the study period, diathermic dilators were not used for puncture tract dilation because their use had been reported to increase AEs[18].

Selection of initial drainage methods

In principle, ERCP has been performed in our institution as a primary biliary drainage technique in cases of biliary obstruction. EUS-BD has been considered when initial ERCP was unsuccessful or reintervention with ERCP was unsuccessful or ineffective. Thus, all EUS-BD procedures have been performed as rescue biliary drainage after failed conventional ERCP. EUS-BD is judged to be contraindicated in the following situations: Eastern Cooperative Oncology Group performance status of 4, bleeding tendency (prothrombin time international normalized ratio > 1.5 or < 50000 platelets), the continuous use of antithrombotic agents, or the presence of massive ascites. The treatment algorithm for initial EUS-BD in our institution is shown in Figure 1. The algorithm was tentatively established, mainly based on patient anatomy, underlying disease, and the location of the biliary stricture as described previously[9,12]. In brief, transmural stenting was selected as an initial EUS-BD procedure when the papilla was endoscopically inaccessible due to an anatomical issue or duodenal stricture. EUS-HGS was used as an initial plan of EUS-BD in cases with hilar biliary obstruction, whereas either EUS-CDS or EUS-HGS was considered the initial plan in distal biliary obstruction with patent duodenal bulb. If the duodenal bulb was inaccessible, EUS-HGS was selected. On the other hand, if the papilla was endoscopically accessible, EUS-RV was considered the first-choice EUS-BD technique in cases with benign or resectable malignant biliary obstruction. In inoperable cases, transmural stenting was indicated as the first choice. As with cases with an inaccessible papilla, the choice of EUS-CDS or EUS-HGS for transmural stenting was based on the site of biliary obstruction. In summary, EUS-RV or transmural stenting with EUS-CDS or EUS-HGS were used as the first-choice drainage method for EUS-BD in this study. Antegrade stenting was not chosen as the initial EUS-BD method.

Conversion of treatment methods in EUS-BD

When the initial EUS-BD failed, endoscopists selected alternative EUS treatment methods to achieve successful biliary drainage after careful consideration of several factors. If the initial EUS-RV had failed, EUS-RV via another approach route or transmural stenting (EUS-CDS or EUS-HGS) could be considered as an alternative drainage technique. When the initial EUS-HGS was unsuccessful, antegrade stenting or EUS-CDS was considered as an alternative approach. In cases with distal biliary obstruction, EUS-guided gallbladder drainage (EUS-GBD) was also indicated if the gallbladder was swollen due to biliary obstruction[19]. Thus, there could be multiple conversion techniques as an alternative to EUS-BD, and the endoscopists selected the technique that seemed most appropriate for each case.

Study endpoints and definitions

The primary outcome of the current study was to assess improvements in the technical and clinical success rates of EUS-BD by converting the treatment method during a single endoscopic session. Secondary outcomes assessed reasons for the conversion of the initial EUS-BD and the methods that were altered; and clinical outcomes of the secondary EUS-BD, including technical and clinical success rates, procedure times, and AE rates. Technical success was defined as successful stent deployment at the target site, as confirmed by a combination of endoscopy and fluoroscopy. Clinical success was defined as an improvement in cholangitis or a decrease in serum bilirubin levels either to a normal level or reduced by more than 50% within 2 weeks following EUS-BD. AE severity was classified according to the American Society for Gastrointestinal Endoscopy lexicon[20].

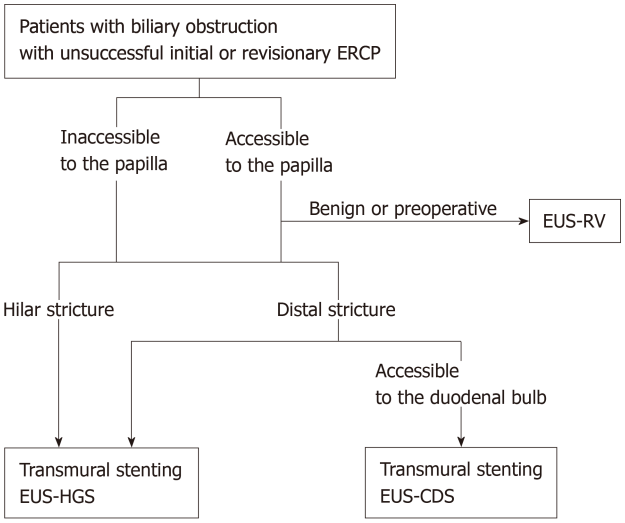

Figure 1 Treatment algorithm for initial endoscopic ultrasound-guided biliary drainage in this study. ERCP: Endoscopic retrograde cholangiopancreatography; EUS-RV: EUS-guided rendezvous technique; EUS-HGS: EUS-guided hepaticogastrostomy; EUS-CDS: EUS-guided choledochoduodenostomy.

Statistical analysis

Continuous variables are presented as medians and ranges, and categorial variables as numbers and percentages. The rates of technical and clinical success and AEs are presented with a 95%CI. Statistical analyses were performed using SAS version 9.4 software (SAS Institute Inc., Cary, NC, United States).

RESULTS

Patient characteristics

During the study period, a total of 208 patients underwent EUS-BD as rescue biliary drainage at our institution. As an initial EUS-BD technique, EUS-RV, transmural stenting with EUS-CDS, and EUS-HGS were performed in 43, 52, and 113 patients, respectively. In 18.8% (39/208) of the cases, the initial EUS-BD technique was converted to a different EUS-BD technique. The initial EUS-BD technique used for the patients who required conversion was EUS-RV in 11, EUS-CDS in 12, and EUS-HGS in 16 patients. Demographic and clinical characteristics of this population (n = 39) are shown in Table 1. The median patient age was 74 years (range, 40-89), and 26 were men. Biliary obstructions were caused by pancreatobiliary malignancies, other malignant lesions, biliary stones, and other benign lesions in 22, 11, 4, and 2 patients, respectively. Malignant lesions in locations other than the pancreatobiliary systems included 6 cases of gastric cancer, 4 cases of colon cancer, and 1 case of malignant lymphoma. Two benign lesions other than biliary stones included anastomotic biliary strictures and inflammatory biliary wall thickening.

These 39 cases consisted of 19 (48.7%) with failure of duodenal scope insertion, 5 (12.8%) with inability to access the papilla after duodenal stent placement, 11 (28.2%) with failure of biliary deep cannulation or selection, and 4 (10.3%) with surgically altered anatomy (Table 2). The reasons for technical difficulty with the initial EUS-BD techniques are shown in Figure 2. Three major factors causing difficulties with the initial EUS-BD were noted: Failure of target puncture (n = 13, 33.3%), failure of puncture tract dilation (n = 8, 20.5%), and failure of guidewire manipulation (n = 18, 46.2%). Thus, the proportion of patients who required conversion was 18.8% of 208 total initial EUS-BD procedures. Moreover, target puncture and guidewire manipulation were identified as critical steps for successful initial EUS-BD.

Treatment method conversion from the initial EUS-BD

We examined final outcomes and causes of failure in patients who required treatment conversion in terms of the initial EUS-BD procedures.

Outcomes of patients with attempted EUS-RV as the initial EUS-BD plan

EUS-RV was attempted as the initial EUS-BD in 43 (20.7%) of 208 patients. The initial EUS-RV was successful in 30 (69.8%) patients. Among the 13 unsuccessful treatments, 2 patients were successfully treated with reattempted ERCP without considering an

Table 1 Demographic and clinical characteristics of 39 patients who underwent treatment method conversion from the initially planned endoscopic ultrasound-guided biliary drainage

Patient characteristics	*n* = 39
Age, median (range), yr	74 (40-89)
Sex, male/female, *n* (%)	26 (66.7)/13 (33.3)
ECOG performance status, median (range)	1 (0-3)
Total bilirubin, median (range), mg/dL	6.4 (1.2-18.4)
Etiology of biliary stricture, *n* (%)	
Malignant lesions	33 (84.6)
Pancreatobiliary cancer	22 (56.4)
Other	11 (28.2)
Benign lesions	6 (15.4)
Bile duct stones	4 (10.2)
Other	2 (5.1)
Reasons for EUS-BD, *n* (%)	
Failure of duodenal scope insertion	19 (48.7)
Failure to access the papilla after duodenal stent insertion	5 (12.8)
Failure of biliary cannulation/selection	11 (28.2)
Surgically altered gastrointestinal anatomy	4 (10.2)

ECOG: Eastern Cooperative Oncology Group; EUS-BD: Endoscopic ultrasound-guided biliary drainage.

alternative EUS-BD. Alternative EUS-BD techniques were performed in the remaining 11 patients. Difficulty with guidewire manipulation led to unsuccessful EUS-RV in all 11 patients. Regarding the alteration of treatment methods, the puncture target was altered in 1 (9.1%) patient, and the drainage technique was changed from RV to transmural stenting in the remaining 10 (90.9%) patients. EUS-RV, EUS-HGS, and EUS-CDS were performed as the EUS-BD conversion technique in 1 (9.1%), 4 (36.4%), and 6 (54.5%) patients, respectively (Figure 3A).

Outcomes of patients with attempted EUS-CDS as the initial EUS-BD plan

Transmural stenting with EUS-CDS was attempted as the initial EUS-BD plan in 52 (25.0%) of 208 patients. The initial EUS-CDS was successful in 40 (76.9%) patients. The initial EUS-CDS was converted to another EUS-BD technique in the 12 unsuccessful treatments. Failures in the initial EUS-CDS were caused by difficulty with the puncture target (*n* = 6, 50%), guidewire manipulation (*n* = 3, 25%), and puncture tract dilation (*n* = 3, 25%). The puncture target was changed in all 12 patients in the subsequent EUS-BD procedures, including EUS-HGS (*n* = 8, 66.7%) and EUS-GBD (*n* = 4, 33.3%). No changes in the drainage method were noted (Figure 3B).

Outcomes of patients who attempted EUS-HGS as the initial EUS-BD plan

Transmural stenting with EUS-HGS was attempted in 113 (54.3%) of 208 patients. The initial EUS-HGS was successful in 94 (83.2%). Among the 19 unsuccessful treatments, surgical drainage was performed in 1 patient because the stent had migrated into the abdominal cavity during EUS-HGS. In addition, PTBD was immediately performed in 2 patients after failed initial EUS-HGS. For the remaining 16 patients, the initial EUS-HGS was changed to an alternative EUS-BD technique. Failures in the initial EUS-HGS were caused by difficulty with the target puncture (*n* = 7, 43.8%), guidewire manipulation (*n* = 4, 25%), and puncture tract dilation (*n* = 5, 31.3%). The puncture target was altered in 12 (75%) patients, whereas the drainage method was altered in the remaining 4 (25%). For patients in whom the puncture target was changed, EUS-CDS (*n* = 4), EUS-HGS (*n* = 4), and EUS-GBD (*n* = 4) were performed as the alternative EUS-BD technique. In 1 patient, EUS-HGS was attempted via a different biliary branch, but was unsuccessful due to difficulty with the puncture. In this case, PTBD was performed after failed EUS-BD. For 4 patients in whom the drainage method was changed, EUS-RV (*n* = 2) and antegrade stenting (*n* = 2) were performed (Figure 3C).

Clinical outcome and impact of alteration from initial EUS-BD methods

Technical success was achieved in 38 (97.4%) of 39 patients who underwent conversion of EUS-BD techniques in a single endoscopic session, and clinical success was verified in 34 (89.5%) of 38 patients. In 1 patient with an unsuccessful alternative

Table 2 Clinical outcomes of patients who underwent treatment method conversion from initially planned endoscopic ultrasound-guided biliary drainage

Patient characteristics	*n* = 39
[1]Technical success, *n* (%)	38[3] (97.4)
Median procedural time (range, min)	65 (26-115)
[2]Clinical success, *n* (%)	34 (89.5)
Adverse events (%)	4 (10.3)
Bile leakage	2 (5.1)
Bleeding	1 (2.6)
Cholecystitis	1 (2.6)

[1]Technical success was defined as successful stent deployment at the target site.
[2]Clinical success was defined as the improvement of cholangitis or a decrease in serum bilirubin levels to normal or by ≥ 50% within 2 wk following endoscopic ultrasound-guided biliary drainage.
[3]In one patient, endoscopic ultrasound-guided hepaticogastrostomy (EUS-HGS) was unsuccessful due to failed guidewire manipulation, and alternative EUS-HGS via another biliary branch was also unsuccessful due to the difficulty in puncture. In this case, percutaneous drainage was successfully performed instead.

EUS-BD, the initial HGS failed due to difficulty with guidewire manipulation, and an alternative HGS via another biliary branch was also unsuccessful due to difficulty with the target puncture. As previously described, this patient was successfully treated with PTBD.

AEs occurred in 4 (10.3%) of 39 patients. These AEs included bile leakage (*n* = 2), bleeding (*n* = 1), and cholecystitis (*n* = 1), all of which were conservatively managed. The median procedure time was 65 min (range, 26-115 min). The overall technical success rate, including alternative EUS-BD procedures, was 97.1% (202/208, 95%CI: 0.938-0.989) though that of the initially planned EUS-BDs was 78.8% (164/208, 95%CI: 0.727-0.842). Similarly, the clinical success rate was 74.0% (154/208, 95%CI: 0.675-0.799) for EUS-BD with initial treatment alone, but this increased to 90.4% (188/208, 95%CI: 0.855-0.940) when alternative EUS-BD procedures were included. The rate of AEs with the initial EUS-BD was 17.8% (37/208, 95%CI: 0.128-0.237), whereas that of all cases, including those treated with alternative EUS-BD procedures, was 19.7% (41/208, 95%CI: 0.145-0.258).

DISCUSSION

In this study, we retrospectively evaluated the usefulness of treatment method conversion from the initial EUS-BD technique during a single endoscopic session. We found that the conversions contributed to significant improvements in the overall technical and clinical success of EUS-BD, regardless of the initial EUS-BD technique used (EUS-RV, EUS-CDS, or EUS-HGS). Thus, we have found evidence that treatment method conversion immediately after failure of initial EUS-BD can be beneficial for patients in whom ERCP-based biliary drainage is impossible or unsuccessful. In the subgroup analyses based on the type of initial EUS-BD technique, we found that the success of EUS-BD depended upon the management of the target puncture, the dilation of puncture tract, and guidewire manipulation. Given the limited data on the conversion methods after initial EUS-BD, our results might be useful not only for establishing the treatment algorithm but also for troubleshooting guidance in EUS-BD.

It is generally accepted that patient anatomy, underlying diseases, and location of the biliary stricture are important factors affecting the selection of the initial EUS-BD technique. Along these lines, the treatment algorithm for EUS-BD in our institution (Figure 1) is based on the accessibility of the papilla by endoscopy, the presence or absence of malignant diseases, and the location of biliary strictures (distal or hilar). According to this algorithm, EUS-HGS was selected as the initial EUS-BD in more than half of the cases, and EUS-RV was the least often chosen. The technical success rate of the initial EUS-BD was highest for EUS-HGS at 83.2%, followed by EUS-CDS at 76.9%, and lowest in EUS-RV at 69.8%. However, the ideal method as a first-choice technique among a wide variety of EUS-BD techniques is under debate. Thus, we emphasize that future studies are required to verify the safety and efficacy of our tentative algorithm for EUS-BD.

Previous reviews focusing on the utility of drainage methods have shown that the technical success rate of EUS-RV was 81%[8,21] lower than that of transmural stenting.

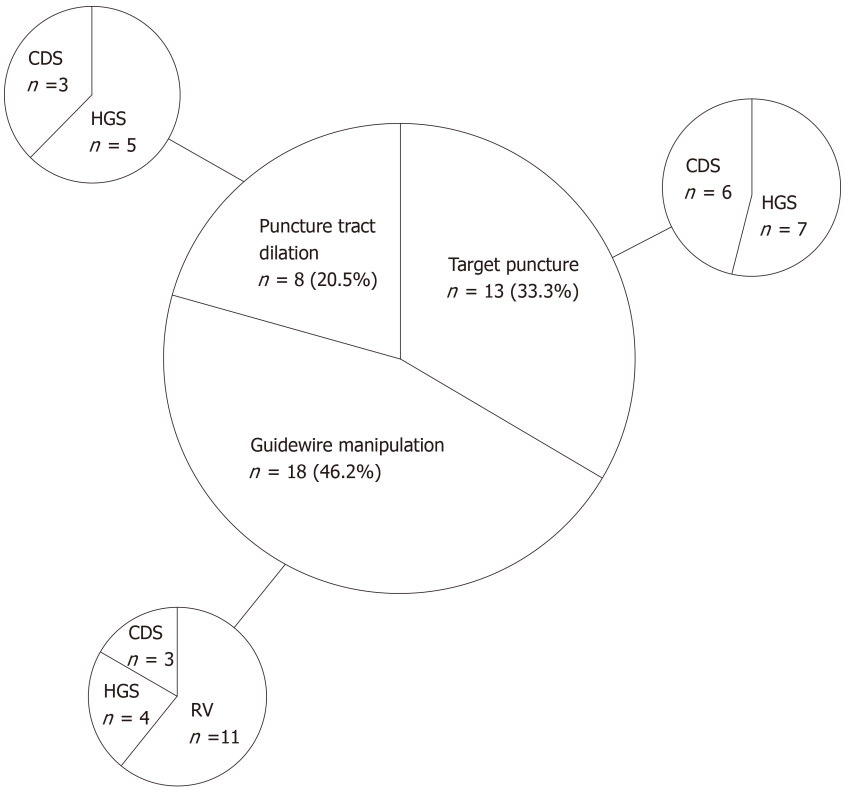

Figure 2 Reasons for difficulties in initial endoscopic ultrasound-guided biliary drainage. CDS: Choledochoduodenostomy; HGS: Hepaticogastrostomy; RV: Rendezvous technique.

Indeed, the success rate of EUS-RV was lower than EUS-HGS and EUS-CDS in this study. EUS-RV is superior to transmural stenting techniques in that it preserves the anatomical integrity of the biliary tracts without creating a permanent anastomosis. On the other hand, EUS-RV procedures are complicated, given scope exchange and skillful guidewire manipulation are required. Thus, the lower success rates of EUS-RV can be partially explained by its complicated procedures. In fact, all the 11 unsuccessful treatments of initial EUS-RV had difficulty with guidewire manipulation in passing through the biliary stricture or the papilla. As shown in Figure 3A, most of these cases were rescued by converting to transmural stenting without changing the access route. A recent study has shown that the extrahepatic approach from the second portion of the duodenum, called the D2 approach, had the highest technical success rate because this route facilitates guidewire manipulation[22]. However, unsuccessful EUS-RV *via* this approach compels endoscopists to change the access route in subsequent EUS-BD. Given that change of access route was unnecessary for the success of subsequent transmural stenting in this study, we need to be cautious about the selection of the D2 approach. This idea is supported by a novel individualized EUS-BD algorithm based on patient anatomy[23]. In this algorithm, Tyberg *et al*[23] have proposed that the intrahepatic approach should be chosen when the intrahepatic bile duct is dilated. The extrahepatic approach needs to be considered if the intrahepatic bile duct is not dilated or when the intrahepatic method is unsuccessful. From the viewpoint of troubleshooting in cases of unsuccessful initial EUS-RV, the intrahepatic approach could be the first choice of EUS-RV for patients exhibiting intrahepatic bile duct dilation, given this approach is easy to convert to transmural stenting. Support for this idea comes from recent studies in which no significant difference in success or AE rates have been observed between the intrahepatic and extrahepatic bile duct approaches[24,25]. In any case, our results provide evidence that transmural stenting is useful as a rescue EUS-BD method when the initial EUS-RV is unsuccessful.

In this study, 4 cases of bile duct stones treated with EUS-BD were included. Among these 4 cases, 3 cases were converted from EUS-RV to transmural stenting. In these cases, the rendezvous technique via the fistula was performed after fistula formation by transmural stenting, and the stones were successfully extracted. These results suggest that transmural stenting and biliary drainage followed by the rendezvous technique via the created fistula might be a useful treatment strategy for patients exhibiting obstructive jaundice or cholangitis due to biliary stones[26].

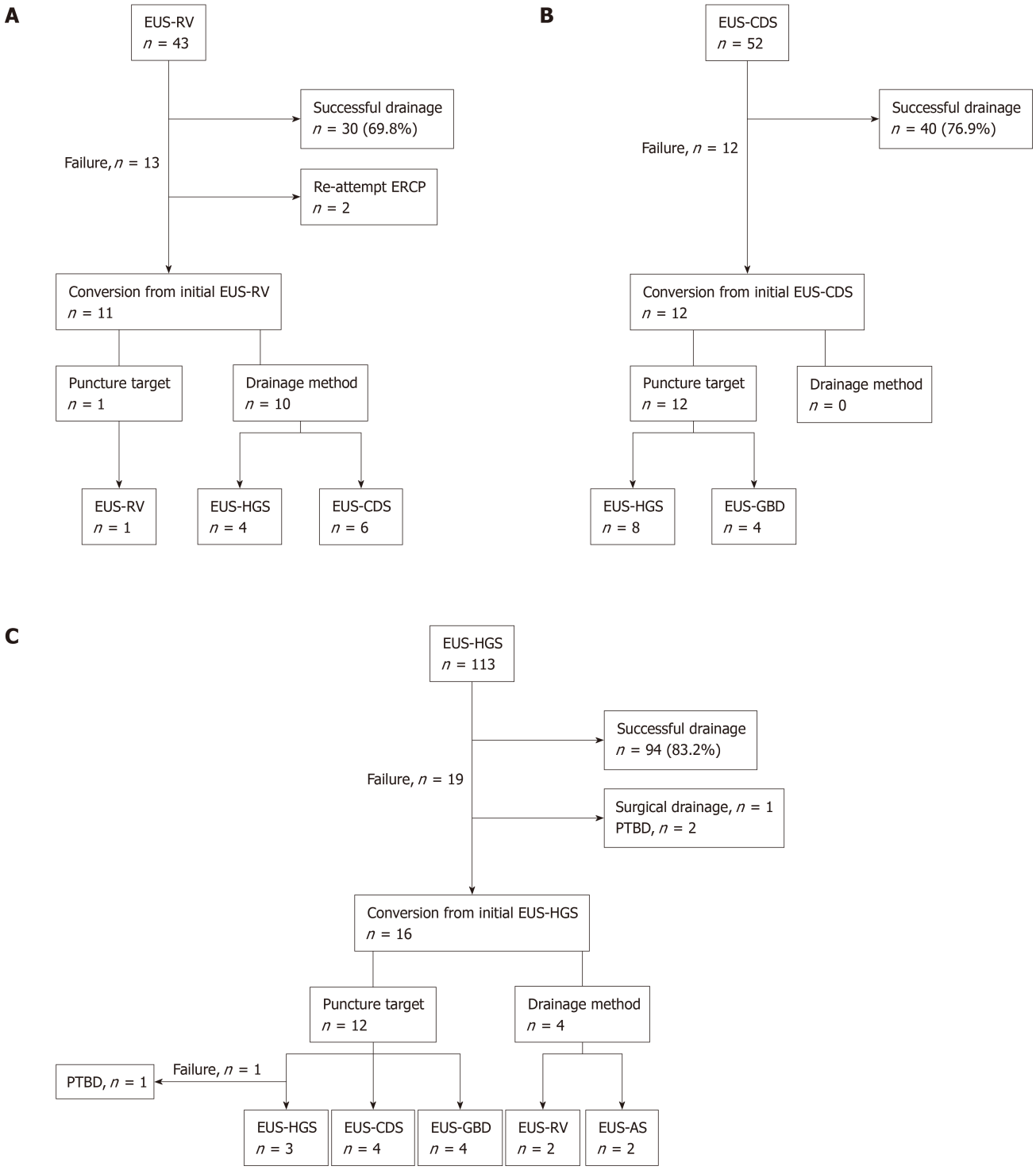

Figure 3 Technical outcomes of each initial endoscopic ultrasound-guided biliary drainage technique in this study. A: EUS-guided rendezvous technique; B: EUS-guided choledochoduodenostomy; C: EUS-guided hepaticogastrostomy. EUS-RV: EUS-guided rendezvous technique; EUS-CDS: EUS-guided choledochoduodenostomy; EUS-HGS: EUS-guided hepaticogastrostomy; EUS-AS: EUS-guided antegrade stenting; PTBD: Percutaneous transhepatic biliary drainage.

The technical success rate of the initial EUS-CDS in this study was 76.9%, which is lower than that published in recent reviews[16,25]. Failures in target puncture and puncture tract dilatation comprised 75% of the unsuccessful cases in this study. Currently, several useful dilators dedicated to EUS-BD have been developed, such as a tip-tapered bougie dilator (ES Dilator; Zeon Medical Co., Tokyo, Japan)[27], a fine-gauge balloon dilator (REN Biliary Dilation Catheter; Kaneka Co., Ltd, Osaka, Japan)[28], and a fine-gauge electrocautery dilator (Fine 025; Medico's Hirata Inc., Osaka, Japan)[29]. Unfortunately, these useful dilators were not available during the study period. Therefore, the lack of diathermic dilator use might have contributed to

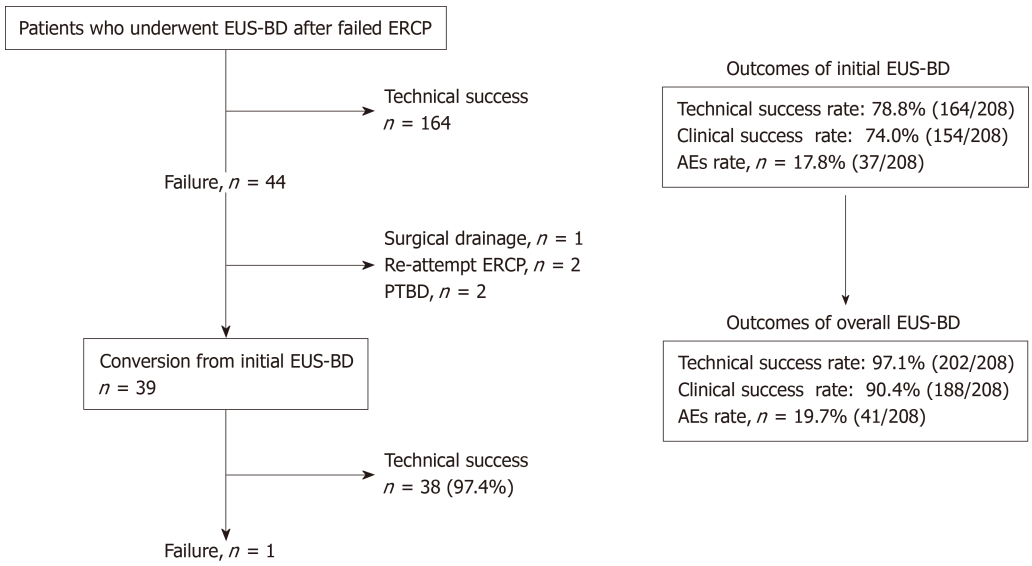

Figure 4 Technical and clinical outcomes of endoscopic ultrasound-guided biliary drainage in all 208 cases. Treatment method conversion for unsuccessful initial EUS-BD cases improved both technical and clinical success rates. EUS-BD: EUS-guided biliary drainage; ERCP: Endoscopic retrograde cholangiopancreatography; PTBD: Percutaneous transhepatic biliary drainage; AE: Adverse event.

the low technical success of EUS-CDS in this study. Regarding conversion from the initial EUS-CDS technique, EUS-HGS is theoretically a good indication, and EUS-GBD can also be a treatment option in cases with a patent cystic duct[19]. As shown in Figure 3B, the treatment methods were converted to EUS-HGS in two-thirds of the unsuccessful EUS-CDS cases.

The indications for EUS-HGS are much broader than EUS-CDS because the latter technique is contraindicated in cases with surgically altered anatomy and duodenal obstruction. EUS-HGS can be performed in those cases as well as in cases with distal bile duct obstruction. In fact, more than half of the cases underwent EUS-HGS as the initial EUS-BD in this study. Regarding troubleshooting for unsuccessful initial EUS-HGS, it is difficult to select the optimal conversion treatment method among the following: Rechallenge of EUS-HGS on another bile duct branch, change of puncture target from the intrahepatic bile duct to the extrahepatic bile duct or gallbladder, or change of drainage methods to EUS-RV or antegrade stenting. Selection of the treatment methods requires careful consideration of a combination of factors, such as patient anatomy, underlying disease, and the location of the biliary stricture. Even in the presence of the influential factors described above, the selection of the intrahepatic approach as the initial EUS-BD allows us to perform transmural stenting, antegrade stenting, and EUS-RV without changing the puncture route. Although some studies have shown a higher incidence of AEs with the intrahepatic approach than that in the extrahepatic[30,31], a recent meta-analysis found no difference[24]. Considering that various dedicated devices for EUS-BD are available and the safety of EUS-BD has been confirmed, giving priority to the intrahepatic approach might be acceptable from the viewpoint of ease of conversion. A recent study proposed the algorithm of conversion from the intrahepatic to the extrahepatic approach after unsuccessful intrahepatic drainage based on 2 cases of this conversion[24]. Along the lines of this small case study, our results could provide further clinical evidence of the usefulness of the conversion technique to select in cases of initial failure of EUS-HGS.

There are some limitations in this study. First, it was a retrospective study conducted in a single center with a relatively small number of patients. Second, selection bias might have occurred due to the nonrandomized nature of the study, although the EUS-BD treatment algorithm was established to minimize the selection bias. Third, lumen-apposing metal stents (LAMSs) were not used in this study. Recent studies have described the efficacy and safety of LAMSs for EUS-BD procedures, and LAMSs are increasingly applied in EUS-BD[32-34]. The advantage of the LAMSs is a reduction in the risk of stent migration and bile leakage, given they facilitate the creation of a sealed transmural conduit between the drainage lumen and the gastrointestinal tract. Unfortunately, LAMSs were not commercially available in Japan during the study period.

In conclusion, target puncture, puncture tract dilation, and guidewire manipulation are 3 major procedural steps associated with failure of initial EUS-BD. Among the 3 steps, guidewire manipulation is the most technically challenging aspect, especially in

the EUS-RV technique. To date, no consensus for the choice of initial EUS-BD technique has been reached. Given the high success rate in this study, when initially planned EUS-BD is difficult, treatment method conversion during a single endoscopic session appears to be feasible and safe. Further multicenter and prospective studies with a larger cohorts are necessary to confirm the suitability and utility of the conversion to another EUS-BD technique from the initial one.

ARTICLE HIGHLIGHTS

Research background

Since it was initially described in 2001, endoscopic ultrasound-guided biliary drainage (EUS-BD) has been developed as an alternative therapeutic technique for biliary obstruction. Although many EUS-BD techniques are available, the optimal algorithm of EUS-BD techniques has not yet been well established.

Research motivation

To date, limited data are available on troubleshooting when the initial EUS-BD plan is challenging. When it was difficult to accomplish the initial EUS-BD procedure, we attempted to convert the puncture target or drainage method in the same endoscopic session.

Research objectives

This study aimed to evaluate the usefulness of converting the treatment methods during a single endoscopic session for difficult cases in initially planned EUS-BD.

Research methods

Patients with biliary obstruction undergoing EUS-BD between May 2008 and April 2016 in a single tertiary-care center were retrospectively reviewed based on our prospectively accumulated database.

Research results

During the study period, 208 patients underwent EUS-BD. In 18.8% of the patients, the treatment methods were converted from the initial plan. The technical and clinical success rates of the conversion cases were 97.4% and 89.5%, respectively. The rate of AEs was 10.3% and all were graded as mild. Puncture target and drainage technique were altered in 25 and 14 cases, respectively. The final technical success rate of all the 208 cases was 97.1%, and that of the initially planned EUS-BD was 78.8%.

Research conclusions

When initially planned EUS-BD is technically challenging, alteration of treatment methods during the single endoscopic session contributed to improvements in the technical success of EUS-BD, without incurring serious AEs.

Research perspectives

Future, multicenter, and prospective studies with larger cohorts are necessary to confirm the suitability and utility of converting the treatment methods in the same endoscopic session from the initially planned EUS-BD technique.

REFERENCES

1 **Coté GA**, Singh S, Bucksot LG, Lazzell-Pannell L, Schmidt SE, Fogel E, McHenry L, Watkins J, Lehman G, Sherman S. Association between volume of endoscopic retrograde cholangiopancreatography at an academic medical center and use of pancreatobiliary therapy. *Clin Gastroenterol Hepatol* 2012; **10**: 920-924 [PMID: 22387254 DOI: 10.1016/j.cgh.2012.02.019]

2 **Dumonceau JM**, Tringali A, Papanikolaou IS, Blero D, Mangiavillano B, Schmidt A, Vanbiervliet G, Costamagna G, Devière J, García-Cano J, Gyökeres T, Hassan C, Prat F, Siersema PD, van Hooft JE. Endoscopic biliary stenting: indications, choice of stents, and results: European Society of Gastrointestinal Endoscopy (ESGE) Clinical Guideline - Updated October 2017. *Endoscopy* 2018; **50**: 910-930 [PMID: 30086596 DOI: 10.1055/a-0659-9864]

3 **Mukai S**, Itoi T, Baron TH, Takada T, Strasberg SM, Pitt HA, Ukai T, Shikata S, Teoh AYB, Kim MH, Kiriyama S, Mori Y, Miura F, Chen MF, Lau WY, Wada K, Supe AN, Giménez ME, Yoshida M, Mayumi T, Hirata K, Sumiyama Y, Inui K, Yamamoto M. Indications and techniques of biliary drainage for acute cholangitis in updated Tokyo Guidelines 2018. *J Hepatobiliary Pancreat Sci* 2017; **24**: 537-549 [PMID: 28834389 DOI: 10.1002/jhbp.496]

4 **Günther RW**, Schild H, Thelen M. Percutaneous transhepatic biliary drainage: experience with 311 procedures. *Cardiovasc Intervent Radiol* 1988; **11**: 65-71 [PMID: 2455599 DOI: 10.1007/]

5 **Oh HC**, Lee SK, Lee TY, Kwon S, Lee SS, Seo DW, Kim MH. Analysis of percutaneous transhepatic cholangioscopy-related complications and the risk factors for those complications. *Endoscopy* 2007; **39**: 731-736 [PMID: 17661249 DOI: 10.1055/s-2007-966577]

6 **Nennstiel S**, Weber A, Frick G, Haller B, Meining A, Schmid RM, Neu B. Drainage-related Complications in Percutaneous Transhepatic Biliary Drainage: An Analysis Over 10 Years. *J Clin Gastroenterol* 2015; **49**: 764-770 [PMID: 25518004 DOI: 10.1097/MCG.0000000000000275]

7 **Giovannini M**, Moutardier V, Pesenti C, Bories E, Lelong B, Delpero JR. Endoscopic ultrasound-guided

bilioduodenal anastomosis: a new technique for biliary drainage. *Endoscopy* 2001; **33**: 898-900 [PMID: 11571690]
8 **Iwashita T**, Doi S, Yasuda I. Endoscopic ultrasound-guided biliary drainage: a review. *Clin J Gastroenterol* 2014; **7**: 94-102 [PMID: 24765215 DOI: 10.1007/s12328-014-0467-5]
9 **Minaga K**, Kitano M. Recent advances in endoscopic ultrasound-guided biliary drainage. *Dig Endosc* 2018; **30**: 38-47 [PMID: 28656640 DOI: 10.1111/den.12910]
10 **Teoh AYB**, Dhir V, Kida M, Yasuda I, Jin ZD, Seo DW, Almadi M, Ang TL, Hara K, Hilmi I, Itoi T, Lakhtakia S, Matsuda K, Pausawasdi N, Puri R, Tang RS, Wang HP, Yang AM, Hawes R, Varadarajulu S, Yasuda K, Ho LKY. Consensus guidelines on the optimal management in interventional EUS procedures: results from the Asian EUS group RAND/UCLA expert panel. *Gut* 2018; **67**: 1209-1228 [PMID: 29463614 DOI: 10.1136/gutjnl-2017-314341]
11 **Isayama H**, Nakai Y, Itoi T, Yasuda I, Kawakami H, Ryozawa S, Kitano M, Irisawa A, Katanuma A, Hara K, Iwashita T, Fujita N, Yamao K, Yoshida M, Inui K. Clinical practice guidelines for safe performance of endoscopic ultrasound/ultrasonography-guided biliary drainage: 2018. *J Hepatobiliary Pancreat Sci* 2019; **26**: 249-269 [PMID: 31025816 DOI: 10.1002/jhbp.631]
12 **Itoi T**, Isayama H, Sofuni A, Itokawa F, Kurihara T, Tsuchiya T, Tsuji S, Ishii K, Ikeuchi N, Tanaka R, Umeda J, Moriyasu F, Kawakami H. Stent selection and tips on placement technique of EUS-guided biliary drainage: transduodenal and transgastric stenting. *J Hepatobiliary Pancreat Sci* 2011; **18**: 664-672 [PMID: 21688214 DOI: 10.1007/s00534-011-0410-9]
13 **Khan MA**, Akbar A, Baron TH, Khan S, Kocak M, Alastal Y, Hammad T, Lee WM, Sofi A, Artifon EL, Nawras A, Ismail MK. Endoscopic Ultrasound-Guided Biliary Drainage: A Systematic Review and Meta-Analysis. *Dig Dis Sci* 2016; **61**: 684-703 [PMID: 26518417 DOI: 10.1007/s10620-015-3933-0]
14 **Wang K**, Zhu J, Xing L, Wang Y, Jin Z, Li Z. Assessment of efficacy and safety of EUS-guided biliary drainage: a systematic review. *Gastrointest Endosc* 2016; **83**: 1218-1227 [PMID: 26542374 DOI: 10.1016/j.gie.2015.10.033]
15 **Logiudice FP**, Bernardo WM, Galetti F, Sagae VM, Matsubayashi CO, Madruga Neto AC, Brunaldi VO, de Moura DTH, Franzini T, Cheng S, Matuguma SE, de Moura EGH. Endoscopic ultrasound-guided *vs* endoscopic retrograde cholangiopancreatography biliary drainage for obstructed distal malignant biliary strictures: A systematic review and meta-analysis. *World J Gastrointest Endosc* 2019; **11**: 281-291 [PMID: 31040889 DOI: 10.4253/wjge.v11.i4.281]
16 **Hathorn KE**, Bazarbashi AN, Sack JS, McCarty TR, Wang TJ, Chan WW, Thompson CC, Ryou M. EUS-guided biliary drainage is equivalent to ERCP for primary treatment of malignant distal biliary obstruction: a systematic review and meta-analysis. *Endosc Int Open* 2019; **7**: E1432-E1441 [PMID: 31673615 DOI: 10.1055/a-0990-9488]
17 **Hedjoudje A**, Sportes A, Grabar S, Zhang A, Koch S, Vuitton L, Prat F. Outcomes of endoscopic ultrasound-guided biliary drainage: A systematic review and meta-analysis. *United European Gastroenterol J* 2019; **7**: 60-68 [PMID: 30788117 DOI: 10.1177/2050640618808147]
18 **Park DH**, Jang JW, Lee SS, Seo DW, Lee SK, Kim MH. EUS-guided biliary drainage with transluminal stenting after failed ERCP: predictors of adverse events and long-term results. *Gastrointest Endosc* 2011; **74**: 1276-1284 [PMID: 21963067 DOI: 10.1016/j.gie.2011.07.054]
19 **Imai H**, Kitano M, Omoto S, Kadosaka K, Kamata K, Miyata T, Yamao K, Sakamoto H, Harwani Y, Kudo M. EUS-guided gallbladder drainage for rescue treatment of malignant distal biliary obstruction after unsuccessful ERCP. *Gastrointest Endosc* 2016; **84**: 147-151 [PMID: 26764194 DOI: 10.1016/j.gie.2015.12.024]
20 **Cotton PB**, Eisen GM, Aabakken L, Baron TH, Hutter MM, Jacobson BC, Mergener K, Nemcek A, Petersen BT, Petrini JL, Pike IM, Rabeneck L, Romagnuolo J, Vargo JJ. A lexicon for endoscopic adverse events: report of an ASGE workshop. *Gastrointest Endosc* 2010; **71**: 446-454 [PMID: 20189503 DOI: 10.1016/j.gie.2009.10.027]
21 **Tsuchiya T**, Itoi T, Sofuni A, Tonozuka R, Mukai S. Endoscopic ultrasonography-guided rendezvous technique. *Dig Endosc* 2016; **28** Suppl 1: 96-101 [PMID: 26786389 DOI: 10.1111/den.12611]
22 **Iwashita T**, Yasuda I, Mukai T, Iwata K, Ando N, Doi S, Nakashima M, Uemura S, Mabuchi M, Shimizu M. EUS-guided rendezvous for difficult biliary cannulation using a standardized algorithm: a multicenter prospective pilot study (with videos). *Gastrointest Endosc* 2016; **83**: 394-400 [PMID: 26089103 DOI: 10.1016/j.gie.2015.04.043]
23 **Tyberg A**, Desai AP, Kumta NA, Brown E, Gaidhane M, Sharaiha RZ, Kahaleh M. EUS-guided biliary drainage after failed ERCP: a novel algorithm individualized based on patient anatomy. *Gastrointest Endosc* 2016; **84**: 941-946 [PMID: 27237786 DOI: 10.1016/j.gie.2016.05.035]
24 **Uemura RS**, Khan MA, Otoch JP, Kahaleh M, Montero EF, Artifon ELA. EUS-guided Choledochoduodenostomy Versus Hepaticogastrostomy: A Systematic Review and Meta-analysis. *J Clin Gastroenterol* 2018; **52**: 123-130 [PMID: 29095426 DOI: 10.1097/MCG.0000000000000948]
25 **Minaga K**, Ogura T, Shiomi H, Imai H, Hoki N, Takenaka M, Nishikiori H, Yamashita Y, Hisa T, Kato H, Kamada H, Okuda A, Sagami R, Hashimoto H, Higuchi K, Chiba Y, Kudo M, Kitano M. Comparison of the efficacy and safety of endoscopic ultrasound-guided choledochoduodenostomy and hepaticogastrostomy for malignant distal biliary obstruction: Multicenter, randomized, clinical trial. *Dig Endosc* 2019; **31**: 575-582 [PMID: 30908711 DOI: 10.1111/den.13406]
26 **Minaga K**, Kitano M, Imai H, Yamao K, Kamata K, Miyata T, Omoto S, Kadosaka K, Yoshikawa T, Kudo M. Urgent endoscopic ultrasound-guided choledochoduodenostomy for acute obstructive suppurative cholangitis-induced sepsis. *World J Gastroenterol* 2016; **22**: 4264-4269 [PMID: 27122677 DOI: 10.3748/wjg.v22.i16.4264]
27 **Kanno Y**, Ito K, Koshita S, Ogawa T, Masu K, Masaki Y, Noda Y. Efficacy of a newly developed dilator for endoscopic ultrasound-guided biliary drainage. *World J Gastrointest Endosc* 2017; **9**: 304-309 [PMID: 28744342 DOI: 10.4253/wjge.v9.i7.304]
28 **Amano M**, Ogura T, Onda S, Takagi W, Sano T, Okuda A, Miyano A, Masuda D, Higuchi K. Prospective clinical study of endoscopic ultrasound-guided biliary drainage using novel balloon catheter (with video). *J Gastroenterol Hepatol* 2017; **32**: 716-720 [PMID: 27420770 DOI: 10.1111/jgh.13489]
29 **Ogura T**, Nakai Y, Iwashita T, Higuchi K, Itoi T. Novel fine gauge electrocautery dilator for endoscopic ultrasound-guided biliary drainage: experimental and clinical evaluation study (with video). *Endosc Int Open* 2019; **7**: E1652-E1657 [PMID: 31788548 DOI: 10.1055/a-0961-7890]
30 **Dhir V**, Artifon EL, Gupta K, Vila JJ, Maselli R, Frazao M, Maydeo A. Multicenter study on endoscopic ultrasound-guided expandable biliary metal stent placement: choice of access route, direction of stent insertion, and drainage route. *Dig Endosc* 2014; **26**: 430-435 [PMID: 23941261 DOI: 10.1111/den.12153]

31 **Alvarez-Sánchez MV**, Jenssen C, Faiss S, Napoléon B. Interventional endoscopic ultrasonography: an overview of safety and complications. *Surg Endosc* 2014; **28**: 712-734 [PMID: 24196551 DOI: 10.1007/s00464-013-3260-5]

32 **Kunda R**, Pérez-Miranda M, Will U, Ullrich S, Brenke D, Dollhopf M, Meier M, Larghi A. EUS-guided choledochoduodenostomy for malignant distal biliary obstruction using a lumen-apposing fully covered metal stent after failed ERCP. *Surg Endosc* 2016; **30**: 5002-5008 [PMID: 26969661 DOI: 10.1007/s00464-016-4845-6]

33 **Anderloni A**, Fugazza A, Troncone E, Auriemma F, Carrara S, Semeraro R, Maselli R, Di Leo M, D'Amico F, Sethi A, Repici A. Single-stage EUS-guided choledochoduodenostomy using a lumen-apposing metal stent for malignant distal biliary obstruction. *Gastrointest Endosc* 2019; **89**: 69-76 [PMID: 30189198 DOI: 10.1016/j.gie.2018.08.047]

34 **El Chafic AH**, Shah JN, Hamerski C, Binmoeller KF, Irani S, James TW, Baron TH, Nieto J, Romero RV, Evans JA, Kahaleh M. EUS-Guided Choledochoduodenostomy for Distal Malignant Biliary Obstruction Using Electrocautery-Enhanced Lumen-Apposing Metal Stents: First US, Multicenter Experience. *Dig Dis Sci* 2019; **64**: 3321-3327 [PMID: 31175495 DOI: 10.1007/s10620-019-05688-2]

World Journal of Gastroenterology

Submit a Manuscript: https://www.f6publishing.com

World J Gastroenterol 2020 March 7; 26(9): 960-972

DOI: 10.3748/wjg.v26.i9.960

ISSN 1007-9327 (print) ISSN 2219-2840 (online)

ORIGINAL ARTICLE

Retrospective Study

Differentiation of atypical hepatic hemangioma from liver metastases: Diagnostic performance of a novel type of color contrast enhanced ultrasound

Xiao-Feng Wu, Xiu-Mei Bai, Wei Yang, Yu Sun, Hong Wang, Wei Wu, Min-Hua Chen, Kun Yan

ORCID number: Xiao-Feng Wu (0000-0002-7958-1228); Xiu-Mei Bai (0000-0001-9581-6851); Wei Yang (0000-0002-5836-0573); Yu Sun (0000-0003-3024-0331); Hong Wang (0000-0002-4417-6855); Wei Wu (0000-0003-1190-8068); Min-Hua Chen (0000-0001-7550-2601); Kun Yan (0000-0002-6422-5060).

Author contributions: All authors performed the research; Wu XF, Bai XM and Yang W wrote the manuscript; Wu XF, Bai XM and Wang H performed the color contrast ultrasound and data analysis; Yang W, Wu W, Chen MH, and Yan K conceived and designed the study, performed the examinations, and the data analysis; Sun Y performed the pathologic analysis. Wu XF and Bai XM contributed equally to this work.

Supported by Capital Medical Development Program, No. 2018-2-2154; and National Natural Science Foundation of China, No. 81773286.

Institutional review board statement: This study was reviewed and approved by the Peking University School of Oncology

Informed consent statement: Patients were not required to give informed consent to the study because the analysis used anonymous clinical data that were obtained after each patient agreed to treatment by written consent.

Xiao-Feng Wu, Xiu-Mei Bai, Wei Yang, Hong Wang, Wei Wu, Min-Hua Chen, Kun Yan, Key Laboratory of Carcinogenesis and Translational Research (Ministry of Education/Beijing), Department of Ultrasound, Peking University Cancer Hospital & Institute, Beijing 100142, China

Yu Sun, Key laboratory of Carcinogenesis and Translational Research (Ministry of Education/Beijing), Department of Pathology, Peking University Cancer Hospital & Institute, Beijing 100142, China

Corresponding author: Wei Yang, MD, Professor, Key Laboratory of Carcinogenesis and Translational Research (Ministry of Education/Beijing), Department of Ultrasound, Peking University Cancer Hospital & Institute, Number 52 Fucheng Road, District of Haidian, Beijing 100142, China. 13681408183@163.com

Abstract

BACKGROUND

In clinical practice, the diagnosis is sometimes difficult with contrast-enhanced ultrasound (CEUS) when the case has an atypical perfusion pattern. Color parametric imaging (CPI) is an analysis software for CEUS with better detection of temporal differences in CEUS imaging using arbitrary colors. It measures the differences in arrival time of the contrast agent in lesions so that the perfusion features of atypical hemangioma and colorectal cancer (CRC) liver metastasis can be distinguished.

AIM

To evaluate the role of a novel type of CPI of CEUS in the differential diagnosis of atypical hemangioma from liver metastases in patients with a history of CRC.

METHODS

From January 2016 to July 2018, 42 patients including 20 cases of atypical hemangioma and 22 cases of liver metastases from CRC were enrolled. These patients had a mean age of 60.5 ± 9.3 years (range: 39-75 years). All patients received ultrasound, CEUS and CPI examinations. Resident and staff radiologists independently and retrospectively reviewed CEUS and CPI images. Two sets of criteria were assigned: (1) Routine CEUS alone; and (2) CEUS and CPI. The diagnostic sensitivity, specificity, accuracy and receiver operating characteristic (ROC) curve of resident and staff radiologists were analyzed.

Conflict-of-interest statement: All authors declare no conflicts of interest related to this article.

Data sharing statement: No additional data are available.

Manuscript source: Invited Manuscript

Received: November 28, 2019
Peer-review started: November 28, 2019
First decision: December 23, 2019
Revised: January 12, 2020
Accepted: January 19, 2020
Article in press: January 19, 2020
Published online: March 7, 2020

P-Reviewer: Rolle U, Sporea I
S-Editor: Ma YJ
L-Editor: A MedE-Ma JY
E-Editor: Liu MY

RESULTS

The following CPI features were significantly different between liver hemangioma and liver metastases analyzed by staff and resident radiologists: Peripheral nodular enhancement (65%-70.0% *vs* 4.5%-13.6%, $P < 0.001$, $P = 0.001$), mosaic/chaotic enhancement (5%-10% *vs* 68.2%-63.6%, $P < 0.001$, $P < 0.001$) and feeding artery (20% *vs* 59.1%-54.5%, $P = 0.010$, $P = 0.021$). CPI imaging offered significant improvements in detection rates compared with routine CEUS in both resident and staff groups. By resident radiologists, the specificity and accuracy of CEUS+CPI were significantly increased compared with that of CEUS (77.3% *vs* 45.5%, $P = 0.030$; 78.6% *vs* 50.0%, $P = 0.006$). In addition, the area under the curve (AUC) of CEUS+CPI was significantly higher than that of CEUS (0.803 *vs* 0.757, $P = 0.036$). By staff radiologists, accuracy was improved in CEUS+CPI (81.0% *vs* 54.8%, $P = 0.010$), whereas no significant differences in specificity and sensitivity were found ($P = 0.144$, $P = 0.112$). The AUC of CEUS+CPI was significantly higher than that of CEUS (0.890 *vs* 0.825, $P = 0.013$) by staff radiologists.

CONCLUSION

Compared with routine CEUS, CPI could provide specific information on the hemodynamic features of liver lesions and help to differentiate atypical hemangioma from liver metastases in patients with CRC, even for senior radiologists.

Key words: Color parametric imaging; Contrast enhanced ultrasound; Liver hemangioma; Liver metastases

Core tip: Features of atypical hemangioma and liver metastases on routine contrast-enhanced ultrasound are complicated. Color parametric imaging is a new approach that provides specific information on hemodynamic features. The following color parametric imaging features were significantly different between atypical liver hemangioma and liver metastases analyzed by staff and resident radiologists: Peripheral nodular enhancement, mosaic/chaotic enhancement and feeding artery. These findings could help radiologists and even senior radiologists with better identification of the diseases.

Citation: Wu XF, Bai XM, Yang W, Sun Y, Wang H, Wu W, Chen MH, Yan K. Differentiation of atypical hepatic hemangioma from liver metastases: Diagnostic performance of a novel type of color contrast enhanced ultrasound. *World J Gastroenterol* 2020; 26(9): 960-972
URL: https://www.wjgnet.com/1007-9327/full/v26/i9/960.htm
DOI: https://dx.doi.org/10.3748/wjg.v26.i9.960

INTRODUCTION

Sonography is the most common imaging modality to detect focal hepatic lesions, but its diagnostic ability to differentiate between benign and malignant lesions is comparatively low. Many studies have shown that contrast-enhanced sonography (CEUS) with low–mechanical index techniques could provide important information about tissue perfusion and vascularity architecture and improve the differential diagnosis in focal hepatic lesions[1-3]. However, the diagnosis is difficult with CEUS when the case has an atypical perfusion pattern.

On CEUS, the typical feature of liver hemangioma is peripheral nodular and centripetal enhancement during the arterial phase followed by hyper- or isoenhancement during the portal venous and late phases[4-7]. In contrast, the feature of liver metastases is complete or rim-like hyperenhancement during the arterial phase followed by hypoenhancement in the portal venous and late phase. There were different perfusion patterns between the two diseases. However, hemangioma also has an atypical pattern on CEUS, such as rapid homogeneous hyperenhancement in arterial phase like malignant tumors or lack of enhancement in the center, which may be misinterpreted as wash out[8-10]. The atypical pattern makes the differentiated

diagnosis quite difficult from liver metastases, especially in patients with a previous history of malignant tumor. In our center, we misdiagnosed several lesions of atypical hemangioma as liver metastases on CEUS in patients with a history of colorectal cancer (CRC). Consequently, these patients received unnecessary surgical resection for these lesions. These misdiagnosed cases encouraged us to explore a better way to differentiate between them.

Color parametric imaging (CPI) is an image analysis software for CEUS with better detection of temporal differences in CEUS imaging using arbitrary colors. It measures the differences in arrival time of the contrast agent between the target region and reference points determined arbitrarily at a structure in the liver such as the hepatic artery and portal vein. The arrival time was defined as zero and represented the time differences in different colors. A few studies demonstrated that CPI was useful in the diagnosis of hepatic parenchymal diseases[11,12] and in identifying spoke-wheel patterns of FNH[13]. To our knowledge, this is the first study to analyze whether CPI could provide useful information to differentially diagnose atypical hemangioma and liver metastases.

The aim of this study was to evaluate the role of CPI in the differential diagnosis of atypical hemangioma and liver metastases and the diagnostic performance of staff and resident radiologists.

MATERIALS AND METHODS

Patients

This retrospective study was approved by the Institutional Review Board of the Peking University School of Oncology, and written informed consent was waived. From January 2016 to July 2018, a total of 1468 consecutive patients with focal liver lesions were referred to our department for CEUS examinations. Of the 109 hemangioma cases, 23 cases had atypical CEUS patterns and previous CRC histories, which were difficult to exclude from liver metastasis. During the same period, 480 patients with suspected liver metastasis from CRCs were diagnosed based on CEUS. Because there were much more liver metastasis cases (n = 480) than hemangioma cases (n = 20), we randomly selected 24 cases from the liver metastasis pool according to a 1:20 proportion. If patients had more than one lesion, the largest and most clearly presented lesion was chosen for CPI evaluation. Five patients who had deep breath during the arterial phase and poor imaging quality were excluded. Finally, 20 hemangiomas and 22 liver metastases were entered into this retrospective study (Figure 1).

According to the liver CEUS guidelines[14] and other studies[10], the atypical pattern of CEUS for hemangioma included rapid homogeneous hyperenhancement at the arterial phase and hypoenhancement at the portal/late phase and peripheral nodular enhancement at the arterial phase and lack of enhancement in the center at the late phase. The CEUS pattern for liver metastasis included hyperenhancement at the arterial phase and washout at the late phase or rim-like enhancement at the arterial phase and a nonenhancement area at the late phase. Among the 22 patients with liver metastasis, the final diagnosis was confirmed by pathologic analysis of specimens obtained via US-guided percutaneous biopsy (n = 16) or surgical resection (n = 6). Among the 20 hemangiomas, the final diagnosis was based on either pathological results (n = 9) or contrast-enhanced computed tomography or contrast-enhanced magnetic resonance imaging findings with at least one year follow-up (n = 11). Among the 42 patients, 19 were male and 23 were female. The average age was 60.5 ± 9.3 years (range: 39-75 years). The mean size of liver lesions was 3.2 ± 1.8 cm (range: 1.3-11 cm).

Ultrasound examination machine and technique

A Logiq E9 ultrasonic machine (GE Healthcare, Milwaukee, WI, United States) was used with a C1-5 convex probe to obtain routine US and CEUS images. The ultrasound contrast agent was SonoVue (Bracco, Milan, Italy). Lyophilized SonoVue powder was dissolved in 5 mL saline. Bolus injection (2 mL the suspension) was performed at the antecubital vein *via* a 20G cannula within 2-3 s, followed by a 5-mL saline flush.

Before the examination, the patients were required to lie in the left lateral position or supine position and breathe steadily. The liver lesions were scanned and located using routine US. The echogenicity, diameter, border, morphology, necrosis, halo sign and vessels were observed. It was defined as necrosis in ultrasound imaging if there was an anechoic area within the lesions, clear boundaries, and color Doppler flow imaging showed no blood flow within the anechoic area. The halo sign was defined as

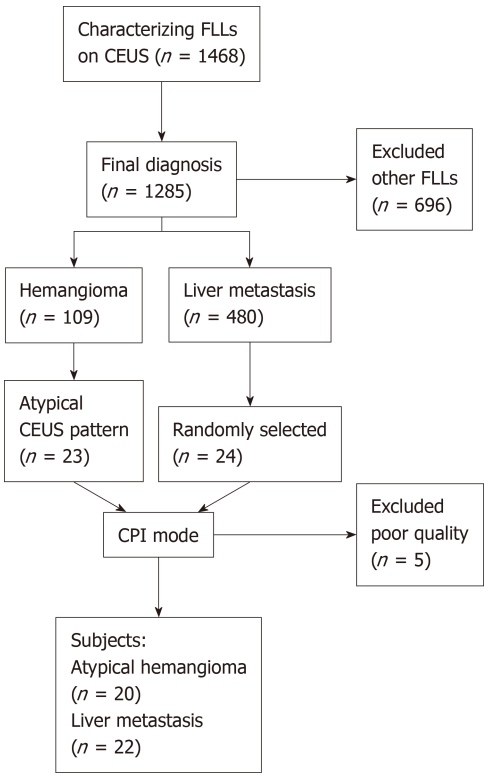

Figure 1 Flow diagram of the study population. CPI: Color parametric imaging; FLL: Focal liver lesions, CEUS: Contrast enhanced ultrasound.

a hypoechoic rim found around the solid mass with a distinct difference between the lesion and the surrounding liver. At least two vessels inside the lesion on color Doppler flow imaging indicated rich flow.

Then, the contrast mode was entered. The imaging settings, such as gain, depth, and focus, were optimal. The mechanical index was set at 0.11-0.13. After injecting contrast agent, the liver was scanned using contrast-enhanced harmonic grayscale sonography, and timer was initiated simultaneously. The dynamic blood perfusion of lesions was observed from baseline to the late phase. Consecutive cine clips (90 s each) were recorded and stored on the hard disk for further analysis. The enhancement phases were divided into the arterial phase (10-30 s), portal vein phase (31-120 s), and late phase (120-360 s) after injection of contrast agent. The same ultrasound machine with the procedure software of parametric imaging was used to obtain CPI.

CEUS and CPI imaging analysis

Two resident radiologists (W. X. F. and W. H.) each with at least one year of experience in the evaluation of liver CEUS images as well as two staff radiologists (Y. W. and W. W.) each with at least 10 years of experience in the liver CEUS images retrospectively read all the CEUS and CPI images independently. Two radiologists at the same level retrospectively interpreted the CEUS images without knowledge of the patients' final diagnosis. In all cases, consensus agreement between the two radiologists was used to determine the CEUS feature and possible diagnosis. According to CEUS guidelines[14], the enhancement patterns at the arterial phase to portal phase of liver lesions included four patterns: Peripheral nodular enhancement (peripheral focal enhancement in the arterial phase, progressing in a centripetal direction to partial fill-in.), rim-like enhancement (peripheral enhancement in the arterial phase, without gradual fill-in.), homogenous hyperenhancement, and heterogeneous enhancement.

All of the CEUS images of the arterial phase were reconstructed with the Parametric Imaging program using a Logiq E9 XD Clear ultrasonic machine (GE Healthcare, Milwaukee, WI, United States). The CEUS video clips were reviewed to record the starting and ending points of lesion enhancement. In the CPI system, time zero was regarded as the point at which the contrast agent reached the liver, and the arrival time was then calculated between the current time and time zero. If the time zero was set at the time when contrast agent was injected, the arrival time of contrast agent at each pixel could be calculated. Thus, the color map consisted of individual pixels representing the arrival time of the contrast agent in the tumor. The residents

and staff radiologists read all the CPI images blindly and independently. The CPI enhancement patterns of liver lesions were summarized and classified into four patterns: (1) Peripheral nodular enhancement (round or semicircle shaped enhancement visualized at the peripheral area of lesions and no enhancement in the center); (2) Peripheral rim-like enhancement (peripheral enhancement without nodular or regular shape); (3) Concentric circle enhancement (multiple circles with the same center); and (4) Mosaic enhancement (enhancing lines of the vascular tree, defined as one or more hypertrophic tortuous arteries that reached the edge of the lesion, partially encircling the nodule and penetrating internally with a basket or chaotic distribution) (Figure 2). The feeding artery, defined as a hypertrophic artery that was directed toward the lesion and was larger than the branches at the same depth during the arterial phase, was red in the central area, which was surrounded by yellow, or was a scattered distribution of red and yellow (Figure 2). In all cases, consensus agreement between the two radiologists was used to determine the CPI feature and possible diagnosis.

In the training, both staff and resident radiologists were required to review all 20 cases of hemangioma and liver metastasis with typical CEUS and CPI features. CEUS and CPI diagnoses were scored using a 5-point scale: 1 = hemangioma with strong evidence, 2 = possible hemangioma, 3 = undetermined, 4 = possible liver metastasis, and 5= liver metastasis with strong evidence.

The arrival time of the contrast agent after injection could be displayed at any point of CPI. The arrival time of a lesion was defined as the arrival time of the earliest color point in the lesion, and the peak time was regarded as the arrival time of the last color point in the lesion. The peak time of CPI was regarded as the time point where the brightest color was in the lesion. AT was regarded as the difference in peak time and arrival time of CPI of atypical hemangioma or liver metastasis.

Statistical analysis

SPSS 21.0 statistical software was used for statistical analysis. The quantitative data are displayed as the mean ± SD and were compared by *t* test. The Kappa test was used to analyze the interrater agreement between the staff and resident radiologists. The agreement was graded as follows: Moderate (0.2-0.39), fair (0.40-0.59), good (0.60-0.79), and perfect (0.80-1.0) agreement. The diagnostic sensitivity, specificity, and accuracy between CEUS and CPI patterns were compared by the McNemar test. The count data were analyzed using χ^2 test and Fisher's exact test. A *P* value less than 0.05 was considered statistically significant.

RESULTS

Routine CEUS patterns of liver atypical hemangioma and liver metastases

The routine CEUS features of liver atypical hemangioma and liver metastases analyzed by staff and resident radiologists are shown in Table 1.

The CEUS features of peripheral nodular enhancement were observed during the arterial phase more frequently in patients with atypical hemangioma than in those with metastasis ($P = 0.003$) by staff radiologists. The CEUS features of heterogeneous hyperenhancement were observed during the arterial phase significantly more frequently in patients with metastasis than in those with atypical hemangioma by staff radiologists ($P = 0.023$). However, the perfusion patterns detected by resident radiologists were not as sensitive as those detected by staff radiologists (Table 1). The features of peripheral nodular enhancement and heterogeneous hyperenhancement for resident radiologists were not significantly different between atypical hemangioma and metastasis ($P = 0.052$, $P = 0.096$). The feeding arteries for the staff and resident radiologists were at a power of 25%–45.5%.

CPI features of liver atypical hemangioma and liver metastases

The CPI features of liver atypical hemangioma and liver metastases analyzed by staff and resident radiologists are shown in Table 2.

The CPI features of peripheral nodules were observed during the arterial phase more frequently in patients with atypical hemangioma than in those with metastasis by both groups of radiologists (65%-70.0% *vs* 4.5%-13.6%, $P < 0.001$, $P = 0.001$). In addition, the CPI features of mosaic enhancement (5%-10% *vs* 68.2%-63.6%, $P < 0.001$, $P < 0.001$) and feeding artery (20% *vs* 59.1%-54.5%, $P = 0.010$, $P = 0.021$) were found during the arterial phase more frequently in patients with metastasis than in those with atypical hemangioma by both groups of radiologists. The feeding arteries for the staff and resident radiologists were at a power of 20%–59.1%. CPI imaging offered significant improvements in detection rates compared with routine CEUS signs in

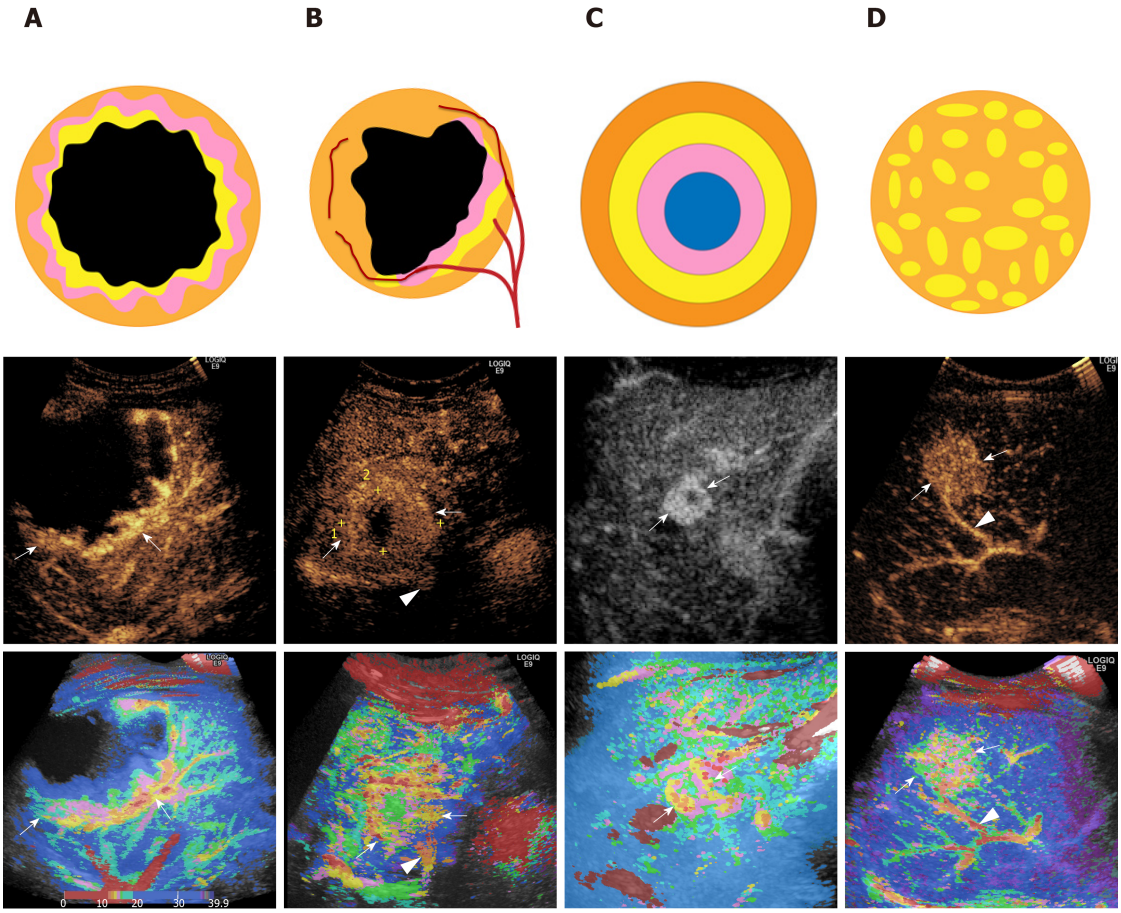

Figure 2 color parametric imaging patterns of liver atypical hemangioma and liver metastases. First line was sketch figures for the four enhancement patterns of color parametric imaging. Second line was representative routine contrast-enhanced ultrasound images corresponding to the four enhancement patterns. Third line was representative color parametric images corresponding to the four patterns. A: Peripheral nodular enhancement; B: Peripheral rim-like with feeding artery (▲); C: Concentric circles enhancement; D: Mosaic enhancement with feeding artery (▲).

both groups.

Consistency of CEUS and CPI features between staff and resident radiologists

The consistency of CEUS and CPI between staff and resident radiologists was analyzed (Table 3). With regard to CEUS features found by staff and resident radiologists, the diagnostic consistency in homogenous hyperenhancement and heterogeneous enhancement was perfect (k = 0.835, k = 0.804), and the diagnostic consistency in peripheral nodular enhancement and rim-like enhancement was good (k = 0.602, k = 0.692).

With regard to CPI features found by staff and resident radiologists, the diagnostic consistency in peripheral nodular enhancement and mosaic enhancement was perfect (k = 0.885, k = 0.803), and the diagnostic consistency in peripheral rim-like enhancement and concentric circle enhancement was good (k = 0.713, k = 0.760).

Diagnostic confidence scoring by CPI and CEUS imaging

The diagnostic confidence scoring of lesions by staff and resident radiologists is summarized in Figure 3. There were significant differences in the final score distribution between the two methods. The number of 3-score (undetermined diagnosis) in CEUS was obviously higher than that in CPI by both the groups of staff (45.2% *vs* 4.8%, P < 0.001) and resident radiologists (35.7% *vs* 7.1%, P = 0.001).

Diagnostic performance of CEUS and CPI in staff and resident radiologists

The diagnostic performance of CEUS and CPI by staff and resident radiologists is shown in Table 4.

By resident radiologists, the specificity of CEUS+CPI was significantly increased compared with that of CEUS (77.3% *vs* 45.5%, P = 0.030). The sensitivity of CEUS+CPI was higher than that of CEUS, but the differences were not significant (80.0% *vs* 55.0%, P = 0.456). The accuracy of CEUS+CPI was significantly higher than the accuracy of CEUS (78.6% *vs* 50%, P = 0.006). Additionally, the AUC of CEUS+CPI was

Table 1 Comparison of routine contrast enhanced ultrasound features between atypical hemangioma and liver metastasis

CEUS	Staff			Resident		
	H (*n* = 20)	M (*n* = 22)	*P* value	H (*n* = 20)	M (*n* = 22)	*P* value
Peripheral nodular	10 (50)	2 (9.1)	0.003	8 (40)	3 (13.6)	0.052
Peripheral rim-like	6 (30)	5 (22.7)	0.592	8 (40)	4 (18.2)	0.118
Homogenous hyper	2 (10)	6 (27.3)	0.135	3 (15)	9 (40.9)	0.063
Heterogeneous hyper	2 (10)	9 (40.9)	0.023	1 (5)	6 (27.3)	0.096
Feeding artery	6 (30)	10 (45.5)	0.303	5 (25)	8 (36.4)	0.426

Numbers in parentheses are percentages. The difference between peripheral nodular enhancement and heterogeneous enhancement of contrast enhanced ultrasound patterns were observed (P = 0.003, P = 0.023) in staff group. CEUS: Contrast enhanced ultrasound; H: Hemangioma; M: Metastasis.

significantly higher than that of CEUS (AUC = 0.803 *vs* AUC = 0.757, P = 0.036).

By staff radiologists, accuracy was improved in CEUS+CPI (81.0% *vs* 54.8%, P = 0.010), whereas no significant differences in specificity and sensitivity were found (P = 0.144, P = 0.112). The AUC of CEUS+CPI was significantly higher than the AUC of CEUS (0.890 *vs* 0.825, P = 0.013) by staff radiologists.

Comparison of the AT of CPI between atypical hemangioma and liver metastasis

The comparison of the AT of CPI between atypical hemangioma and liver metastasis is summarized in Figure 4. The difference in peak time and arrival time of CPI of atypical hemangioma was significantly longer than that of liver metastasis (8.31 ± 3.05 s *vs* 5.13 ± 0.99 s, P < 0.001).

DISCUSSION

Ultrasonography is useful for the diagnosis of hepatic focal lesions, which is based on their distinctive echogenicities—the grayscale morphologic features. The development of ultrasound contrast agents provided us with more information about tissue perfusion and helped to improve diagnostic accuracy, particularly in focal liver lesions (FLLs)[15-17]. Compared with first-generation agents, the second-generation ultrasound contrast agent SonoVue consisting of sulfur hexafluoride microbubbles (Bracco, Milan, Italy) has a high flexibility shell and is more stable to acoustic pressure. SonoVue microbubbles produce a longer duration and stable continuous nonlinear harmonic signal when insonated with low acoustic power. With SonoVue, we could acquire important information on both the macrovasculature and microvasculature and then evaluate the flow dynamic features of FLLs in real time[18-21]. Many studies have reported the typical or atypical features of different liver tumors in CEUS performance, and many clinical centers and guidelines have recommended a diagnostic criterion of FLLs using CEUS in clinical practice[18,22,23].

It was reported that the incidence of hemangioma in the general population varies from 0.4% to 20%[24], the latter resulting from a thorough prospective search of the liver in an unselected autopsy series. CEUS imaging of hemangioma can be performed during the vascular phase assessing the dynamic enhancement pattern and the vascular morphology of the lesion[25]. Moreover, the majority of hemangiomas presents as peripheral nodular or rim enhancement at arterial phase with centripetal progression in portal venous and late phase on CEUS. However, some cases had the atypical pattern of CEUS for hemangioma as hyperenhancement during the arterial phase or have nonenhancement area at portal and late phases, which often caused various misdiagnoses, including malignant liver tumors. When the case had a history of malignant tumors, it was a challenge to differentiate the atypical hemangioma from liver metastasis. As the treatments for these diseases are completely different, misdiagnosis might result in the unnecessary traumatic resection of benign lesions or miss the opportunity for radical resection of malignant lesions. In our center, 7 cases of atypical hemangioma with a history of colon-rectal cancer had been misdiagnosed as liver metastasis on CEUS and received unnecessary surgical resection of liver lesions before we started this study. These misdiagnosed cases encouraged us to carry out the present study. This study mainly assessed the value of the combination of CEUS and CPI for differentiating hemangioma and liver metastases.

In our study, the CEUS feature of atypical hemangioma included homogenous

Table 2 Comparison of color parametric imaging features between atypical hemangioma and liver metastasis

CPI	Staff			Resident		
	H (*n* = 20)	M (*n* = 22)	*P* value	H (*n* = 20)	M (*n* = 22)	*P* value
Peripheral nodular[1]	14 (70.0)	1 (4.5)	< 0.001	13 (65.0)	3 (13.6)	0.001
Peripheral rim-like	2 (10.0)	6 (27.3)	0.152	3 (15.0)	4 (18.2)	0.556
Concentric circles[1]	3 (15.0)	0 (0)	0.099	2 (10.0)	1 (4.5)	0.463
Mosaic/ chaotic.	1 (5.0)	15 (68.2)	<0.001	2 (10.0)	14 (63.6)	< 0.001
Feeding artery	4 (20)	13 (59.1)	0.010	4 (20)	12 (54.5)	0.021

Numbers in parentheses are percentages.
[1]The difference between peripheral nodular,Mosaic/chaotic enhancement and feeding artery of CPI patterns were observed ($P < 0.001$, $P < 0.001$, $P = 0.010$) in staff group and ($P = 0.001$, $P < 0.001$, $P = 0.021$) in resident group. CPI: Color parametric imaging; H: Hemangioma; M: Metastasis.

hyperenhancement/rim-like enhancement during the arterial phase and nonenhancement during the late phase, and these appearances might also be found in liver metastasis. Thus, the similar manifestations made it difficult for radiologists to differentiate them. The newly developed technique of CPI offered a more objective color-coded map to display FLL dynamic perfusion, which can provide more information for differential diagnosis. Parametric images could quantify the dynamic procedure of CEUS and then evaluate the vascular architecture in lesions more objectively than the regular CEUS review[23]. One of the CEUS shortcomings was that CEUS could not detect tiny changes in contrast agent dynamics due to rapid monochromatic enhancement of small lesions or lesions that were enhanced very shortly. In this line, CPI could overcome the disadvantage of conventional CEUS because CPI has higher ability to demonstrate temporal changes in contrast-enhanced imaging findings. Therefore, CPI has better potential for detecting concentric circles or peripheral nodular enhancement of hemangioma and mosaic enhancement of liver metastasis.

Since the application period was short after the CPI technique was put to market, there were only a few clinical reports[26-28]. Some researchers indicated that CPI using Sonazoid as a contrast agent was better for detecting spoke-wheel patterns of FNH less than 3 cm in size[13]. In Li *et al*[28]'s study, the diagnostic sensitivity, specificity, accuracy, PPV, and NPV of CPI for atypical hepatocellular carcinoma from focal nodular hyperplasia were higher than those of CEUS only. They concluded that the newly developed technique of CPI offered a more objective color-coded map to display focal liver lesion dynamic perfusion and greatly improved the differentiation of focal liver lesions, especially in the resident radiologist group. To our knowledge, our study is the first report on the role of CPI in the differential diagnosis of atypical hemangioma and liver metastasis. In our study, CPI improved the diagnostic performance in the resident group. The diagnostic specificity and accuracy rate of the combination CPI and CEUS (77.3% and 78.6%, respectively) were significantly higher than those of CEUS alone (45.5% and 50.0%, respectively) in the resident group. The accuracy rate of the combination (81.0%) was also higher than that of CEUS alone (54.8%) in the staff group. Our data indicated that the differential diagnosis of atypical hemangioma and liver metastasis was still challenging, even for experienced radiologists, and CPI provided a very useful tool to improve diagnosis.

Our study showed that the 3-score (undetermined diagnosis) in CEUS was obviously higher than that in CPI+CEUS in both the staff group (45.2% *vs* 4.8%, $P < 0.001$) and in the resident group (35.7% *vs* 7.1%, $P = 0.001$). Our data confirmed that the application of CPI significantly increased the diagnostic confidence of focal liver lesions compared with CEUS, and the number of undetermined cases decreased greatly compared with CEUS. CPI can display the color-coded imaging of regional flow dynamics based on the arrival time parameter. The color map emphasized the difference in perfusion viscosity of lesions and revealed the features of blood flow perfusion and pathological structures. On CPI imaging, we found that the flow perfusion gradually filled from the peripheral area to the center of the hemangioma. Additionally, the visualization of tumor vessels, such as mosaic enhancement, was made possible by CPI. The clear depiction of tumor microvascular structures provides a clue for the diagnosis of liver metastasis.

In addition to consensus review by two readers from each group, we found that inter-reader agreement between the staff and resident radiologists for CEUS and CPI

Table 3 Inter-reader agreement of contrast enhancement ultrasound and color parametric imaging feature between staff and resident radiologists

Feature	Kappa value
CEUS	
Peripheral nodular enhancement	0.602 ± 0.142
Peripheral Rim-like enhancement	0.692 ± 0.127
Homogenous hyper-enhancement	0.835 ± 0.064
Heterogeneous enhancement	0.804 ± 0.132
CPI	
Peripheral nodular enhancement	0.885 ± 0.079
Peripheral rim-like enhancement	0.713 ± 0.177
Concentric circles enhancement	0.760 ± 0.112
Mosaic enhancement	0.803 ± 0.134

Data are mean ± SD. CEUS: Contrast enhancement ultrasound; CPI: Color parametric imaging.

imaging was good. With regard to CEUS features by staff and resident radiologists, the diagnostic consistency in homogenous hyperenhancement and heterogeneous enhancement was perfect (k = 0.835, k = 0.804), and the diagnostic consistency in peripheral nodular enhancement and rim-like enhancement was good (k = 0.602, k = 0.692). For CPI features by staff and resident radiologists, the diagnostic consistency in peripheral nodular enhancement and mosaic enhancement was perfect (k = 0.885, k = 0.803) and the diagnostic consistency in concentric circle enhancement and peripheral rim-like enhancement was good (k = 0.760, k = 0.713). These findings showed that CPI imaging could provide an objective tool to improve the learning curve.

This study has several limitations. First, the comparative analysis was from retrospective research. Second, the sample size was small to show the benefits in some of the subgroup analyses. Because patients with atypical CEUS patterns of hemangioma accounted for a small percentage of the regular patient population, only 20 cases were enrolled in this study during the 3-year period. Third, a score of 3 was classified as undetermined diagnosis or diagnosed errors, reducing the diagnostic performance of CEUS and CPI. Finally, the application of CPI requires specific hardware, and software standardization of the conditions of examination needs further improvement in the future.

In the present study, we used SonoVue as a contrast agent together with color parameter imaging of the liver lesion. Compared to CT imaging, low-MI CEUS has several advantages, including no ionizing radiation, real-time imaging and low cost[29,30]. However, multiple imaging modalities and referring to the results of laboratory examinations and needle biopsy are still required for final diagnosis when necessary.

In conclusion, compared with CEUS, CPI could provide specific information on the hemodynamic features of liver lesions and help to differentiate atypical hemangioma from liver metastases, for both staff and resident radiologists. CPI is useful especially for radiologists with less CEUS experience. It is anticipated that in the future, new methods of contrast ultrasonography will gain importance.

Table 4 Diagnostic performance of contrast enhancement ultrasound and color parametric imaging by staff and resident radiologists (%)

Criteria	Sensitivity	*P* value	Specificity	*P* value	Accuracy	*P* value	AUC	*P* value
Resident								
CEUS	55.0 (11/20)	0.456	45.5 (10/22)	0.030	50.0 (21/42)	0.006	0.757	0.036
CEUS+CPI	80.0 (16/20)		77.3 (17/22)		78.6 (33/42)		0.803	
Staff								
CEUS	65.0 (13/20)	0.144	54.5 (12/22)	0.112	54.8 (23/42)	0.010	0.825	0.013
CEUS+CPI	85.0 (17/20)		77.3 (17/22)		81.0 (34/42)		0.890	

CEUS: Contrast enhancement ultrasound; CPI: Color parametric imaging; AUC: Area under curve.

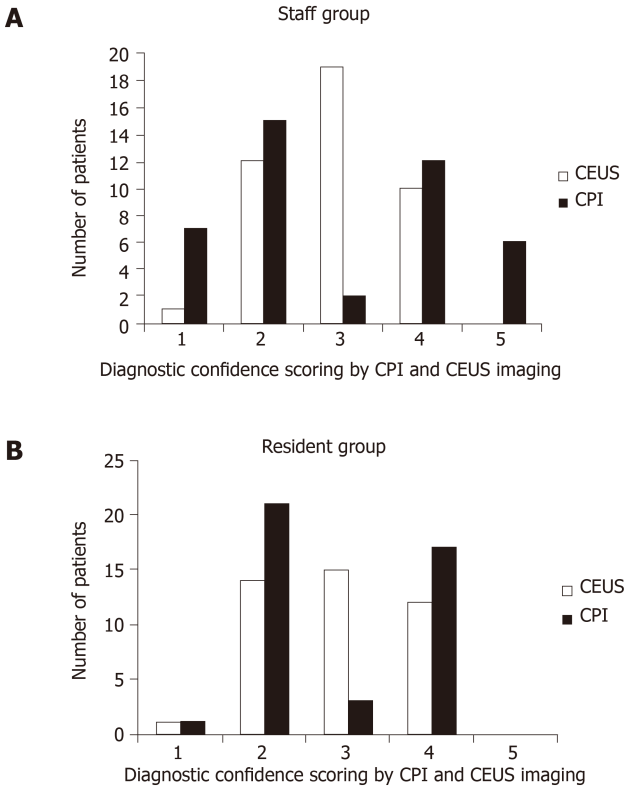

Figure 3 Diagnostic confidence of atypical hemangioma and liver metastasis by staff and resident radiologists. The number of 3-score (undetermined diagnosis) in contrast enhancement ultrasound was significantly higher than that in color parametric imaging in both staff group (A) and resident group (B). CEUS: Contrast enhancement ultrasound; CPI: Color parametric imaging.

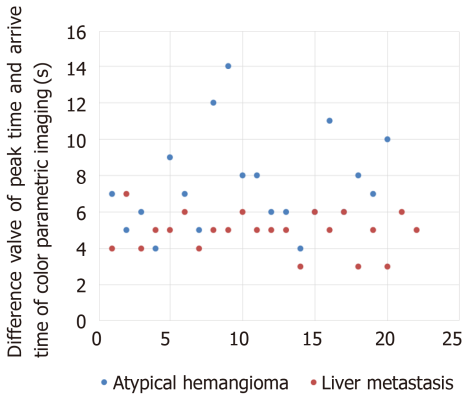

Figure 4 Spot diagram of AT in atypical hemangioma and liver metastasis. AT = Difference valve of peak time and arrival time of color parametric imaging of liver lesions. AT of atypical hemangioma was significantly longer than that of liver metastasis (8.31 ± 3.05 s *vs* 5.13 ± 0.99 s, $P < 0.001$).

ARTICLE HIGHLIGHTS

Research background

In clinical practice, the diagnosis is sometimes difficult with contrast-enhanced ultrasound (CEUS) when the case has an atypical perfusion pattern. Color parametric imaging (CPI) is an analysis software for CEUS with better detection of temporal differences in CEUS imaging using arbitrary colors. It measures the differences in arrival time of the contrast agent in lesions so that the perfusion features of atypical hemangioma and colorectal cancer liver metastasis can be distinguished.

Research motivations

The motivation of this study was to evaluate the role of CPI in the differential diagnosis of atypical hemangioma from liver metastases and the diagnostic performance by staff and resident radiologists. The patients with atypical hemangioma would be benefited by avoiding invasive test or even surgical resection. Furthermore, a junior radiologist can be more confident in the differential diagnosis of liver lesions by CPI.

Research objectives

To evaluate the role of a novel type of CPI of CEUS in the differential diagnosis of atypical hemangioma from liver metastases in patients with a history of colorectal cancer.

Research methods

All enrolled patients received ultrasound, CEUS and CPI examinations. Resident and staff radiologists independently and retrospectively reviewed CEUS and CPI images. Two sets of criteria were assigned: (1) Routine CEUS alone; and (2) CEUS and CPI. The diagnostic sensitivity, specificity, accuracy and receiver operating characteristic (ROC) curve of resident and staff radiologists were analyzed.

Research results

The following CPI features were significantly different between liver hemangioma and liver metastases analyzed by staff and resident radiologists: Peripheral nodular enhancement (65%-70.0% *vs* 4.5%-13.6%, $P < 0.001$, $P = 0.001$), mosaic/chaotic enhancement (5%-10% *vs* 68.2%-63.6%, $P < 0.001$, $P < 0.001$) and feeding artery (20% *vs* 59.1-54.5%, $P = 0.010$, $P = 0.021$). CPI imaging offered significant improvements in detection rates compared with routine CEUS signs in both resident and staff groups.

Research conclusions

CPI could provide specific information on the hemodynamic features of liver lesions and help to differentiate atypical hemangioma from liver metastases, for both staff and resident radiologists. CPI is useful especially for radiologists with less CEUS experience.

Research perspectives

In this study, a novel type of color contrast enhanced ultrasound provided supplemental information for differential diagnosis between atypical hemangioma and liver metastasis. This technique is safe and effective in clinical practice. However, to confirm the performance of this new imaging method, studies on a larger sample set are required.

ACKNOWLEDGEMENTS

We thank Dan Yan for her assistance with software technique.

REFERENCES

1 **Jang JY**, Kim MY, Jeong SW, Kim TY, Kim SU, Lee SH, Suk KT, Park SY, Woo HY, Kim SG, Heo J, Baik SK, Kim HS, Tak WY. Current consensus and guidelines of contrast enhanced ultrasound for the characterization of focal liver lesions. *Clin Mol Hepatol* 2013; **19**: 1-16 [PMID: 23593604 DOI: 10.3350/cmh.2013.19.1.1]

2 **D'Onofrio M**, Romanini L, Serra C, Magnolfi F, Bertolotto M, Quaia E, Puntel G, Colleoni A, Fiorini E, Cenci C, Santi E, Ciaravino V, Laffranchi F, Catalano O, Cantisani V, Calliada F, Derchi L. Contrast enhancement ultrasound application in focal liver lesions characterization: a retrospective study about guidelines application (SOCEUS-CEUS survey). *J Ultrasound* 2016; **19**: 99-106 [PMID: 27298641 DOI: 10.1007/s40477-015-0185-y]

3 **Fan ZH**, Chen MH, Dai Y, Wang YB, Yan K, Wu W, Yang W, Yin SS. Evaluation of primary malignancies of the liver using contrast-enhanced sonography: correlation with pathology. *AJR Am J Roentgenol* 2006; **186**: 1512-1519 [PMID: 16714638 DOI: 10.2214/AJR.05.0943]

4 **Fang L**, Zhu Z, Huang B, Ding H, Mao F, Li C, Zeng M, Zhou J, Wang L, Wang W, Chen Y. A comparative study of contrast enhanced ultrasound and contrast enhanced magnetic resonance imaging for the detection and characterization of hepatic hemangiomas. *Biosci Trends* 2015; **9**: 104-110 [PMID: 25971695 DOI: 10.5582/bst.2015.01026]

5 **Sirli R**, Sporea I, Săndulescu DL, Popescu A, Dănilă M, Săftoiu A, Spârchez Z, Badea R. Contrast enhanced ultrasound for the diagnosis of liver hemangiomas - results of a Romanian multicentre study. *Med Ultrason* 2015; **17**: 444-450 [PMID: 26649337 DOI: 10.11152/mu.2013.2066.174.csu]

6 **Dietrich CF**, Mertens JC, Braden B, Schuessler G, Ott M, Ignee A. Contrast-enhanced ultrasound of histologically proven liver hemangiomas. *Hepatology* 2007; **45**: 1139-1145 [PMID: 17464990 DOI: 10.1002/hep.21615]

7 **Jang H**, Kim TK, Lee JS, Sim JS, Kim EA. Hepatic hemangioma: typical and atypical appearances on various ultrasound imaging techniques. *Ultrasound Med Biol* 2003; **29**: 166-167 [DOI: 10.1016/s0301-5629(03)00664-1]

8 **Zviniene K**, Zaboriene I, Basevicius A, Jurkiene N, Barauskas G, Pundzius J. Comparative diagnostic value of contrast-enhanced ultrasonography, computed tomography, and magnetic resonance imaging in diagnosis of hepatic hemangiomas. *Medicina (Kaunas)* 2010; **46**: 329-335 [PMID: 20679748 DOI: 10.1159/000320314]

9 **Huang M**, Zhao Q, Chen F, You Q, Jiang T. Atypical appearance of hepatic hemangiomas with contrast-enhanced ultrasound. *Oncotarget* 2018; **9**: 12662-12670 [PMID: 29560099 DOI: 10.18632/oncotarget.24185]

10 **Giannetti A**, Franci L, Grechi C, Giangregorio F. Contrast-enhanced sonography in the diagnosis of hepatic hemangiomas: atypical appearance due to the washout of microbubbles. *J Clin Ultrasound* 2013; **41**: 361-365 [PMID: 22610668 DOI: 10.1002/jcu.21939]

11 **Shiozawa K**, Watanabe M, Takayama R, Kudo T, Maruyama K, Sumino Y. Hepatic parenchymal hemodynamics of cholangitis with portal trunk thrombus using contrast-enhanced ultrasonography with Sonazoid: delineation of so-called central and peripheral zonal differentiation by arrival-time parametric imaging. *J Med Ultrason (2001)* 2013; **40**: 73-76 [PMID: 27276930 DOI: 10.1007/s10396-012-0387-2]

12 **Watanabe M**, Shiozawa K, Takahashi M, Wakui N, Otsuka Y, Kaneko H, Tanikawa K, Shibuya K, Kamiyama N, Sumino Y. Parametric imaging using contrast-enhanced ultrasound with Sonazoid for hepatocellular carcinoma. *J Med Ultrason (2001)* 2010; **37**: 81-86 [PMID: 27277718 DOI: 10.1007/s10396-009-0254-y]

13 **Wakui N**, Takayama R, Kamiyama N, Kobayashi K, Matsui D, Matsukiyo Y, Kanekawa T, Ikehara T, Ishii K, Sumino Y. Arrival time parametric imaging using Sonazoid-enhanced ultrasonography is useful for the detection of spoke-wheel patterns of focal nodular hyperplasia smaller than 3 cm. *Exp Ther Med* 2013; **5**: 1551-1554 [PMID: 23837029 DOI: 10.3892/etm.2013.1048]

14 **Claudon M**, Dietrich CF, Choi BI, Cosgrove DO, Kudo M, Nolsøe CP, Piscaglia F, Wilson SR, Barr RG, Chammas MC, Chaubal NG, Chen MH, Clevert DA, Correas JM, Ding H, Forsberg F, Fowlkes JB, Gibson RN, Goldberg BB, Lassau N, Leen EL, Mattrey RF, Moriyasu F, Solbiati L, Weskott HP, Xu HX; World Federation for Ultrasound in Medicine; European Federation of Societies for Ultrasound. Guidelines and good clinical practice recommendations for Contrast Enhanced Ultrasound (CEUS) in the liver - update 2012: A WFUMB-EFSUMB initiative in cooperation with representatives of AFSUMB, AIUM, ASUM, FLAUS and ICUS. *Ultrasound Med Biol* 2013; **39**: 187-210 [PMID: 23137926 DOI: 10.1016/j.ultrasmedbio.2012.09.002]

15 **Dill-Macky MJ**, Burns PN, Khalili K, Wilson SR. Focal hepatic masses: enhancement patterns with SH U 508A and pulse-inversion US. *Radiology* 2002; **222**: 95-102 [PMID: 11756711 DOI: 10.1148/radiol.2221010092]

16 **Klibanov AL**. Microbubble contrast agents: targeted ultrasound imaging and ultrasound-assisted drug-delivery applications. *Invest Radiol* 2006; **41**: 354-362 [PMID: 16481920 DOI: 10.1097/01.rli.0000199292.88189.0f]

17 **Ta CN**, Kono Y, Eghtedari M, Oh YT, Robbin ML, Barr RG, Kummel AC, Mattrey RF. Focal Liver Lesions: Computer-aided Diagnosis by Using Contrast-enhanced US Cine Recordings. *Radiology* 2018; **286**: 1062-1071 [PMID: 29072980 DOI: 10.1148/radiol.2017170365]

18 **Quaia E**, Calliada F, Bertolotto M, Rossi S, Garioni L, Rosa L, Pozzi-Mucelli R. Characterization of focal liver lesions with contrast-specific US modes and a sulfur hexafluoride-filled microbubble contrast agent: diagnostic performance and confidence. *Radiology* 2004; **232**: 420-430 [PMID: 15286314 DOI: 10.1148/radiol.2322031401]

19 **Dai Y**, Chen MH, Yin SS, Yan K, Fan ZH, Wu W, Wang YB, Yang W. Focal liver lesions: can SonoVue-enhanced ultrasound be used to differentiate malignant from benign lesions? *Invest Radiol* 2007; **42**: 596-603 [PMID: 17620943 DOI: 10.1097/RLI.0b013e318050ab29]

20 **Huang-Wei C**, Bleuzen A, Bourlier P, Roumy J, Bouakaz A, Pourcelot L, Tranquart F. Differential diagnosis of focal nodular hyperplasia with quantitative parametric analysis in contrast-enhanced sonography. *Invest Radiol* 2006; **41**: 363-368 [PMID: 16481921 DOI: 10.1097/01.rli.0000195835.56589.55]

21 **Mandai M**, Koda M, Matono T, Nagahara T, Sugihara T, Ueki M, Ohyama K, Murawaki Y. Assessment of hepatocellular carcinoma by contrast-enhanced ultrasound with perfluorobutane microbubbles: comparison with dynamic CT. *Br J Radiol* 2011; **84**: 499-507 [PMID: 20959373 DOI: 10.1259/bjr/38682601]

22 **Ding H**, Wang WP, Huang BJ, Wei RX, He NA, Qi Q, Li CL. Imaging of focal liver lesions: low-mechanical-index real-time ultrasonography with SonoVue. *J Ultrasound Med* 2005; **24**: 285-297 [PMID: 15723841 DOI: 10.7863/jum.2005.24.3.285]

23 **Catalano O**, Nunziata A, Lobianco R, Siani A. Real-time harmonic contrast material-specific US of focal liver lesions. *Radiographics* 2005; **25**: 333-349 [PMID: 15798053 DOI: 10.1148/rg.252045066]

24 **Karhunen PJ**. Benign hepatic tumours and tumour like conditions in men. *J Clin Pathol* 1986; **39**: 183-188 [PMID: 3950039 DOI: 10.1136/jcp.39.2.183]

25 **Strobel D**, Seitz K, Blank W, Schuler A, Dietrich CF, von Herbay A, Friedrich-Rust M, Bernatik T. Tumor-specific vascularization pattern of liver metastasis, hepatocellular carcinoma, hemangioma and focal nodular hyperplasia in the differential diagnosis of 1,349 liver lesions in contrast-enhanced ultrasound (CEUS). *Ultraschall Med* 2009; **30**: 376-382 [PMID: 19688669 DOI: 10.1055/s-0028-1109672]

26 **Sugimoto K**, Moriyasu F, Kamiyama N, Metoki R, Iijima H. Parametric imaging of contrast ultrasound for the evaluation of neovascularization in liver tumors. *Hepatol Res* 2007; **37**: 464-472 [PMID: 17539818 DOI: 10.1111/j.1872-034X.2007.00060.x]

27 **Van Beers BE**, Daire JL, Garteiser P. New imaging techniques for liver diseases. *J Hepatol* 2015; **62**: 690-700 [PMID: 25457198 DOI: 10.1016/j.jhep.2014.10.014]

28 **Li W**, Wang W, Liu GJ, Chen LD, Wang Z, Huang Y, Liu JY, Xie XY, Lu MD. Differentiation of Atypical Hepatocellular Carcinoma from Focal Nodular Hyperplasia: Diagnostic Performance of Contrast-enhanced US and Microflow Imaging. *Radiology* 2015; **275**: 870-879 [PMID: 25584708 DOI: 10.1148/radiol.14140911]

29 **Sandrose SW**, Karstrup S, Gerke O, Rafaelsen S. Contrast Enhanced Ultrasound in CT-undetermined Focal Liver Lesions. *Ultrasound Int Open* 2016; **2**: E129-E135 [PMID: 28286878 DOI: 10.1055/s-0042-120272]
30 **Chung YE**, Kim KW. Contrast-enhanced ultrasonography: advance and current status in abdominal imaging. *Ultrasonography* 2015; **34**: 3-18 [PMID: 25342120 DOI: 10.14366/usg.14034]

World Journal of Gastroenterology

Submit a Manuscript: https://www.f6publishing.com

World J Gastroenterol 2020 March 7; 26(9): 973-983

DOI: 10.3748/wjg.v26.i9.973

ISSN 1007-9327 (print) ISSN 2219-2840 (online)

ORIGINAL ARTICLE

Retrospective Study

Effect and safety of mark-guided *vs* standard peroral endoscopic myotomy: A retrospective case control study

De-Feng Li, Feng Xiong, Zhi-Chao Yu, Hai-Yang Zhang, Ting-Ting Liu, Yan-Hui Tian, Rui-Yue Shi, Ming-Guang Lai, Yang Song, Zheng-Lei Xu, Ding-Guo Zhang, Jun Yao, Li-Sheng Wang

ORCID number: De-Feng Li (0000-0003-3118-6840); Feng Xiong (0000-0002-4021-0817); Zhi-Chao Yu (0000-0001-5123-9191); Hai-Yang Zhang (0000-0002-0899-827X); Ting-Ting Liu (0000-0002-1533-5220); Yan-Hui Tian (0000-0003-4671-2938); Rui-Yue Shi (0000-0001-9123-2103); Ming-Guang Lai (0000-0001-5432-0921); Yang Song (0000-0003-4124-9286); Zheng-Lei Xu (0000-0002-5413-7390); Ding-Guo Zhang (0000-0001-7728-9672); Jun Yao (0000-0002-3472-1602); Li-Sheng Wang (0000-0002-7418-6114).

Author contributions: Wang LS and Yao J were responsible for design of the study and reviewed the manuscript. Li DF and Xiong F drafted the manuscript. Li DF, Xiong F and Yu ZC abstracted data. Liu TT, Tian YH, Shi RY, Lai MG, Song Y, Xu ZL and Zhang DG performed the POEM. Yao J and Wang LS were responsible for revising manuscript. All authors have read and approved the final manuscript.

Supported by Natural Science Foundation of Guangdong Province, No. 2018A0303100024; Shenzhen Health Planning Commission, No. SZXJ2017030.

Institutional review board statement: The research was reviewed and approved by the Institutional review board of Shenzhen Municipal People's Hospital.

Informed consent statement: Patients were not required to give informed consent to the study

De-Feng Li, Feng Xiong, Zhi-Chao Yu, Hai-Yang Zhang, Ting-Ting Liu, Yan-Hui Tian, Rui-Yue Shi, Ming-Guang Lai, Yang Song, Zheng-Lei Xu, Ding-Guo Zhang, Jun Yao, Li-Sheng Wang, Department of Gastroenterology, the Second Clinical Medicine College (Shenzhen People's Hospital) of Jinan University, Shenzhen 518020, Guangdong Province, China

Corresponding author: Li-Sheng Wang, MD, Doctor, Department of Gastroenterology, the Second Clinical Medicine College (Shenzhen People's Hospital) of Jinan University, 1017 East Gate Road, Shenzhen 518020, Guangdong Province, China. wanglsszrmyy@163.com

Abstract

BACKGROUND

Peroral endoscopic myotomy (POEM) is a promising therapeutic modality for esophageal achalasia worldwide. However, clinical failure and adverse events of POEM have still been concerned.

AIM

To compare the efficacy and safety of a novel mark-guided POEM with standard POEM.

METHODS

A total of 133 patients with esophageal achalasia who underwent POEM from May 2013 to May 2019 were enrolled in this retrospective study. Of the 133 patients, there were 64 patients in the mark-guided POEM group and 69 patients in the standard POEM group. The clinical success, procedural duration and adverse events were compared between the two groups at 3 mo, 12 mo and 24 mo postoperatively.

RESULTS

Characteristic baseline was similar in the mark-guided POEM group and standard POEM group. The clinical success was comparable between the two groups, ranging from 92% to 98%, at 3 mo, 12 mo and 24 mo postoperatively (all $P > 0.5$). Eckart score, Gastroesophageal Reflux Disease Questionnaire score and SF-36 score were not different between the two groups after treatment (all $P > 0.05$). No severe adverse events occurred in the two groups. However, mark-guided POEM required shorter procedural duration, and less use of proton pump inhibitors and lower incidence of reflux symptoms than the standard POEM (all $P < 0.001$).

CONCLUSION

because the analysis used anonymous data that were obtained after each patient agreed to treatment by written consent.

Conflict-of-interest statement: The authors of this manuscript have no conflicts of interest to disclose.

Data sharing statement: No additional data are available.

Manuscript source: Unsolicited manuscript

Received: October 30, 2019
Peer-review started: October 30, 2019
First decision: December 12, 2019
Revised: January 9, 2020
Accepted: January 19, 2020
Article in press: January 19, 2020
Published online: March 7, 2020

P-Reviewer: Abdelfatah MM, Eleftheriadis N
S-Editor: Dou Y
L-Editor: MedE-Ma JY
E-Editor: Zhang YL

Mark-guided POEM and standard POEM were both effective and safe for the treatment of esophageal achalasia. However, the mark-guided POEM was characterized by shorter procedural duration, less use of proton pump inhibitors and lower incidence of reflux symptoms.

Key words: Mark-guided peroral endoscopic myotomy; Standard peroral endoscopic myotomy; Achalasia; Endoscopy; Efficacy; Adverse event

Core tip: Mark-guided Peroral endoscopic myotomy (POEM) can create full and large separation through sufficient sub-mucosal injection, which can improve the operative filed, decrease the incidence of bleeding, perforation and intra-procedural mucosal injury, and enhance the clinical success. By mark-guided POEM, it was not necessary to repeatedly pull out the tunnel to check the direction, thus saving the procedural time. Moreover, mark-guided POEM required less use of proton pump inhibitors and showed a lower incidence of reflux symptoms after the procedure.

Citation: Li DF, Xiong F, Yu ZC, Zhang HY, Liu TT, Tian YH, Shi RY, Lai MG, Song Y, Xu ZL, Zhang DG, Yao J, Wang LS. Effect and safety of mark-guided *vs* standard peroral endoscopic myotomy: A retrospective case control study. *World J Gastroenterol* 2020; 26(9): 973-983
URL: https://www.wjgnet.com/1007-9327/full/v26/i9/973.htm
DOI: https://dx.doi.org/10.3748/wjg.v26.i9.973

INTRODUCTION

As a rare esophageal motility disorder, esophageal achalasia is characterized by a failure of peristalsis in the esophageal body, leading to impaired lower esophageal sphincter relax and esophageal emptying[1,2]. The hampered passage of food from the esophagus to the stomach contributes to symptoms of dysphagia, regurgitation, chest pain and weight loss, as well as pulmonary complications[3,4].

Peroral endoscopic myotomy (POEM) was first described by Inoue *et al*[5] for achalasia treatment in 2010. Subsequently, it was demonstrated that POEM was effective and safe and has become the standard procedure for achalasia treatment worldwide[6-8]. Although several prospective studies have shown that POEM was superior in controlling symptoms of achalasia, POEM-associated clinical failure and adverse events have still been concerned[9-11]. The clinical success rate of POEM was reported to be more than 90%, however, reflux esophagitis which was the main adverse event developed in more than 40% of the patients after POEM treatment[12].

Several factors are associated with the efficacy and safety of POEM, such as mucosal injury, direction lossin the tunnel and oblique muscle damage[12,13]. Therefore, we here described a novel POEM procedure named mark-guided POEM, which may solve above-mentioned problems. We retrospectively compared the novel mark-guided POEM and standard POEM described by Inoue *et al*[5] in terms of clinical success, technical success and adverse events in our clinical center.

MATERIALS AND METHODS

From May 2013 to May 2019, patients diagnosed with achalasia based on Eckardt score, barium esophagography and high-resolution manometry (HRM) were retrospectively collected at the Department of Gastroenterology of the Second Clinical Medicine College (Shenzhen People's Hospital) of Jinan University (Guangdong, China). The patients who were lost to follow-up were excluded. Demographic and clinical data included patient's age, gender, disease duration, follow-up, procedural duration, clinical success, technical success, pre-operative and post-operative Eckardt score, post-operative length of stay, recurrence and adverse events (bleeding, perforation and reflux symptoms). A total of 133 patients who underwent POEM were included in this study. Of these patients, there were 64 patients in the mark-guided POEM group treated from September 2018 to May 2019 and 69 patients in the

standard POEM group treated from May 2013 to September 2018. The initial follow-up barium esophagography was conducted at 3 mo post-operatively. Subsequently, Eckardt score, Medical Outcomes Study 36-Item Short-Form Health Survey (SF-36), reflux symptoms and proton pump inhibitor (PPI) use were assessed *via* telephone at 3, 12 and 24 mo post-operatively (Figure 1). The study protocol was approved by Shenzhen People's Hospital Ethics Committee.

Definitions

Achalasia is divided into three distinct subtypes (type I, II and III) according to the pattern of esophageal contractility observed during high-resolution manometry (HRM) according to the Chicago Classification system[3]. Eckardt scores in 4-item questionnaire including dysphagia, regurgitation and chest pain ranging from 0 to 3 (0, none; 1, occasionally; 2, daily; 3, with every meal), and weight loss (0, no weight loss; 1, < 5 kg; 2, 5-10 kg; 3, > 10 kg) were used to evaluate the severity of achalasia, which were rated from the lowest severity (0 score) to the highest severity (12 scores)[14]. Clinical success was assessed using the Eckardt scores (≤ 3 scores), and failure of treatment was defined as Eckardt scores of more than 3 after treatment. The Gastroesophageal Reflux Disease Questionnaire (GERDQ) was used to assess reflux symptoms, including heartburn, regurgitation, epigastric pain, nausea, sleep disorder and use of over-the-counter drugs, and each of them was rated from 0 to 3 scores. Therefore, the total scores ranged from 0 to 18 points, and > 8 points was regarded as GERD[15]. SF-36 scoring system was composed of physical and mental components ranging from 0 to 100 scores, and higher scores indicated better quality of life[16]. Severe adverse events consisted of perforation and bleeding (defined as need of blood transfusion or endoscopy, radiologic and surgical intervention).

POEM procedure

Patients were fasted for 24 h before the procedure. POEM was performed under general anesthesia with endotracheal intubation and CO_2 insufflation. All participating endoscopists were experts, and standard POEM procedure in this study was in accordance with Inoue *et al*[5]. The steps of standard POEM were briefly described as follows. (1) At the middle of esophagus, a submucosal bleb was created by injecting saline containing 0.3% indigo carmine. Subsequently, a 2-cm longitudinal mucosal incision was made by Dual Knife (Olympus, Japan) to create submucosal tunnel using Endocut mode (30 W, effect 3) (ERBE, Germany); (2) A tunnel passing gastroesophageal junction (GEJ) 2-3 cm into proximal stomach was created by Dual Knife on the plane of dissection of submucosal layer; (3) Circular muscle bundle dissection was extended from 3 cm below the mucosal entry onto the proximal gastric cardia using Triangle Knife; and (4) Clips were placed close to the mucosal entity site (Anrei, China) (Video 1 standard peroral endoscopic myotomy procedure) through endoscopy. In the first step of mark-guided POEM, the middle of esophagus to gastric cardia at esophageal mucosal surface was marked using Dual Knife. Then, submucosal injection was administered through the mark with saline containing 0.3% indigo carmine. Next, submucosal layer dissection, circular muscle bundle dissection and closure of mucosal entity site were the same as standard POEM (Video 2 mark-guided peroral endoscopic myotomy procedure).

Postoperative management

All patients were given antibiotics (Cefatriaxone and Metronidazole) and a double-dose PPI (Omeprazole) intravenously at the day of the procedure and kept nothing by mouth (NPO) at the night of the procedure. The next day, a gastrografin esophagram was performed to rule out leakage and perforation. All patients with no evidence of adverse events were discharged, and they were advised to take soft food for 2 wk and PPI (Omeprazole, 20 mg, once a day) was prescribed for 2 wk.

Follow-up

All patients were followed up with barium esophagography at 3 mo post-operatively, and Eckart score, GERDQ score, SF-36 score, reflux symptoms and PPI use were also assessed *via* telephone at 12 mo and 24 mo post-operatively.

Outcomes

The primary outcome was clinical success, and the second outcome included procedure duration, severe adverse events, Eckart score, GERDQ score, SF-36 score, reflux symptoms and PPI use.

Statistical analysis

All analyses were performed using the SPSS 23.0 software package (SPSS Company, Chicago, IL, United States). All categorical variables were expressed as the frequency

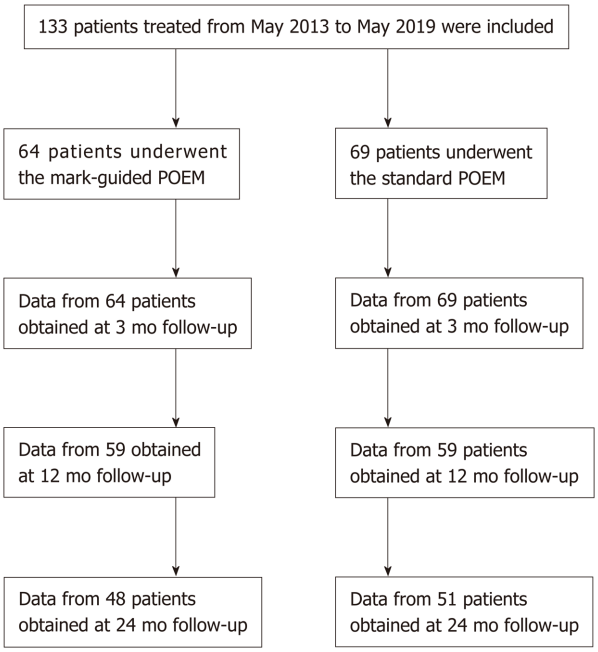

Figure 1 Flow chart.

with respective percentages. Continuous data were presented as mean ± SD or median (interquartile range) according to distribution. χ^2 test or Fisher's exact test was used to assess categorical variables, and unpaired *t*-test or Mann-Whitney test was used to assess continuous data. *P* values < 0.05 were considered statistically significant.

RESULTS

Patient characteristics

A total of 133 consecutive patients were included in this retrospective study. Of these patients, there were 64 patients in the mark-guided POEM group and 69 patients in the standard POEM group. There was no significant difference between the two groups in terms of sex, age, type of achalasia, disease duration, Eckardt score, esophageal height, esophageal diameter, HRM, GERDQ score and SF-36 score (Table 1).

Comparison of procedure-related parameters

Both groups successfully underwent POEM without any severe adverse events (perforation and bleeding) ($P = 1$). In addition, the hospital stay was not significantly different between the two groups ($P = 0.56$). However, the procedure duration was significantly shorter in the mark-guided POEM group compared with the standard POEM group ($P < 0.001$) (Table 1).

Primary outcome and second outcome at 3-mo follow-up

There were 64 and 69 patients in the mark-guided POEM group and standard POEM group at 3-mo follow-up, respectively. No significant difference was observed in the clinical success between the two groups (98.4% *vs* 98.6%, $P = 0.3$). Figure 2 shows that the pre-operative HRM and Eckart scores were significantly decreased compared with the post-operative values in both groups (Figure 2A-2D, all $P < 0.001$). Furthermore, the pre-operative SF-36 score was significantly improved compared with the postoperative value in both groups (Figure 2E, 2F, all $P < 0.001$). However, there was no significant difference between the two groups (Table 2). The post-operative height and diameter of barium esophagography were significantly decreased in both groups (Figure 3A-3D, all $P < 0.001$), whereas there was no significant difference between the two groups (Table 2). Moreover, the pre-operative GERDQ score was significantly decreased compared with its post-operative value in the standard POEM group ($P = 0.01$, Figure 3E), while such significant difference was not observed in the mark-guided POEM group ($P = 0.09$, Figure 3F). However, the incidence of reflux symptoms and PPI use were significantly different between mark-guided POEM and

Table 1 Baseline characteristics and comparison of procedurerelated parameters

Characteristics	Mark-guided POEM (*n* = 64)	Standard POEM (*n* = 69)	*P* value
Sex			
Male (*n*)	33 (51.6%)	36 (52.2%)	0.94
Female (*n*)	31 (48.4%)	33 (47.8%)	
Age (yr)	33.5 (28-48.75)	40 (30-47.75)	0.22
Achalasia Type			
I	21 (32.8%)	23 (33.3%)	0.98
II	36 (56.3%)	38 (55.1%)	
III	7 (10.9%)	8 (11.6%)	
Disease duration (mo)	32.5 (23-49.50)	33 (22.5-49.50)	0.95
Eckardt score	9.0 (8-9.75)	8.0 (7-9)	0.32
Barium esophagraphy			
Height (cm)	8 (8-9)	8 (7-9)	0.55
Diameter (cm)	5 (4-6)	5 (5-6)	0.29
HRM (mmHg)	38 (28-41)	38 (28-41.5)	0.64
GERDQ score	7 (6-9)	7 (6-8.5)	0.74
SF-36 score	47.22 ± 7.25	46.81 ± 7.60	0.75
Procedure duration (min)	40 (38-43)	49 (47-51)	< 0.001
Technical success (*n*)	64 (100%)	69 (100%)	1
Postoperative stay (d)	1 (1-2)	1 (1-2)	0.56
Perforation (*n*)	0	0	1
Bleeding (*n*)	0	0	1

POEM: Peroral endoscopic myotomy; HRM: High-resolution manometry; GERDQ: Gastroesophageal reflux disease questionnaire; SF-36: 36-Item Short-Form Health Survey.

standard POEM groups (10.9% *vs* 24.6%, $P = 0.04$; and 12.7% *vs* 27.5%, $P = 0.03$, respectively) (Table 2).

Primary outcome and second outcome at 12-mo follow-up

Table 3 shows that there were 59 patients in each group at 12-mo follow-up, and the clinical success was 93.5% (55/59) and 91.5% (54/59) in the mark-guided POEM group and standard POEM group, respectively, with no significant difference between the two groups ($P = 0.73$). Moreover, there was no significant difference between the two groups in terms of Eckart score, GERDQ score and SF-36 score ($P = 0.9$, $P = 0.67$ and $P = 0.94$, respectively). However, the incidence of reflux symptoms and PPI use was 16.9% and 18.6% in the mark-guided POEM group and 37.3% and 40.7% in the standard POEM group, respectively ($P = 0.01$ and $P = 0.009$).

Primary outcome and second outcome at 24-mo follow-up

There were 48 patients in the mark-guided POEM group and 51 patients in the standard POEM group at 24-mo follow-up. The results showed that there was no significant difference in clinical success between the mark-guided POEM group and standard POEM group (92.7% *vs* 92.2%, $P = 0.93$). Furthermore, there was no significant difference between the two groups in terms of Eckart score, GERDQ score and SF-36 score ($P = 0.92$, $P = 0.74$ and $P = 0.73$, respectively), whereas the incidence of reflux symptoms and PPI use were significantly lower in the mark-guided POEM group compared with the standard POEM group (27.1% *vs* 47.1%, $P = 0.04$ and 29.2% *vs* 51%, $P = 0.02$) (Table 4).

Unsuccessful treatment analysis

Nine and 10 patients with unsuccessful treatment in the mark-guided POEM group and standard POEM group, respectively, were all symptomatic (Eckart score > 3). Of the nine patients in the mark-guided POEM group, five patients required re-treatment and recovered uneventfully, whereas the other four patients refused additional treatments because of symptom improvement. Of the 10 patients in the standard POEM group, six patients successfully underwent re-treatment of POEM, while the other four patients refused additional re-treatment.

Table 2 Primary and secondary outcomes in patients at 3 mo follow-up

	Mark-guided POEM (*n* = 64)	Standard POEM (*n* = 69)	*P* value
Overall clinical success (*n*)	63 (98.4%)	68 (98.6%)	0.3
Eckart score	1 (1-2)	1 (1-2)	0.78
GERDQ score	6 (5-9)	6 (5-7)	0.35
SF-36 score	78 (76-80)	78 (75-80.5)	0.87
Barium esophagraphy			
Height (cm)	3 (2-4)	3 (2-4)	0.94
Diameter (cm)	2 (2-2.5)	2 (2-2.75)	0.86
HRM (mmHg)	12.2 ± 2.37	12.06 ± 1.93	0.7
Reflux symptom (*n*)			
Yes	7 (10.9%)	17 (24.6%)	0.04
No	57 (89.1%)	52(75.4%)	
PPI use (*n*)			
Yes	8 (12.7%)	19 (27.5%)	0.03
No	56 (87.3%)	60 (72.5%)	

POEM: Peroral endoscopic myotomy; HRM: High-resolution manometry; GERDQ: Gastroesophageal reflux disease questionnaire; SF-36: 36-Item Short-Form Health Survey; PPI: Proton pump inhibitor.

DISCUSSION

In this retrospective study, we compared the mark-guided POEM with standard POEM in terms of the clinical success, procedure duration, adverse events, reflux symptoms and PPI use at 3-mo, 12-mo and 24-mo follow-up. The results showed that the overall clinical success, hospital stay and severe adverse events were not significantly different between the two groups. However, the procedural duration, and incidence of reflux symptoms and PPI use were significantly lower in the mark-guided POEM group compared with the standard POEM group.

In the present study, we found that the clinical success ranged from 92.7% to 98.4% and 92.2% to 98.6% at 3-mo follow-up and 24-mo follow-up, respectively, in the mark-guided POEM group and standard POEM group, which was similar to a previous meta-analysis[17]. Moreover, there was no severe adverse event (perforation and bleeding) in the patients in this study. However, a previous study has shown that the overall rate of adverse events is 7.5%, and severe adverse events only occur in 90 cases of 1800 POEM procedures[18]. Our results indicated that the clinical success could be decreased with time in both groups, which was consistent with previous data that the recurrence rate after POEM can be increased with time[19,20]. However, POEM re-treatment was also effective for the recurrent patients, and some of them refused additional treatment because of symptom improvement. Therefore, both the mark-guided and standard POEM was effective for achalasia. Interestingly, we found that the mark-guided POEM showed a lower incidence of reflux symptoms and less PPI use compared with standard POEM, which wasmarkedly lower compared with the previous study as well[6]. Ponds *et al*[10] have demonstrated that the reflux esophagitis rate is 49%, and 8% are severe cases on endoscopy examination at 1-year follow-up after POEM treatment, which is markedly higher compared with the mark-guided POEM in the present study. Furthermore, Shiwaku *et al*[21] have found that the erosive esophagitis (Los Angeles grade A-D) and severe erosive esophagitis (Los Angeles grade C-D) account for 63% and 6.2%, respectively, whereas, symptomatic GERD is only observed in 14.8% of 1300 patients at 6-mo follow-up after POEM. Therefore, the erosive esophagitis might be more in this study. Fortunately, many studies including our current study have shown that reflux symptoms respond to treatment with a PPI[10,21].

To the best of our knowledge, we, for the first time, compared the mark-guided POEM with standard POEM. In addition to less procedure duration, and lower incidence of reflux symptoms and PPI use in the mark-guided POEM, there was no significant difference between the two groups. We considered that the mark-guided POEM had the following advantages: First, it could create full and large separation through sufficient sub-mucosal injection, which could improve operative filed, decrease the incidence of bleeding, perforation and intra-procedural mucosal injury, and increase the clinical success. Liu *et al*[22] have shown that intra-procedural mucosal injury is a risk factor for clinical failure. Second, it was not necessary to repeatedly

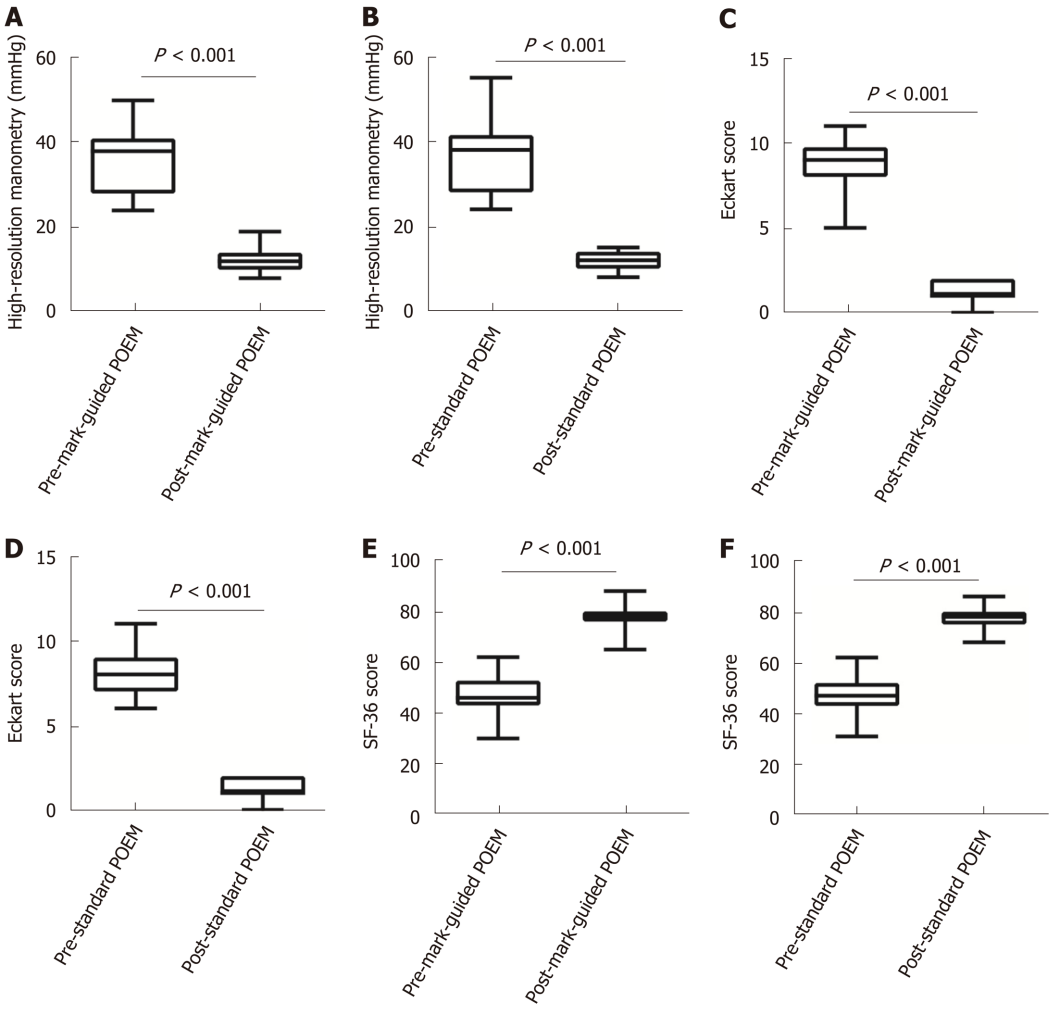

Figure 2 High-resolution manometry, Eckart score and 36-Item Short-Form Health Survey scores at 3-mo follow-up in the mark-guided peroral endoscopic myotomy group and standard peroral endoscopic myotomy group. A-D: The pre-operative high-resolution manometry and Eckart scores were significantly decreased compared with the postoperative values in the two groups (all $P < 0.001$); E, F: The pre-operative 36-Item Short-Form Health Survey scores were significantly improved compared with the postoperative values in both groups (all $P < 0.001$).

pull out the tunnel to check the direction, thus saving much operating time.

There are several limitations in this study. First, this was a retrospective study from a single tertiary hospital, and the results need to be confirmed by multi-centers randomized controlled trials. Second, the Eckardt score was used to determine clinical success. However, its construct validity has recently been questioned[23]. Third, GERDQ has limitations to identify reflux symptoms or GERD after POEM. Fourth, patients were followed up at 3, 12 and 24 mo *via* telephone, and long-term conclusion is unavailable.

In summary, this retrospective study confirmed that the mark-guided POEM and standard POEM were both effective and safe for esophageal achalasia. However, the mark-guided POEM required less procedural duration and showed a lower incidence of reflux symptoms and PPI use compared with the standard POEM.

Table 3 Primary and secondary outcomes in patients at 12 mo follow-up

	Mark-guided POEM (*n* = 59)	Standard POEM (*n* = 59)	*P* value
Overall clinical success (*n*)	55 (93.2%)	54 (91.5%)	0.73
Eckart score	1 (1-2)	1 (1-2)	0.9
GERDQ score	7 (6-9)	6 (6-9)	0.67
SF-36 score	75 (67-78)	74 (70-78)	0.94
Reflux symptom (*n*)			
Yes	10 (16.9%)	22 (37.3%)	0.01
No	49 (83.1%)	37 (62.7%)	
PPI use (*n*)			
Yes	11 (18.6%)	24 (40.7%)	0.009
No	48 (81.4%)	35 (59.3%)	

POEM: Peroral endoscopic myotomy; GERDQ: Gastroesophageal reflux disease questionnaire; SF-36: 36-Item Short-Form Health Survey; PPI: Proton pump inhibitor.

Table 4 Primary and secondary outcomes in patients at 24 mo follow-up

	Mark-guided POEM (*n* = 48)	Standard POEM (*n* = 51)	*P* value
Overall clinical success (*n*)	44 (92.7%)	47 (92.2%)	0.93
Eckart score	1 (1-2)	1 (1-2)	0.92
GERDQ score	7 (6-9)	7 (6-9)	0.74
SF-36 score	77 (71-80)	76 (72-80)	0.73
Reflux symptom (*n*)			
Yes	13 (27.1%)	24(47.1%)	0.04
No	35(72.9%)	27 (52.9%)	
PPI use (*n*)			
Yes	14 (29.2%)	26 (51%)	0.02
No	34 (70.8%)	25 (49%)	

POEM: Peroral endoscopic myotomy; GERDQ: Gastroesophageal reflux disease questionnaire; SF-36: 36-Item Short-Form Health Survey; PPI: Proton pump inhibitor.

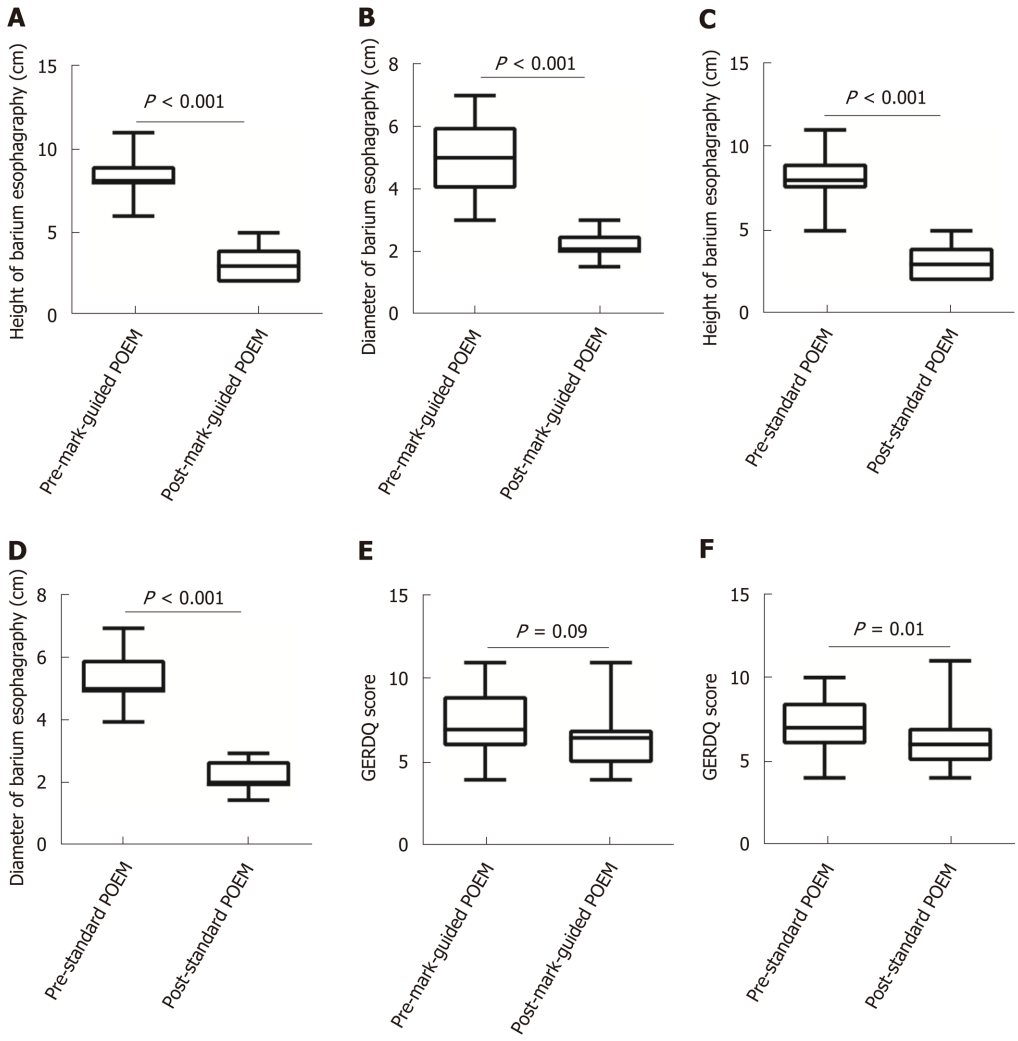

Figure 3 Barium esophagography at 3-mo follow-up in the mark-guided peroral endoscopic myotomy group and standard peroral endoscopic myotomy group. A-D: The post-operative height and diameter of barium esophagography were significantly decreased compared with the pre-operative values in the two groups (all $P < 0.001$); E: The pre-operative Gastroesophageal reflux disease questionnaire score was significantly decreased compared with the post-operative value in the standard peroral endoscopic myotomy group ($P = 0.01$); F: No significant difference was observed between pre-operative and post-operative values in the mark-guided peroral endoscopic myotomy group ($P = 0.09$).

ARTICLE HIGHLIGHTS

Research background

Peroral endoscopic myotomy (POEM) was first described by a study on achalasia treatment in 2010. Subsequently, it was demonstrated that POEM was effective and safe and has become the standard procedure for achalasia worldwide. However, clinical failure and adverse events of POEM have still been concerned. Indeed, POEM procedure can lead to a high incidence of reflux esophagitis.

Research motivation

Several factors are associated with the efficacy and safety of POEM, such as sufficient sub-mucosal injection, limiting mucosal injury and constructing sub-mucosal tunnel straightly. Therefore, we described a novel POEM procedure named mark-guided POEM, which may solve afore-mentioned problems.

Research objectives

This study aimed to compare the efficacy and safety of the novel mark-guided POEM with standard POEM in the improvement of efficacy and safety of achalasia treatment. This retrospective case control study will encourage us to explore the efficacy and safety of the mark-guided POEM for further research, such as multi-centers randomized controlled trials.

Research methods

This retrospective case control study compared the efficacy and safety between the mark-guided POEM and standard POEM.

Research results
This study showed that mark-guided POEM and standard POEM were both effective and safe for achalasia treatment, however, the mark-guided POEM seemed to require less procedural duration and proton pump inhibitor (PPI) use and show a lower incidence of reflux symptoms. However, these results will be confirmed by randomized controlled trials.

Research conclusions
POEM is a promising therapeutic procedure for esophageal achalasia worldwide. However, clinical failure and adverse events of POEM have still been concerned. In order to improve efficacy and safety of achalasia treatment, we described a novel POEM procedure named the mark-guided POEM. We retrospectively compared the efficacy and safety of the mark-guided POEM with standard POEM. The results showed that the clinical success was comparable between the two groups, ranging from 92% to 98%, at 3 mo, 12 mo and 24 mo postoperatively. However, the mark-guided POEM required less procedural duration, less use of PPI and lower incidence of reflux symptoms than the standard POEM. We will conduct multi-centers randomized controlled trial to confirm these results.

Research perspectives
The mark-guided POEM may be superior to standard POEM for achalasia treatment; however, the findings need to be further confirmed using multi-centers randomized controlled trials.

REFERENCES

1 **Richter JE**. Achalasia - an update. *J Neurogastroenterol Motil* 2010; **16**: 232-242 [PMID: 20680161 DOI: 10.5056/jnm.2010.16.3.232]
2 **Sadowski DC**, Ackah F, Jiang B, Svenson LW. Achalasia: incidence, prevalence and survival. A population-based study. *Neurogastroenterol Motil* 2010; **22**: e256-e261 [PMID: 20465592 DOI: 10.1111/j.1365-2982.2010.01511.x]
3 **Boeckxstaens GE**, Zaninotto G, Richter JE. Achalasia. *Lancet* 2014; **383**: 83-93 [PMID: 23871090 DOI: 10.1016/S0140-6736(13)60651-0]
4 **Boeckxstaens GE**. The lower oesophageal sphincter. *Neurogastroenterol Motil* 2005; **17** Suppl 1: 13-21 [PMID: 15836451 DOI: 10.1111/j.1365-2982.2005.00661.x]
5 **Inoue H**, Minami H, Kobayashi Y, Sato Y, Kaga M, Suzuki M, Satodate H, Odaka N, Itoh H, Kudo S. Peroral endoscopic myotomy (POEM) for esophageal achalasia. *Endoscopy* 2010; **42**: 265-271 [PMID: 20354937 DOI: 10.1055/s-0029-1244080]
6 **Kahrilas PJ**, Katzka D, Richter JE. Clinical Practice Update: The Use of Per-Oral Endoscopic Myotomy in Achalasia: Expert Review and Best Practice Advice From the AGA Institute. *Gastroenterology* 2017; **153**: 1205-1211 [PMID: 28989059 DOI: 10.1053/j.gastro.2017.10.001]
7 **Benias PC**, Korrapati P, Raphael KL, D'Souza LS, Inamdar S, Trindade AJ, Lee C, Kumbhari V, Sejpal DV, Okolo P, Khashab MA, Miller L, Carr-Locke D. Safety and feasibility of performing peroral endoscopic myotomy as an outpatient procedure with same-day discharge. *Gastrointest Endosc* 2019; **90**: 570-578 [PMID: 31078571 DOI: 10.1016/j.gie.2019.04.247]
8 **Liu Z**, Wang Y, Fang Y, Huang Y, Yang H, Ren X, Xu M, Chen S, Chen W, Zhong Y, Zhang Y, Qin W, Hu J, Cai M, Yao L, Li Q, Zhou P. Short-term safety and efficacy of peroral endoscopic myotomy for the treatment of achalasia in children. *J Gastroenterol* 2019 [PMID: 31679066 DOI: 10.1007/s00535-019-01607-4]
9 **Werner YB**, Hakanson B, Martinek J, Repici A, von Rahden BHA, Bredenoord AJ, Bisschops R, Messmann H, Vollberg MC, Noder T, Kersten JF, Mann O, Izbicki J, Pazdro A, Fumagalli U, Rosati R, Germer CT, Schijven MP, Emmermann A, von Renteln D, Fockens P, Boeckxstaens G, Rösch T. Endoscopic or Surgical Myotomy in Patients with Idiopathic Achalasia. *N Engl J Med* 2019; **381**: 2219-2229 [PMID: 31800987 DOI: 10.1056/NEJMoa1905380]
10 **Ponds FA**, Fockens P, Lei A, Neuhaus H, Beyna T, Kandler J, Frieling T, Chiu PWY, Wu JCY, Wong VWY, Costamagna G, Familiari P, Kahrilas PJ, Pandolfino JE, Smout AJPM, Bredenoord AJ. Effect of Peroral Endoscopic Myotomy vs Pneumatic Dilation on Symptom Severity and Treatment Outcomes Among Treatment-Naive Patients With Achalasia: A Randomized Clinical Trial. *JAMA* 2019; **322**: 134-144 [PMID: 31287522 DOI: 10.1001/jama.2019.8859]
11 **Shiwaku H**, Inoue H, Sato H, Onimaru M, Minami H, Tanaka S, Sato C, Ogawa R, Okushima N, Yokomichi H. Peroral endoscopic myotomy for achalasia: a prospective multicenter study in Japan. *Gastrointest Endosc* 2019 [PMID: 31759035 DOI: 10.1016/j.gie.2019.11.020]
12 **Khashab MA**, Vela MF, Thosani N, Agrawal D, Buxbaum JL, Abbas Fehmi SM, Fishman DS, Gurudu SR, Jamil LH, Jue TL, Bijun Sai Kannadath, Law JK, Lee JK, Naveed M, Qumseya BJ, Sawhney MS, Yang J, Wani S. ASGE guideline on the management of achalasia. *Gastrointest Endosc* 2019 [PMID: 31839408 DOI: 10.1016/j.gie.2019.04.231]
13 **Chiu PW**, Inoue H, Rösch T. From POEM to POET: Applications and perspectives for submucosal tunnel endoscopy. *Endoscopy* 2016; **48**: 1134-1142 [PMID: 27855465 DOI: 10.1055/s-0042-119395]
14 **Perbtani YB**, Mramba LK, Yang D, Suarez J, Draganov PV. Life after per-oral endoscopic myotomy: long-term outcomes of quality of life and their association with Eckardt scores. *Gastrointest Endosc* 2018; **87**: 1415-1420.e1 [PMID: 29410304 DOI: 10.1016/j.gie.2018.01.019]
15 **Wang M**, Zhang JZ, Kang XJ, Li L, Huang XL, Aihemaijiang K, Ayinuer A, Li YX, He XL, Gao F. Relevance between GerdQ score and the severity of reflux esophagitis in Uygur and Han Chinese. *Oncotarget* 2017; **8**: 74371-74377 [PMID: 29088793 DOI: 10.18632/oncotarget.20146]
16 **Vigneswaran Y**, Tanaka R, Gitelis M, Carbray J, Ujiki MB. Quality of life assessment after peroral endoscopic myotomy. *Surg Endosc* 2015; **29**: 1198-1202 [PMID: 25249144 DOI: 10.1007/s00464-014-3793-2]
17 **Lee Y**, Brar K, Doumouras AG, Hong D. Peroral endoscopic myotomy (POEM) for the treatment of pediatric achalasia: a systematic review and meta-analysis. *Surg Endosc* 2019; **33**: 1710-1720 [PMID: 30767141 DOI: 10.1007/s00464-019-06701-5]

18 **Haito-Chavez Y**, Inoue H, Beard KW, Draganov PV, Ujiki M, Rahden BHA, Desai PN, Pioche M, Hayee B, Haji A, Saxena P, Reavis K, Onimaru M, Balassone V, Nakamura J, Hata Y, Yang D, Pannu D, Abbas A, Perbtani YB, Patel LY, Filser J, Roman S, Rivory J, Mion F, Ponchon T, Perretta S, Wong V, Maselli R, Ngamruengphong S, Chen YI, Bukhari M, Hajiyeva G, Ismail A, Pieratti R, Kumbhari V, Galdos-Cardenas G, Repici A, Khashab MA. Comprehensive Analysis of Adverse Events Associated With Per Oral Endoscopic Myotomy in 1826 Patients: An International Multicenter Study. *Am J Gastroenterol* 2017; **112**: 1267-1276 [PMID: 28534521 DOI: 10.1038/ajg.2017.139]

19 **Von Renteln D**, Fuchs KH, Fockens P, Bauerfeind P, Vassiliou MC, Werner YB, Fried G, Breithaupt W, Heinrich H, Bredenoord AJ, Kersten JF, Verlaan T, Trevisonno M, Rösch T. Peroral endoscopic myotomy for the treatment of achalasia: an international prospective multicenter study. *Gastroenterology* 2013; **145**: 309-11.e1-3 [PMID: 23665071 DOI: 10.1053/j.gastro.2013.04.057]

20 **Werner YB**, Costamagna G, Swanström LL, von Renteln D, Familiari P, Sharata AM, Noder T, Schachschal G, Kersten JF, Rösch T. Clinical response to peroral endoscopic myotomy in patients with idiopathic achalasia at a minimum follow-up of 2 years. *Gut* 2016; **65**: 899-906 [PMID: 25934759 DOI: 10.1136/gutjnl-2014-308649]

21 **Shiwaku H**, Inoue H, Onimaru M, Minami H, Sato H, Sato C, Tanaka S, Ogawa R, Okushima N. Multicenter collaborative retrospective evaluation of peroral endoscopic myotomy for esophageal achalasia: analysis of data from more than 1300 patients at eight facilities in Japan. *Surg Endosc* 2020; **34**: 464-468 [PMID: 31183791 DOI: 10.1007/s00464-019-06833-8]

22 **Liu XY**, Cheng J, Chen WF, Liu ZQ, Wang Y, Xu MD, Chen SY, Zhong YS, Zhang YQ, Yao LQ, Zhou PH, Li QL. A risk-scoring system to predict clinical failure for patients with achalasia after peroral endoscopic myotomy. *Gastrointest Endosc* 2020; **91**: 33-40.e1 [PMID: 31421076 DOI: 10.1016/j.gie.2019.07.036]

23 **Taft TH**, Carlson DA, Triggs J, Craft J, Starkey K, Yadlapati R, Gregory D, Pandolfino JE. Evaluating the reliability and construct validity of the Eckardt symptom score as a measure of achalasia severity. *Neurogastroenterol Motil* 2018; **30**: e13287 [PMID: 29315993 DOI: 10.1111/nmo.13287]

World Journal of Gastroenterology

Submit a Manuscript: https://www.f6publishing.com

World J Gastroenterol 2020 March 7; 26(9): 984-991

DOI: 10.3748/wjg.v26.i9.984

ISSN 1007-9327 (print) ISSN 2219-2840 (online)

CASE REPORT

Two case reports of novel syndrome of bizarre performance of gastrointestinal endoscopy due to toxic encephalopathy of endoscopists among 181767 endoscopies in a 13-year-university hospital review: Endoscopists, first do no harm!

Mitchell S Cappell

ORCID number: Mitchell S Cappell (0000-0003-3445-5428).

Author contributions: Cappell MS designed the research, performed the research, analyzed the data, and wrote the paper.

Informed consent statement: Informed written consent was obtained from the patients for publication of this report and accompanying images.

Conflict-of-interest statement: None. Dr. Cappell, as a consultant of the United States Food and Drug Administration (FDA) Advisory Committee for Gastrointestinal Drugs, affirms that this paper does not discuss any proprietary confidential pharmaceutical data submitted to the FDA and reviewed by Dr. Cappell. Dr. Cappell was until 2 years ago a member of the speaker's bureau for AstraZeneca and Daiichi Sankyo, co-marketers of Movantik. Dr. Cappell has had one-time consultancies for Mallinckrodt and Shire > 1 year ago. This work does not discuss any drug manufactured or marketed by AstraZeneca, Daiichi Sankyo, Shire, or Mallinckrodt.

CARE Checklist (2016) statement: The author has read the CARE Checklist (2016), and the manuscript was prepared and revised according to the CARE Checklist (2016).

Mitchell S Cappell, Division of Gastroenterology & Hepatology, William Beaumont Hospital, Royal Oak, MI 48073, United States

Mitchell S Cappell, Oakland University William Beaumont School of Medicine, Royal Oak, MI 48073, United States

Corresponding author: Mitchell S Cappell, MD, PhD, Professor, Division of Gastroenterology and Hepatology, William Beaumont Hospital, MOB Suite 602, Thirteen Mile Rd, Royal Oak, MI 48073, United States. mitchell.cappell@beaumont.edu

Abstract

BACKGROUND

Although deficient procedures performed by impaired physicians have been reported for many specialists, such as surgeons and anesthesiologists, systematic literature review failed to reveal any reported cases of deficient endoscopies performed by gastroenterologists due to toxic encephalopathy. Yet gastroenterologists, like any individual, can rarely suffer acute-changes-in-mental-status from medical disorders, and these disorders may first manifest while performing gastrointestinal endoscopy because endoscopy comprises so much of their workday.

CASE SUMMARIES

Among 181767 endoscopies performed by gastroenterologists at William-Beaumont-Hospital at Royal-Oak, two endoscopies were performed by normally highly qualified endoscopists who manifested bizarre endoscopic interpretation and technique during these endoscopies due to toxic encephalopathy. Case-1-endoscopist repeatedly insisted that gastric polyps were colonic polyps, and absurdly "pressed" endoscopic steering dials to "take" endoscopic photographs; Case-2-endoscopist repeatedly insisted that had intubated duodenum when intubating antrum, and wildly turned steering dials and bumped endoscopic tip forcefully against antral wall. Endoscopy nurses recognized endoscopists as impaired and informed endoscopy-unit-nurse-manager. She called Chief-of-Gastroenterology who advised endoscopists to terminate their esophagogastroduodenoscopies (fulfilling ethical imperative of "physician, first-do-no-harm"), and go to emergency room for medical evaluation. Both endoscopists complied. In-hospital-work-up revealed toxic encephalopathy in

Manuscript source: Invited manuscript

Received: October 16, 2019
Peer-review started: October 16, 2019
First decision: November 22, 2019
Revised: December 4, 2019
Accepted: February 21, 2020
Article in press: February 21, 2020
Published online: March 7, 2020

P-Reviewer: Dutta A, Efthymiou A, Dinç T
S-Editor: Wang YQ
L-Editor: A
E-Editor: Ma YJ

both from: case-1-urosepsis and left-ureteral-impacted-nephrolithiasis; and case-2-dehydration and accidental ingestion of suspected illicit drug given by unidentified stranger. Endoscopists rapidly recovered with medical therapy.

CONCLUSION
This rare syndrome (0.0011% of endoscopies) may manifest abruptly as bizarre endoscopic interpretation and technique due to impairment of endoscopists by toxic encephalopathy. Recommended management (followed in both cases): 1-recognize incident as medical emergency demanding immediate action to prevent iatrogenic patient injury; 2- inform Chief-of-Gastroenterology; and 3-immediately intervene to abort endoscopy to protect patient. Syndromic features require further study.

Key words: Endoscopy; Iatrogenic injury; Medical ethics; Hippocratic Oath; Quality improvement; Medical malpractice; Morbidity and mortality

Core tip: Two novel cases are reported of impaired endoscopists manifesting bizarre-endoscopic-interpretation-and-technique due to toxic encephalopathy among 181767 endoscopies performed at William-Beaumont-Hospital-Royal-Oak. Case-1-endoscopist repeatedly insisted that gastric polyps were colonic polyps, and absurdly "pressed" endoscopic steering dials to photograph gastric lesions. Case-2-endoscopist repeatedly insisted that had intubated duodenum when intubating antrum, and erratically turned steering dials and bumped endoscopic tip against antral wall. Endoscopists were advised to terminate their esophagogastroduodenoscopies, fulfilling ethical imperative: "physician-first-do-no-harm". In-hospital-work-up revealed toxic encephalopathies from urosepsis, or inadvertently ingesting "illicit drug". Both endoscopists rapidly recovered with medical therapy. These potential-medical-emergencies require aborting endoscopy to prevent iatrogenic patient injury.

Citation: Cappell MS. Two case reports of novel syndrome of bizarre performance of gastrointestinal endoscopy due to toxic encephalopathy of endoscopists among 181767 endoscopies in a 13-year-university hospital review: Endoscopists, first do no harm! *World J Gastroenterol* 2020; 26(9): 984-991
URL: https://www.wjgnet.com/1007-9327/full/v26/i9/984.htm
DOI: https://dx.doi.org/10.3748/wjg.v26.i9.984

INTRODUCTION

Gastroenterologists (GIs), like any individual, can suffer acute-changes-in-mental-status from medical disorders, and these medical disorders may rarely first manifest while performing gastrointestinal (GI) endoscopy because endoscopy comprises so much of their workday. Review of 181767 GI endoscopies performed by GIs at a large university teaching hospital revealed 2 cases (0.0011%) of acute-change-in-mental-status by GIs first manifesting during endoscopy, as reported herein. This novel work reports syndromic features, including nature of bizarre endoscopic performance, health professionals who reported incidents, and medical causes of transient impairment; recommends chain-of-command to manage medical crises; and emphasizes the need to immediately abort endoscopy to prevent iatrogenic patient injury (fulfilling ethical imperative of Hippocratic Oath, "Physician, first do no harm!")[1].

Methods

Dr. Cappell prospectively intervened administratively during both incidents, and was involved soon thereafter in investigating the incidents for quality assurance as Chief-of-Gastroenterology (GI), November 2006-September 2019, at William Beaumont Hospital, Royal Oak, a large university hospital of Oakland University William Beaumont School of Medicine. Computerized search of all outpatient and inpatient esophagogastroduodenoscopies (EGDs), sigmoidoscopies, and colonoscopies performed in hospital endoscopy unit by GIs using Provations (800 Washington

Avenue North, Minneapolis, MN 555401), a computerized endoscopy reporting system (using terms "abort", "aborted", "incomplete", "stop", "stopped", "terminate", "terminated", "impaired", or "unsatisfactory" [endoscopy /endoscopist]), did not reveal any more aborted endoscopies because of impaired endoscopists. Study excluded surgeons performing GI endoscopy because Chief-of-GI lacked prospective knowledge of such incidents due to a separate quality assurance pathway. This study was exempted/approved by the William Beaumont Hospital Institutional Review Board on 9/4/19. Dr. Cappell claims expertise in quality assurance based on professional experience as senior GI administrator (1995-2019) at the five following teaching hospitals (with medical residencies and GI fellowships): Maimonides Hospital, Brooklyn, NY; Woodhull Hospital, Brooklyn, NY; Saint Barnabas Hospital, Bronx, NY; Albert Einstein Hospital, Philadelphia, PA; and William Beaumont Hospital, Royal Oak, MI.

Literature related to impaired endoscopists at endoscopy was systematically searched using Pubmed and Ovid with the following terms ["incapacitated" or "impaired" or "incompetent"] AND ["gastroenterologist" or "endoscopist" or "surgeon" or "physician" or "doctor"]. Abstracts of all identified publications were reviewed. This search failed to reveal prior publications on impaired endoscopists, although several papers were identified about impaired physicians, surgeons, anesthesiologists, or other specialists due to alcoholism or drug dependency.

For clarification, the subjects of these two case reports are not the patients undergoing the endoscopies, but the gastroenterologists performing the endoscopies.

CASE PRESENTATIONS

Case report 1

Chief-of-GI was paged stat by the endoscopy-unit-nurse-administrator about an elderly, highly experienced, and normally, highly competent endoscopist who suffered an acute-change-in-mental-status while performing EGD manifested by bizarre behavior, including repeatedly insisting that gastric polyps were in colon, and attempting to endoscopically photograph these polyps by absurdly pressing the steering dials instead of the photography button. Endoscopy nurse recognized this behavior as bizarre and immediately notified endoscopy-unit-nurse-administrator. The summoned Chief-of-GI noted the endoscopist was confused, dizzy, and unsteady; and advised this endoscopist to immediately abort the EGD, cancel upcoming endoscopies, and go to emergency room (ER) for medical evaluation. The endoscopist complied. The Chief-of-GI accompanied the impaired endoscopist to ER.

The impaired endoscopist was experiencing progressive left lower quadrant abdominal pain, hardly eating or drinking fluids, and experiencing orthostatic dizziness during the past 24 h. He had chronic, benign, prostatic hypertrophy. He had no history of neuropsychiatric-disorders/illicit-drug-use/alcoholism/prior similar episodes. Family history was noncontributory. He was bending over in pain and clutching his left lower abdominal quadrant while walking several steps to a waiting wheelchair. Physical examination on admission revealed blood pressure of 181/85 mmHg, pulse of 84 beats/min with orthostasis, respiratory rate of 18 breaths/min, and temperature of 37.9 °C. Mucous membranes were dry, skin turgor was deceased, and axillary sweat was absent. The abdomen was soft, nontender, non-distended, and without hepatosplenomegaly. The left flank was moderately tender. Digital rectal examination revealed guaiac negative stool, and diffuse severe prostatomegaly, without induration. He was moderately confused; oriented to place, person, and year but not month and day. He was conversant and cognizant of his confusion. Formal neurologic examination by a neurologist revealed no other neurologic abnormalities.

There were 16800 leukocytes/mm^3 (normal: 3500-10100 leukocytes/mm^3), and 13700 neutrophils/mm^3 (normal: 1600-7200 neutrophils/mm^3). Hemoglobin was within normal limits. Levels of routine serum electrolytes, serum glucose, basic metabolic panel, lactic acid, and routine thyroid function tests were within normal limits. An electrocardiogram (EKG) and serial troponin levels showed no cardiac ischemia or cardiac arrhythmia. Blood alcohol level and urine screen for 8 commonly abused drugs were negative.

Blood urea nitrogen (BUN) level was 19 mg/dL (normal: 8-22 mg/dL), and creatinine was 2.01 mg/dL (normal: 0.60-1.40 mg/dL). Abdomino-pelvic CT revealed moderate, left-sided, hydroureteronephrosis, mild left perinephric stranding, a 5.5-mm-wide-radioopaque-stone obstructing the left mid-ureter (Figure 1A and B), and an extremely large prostate gland protruding into the bladder (Figure 1C). Urinalysis revealed ketonuria (likely from early starvation ketosis), and microscopic hematuria (from kidney stone). Head computerized tomography (CT) and brain magnetic

resonance angiography (MRA) showed unremarkable cerebral anatomy and cerebral vessels, respectively.

Case report 2

The Chief-of-GI was paged stat by the endoscopy-unit-nurse-administrator about a middle-aged, highly experienced, and normally highly competent endoscopist who suffered an acute-change-in-mental-status while performing EGD manifested by bizarre behavior, including insisting that he was intubated in duodenum when he had actually intubated gastric antrum, and wildly turning the steering dials and bumping forcefully against antral wall while trying to intubate the pylorus. The prior evening, he had taken diazepam 5 mg orally, and drank 24 ounces of beer to relieve lower back pain after twisting his lower back while carrying a heavy pile of medical charts (incident preceded advent of electronic medical records). The endoscopist had not eaten any food or drank any fluids for 16 h before EGD because of residual back pain. After performing one EGD in the morning without incident, he took two purported "motrin" pills of unknown dosage donated by an unidentified stranger (this event was witnessed). He soon became dizzy and disoriented. The endoscopy nurse noted the endoscopist's bizarre behavior during the next EGD and immediately notified the endoscopy-unit-nurse-administrator who paged the Chief-of-GI stat. After noting that the endoscopist was confused, dizzy, lethargic, unsteady, and oriented to place and person but not time, the summoned Chief-of-GI advised the endoscopist to abort the EGD, cancel upcoming endoscopies, and go to ER for medical evaluation. The endoscopist complied. The Chief-of-GI accompanied the impaired endoscopist to ER.

Past medical history revealed chronic back pain for which he intermittently took motrin 200 mg orally, three times daily; and mild anxiety occasionally requiring diazepam, 5 mg orally, as needed. The endoscopist had no history of neuropsychiatric-disorders/illicit-drug-use/alcoholism/prior similar episodes. Family history was noncontributory. Upon evaluation in ER 30 min later, the endoscopist was asymptomatic and appeared completely recovered from his change-in-mental-status. His blood pressure was 130/91 mmHg, pulse was 82 beats/min and regular, respiratory rate was 18 breaths/min, and temperature was 36.2 °C. He had dry mucous membranes, absent axillary sweat, and poor skin turgor. His abdomen was soft and nontender. He was alert; oriented to time, place, and person; and not anymore confused. Formal neurologic examination by a neurologist revealed no neurologic abnormalities. Routine serum electrolytes, basic metabolic panel, BUN, creatinine, complete hemogram, and urinalysis were within normal limits. Blood alcohol level and urine screen for 8 commonly abused drugs were negative. EKG and serial troponin levels showed no cardiac ischemia or cardiac arrhythmias. Head CT and brain MRA with IV contrast revealed no abnormalities.

FINAL DIAGNOSIS

Case report 1

Endoscopist was confused and disoriented at EGD due to toxic encephalopathy secondary to kidney stone obstructing left ureter, complicated by left-sided hydroureteronephrosis, urosepsis, and dehydration.

Case report 2

Transient confusion during EGD attributed to brief toxic encephalopathy attributed to potential neuropsychiatric effects of alleged "motrin" pills given by a stranger, exacerbated by dehydration and acute back pain.

TREATMENT

Case report 1

Endoscopist received profuse IV hydration, and IV ceftriaxone 1 g/d for presumed urosepsis. Cystourethroscopy revealed left, mid-ureteral obstruction from an impacted kidney stone. A J-stent was inserted into left ureter to bypass the ureteral obstruction, and stone removal was deferred. Urine culture obtained from left ureter during cystourethroscopy revealed > 10000 colony-forming-units/mL (normal: < 10000 cfu/mL). He was discharged 1 d later when the creatinine level declined to 1.8 mg/dL, and received trimethoprim/sulfamethoxazole orally for 5 d as an outpatient. At repeat cystourethroscopy 10 d later, the left ureteral stone was successfully extracted *via* basket.

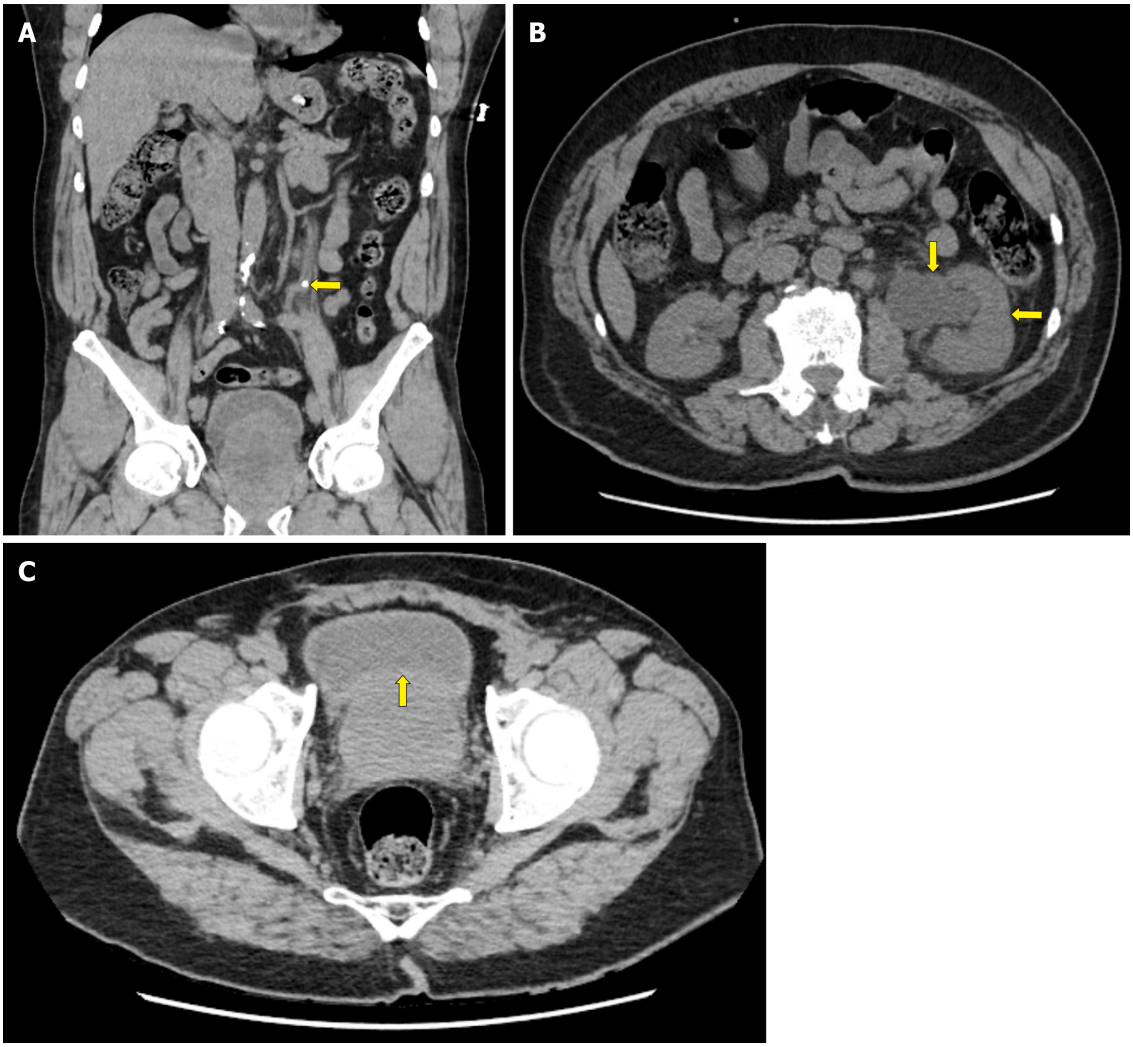

Figure 1 Abdomino-pelvic computed tomography without contrast. A: Left kidney stone. Sagittal section of abdomino-pelvic computerized tomograph without IV contrast (not administered due to elevated creatinine) performed on admission in patient reported as case-1 demonstrates a 5.5-mm-wide, round, radiopaque, kidney stone in left ureter (arrow), just rostral to the level of left iliac crest; B: Left-sided hydroureteronephrosis. Axial section of the same abdomino-pelvic CT at level of mid-kidneys shows that this stone has caused left ureteral obstruction, left-sided hydroureter, and left-sided hydronephrosis. Note the severely dilated left renal calyx (vertical arrow) and compressed left renal parenchyma (horizontal arrow), as compared to normal-sized right calyx and right kidney; C: Moderately severe diffuse prostatomegaly. Axial section of the same abdomino-pelvic CT at level of rectum reveals moderately severe diffuse prostatomegaly, as demonstrated by the prostate compressing the bladder [arrow shows upper (ventral) margin of prostrate compressing bladder].

Case report 2

Patient was admitted overnight for vigorous hydration and observation.

OUTCOME AND FOLLOW-UP

Case report 1

The patient's creatinine and BUN levels rapidly normalized. Chemical analysis revealed a calcium oxalate monohydrate and dehydrate stone. The endoscopist resumed seeing patients and performing GI endoscopy 10 d later with no neurologic sequelae.

Case report 2

Patient became asymptomatic and was discharged the next morning. He resumed seeing patients and performing endoscopy 3 d after hospital discharge, with no neurologic sequelae.

DISCUSSION

Both cases exhibited five notable syndromic features. First, this syndrome is rare (0.0011% of GI endoscopies performed by GIs). This is not surprising because GIs performing endoscopy are generally healthy. Contrariwise, this syndrome can rarely occur because GIs, like other individuals, are subject to human frailties, and these frailties could manifest during endoscopy, which comprises a large part of their workday. Second, impairment first manifested abruptly as bizarre endoscopic interpretation and technique at endoscopy. Changes-in-mental-status may only be first appreciated during endoscopy because endoscopy requires sophisticated cognitive and technical skills which can be readily affected by a change-in-mental-status. Third, in both cases endoscopy nurses first detected this impairment. Endoscopy nurses are highly trained, highly focused on endoscopy, and can directly view endoscopic findings by video-monitor, to detect aberrant cognitive and technical behavior by endoscopists. Both nurses recognizing bizarre behavior were very experienced (> 8 years nursing experience). Fourth, in both cases the change-in-mental-status was caused by metabolic encephalopathy: Case-1-from urosepsis from left ureteral obstruction from kidney stone impacted in left ureter (prostatomegaly a possible predisposing factor), which was compounded by dehydration and ketonuria; and case-2-occurring soon after taking two putative "motrin" pills given by a stranger and resolving soon thereafter, suggesting that the putative "motrin" pills were the proximate cause of impairment, probably exacerbated by dehydration. The impaired endoscopist in case-2 speculated that the pill was not "motrin" but a neuropsychiatric drug which could have been administered mistakenly or deliberately (as in "slipping a Mickey Finn" alluding to Mickey Finn, a bartender who would spike alcoholic drinks with chloral hydrate to make clients sleepy to rob them later)[2]. Change-in-mental-status was not likely an allergic reaction to motrin because the endoscopist had previously taken motrin frequently without toxicity. Fifth, both impaired endoscopists rapidly recovered from their toxic encephalopathies, and resumed seeing patients and performing endoscopy within 10 d after hospitalization.

The following five administrative actions are recommended to manage the crises (Figure 2). First, hospital administrators should recognize such incidents as medical emergencies because of potential iatrogenic patient injury (*e.g.* GI perforation) by impaired endoscopists. For example, the second impaired endoscopist wildly turned the steering dials, and forcefully bumped the endoscopic tip against the antral wall. These effects of metabolic encephalopathy are biologically reasonable. Like a drunken driver crashing a car due to erratic driving, an impaired endoscopist may bump the endoscopic tip forcefully against the GI wall due to erratic steering and potentially cause GI perforation. Inebriated drivers often fail the field sobriety test because they cannot walk in a straight line. The neurologist, Oliver Sacks, published numerous case reports of bizarre behavior due to neurologic impairments, such as a patient who mistook his wife for a hat due to visual agnosia[3]. Second, this work illustrates a reasonable chain-of-command for crisis management: Endoscopy nurse to endoscopy-unit-nurse-administrator to Chief-of-GI. This avoids endoscopy nurses awkwardly confronting endoscopists about faulty endoscopic technique, and defers action until after evaluation by Chief-of-GI, who as a practitioner and peer of impaired endoscopists, should be highly familiar with endoscopic standards of care. Third, the Chief-of-GI was paged stat, and responded immediately, as required for an emergency. Fourth, the Chief-of-GI strongly advised impaired endoscopists in both cases to abort the EGDs, and cancel all upcoming endoscopies to prevent iatrogenic injury (following ethical imperative of "Physician, first do no harm!")[1]; this was accomplished by persuasion. Fifth, impaired endoscopists should be advised to go to ER as recommended for diagnosis and treatment of acute-changes-in-mental-status.

The following two optional recommendations are proposed. First, if the patient agrees, the Chief-of-GI may accompany an impaired endoscopist to demonstrate professional camaraderie and facilitate ER evaluation. Second, with patient consent, a urine screen for commonly abused drugs and a blood alcohol level should be determined, because these agents account for approximately 30% of cases of acute-change-in-mental-status[4]. Moreover, detection of drug addiction by physicians is imperative to prevent patient harm[1,5].

Systematic literature review revealed that the reported cases are novel, even though some literature exists on impaired physicians, surgeons, anesthesiologists, and other specialists, especially from alcoholism or drug dependency[6-10].

Toxic encephalopathy can affect the cognitive behavior of any physician in any specialty or subspecialty performing medical, surgical, or other specialty consults; can affect the technical performance of procedures or surgery by physicians in any medical, surgical, or other specialty, such as cardiac catheterization, interventional angiography, or intestinal surgery, as illustrated for GI endoscopy. Moreover, toxic

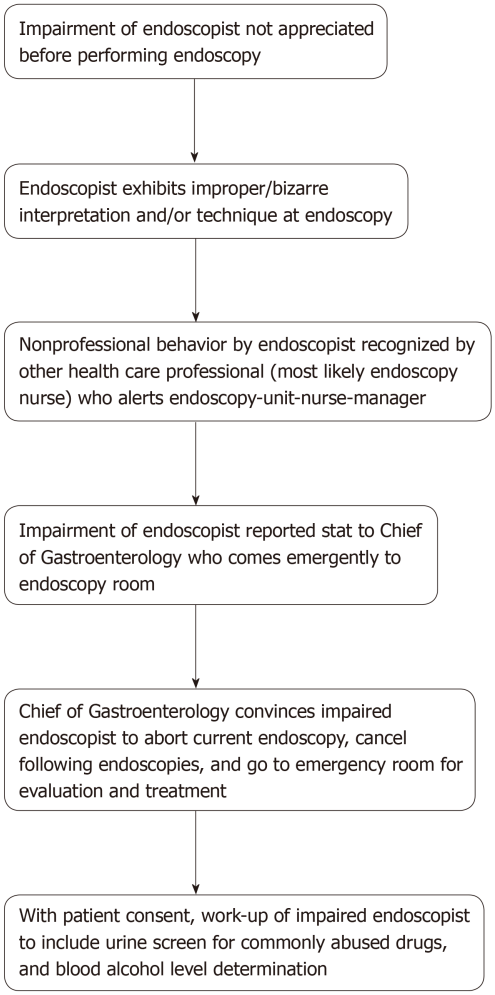

Figure 2 Algorithm. Algorithm summarizing steps to recognize and manage bizarre performance of gastrointestinal endoscopy by an impaired gastroenterologist-endoscopist. The first three steps relate to syndrome recognition. The next two steps describe recommended actions by Chief of Gastroenterology. The last step relates to recommended patient work-up in emergency room. See Discussion section and Supplementary Table 1 for fuller discussion of syndrome recognition and management.

encephalopathy can affect other activities, such as driving a car or operating heavy machinery, due to cognitive impairment. Individuals suffering from toxic encephalopathy should refrain from these activities, and their supervisors should intervene appropriately if necessary.

This study has limitations. First, it is retrospective. However, the author, as Chief-of-GI, prospectively investigated and managed the work-up of the impaired endoscopists in real time, and thoroughly analyzed the events shortly thereafter for quality assurance. Second, the author cannot exclude missed cases of this syndrome during the study period, but such cases seem unlikely because this syndrome is so conspicuous. Third, recommendations on incident management are based on expert opinion by one GI, which may be subject to individual bias. However, Dr. Cappell has extensive experience in senior administrative positions in academic gastroenterology (see Methods), has published very extensively on GI endoscopy[11-13], and has published on GI quality assurance[14,15]. Fourth, this syndrome cannot be reliably characterized by just two cases, and the findings require corroboration, even though all reported syndromic features are biologically reasonable.

CONCLUSION

Two novel cases are reported of acute-change-in-mental-status manifesting as bizarre endoscopic interpretation and technique from toxic encephalopathy. Such incidents should be handled emergently to disengage impaired endoscopists from their patients undergoing endoscopy because of dangers of impaired endoscopists causing

iatrogenic injury (*e.g.*, GI perforation).

REFERENCES

1 **Glasscheibe HS**. New York: Putnam 1964; 164 The march of medicine: The emergence and triumph of modern medicine, 1964: 164
2 **Wikipedia**. Mickey Finn (drugs). Available from: https://en.wikipedia.org/wiki/Mickey_Finn_(drugs)
3 **Sacks O**. The man who mistook his wife for a hat and other clinical tales. New York: Summit Books, 1985: 8-22
4 **Francis J**. Drug-induced delirium: Diagnosis and treatment. *CNS Drugs* 1996; **5**: 103
5 **Watkins D**. Substance abuse and the impaired provider. *J Healthc Risk Manag* 2010; **30**: 26-28 [PMID: 20677242 DOI: 10.1002/jhrm.20040]
6 The impaired surgeon. Diagnosis, treatment, and reentry. Committee on the Impaired Physician, American College of Surgeons Board of Governors. *Bull Am Coll Surg* 1992; **77**: 29-32, 39 [PMID: 10121119]
7 **Jones JW**, McCullough LB, Richman BW. An impaired surgeon, a conflict of interest, and supervisory responsibilities. *Surgery* 2004; **135**: 449-451 [PMID: 15041970 DOI: 10.1016/j.surg.2003.09.011]
8 **Jones JW**, McCullough LB. The question of an impaired surgeon dilemma. *J Vasc Surg* 2012; **56**: 1761-1762 [PMID: 23182487 DOI: 10.1016/j.jvs.2012.10.063]
9 **Killewich LA**. The impaired surgeon: revisiting Halstead. *J Vasc Surg* 2009; **50**: 440-441 [PMID: 19631884 DOI: 10.1016/j.jvs.2009.05.001]
10 **Sudan R**, Seymour K. The Impaired Surgeon. *Surg Clin North Am* 2016; **96**: 89-93 [PMID: 26612022 DOI: 10.1016/j.suc.2015.09.006]
11 **Cappell MS**. Evaluating the Safety of Endoscopy During Pregnancy: The Robust Statistical Power vs Limitations of a National Registry Study. *Gastroenterology* 2017; **152**: 475-479 [PMID: 28038928 DOI: 10.1053/j.gastro.2016.12.014]
12 **Cappell MS**, Iacovone FM Jr. Safety and efficacy of esophagogastroduodenoscopy after myocardial infarction. *Am J Med* 1999; **106**: 29-35 [PMID: 10320114 DOI: 10.1016/s0002-9343(98)00363-5]
13 **Cappell MS**. Safety and efficacy of colonoscopy after myocardial infarction: an analysis of 100 study patients and 100 control patients at two tertiary cardiac referral hospitals. *Gastrointest Endosc* 2004; **60**: 901-909 [PMID: 15605004 DOI: 10.1016/s0016-5107(04)02277-1]
14 **Cappell MS**. Complaints against gastroenterology fellows. *Gastrointest Endosc* 2014; **80**: 153-155 [PMID: 24950643 DOI: 10.1016/j.gie.2014.03.027]
15 **Cappell MS**, Friedel DM. Stricter national standards are required for credentialing of endoscopic-retrograde-cholangiopancreatography in the United States. *World J Gastroenterol* 2019; **25**: 3468-3483 [PMID: 31367151 DOI: 10.3748/wjg.v25.i27.3468]

World Journal of Gastroenterology

Submit a Manuscript: https://www.f6publishing.com

World J Gastroenterol 2020 March 7; 26(9): 992-994

DOI: 10.3748/wjg.v26.i9.992

ISSN 1007-9327 (print) ISSN 2219-2840 (online)

LETTER TO THE EDITOR

Results of meta-analysis should be treated critically

Rong-Qiang Liu, Yi Shao

ORCID number: Rong-Qiang Liu (0000-0001-7993-8891); Yi Shao (0000-0003-1571-2433).

Author contributions: Liu RQ and Shao Y designed and performed the research, and analyzed the data; Liu RQ wrote the letter; Liu RQ revised the letter.

Supported by National Natural Science Foundation of China, No. 81400372; Youth Science Foundation of Jiangxi Province, No. 20151BAB21516; Science and Technology Plan Project of Jiangxi Province, No. 20151BBG70223; Association for Science and Technology of Jiangxi Province, No. 20111BBG70026-2; Science and Technology Plan of Jiangxi Provincial Health and Family Planning Commission, No. 20164017 and No. 20155154.

Conflict-of-interest statement: Osamu Yokosuka has received research funding from Chugai Pharma.

Manuscript source: Unsolicited manuscript

Rong-Qiang Liu, Yi Shao, Department of Ophthalmology, The First Affiliated Hospital of Nanchang University, Nanchang 330006, Jiangxi Province, China

Rong-Qiang Liu, Department of Hepatobiliary Surgery, The First Affiliated Hospital of Guangzhou Medical University, Guangzhou 510220, Guangdong Province, China

Corresponding author: Yi Shao, MD, PhD, Director, Doctor, Department of Ophthalmology, The First Affiliated Hospital of Nanchang University, No. 17, YongWaiZheng Street, DongHu District, Nanchang 330006, Jiangxi Province, China. freebee99@163.com

Abstract

Proton pump inhibitors use increases hepatic encephalopathy risk in patients with liver disease.

Key words: Proton pump inhibitor; Hepatic encephalopathy; Liver disease

Core tip: Proton pump inhibitors (PPIs) have been widely used in patients with liver disease. In general, PPIs are considered safe. However, accumulating evidence indicates that long-term and excessive use of PPIs without clear indication can lead to serious adverse reactions. Some epidemiological studies have investigated the association of PPI use with the risk of hepatic encephalopathy. However, the results are controversial. The study reveals that PPI use increases hepatic encephalopathy risk in patients with liver disease. This reminds clinicians to be more cautious when using PPIs in patients with liver disease.

Citation: Liu RQ, Shao Y. Results of meta-analysis should be treated critically. *World J Gastroenterol* 2020; 26(9): 992-994

URL: https://www.wjgnet.com/1007-9327/full/v26/i9/992.htm

DOI: https://dx.doi.org/10.3748/wjg.v26.i9.992

TO THE EDITOR

We read the recently published meta-analysis on the association between proton pump inhibitor (PPI) and hepatic encephalopathy (HE)[1]. The authors found that there was a significant association between PPI use and HE risk with low

Received: November 25, 2019
Peer-review started: November 25, 2019
First decision: December 23, 2019
Revised: January 14, 2020
Accepted: January 19, 2020
Article in press: January 19, 2020
Published online: March 7, 2020

P-Reviewer: Barreto SG, Chiu CC, Triantafyllou K
S-Editor: Zhang L
L-Editor: Filipodia
E-Editor: Ma YJ

heterogeneity (I^2 = 14.2%). In fact, a correct analysis showed an even stronger association. First, the author made an error in extracting the data. The study by Tsai *et al*[2] provided three dose-related odds ratios (ORs) of 1.41 (1.09-1.84), 1.51 (1.11-2.06) and 3.01 (1.78-5.10), and the meta-analysis by Ma *et al*[1] incorrectly used only the first OR. According to the study of Hamling *et al*[3], we recalculated that the correct OR was 1.59 (1.30-1.95). The results of the meta-analysis revealed that PPI use was significantly associated with the risk of HE with a pooled OR of 1.97 (95% confidence interval [CI]: 1.51–2.58) by using a random effects model (I^2 = 57.1%). The forest plot is shown in Figure 1. In addition, we used the data which were given by Ma *et al*[1] to perform comprehensive analysis. The pooled OR was 1.97 (1.47, 2.65) instead of 1.50 (1.25, 1.75) and the I^2 was 61.2% instead of 14.2%. The results are shown in Figure 2. The incorrect operations of Ma *et al*[1] from using software may be the cause of inconsistencies. Due to the obvious heterogeneity, subgroup analysis and meta-regression should be performed to explore the sources of heterogeneity.

The fixed effects model assumes that all the included studies have the same true effect size, while the true effect size in the random effects model varies with different studies. When the observed effect size of each study approaches or equals its true effect size, the heterogeneity is not obvious and the fixed effect model should be used. Otherwise, the random effects model is used. The Cochrane Handbook has stated that when I^2 is less than 40%, a fixed effects model should be used for meta-analysis. Otherwise, a random effect model should be used. In general, the conclusions obtained by random effects models tend to be conservative, and thus can be used in any case. However, when the heterogeneity is significant, only the random effect model can be used, and further analysis is needed to find the sources of heterogeneity.

In conclusion, our results demonstrated that PPI use increased HE risk, consistent with the study of Ma *et al*[1]. However, the meta-analysis by Ma *et al*[1] is flawed. More accurate statistical analysis is necessary to improve the quality of this meta-analysis.

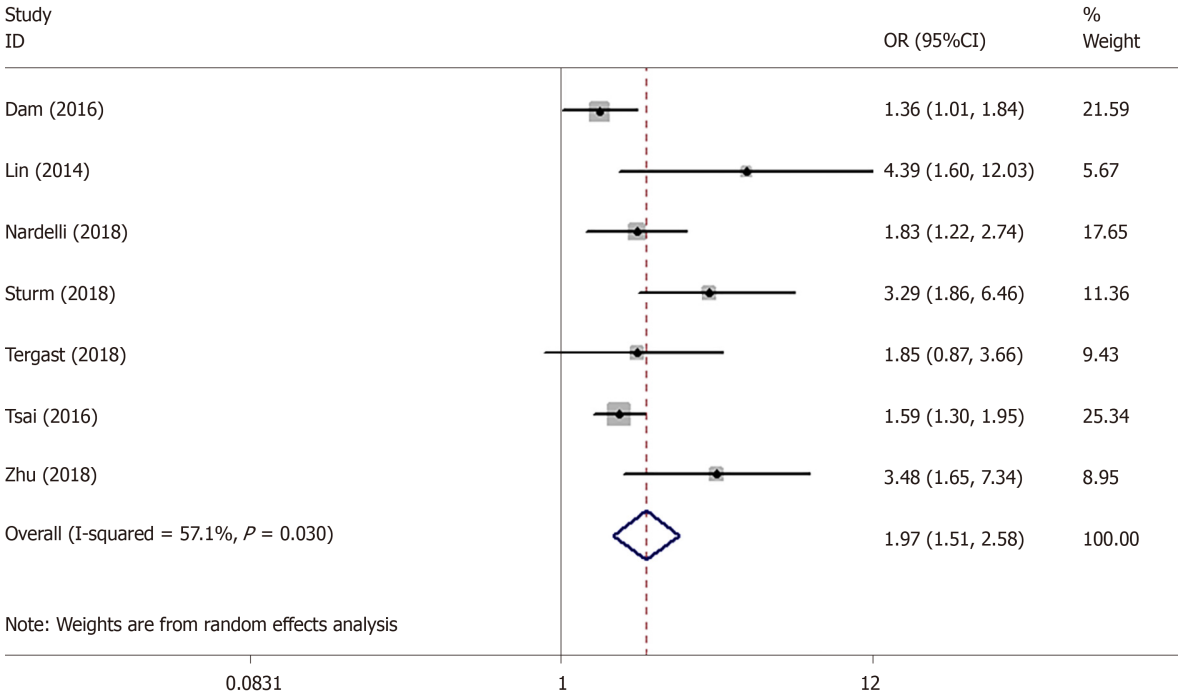

Figure 1 Forest plot of the association between proton pump inhibitor use and hepatic encephalopathy.

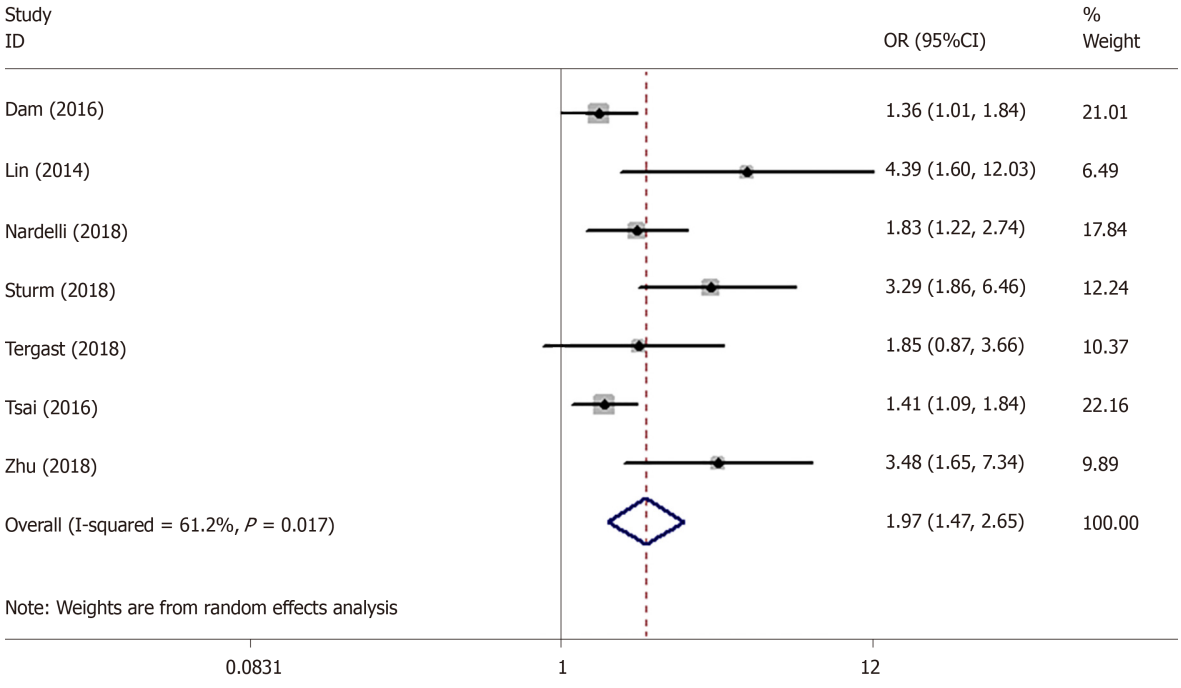

Figure 2 Forest plot of proton pump inhibitor use and risk of hepatic encephalopathy.

REFERENCES

1 **Ma YJ**, Cao ZX, Li Y, Feng SY. Proton pump inhibitor use increases hepatic encephalopathy risk: A systematic review and meta-analysis. *World J Gastroenterol* 2019; **25**: 2675-2682 [PMID: 31210718 DOI: 10.3748/wjg.v25.i21.2675]

2 **Tsai CF**, Chen MH, Wang YP, Chu CJ, Huang YH, Lin HC, Hou MC, Lee FY, Su TP, Lu CL. Proton Pump Inhibitors Increase Risk for Hepatic Encephalopathy in Patients With Cirrhosis in A Population Study. *Gastroenterology* 2017; **152**: 134-141 [PMID: 27639806 DOI: 10.1053/j.gastro.2016.09.007]

3 **Hamling J**, Lee P, Weitkunat R, Ambühl M. Facilitating meta-analyses by deriving relative effect and precision estimates for alternative comparisons from a set of estimates presented by exposure level or disease category. *Stat Med* 2008; **27**: 954-970 [PMID: 17676579 DOI: 10.1002/sim.3013]

Published By Baishideng Publishing Group Inc
7041 Koll Center Parkway, Suite 160, Pleasanton, CA 94566, USA
Telephone: +1-925-3991568
E-mail: bpgoffice@wjgnet.com
Help Desk:http://www.f6publishing.com/helpdesk
http://www.wjgnet.com